THE UNIVERSITY OF MICHIGAN RESEARCH INSTITUTE
ANN ARBOR, MICHIGAN

A SMALL-SIGNAL ANALYSIS OF E-TYPE TRAVELING-WAVE DEVICES

TECHNICAL REPORT NO. 38

Electron Physics Laboratory
Department of Electrical Engineering

By

Walter M. Nunn, Jr.

Approved by: J. E. Rowe

J. E. Rowe, Director
Electron Physics Laboratory

Project 2845

CONTRACT NO. DA-49-186-502-ORD-720
DIAMOND ORDNANCE FUZE LABORATORIES
PROJECT NO. 31030
PLACED BY: THE DEPARTMENT OF THE ARMY ORDNANCE CORPS
WASHINGTON, D. C.

August, 1960

This report has also been submitted as a dissertation in partial fulfillment of the requirements for the degree of Doctor of Philosophy in The University of Michigan, 1960.

ABSTRACT

This dissertation is concerned with a small-signal study of E-type traveling-wave tubes. The investigation includes both a theoretical analysis and an experimental examination.

The theoretical portion of the work is divided into two general phases. The first of these treats the electromagnetic boundary value problem, with special attention being devoted to the allowed field solutions and their formulation in the interaction region. The azimuthally nonre-entrant character of the circular-cylindrical structure, associated with the class of devices studied here, leads to a requirement for general, nonintegral order, real and hyperbolic Bessel functions. The unavailability of these functions has necessitated the derivation of a special set of small-argument approximations which are found to satisfy the required boundary conditions. In addition, a careful consideration of the configuration of a typical E-type device reveals that these simplifications fall within the operating conditions actually encountered.

The electromagnetic analysis not only provides an understanding of the origin and generation of the field components permeating the interaction space in the absence of an energy-carrying electron beam, but it also leads to a general classification of centrifugal-focusing systems and to a prediction of related devices not presently in existence. However, the most important consequences of this study lie in the foundation it provides for an adequate mathematical development of the second part, which treats the electron-wave interaction problem from the viewpoint of the equivalent circuit analysis.

It is primarily this equivalent circuit approach that leads to a prediction of the propagation constants and amplitudes of the excited waves in the presence of an impressed azimuthally-propagating slow electromagnetic wave and a ribbon-shaped electron beam. The circuit and ballistic relations are derived and used in the subsequent development of the generalized determinantal equation, which applies to both forward- and backward-wave E-type devices. The input boundary problem is next formulated and solved in order to obtain predictions of the magnitude of the forward-wave growing- and beating-wave gain, and the backward-wave start-oscillation conditions. The general problem has been solved for a very wide range of operating conditions with the aid of the IBM-704 digital computer.

In addition, the study leads to a small-signal estimate of the efficiency that might be expected from E-type devices. It is found that the important interaction components of the fields are principally azimuthally-oriented, and that the efficiency is comparable to that obtained in O-type devices. Although the study reveals that the E-type incremental propagation constants exhibit properties similar to those of O-type tubes, certain resemblances to M-type devices are also

evident. Furthermore, the study reveals that E-type devices possess certain distinctive characteristics not known to other traveling-wave tubes. One of the most important of these is related to the fact that the gain and start-oscillation characteristics of E-type tubes are strongly influenced by the radius of curvature of the ribbon-shaped electron beam following a circular path in the interaction region.

The experimental portion of the study provides a treatment of those factors which exercise control over the laboratory model of the small-signal device. The design data for the tube is used in conjunction with the theoretical analysis to predict the forward-wave gain characteristics of the amplifier. The measured data are then presented for comparison, and an explanation is provided to determine the probable range of validity of the theoretical analysis.

ACKNOWLEDGMENTS

The author wishes to express his appreciation to the members of his doctoral committee for their assistance, and in particular to Professor J. E. Rowe, chairman of the committee, under whose guidance and supervision the work was carried out. The skill and competence of Mr. L. Flanigan in programming the digital computer, as well as the work of Messrs. H. Sanford, D. Williams and K. McCrath, in constructing the experimental device, is gratefully acknowledged. The author also appreciates the assistance he has received from the administrative staff of the Electron Physics Laboratory in preparing this report.

TABLE OF CONTENTS

LIST OF TABLES

LIST OF ILLUSTRATIONS

CHAPTER I. INTRODUCTION

1.1 The Basic Types of Traveling-Wave Devices

This dissertation is concerned with a small-signal investigation of E-type traveling-wave tubes. As with the more familiar O-type device[7], the E-type traveling-wave tube employs the interaction of an electron beam and a slow electromagnetic wave for the generation and amplification of microwave signals. The very wide bandwidth that may be obtained with these microwave electron beam tubes is primarily responsible for their extensive use in the communications industry.

The O-type traveling-wave tube consists of an electron beam arranged to pass through an environment containing a slow electromagnetic wave, with the beam confinement usually being accomplished by means of a long focusing magnet. The cumulative effect of the interaction between the beam and the wave results in a net transfer of energy to the r-f wave. The general principles of the O-type traveling-wave tube have been extensively treated by Pierce[7], Rowe[25,26], Heffner[20], Watkins[38], and many others, and its operation is now well understood. The device is capable of providing large bandwidths, high gain, moderate efficiency and relatively low noise figures. To date, O-type traveling-wave amplifiers have been successfully constructed to operate at all power levels from milliwatts to megawatts.

It has also been found that higher efficiencies can be achieved by passing the electron beam through a region containing slow electromagnetic waves under the influence of orthogonally-oriented static electric and magnetic fields. These traveling-wave tubes, which are

known as M-type devices, exhibit large efficiencies because the electrons transfer d-c potential energy to the r-f wave, thereby maintaining a phase relation suitable for a continuing energy exchange. The O-type device has a somewhat lower limit of maximum achievable efficiency since energy transformations to the wave take place through a loss of kinetic energy, with the result that the electrons progressively lose the optimum phase relation necessary for most favorable interaction. There are means, however, of maintaining the optimum phase relationship as the electrons slow down.

The operation of both M- and O-type devices depends on the use of generally large and heavy magnets. In recent years a substantial amount of effort has been devoted to a reduction, or complete elimination, of these magnet systems[6]. One method of reducing the weight of the magnet is to replace it by a set of suitably situated small permanent magnets. Although this "periodic-magnetic-focusing" principle has been successfully employed in forward-wave amplifiers, certain operating difficulties have attended its use in backward-wave amplifiers and oscillators. Recent developments have also led to the complete replacement of the magnet by means of properly arranged electrodes, subjected to prescribed voltages, through which the electron beam passes. This "periodic-electrostatic-focusing" principle has been successfully employed in both forward- and backward-wave devices and is presently under intensive investigation.

Another system, which is the subject of this dissertation, that provides for the complete elimination of the focusing magnet is known as the E-type traveling-wave device[20]. The interaction region consists of a coaxial-cylindrical structure with the slow-wave circuit situated

along the inner concentric cylinder and the sole along the outer cylinder, as shown in Fig. 1.1. A ribbon-shaped electron beam is injected along a tangent to the circle of motion in the cross-sectional plane of the system, and a static electric field is applied between the sole and circuit electrodes. The d-c potential of the circuit (measured relative to the cathode) is chosen just sufficiently larger than that of the sole so that the centrifugal force exerted on the electron, as it traverses the circular path through the interaction region, is balanced by an equal and opposite radial electric field force. Although this focusing scheme has often been referred to in the United States[6] as "Harris-flow focusing", the Russian designation[27,28], "Centrifugal-Electrostatic Focusing", abbreviated CEF, seems more informative.

1.2 Devices Employing the Centrifugal-Focusing Principle

The system that Heffner and Watkins[20] have identified as the E-type traveling-wave device in 1955 appears to have been invented by Huber[21] in 1949. His disclosure, filed with the French Patent Office, provides several drawings, one of which employs a filter-type structure as the slow-wave circuit, and another suggesting the use of a helix. Although no mathematical support is provided, the inventor apparently takes the position that an electron which favorably interacts with the r-f wave expends energy and moves radially inward. The slow-wave structure is therefore placed along the inner of the two coaxial cylinders so that the electron beam moves in the direction of increasing field intensity as it loses energy. There is no evidence in the patent, however, which would indicate that the tube was actually constructed or that any experimental data for the device was ever obtained.

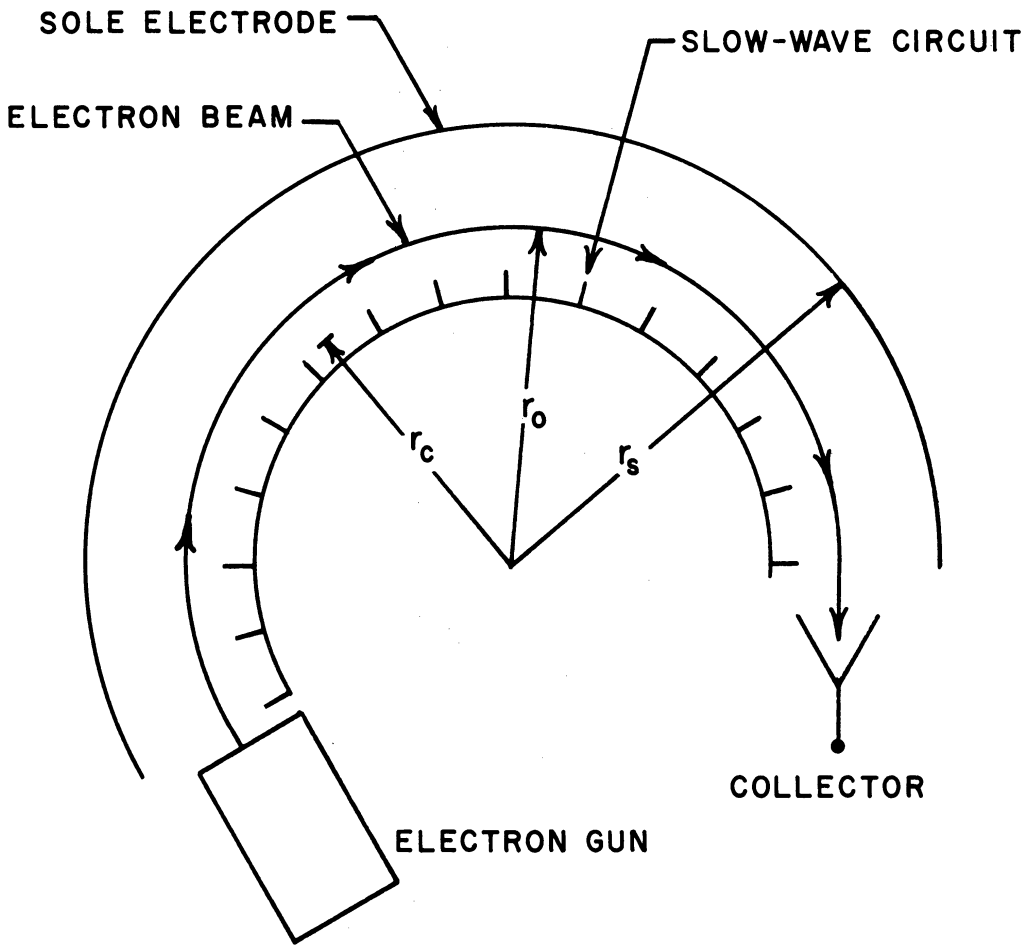

r_c = RADIUS OF THE SLOW-WAVE CIRCUIT

r_o = RADIUS OF THE CENTER-OF-THE-BEAM ELECTRON

r_s = RADIUS OF THE SOLE ELECTRODE

FIG. 1.1 THE BASIC GEOMETRY OF THE E-TYPE TRAVELING-WAVE DEVICE.

A tube referred to as "A Magnetless Magnetron" by Versnel and Jonker[29] in 1954 employs an azimuthally re-entrant slow-wave system situated along the inner coaxial cylinder. The device, which is similar to the French invention in that the beam makes only a single transit through the interaction region, was subsequently described in greater detail by Versnel[30] in 1956. The steady-state voltage and current relations that must be satisfied in order to achieve stable electron orbits, and the frequency of oscillation, were derived. A test model was constructed for operation over the frequency range of 230 to 430 mcs. In addition to obtaining experimental results which are in good agreement with theoretical predictions, Versnel obtained the relatively large power output of some tens of milliwatts.

A significant advance was made by Watkins[20,38] in 1954 when a device that has now come to be known as "The Helitron" was conceived. The tube, which utilizes the CEF principle, employs a ribbon-shaped electron beam that is permitted to drift axially while it interacts with the azimuthal component of one of the space harmonics of an r-f wave propagating along a "guiding system". An interesting aspect of the helitron lies in the fact that the axial velocity of the r-f wave is very nearly equal to the velocity of light, so that the wave actually "sweeps past" the beam as it absorbs energy. Experimental results have shown that a helitron backward-wave oscillator can be made to generate a signal power as large as ten milliwatts in both the UHF and microwave frequency ranges.

A traveling-wave tube which in certain physical respects resembles the helitron was described by Tchernov[27] in 1956. The device, known as "The Spiratron", employs a helical ribbon-shaped electron beam that

spirals about the axis of two concentric cylinders. The inner cylinder contains a structure capable of supporting axially slow waves. Watkins and Wada[38] have pointed out, however, that the spiratron is, in fact, a Harris-flow-focused O-type forward-wave amplifier, since it is only the relatively small axial velocity component of the beam which provides interaction with the wave. Although the analysis has been limited principally to the d-c characteristics of the spiratron[27,28], Tchernov has described several experimental traveling-wave and double-stream amplifiers employing the same principle. A power output as large as two watts at a frequency of 3 kmc, with an overall efficiency of 20 percent, has been obtained[27] for a spiratron traveling-wave amplifier. The maximum small-signal gain for this tube was found to be 40 db over a pass-band as large as 60 percent of the S-band frequency range.

Although the ribbon-shaped electron beam can be made to traverse a helical path in CEF systems such as the helitron and spiratron, it is also possible to achieve the same motion by means of an axial magnetic field. A device was recently constructed by Pantell[23] in which the azimuthal velocity component of a helical ribbon beam was caused to interact with the transverse electric field of a TE_{10} wave propagating in a rectangular waveguide. While the objective of the work was not concerned with the elimination of the focusing magnet, the successful performance of the device as a backward-wave oscillator demonstrated the feasibility of a new class of tubes utilizing the "Centrifugal-Magnetic-Focusing", or CMF, principle. These investigations have shown that CEF and CMF systems exhibit similar focusing properties, although it is known that each possesses distinctive characteristics[36].

1.3 The Present State of Analytical Development of Centrifugal-Focusing Systems

A review of the literature reveals the centrifugal-focusing systems in general, and E-type devices in particular, have received relatively little analytical attention. The properties of a single electron moving between the curved plates of a coaxial-cylindrical capacitor have been treated with varying degrees of completeness by Pierce[6], by Harman[19], and more thoroughly by Waters[33]. In addition, Waters has analyzed the motion of thin electron ribbons subject to purely electrostatic forces[32,35], and has obtained the paraxial-ray equation for these beams when arbitrary curved motions are involved[34]. An important consequence of this work has been the determination of those conditions under which the ribbon beam executes no rippling, but follows a specified circular path with unvarying radial thickness. This work has recently been extended to include CMF as well as CEF systems[36]. As mentioned earlier, brief treatments of the conditions leading to stable electron orbits, under the influence of prescribed steady electric fields, have been presented by Tchernov[27], and by Versnel[30].

In regard to a general study of the r-f interaction phenomena in centrifugal-focusing systems, the subject has received less attention. Moreover, there appears to have been some misunderstanding in the past of the detailed nature of the interaction. Although the first publication of the work on the helitron by Watkins and Wada[38] presented a close correlation between the predicted and observed voltage tuning curve, other aspects of the experimental results were not in good agreement with the analysis.

The first theoretical study of the helitron, which was based on the type of crossed-field analysis originally presented by Pierce[7], presumed that the propagation constants were very nearly the same as those obtained in M-type tubes. However, this and subsequent analyses led to predictions of the performance characteristics of the helitron that did not agree with the observed start-oscillation conditions. Nevertheless, Watkins and Wada concluded[38] that the helitron employs a beam-to-circuit interaction like that of M-type devices.

Heffner and Watkins[20], and later Watkins and Wada[38], advanced nonmathematical arguments to show that when an electron transfers energy to the r-f wave it moves radially inward, but maintains its spatial angular velocity in synchronism with that of the wave. However, Waters[35] has shown that, in the presence of a constant azimuthal retarding r-f field, an electron increases its angular velocity as it moves radially inward, thereby slipping out of synchronism.

More recently, Wada and Pantell[24,31] have presented an analysis of the helitron which leads to predictions of start-oscillation conditions that agree reasonably well with experimental observations made on two such backward-wave oscillators. The small-signal analysis presented by these authors employed a procedure similar to that used by Pierce[7]. The circuit equation was derived from a normal mode expansion, while the ballistic equations were derived in the usual manner from the equations of motion of a single particle. It was found that the principal interaction between the electron beam and the circuit fields takes place due to bunching in the azimuthal direction, and that interaction arising from transverse motion of the beam is a second-order effect. The electron stream is found to transfer energy to the r-f wave through a loss of

kinetic energy of rotation, and in this respect the E- and O-type devices behave similarly[31]. However, it has also been shown[24] that growing waves can exist in a CEF system, even without the presence of a circuit field. This characteristic of the E-type device is similar to that of the M-type tube.

1.4 Objective of the Present Investigation

The work on E-type traveling-wave devices undertaken at this University was initiated to acquire a better understanding of the characteristics of CEF systems. The research, which began shortly before Watkins and Wada[38] published their findings, was concerned with a study of the waves which may propagate in coaxial-cylindrical systems in the presence of a ribbon-shaped electron beam, and with the manner in which these waves combine to produce growing- and beating-wave amplification, and backward-wave oscillation.

These objectives can be most effectively achieved by first examining the solutions of the electromagnetic boundary value problem for the appropriate geometry. A quantitative understanding of the relative magnitudes of the important field components, and the mechanism of their generation, provides the necessary foundation for the formulation of the equivalent circuit analysis. The derivation of the ballistic and circuit equations leads to the generalized determinantal equation, whose solutions yield the incremental propagation constants for both forward- and backward-wave E-type devices. The input boundary problem is subsequently treated in order to determine the forward-wave growing- and beating-wave gain[26], and the backward-wave start-oscillation conditions. The causes for a slipping electron stream in E-type devices, and an approximate

method of accounting for its influence on the growing-wave gain of a small-signal forward-wave amplifier, also receive attention.

The incremental propagation constants, and the gain and start-oscillation characteristics, of E-type devices have been examined over a wide range of operating conditions. Although the results, which appear in five appendices, point to a similarity between E- and O-type devices, the propagation constants exhibit certain properties more closely associated with M-type tubes. In addition, the study brings to light several unusual characteristics not found in other types of traveling-wave tubes. One of the most important of these is related to the fact that the gain and start-oscillation characteristics of the E-type device are strongly influenced by the radius of curvature of the ribbon-shaped beam following a circular path in the interaction space.

A small-signal efficiency estimate is also carried out along lines originally used by Pierce[7], but modified to account for the two-dimensional electron motion of the E-type device. General and special forms of efficiency relations are derived, and it is shown that the principal contribution to electron-wave energy transformations arise as a result of azimuthally-oriented interactions. The range of efficiencies that may be expected from typical E-type tubes is found to be comparable to that obtained in O-type traveling-wave devices. These results are in agreement with the findings of Wada and Pantell[24,31] concerning the relation between E- and O-type devices.

The experimental phase of the investigation includes not only a discussion of the specific details of an azimuthally nonre-entrant device, such as shown in Fig. 1.1, but also a prediction of the expected incremental propagation constants and the growing- and beating-wave gain

characteristics based on the previously developed theory. The experimental results are then presented for correlation with the small-signal analysis.

The treatment advanced in this dissertation differs from the work of Wada and Pantell[24,31] in several important respects. First, the small-signal E-type device studied here involves only circular motion of the electron beam, in contrast to the helical motion of the helitron backward-wave oscillator. Second, an investigation of the conditions leading to complementary mode propagation in azimuthally nonre-entrant circular-cylindrical waveguide structures was necessitated by the present study, whereas the helitron involves TEM wave propagation in an azimuthally re-entrant system[38]. Third, both forward- and backward-wave devices are studied here with attention being devoted to the influence that the tube parameters exert over the incremental propagation constants and the gain and start-oscillation characteristics of E-type devices. Finally, the present study provides a theoretical estimate of the efficiency of E-type devices based on a small-signal analysis.

CHAPTER II. THE ELECTROMAGNETIC ANALYSIS

2.1 Introduction

In order to obtain a proper understanding of the interaction processes that take place between a ribbon-shaped electron beam following a circular path and the r-f fields associated with the slow-wave system, it is necessary to investigate the solutions of the electromagnetic boundary value problem appropriate to the geometry of E-type devices. These solutions are treated only for the condition that the electron beam is not present in the interaction space. Several attempts to solve the inhomogeneous wave equation for propagation in a coaxial-cylindrical interaction space, partially occupied by a ribbon beam, have led to untenable mathematical complexity. Moreover, the effect of the electron stream upon the circuit fields will be accounted for by the analysis presented in the following chapter. It is essential to observe, however, that this approach limits the study to an investigation of energy transformations taking place between the electron stream and the fields propagating along the slow-wave circuit. Energy transformations taking place within the stream, due to the relative motions of electrons, must necessarily be excluded from the present treatment.

There are at least two geometries whose field solutions are of interest in a study of centrifugal-focusing systems. An examination of the first of these involves the investigation of the permissible radial and azimuthal field components that exist in any transverse plane, when electromagnetic waves are guided by one or more pairs of parallel-wire transmission lines. This is the basic configuration of the r-f circuit

used in the helitron[38], where the transverse fields of a TEM wave interact with the azimuthal component of a ribbon-shaped electron beam advancing along a helical path. A significant feature of this system lies in the fact that the multiply-connected region associated with any cross-sectional plane of this structure admits the generation of nonzero radial and azimuthal field components in the presence of plane electromagnetic waves. An excellent treatment of the conditions under which plane waves may exhibit linear, circular or elliptical polarization is presented by Stratton[9]. Furthermore, the distinction between uniform plane waves, where the field intensities are independent of the coordinates of each transverse plane, and nonuniform plane waves, where the field intensities do not possess this independence, is discussed by Schelkunoff[8].

The second geometrical configuration, whose field solutions will be of primary interest in this chapter, is that of a coaxial-cylindrical transmission system in which the inner conductor is replaced by an r-f circuit capable of supporting (azimuthally) slow waves. In addition to the usual difficulties which arise from the limited tabular range of the real and hyperbolic Bessel functions, complications also result from the azimuthally periodic, but spatially discontinuous, boundaries of the slow-wave circuit. Each of these problems is partially circumvented by approximate methods that yield the general forms of functional dependence existing among the various field components.

2.2 Separability Considerations for the Wave Equation in Coaxial-Cylindrical Geometry

One of the central issues of electromagnetic theory pertains to an investigation of the fields which may propagate in a given spatial

environment. The resolution of the vector field into its components is contingent upon the separation of a scalar partial differential equation (derived from Maxwell's equations) into three ordinary differential equations. The well-known product method may be successfully applied to accomplish this separation provided the resulting scalar equation is of the Helmholtz form[5]. The familiar orthogonal, rectangular coordinate system is "completely separable" inasmuch as a scalar Helmholtz, or wave, equation may be obtained from an analysis which presumes that propagation is principally directed along any one of the three coordinate axes. In curvilinear coordinate systems separability can be achieved only for certain axes, if at all. It becomes essential, therefore, to regard separability as a special geometric property restricted to selected axes in a limited class of coordinate systems.

Those curvilinear systems that do yield a scalar wave equation for at least one of the coordinates can be determined by means of a simple test[5]. A scalar Helmholtz equation can be derived from Maxwell's equation if the following set of conditions are simultaneously fulfilled:

1. One of the coordinate scale factors of the expression for differential arc length must be unity.
2. The ratio of the other two scale factors is independent of the unity scale factor coordinate.

The nature of these requirements is such that a wave having a component lying parallel to the "separable axis" is capable of generating all transverse field components lying in a plane normal to this axis. This follows from the fact that the solutions of Maxwell's equations, subject to the appropriate boundary conditions, must provide a complete description of the electromagnetic fields permeating the space under consideration[11].

The coaxial-cylindrical geometry, shown in Fig. 2.1, may be investigated with the aid of the foregoing rules. The vector increment of arc length is known to be[3]

$$d\bar{s} = \bar{l}_r\, dr + \bar{l}_\theta\, r\, d\theta + \bar{l}_z\, dz \quad , \tag{2.1}$$

where s is the scalar magnitude of the arc length and the associated r, θ, z components are chosen to conform to the diagram. The application of the above conditions reveals that separability is feasible only for the axial coordinate, because only in the case of the z-axis is the scale factor unity with the ratio of the remaining scale factors independent of z.

2.3 The Derivation of the Field Relations in Coaxial-Cylindrical Geometry

The first exhaustive treatment of the electromagnetic boundary value problem appears to have been given by Kalähne[13], in 1905, for an azimuthally re-entrant coaxial-cylindrical structure. Although the method involves the reduction of Maxwell's equations to a system of three scalar ordinary differential equations, it differs from the more general approach of seeking solutions to the scalar wave equation in the associated geometry.

A later examination of the related problem of waves propagating around a circular bend in a rectangular waveguide was presented by Buchholz[11] in 1939. The procedure employed the Hertzian vector functions in the derivation of the field components for a long, straight waveguide of rectangular cross section. The field solutions were then subjected to appropriate transformations that apply when the waveguide assumes a large, but finite, radius of curvature.

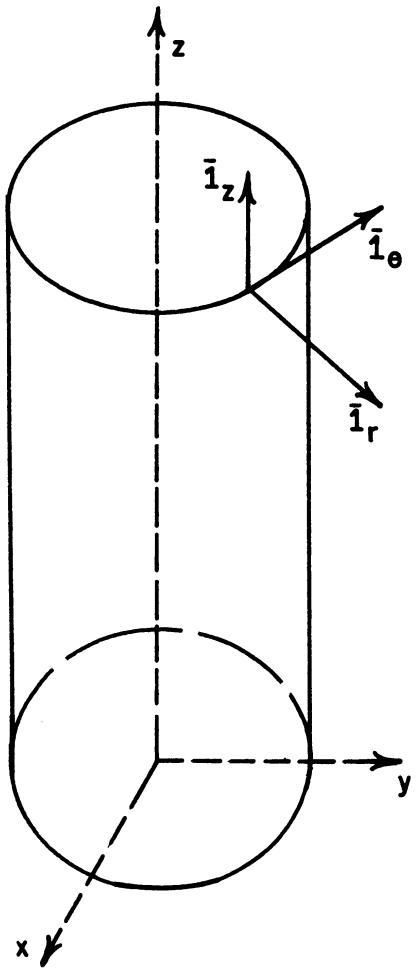

FIG. 2.1 A RIGHT-HANDED ORTHOGONAL CYLINDRICAL SYSTEM.

The present analysis utilizes the fact that solutions of the scalar wave equation, subject to the stipulated boundary conditions, yield functions which completely specify the mathematical forms of all wave fields within the system. It is shown in Appendix A that when the electric and magnetic field intensities are defined according to the relations

$$\bar{E} = \mathrm{Re}\left[(\bar{\psi}_T + \bar{l}_z \psi_z)\, e^{j(\omega t - \gamma z)}\right] , \tag{2.2}$$

$$\bar{H} = \mathrm{Re}\left[(\bar{\xi}_T + \bar{l}_z \xi_z)\, e^{j(\omega t - \gamma z)}\right] , \tag{2.3}$$

then the following set of scalar wave equations follow from Maxwell's equation:

$$\left(\nabla^2_{r,\theta} + k^2\right) \psi_z = 0 , \tag{2.4}$$

$$\left(\nabla^2_{r,\theta} + k^2\right) \xi_z = 0 . \tag{2.5}$$

Although Eqs. 2.4 and 2.5 apply to waves propagating in the assumed positive axial direction, it may easily be shown that precisely the same Helmholtz equations are obtained for waves propagating in the negative axial direction.

It will be convenient to replace ψ_z and ξ_z, which depend on r and θ only, by the scalar function U and thereby obtain

$$\frac{\partial^2 U}{\partial r^2} + \frac{1}{r}\frac{\partial U}{\partial r} + \frac{1}{r^2}\frac{\partial^2 U}{\partial \theta^2} + k^2 U = 0 . \tag{2.6}$$

The familiar product representation of U is given by

$$U = R\,\Theta , \tag{2.7}$$

where R = a scalar function of r only,

Θ = a scalar function of θ only.

Equation 2.7 may be substituted into Eq. 2.6 to obtain, after separation and rearrangement,

$$\Theta'' + \beta_o^2 \Theta = 0 \quad , \tag{2.8}$$

$$R'' + \frac{R'}{r} + \left(k^2 - \frac{\beta_o^2}{r^2}\right) R = 0 \quad , \tag{2.9}$$

where the primes indicate partial differentiation with respect to the associated variables. The solutions of Eq. 2.8 involve the well-known exponential function

$$\Theta = A_1 e^{j\beta_o\theta} + A_2 e^{-j\beta_o\theta} \quad , \tag{2.10}$$

where A_1 and A_2 are arbitrary constants that are evaluated in matching the boundary conditions. Equation 2.9 is recognized as Bessel's differential equation which has the general solution

$$R = A_3 J_{\beta_o}(kr) + A_4 N_{\beta_o}(kr) \quad , \tag{2.11}$$

where A_3, A_4 = arbitrary constants,

$J_{\beta_o}(kr)$ = real Bessel function of the first kind with argument kr and order β_o,

$N_{\beta_o}(kr)$ = real Bessel function of the second kind with argument kr and order β_o.

The scalar function U therefore takes the form

$$U = \left(A_1 e^{j\beta_o\theta} + A_2 e^{-j\beta_o\theta}\right)\left(A_3 J_{\beta_o}(kr) + A_4 N_{\beta_o}(kr)\right) \quad . \tag{2.12}$$

A study of this relation shows that β_o is the circular propagation constant of the r-f wave. From the analogy with the linear propagation constant, it follows that

$$\beta_o = \frac{\omega}{\Omega_w} \text{ electrical radian/spatial radian,} \qquad (2.13)$$

where $\omega = 2\pi f$ = electrical angular velocity of the wave in electrical radians/second,

f = frequency of the r-f wave in electrical cycles/second,

Ω_w = spatial angular velocity of the wave in spatial radians/second.

In view of these results it is apparent that the waves possess a spatial angular velocity which is dependent only upon the electrical angular velocity and the circular propagation constant. The linear (tangential) velocity is, however, a function of the radius according to the relation

$$(v)_r = \Omega_w r = \left(\frac{\omega}{\beta_o}\right) r \quad , \qquad (2.14)$$

where $(v)_r$ = linear tangential velocity of the wave at radius r in meters/second,

r = radius in meters.

The general forms of the separable scalar electric and magnetic field intensities, for waves propagating in both the positive and negative axial and azimuthal directions, may therefore be written

$$E_z = \mathrm{Re}\left[C_1\left(J_{\beta_o}(kr)+C_2N_{\beta_o}(kr)\right)\left(e^{j\gamma z}+C_3e^{-j\gamma z}\right)\left(e^{-j\beta_o\theta}+C_4e^{j\beta_o\theta}\right)e^{j\omega t}\right] \quad , \qquad (2.15)$$

$$H_z = \mathrm{Re}\left[D_1\left(J_{\beta_o}(kr)+D_2N_{\beta_o}(kr)\right)\left(e^{j\gamma z}+D_3e^{-j\gamma z}\right)\left(e^{-j\beta_o\theta}+D_4e^{j\beta_o\theta}\right)e^{j\omega t}\right] \quad , \qquad (2.16)$$

where $C_1,\ldots, C_4, D_1,\ldots, D_4$ are real constants. These are the relations that must be used in evaluating the integration constants, because the total field intensities are the ones given in a statement of the boundary conditions.

One simplification is possible, however, for the azimuthally nonre-entrant structure of the E-type device under consideration. Inasmuch as no stipulations are placed on the total fields within the domain of finite θ values, other than the fact that they may possess any attainable function value, it is possible to limit attention to those waves propagating in the positive azimuthal direction. Under these circumstances, Eqs. 2.15 and 2.16 reduce to

$$E_{z\theta+} = \mathrm{Re}\left[C_1\left(J_{\beta_o}(kr) + C_2 N_{\beta_o}(kr)\right)\left(e^{j\gamma z} + C_3 e^{-j\gamma z}\right)e^{j(\omega t-\beta_o\theta)}\right] , \tag{2.17}$$

$$H_{z\theta+} = \mathrm{Re}\left[D_1\left(J_{\beta_o}(kr) + D_2 N_{\beta_o}(kr)\right)\left(e^{j\gamma z} + D_3 e^{-j\gamma z}\right)e^{j(\omega t-\beta_o\theta)}\right] , \tag{2.18}$$

Nevertheless, the use of these equations in subsequent work carries the implied constraints that

$$0 \leq \beta_o < \infty , \quad 0 \leq \theta < \infty .$$

The $\theta+$ subscript will be dropped from further references to Eqs. 2.17 and 2.18 with these restrictions on β_o and θ being clearly understood.

The remaining components may now be obtained by solving the Maxwell curl equations for the radial and azimuthal field intensities in terms of the axial fields. These expressions are

$$E_r = \frac{1}{k^2}\left[\frac{\partial}{\partial z}\left(\frac{\partial E_z}{\partial r}\right) - j\frac{\omega\mu_m}{r}\frac{\partial H_z}{\partial \theta}\right] , \tag{2.19}$$

$$E_\theta = \frac{1}{k^2}\left[\frac{1}{r}\frac{\partial}{\partial z}\left(\frac{\partial E_z}{\partial \theta}\right) + j\omega\mu_m\frac{\partial H_z}{\partial r}\right] , \tag{2.20}$$

$$H_r = \frac{1}{k^2}\left[\frac{j\omega\epsilon_m}{r}\frac{\partial E_z}{\partial \theta} + \frac{\partial}{\partial z}\left(\frac{\partial H_z}{\partial r}\right)\right] , \tag{2.21}$$

$$H_\theta = \frac{1}{k^2}\left[-j\omega\epsilon_m\frac{\partial E_z}{\partial r} + \frac{1}{r}\frac{\partial}{\partial z}\left(\frac{\partial H_z}{\partial \theta}\right)\right] , \tag{2.22}$$

where μ_m = permeability of the medium in henry/meter,

ϵ_m = permittivity of the medium in farad/meter,

$k = \sqrt{\omega^2\mu_m\epsilon_m - \gamma^2}$ electrical radians/meter,

γ = axial propagation constant in electrical radians/meter.

The general forms of the transverse field components follow at once upon substituting Eqs. 2.17 and 2.18 into Eqs. 2.19-2.22. The relations become

$$E_r = \mathrm{Re}\left[\left\{\frac{j\gamma C_1}{k}\left(J'_{\beta_o}(kr)+C_2N'_{\beta_o}(kr)\right)\left(e^{j\gamma z}-C_3e^{-j\gamma z}\right)\right.\right.$$
$$\left.\left. - \frac{\omega\mu_m\beta_o D_1}{k^2r}\left(J_{\beta_o}(kr)+D_2N_{\beta_o}(kr)\right)\left(e^{j\gamma z}+D_3e^{-j\gamma z}\right)\right\}e^{j(\omega t-\beta_o\theta)}\right] , \tag{2.23}$$

$$E_\theta = \mathrm{Re}\left[\left\{\frac{\gamma\beta_o C_1}{k^2r}\left(J_{\beta_o}(kr)+C_2N_{\beta_o}(kr)\right)\left(e^{j\gamma z}-C_3e^{-j\gamma z}\right)\right.\right.$$
$$\left.\left. + \frac{j\omega\mu_m D_1}{k}\left(J'_{\beta_o}(kr)+D_2N'_{\beta_o}(kr)\right)\left(e^{j\gamma z}+D_3e^{-j\gamma z}\right)\right\}e^{j(\omega t-\beta_o\theta)}\right] , \tag{2.24}$$

$$H_r = \mathrm{Re}\left[\left\{ \frac{\omega\epsilon_m \beta_o C_1}{k^2 r} \left(J_{\beta_o}(kr) + C_2 N_{\beta_o}(kr) \right) \left(e^{j\gamma z} + C_3 e^{-j\gamma z} \right) \right.\right.$$

$$\left.\left. + j \frac{\gamma D_1}{k} \left(J'_{\beta_o}(kr) + D_2 N'_{\beta_o}(kr) \right) \left(e^{j\gamma z} - D_3 e^{-j\gamma z} \right) \right\} e^{j(\omega t - \beta_o \theta)} \right] , \tag{2.25}$$

$$H_\theta = \mathrm{Re}\left[\left\{ \frac{-j\omega\epsilon_m C_1}{k} \left(J'_{\beta_o}(kr) + C_2 N'_{\beta_o}(kr) \right) \left(e^{j\gamma z} + C_3 e^{-j\gamma z} \right) \right.\right.$$

$$\left.\left. + \frac{\gamma \beta_o D_1}{k^2 r} \left(J_{\beta_o}(kr) + D_2 N_{\beta_o}(kr) \right) \left(e^{j\gamma z} - D_3 e^{-j\gamma z} \right) \right\} e^{j(\omega t - \beta_o \theta)} \right] , \tag{2.26}$$

where the primes in the above equations indicate partial differentiation with respect to the argument kr. The foregoing results show that two possible field configurations may exist for waves propagating in cylindrical geometry. Those produced by a nonzero axial electric field ($E_z \neq 0$) are known as "E-waves", while those produced by a nonzero axial magnetic field ($H_z \neq 0$) are known as "H-waves". Although the most general field solutions consist of a superposition of the two wave types, as given by Eqs. 2.23-2.26, it will be more convenient to treat the E- and H-mode fields separately when evaluating the integration constants.

2.3.1 The E-Mode Fields. The mathematical analysis is facilitated by first deriving the field relations for the smooth, perfectly conducting, rectangular waveguide bent into a circle, and thereafter modifying the results to account for the presence of the slow-wave structure. Therefore, the boundary conditions appropriate to the E-mode fields are of the well-known Dirichlet form[5]

$$E_r = 0 \quad \text{at} \quad z = 0, L \ , \tag{2.27}$$

$$E_\theta = 0 \quad \text{at} \quad z = 0, L \ , \tag{2.28}$$

$$E_\theta = 0 \quad \text{at} \quad r = r_a, r_s \ , \tag{2.29}$$

and

$$E_z = 0 \quad \text{at} \quad r = r_a, r_s \ , \tag{2.30}$$

where L = height of the waveguide parallel to the z-axis in meters,

r_a = radius to the inside wall of the curved, rectangular waveguide in meters,

r_s = radius to the outside wall of the curved, rectangular waveguide in meters.

These constraints may be used in conjunction with Eqs. 2.23-2.26 to evaluate the integration constants. Thus, upon applying condition 2.30 to Eq. 2.17 the characteristic equation for the E-modes is found to be

$$\begin{vmatrix} J_{\beta_o}(kr_a) & N_{\beta_o}(kr_a) \\ J_{\beta_o}(kr_s) & N_{\beta_o}(kr_s) \end{vmatrix} = 0 \ , \tag{2.31}$$

which evidently results from the fact that

$$C_2 = - J_{\beta_o}(kr_a) \Big/ N_{\beta_o}(kr_a) \ ,$$

$$= - J_{\beta_o}(kr_s) \Big/ N_{\beta_o}(kr_s) \ . \tag{2.32}$$

The remaining boundary conditions may be used in conjunction with Eqs. 2.23-2.26, after setting D_1, D_2 and D_3 to zero, to obtain

$$E_r = \mathrm{Re}\left[A \left(\frac{-n\pi}{kL} \right) X'_{\beta_o}(kr) \sin\left(\frac{n\pi}{L} z \right) e^{j(\omega t - \beta_o \theta)} \right] \ , \tag{2.33}$$

$$E_\theta = \mathrm{Re}\left[A\left(\frac{jn\pi\beta_o}{k^2rL}\right)X_{\beta_o}(kr)\sin\left(\frac{n\pi}{L}z\right)e^{j(\omega t-\beta_o\theta)}\right] , \qquad (2.34)$$

$$E_z = \mathrm{Re}\left[AX_{\beta_o}(kr)\cos\left(\frac{n\pi}{L}z\right)e^{j(\omega t-\beta_o\theta)}\right] , \qquad (2.35)$$

$$H_r = \mathrm{Re}\left[A\left(\frac{\omega\epsilon_m\beta_o}{k^2r}\right)X_{\beta_o}(kr)\cos\left(\frac{n\pi}{L}z\right)e^{j(\omega t-\beta_o\theta)}\right] , \qquad (2.36)$$

$$H_\theta = \mathrm{Re}\left[A\left(\frac{-j\omega\epsilon_m}{k}\right)X'_{\beta_o}(kr)\cos\left(\frac{n\pi}{L}z\right)e^{j(\omega t-\beta_o\theta)}\right] , \qquad (2.37)$$

$$H_z = 0 , \qquad (2.38)$$

where $A = 2C_1/N_{\beta_o}(kr_s)$,

$k = \sqrt{\omega^2\mu_m\epsilon_m-(n\pi/L)^2}$ electrical radians/meter,

n = integer,

$$X_{\beta_o}(kr) = J_{\beta_o}(kr)N_{\beta_o}(kr_s)-N_{\beta_o}(kr)J_{\beta_o}(kr_s) ,$$

$$X'_{\beta_o}(kr) = \frac{dX_{\beta_o}(kr)^*}{d(kr)} .$$

2.3.2 The H-Mode Fields. The boundary conditions applicable to the H-mode fields are of the Neumann form[5]

$$\frac{\partial H_r}{\partial z} = 0 \quad \text{at} \quad z = 0,L , \qquad (2.39)$$

---

* The transformation from partial to total differentiation is made possible by the fact that only $X_{\beta_o}(kr)$ depends on r.

$$\frac{\partial H_\theta}{\partial z} = 0 \qquad \text{at} \qquad z = 0, L \quad , \tag{2.40}$$

$$\frac{\partial H_\theta}{\partial (kr)} = 0 \qquad \text{at} \qquad r = r_a, r_s \quad , \tag{2.41}$$

and

$$\frac{\partial H_z}{\partial (kr)} = 0 \qquad \text{at} \qquad r = r_a, r_s \quad . \tag{2.42}$$

The characteristic equation for the H-modes can be obtained by substituting Eq. 2.18 into 2.42, leading to the result

$$\begin{vmatrix} J'_{\beta_o}(kr_a) & N'_{\beta_o}(kr_a) \\ J'_{\beta_o}(kr_s) & N'_{\beta_o}(kr_s) \end{vmatrix} = 0 \quad , \tag{2.43}$$

in consequence of the fact that

$$D_2 = -J'_{\beta_o}(kr_a) \Big/ N'_{\beta_o}(kr_a) \quad ,$$

$$= -J'_{\beta_o}(kr_s) \Big/ N'_{\beta_o}(kr_s) \quad . \tag{2.44}$$

The boundary conditions given by Eqs. 2.39-2.41 may be used in conjunction with Eqs. 2.23-2.26, after setting C_1, C_2 and C_3 to zero, to obtain

$$E_r = \mathrm{Re}\left[B \left(\frac{-j\omega_m \beta_o}{k^2 r} \right) Z_{\beta_o}(kr) \sin\left(\frac{n\pi}{L} z \right) e^{j(\omega t - \beta_o \theta)} \right] \quad , \tag{2.45}$$

$$E_\theta = \mathrm{Re}\left[B \left(\frac{-\omega \mu_m}{\quad} \right) Z'_{\beta_o}(kr) \sin\left(\frac{n\pi}{L} z \right) e^{j(\omega t - \beta_o \theta)} \right] \quad , \tag{2.46}$$

$$E_z = 0 \quad , \tag{2.47}$$

$$H_r = \mathrm{Re}\left[B \left(\frac{jn\pi}{kL}\right) Z'_{\beta_o}(kr) \cos\left(\frac{n\pi}{L} z\right) e^{j(\omega t - \beta_o \theta)} \right] \quad , \tag{2.48}$$

$$H_\theta = \mathrm{Re}\left[B \left(\frac{n\pi\beta_o}{k^2 rL}\right) Z_{\beta_o}(kr) \cos\left(\frac{n\pi}{L} z\right) e^{j(\omega t - \beta_o \theta)} \right] \quad , \tag{2.49}$$

$$H_z = \mathrm{Re}\left[jBZ_{\beta_o}(kr) \sin\left(\frac{n\pi}{L} z\right) e^{j(\omega t - \beta_o \theta)} \right] \quad , \tag{2.50}$$

where $B = 2D_1 / N'_{\beta_o}(kr_s)$,

$$Z_{\beta_o}(kr) = J_{\beta_o}(kr) N'_{\beta_o}(kr_s) - N_{\beta_o}(kr) J'_{\beta_o}(kr_s) \quad ,$$

$$Z'_{\beta_o}(kr) = \frac{dZ_{\beta_o}(kr)}{d(kr)} \quad .$$

2.3.3 The Fields in the Slow-Wave Region. The function of the slow-wave structure of the E-type device is to sufficiently reduce the spatial angular velocity of the r-f wave so that its linear tangential velocity at a given radius is nearly equal to that of the electron beam. The use of azimuthally periodic slow-wave circuits along the inner vertical wall of the curved rectangular waveguide, to control the wave's spatial angular velocity, requires the boundary matching procedure (involved in the determination of the space harmonics) to be accomplished subject to the spatial discontinuity.

The mathematical process of evaluating the space harmonics becomes extremely tedious for any but the simplest systems. In view of this

complexity, it is customary to carry out solutions for only a few such harmonic terms. Moreover, each time the physical structure is changed the evaluation must be repeated, so that practical considerations tend to restrict the analysis to a small number of potentially important configurations.

In spite of this arraignment, analytical procedures can be used to advantage for investigating certain general properties of azimuthally periodic slow-wave circuits. Thus, the angular description of all fields may be expressed in terms of a countably infinite set of space-periodic components for both re-entrant and nonre-entrant structures. In the case of a re-entrant circuit, or a nonre-entrant circuit whose fields would be undisturbed by making it re-entrant, the azimuthal variation of all fields involves an infinite set of integral space harmonics, since these fields must repeat their initial values after a spatial excursion of 2π radians. If the fields of the nonre-entrant structure would be disturbed by making it re-entrant, then the space harmonics are associated with a set of either rational fractional order, or general nonintegral order, components. In the ensuing work, discrete summations involving β_o therefore apply to both re-entrant and nonre-entrant circuits.

The actual slow-wave circuit will be replaced by the simplified model shown in Fig. 2.2. The structure consists of smooth, perfectly conducting, circular waveguide walls located at radii r_a and r_s, and a dielectric annular ring whose inside surface coincides with radius r_a. The dielectric is assumed to be lossless and its permeability is taken to be that of free space. Hence, the phase velocity of electromagnetic waves propagating in this medium is

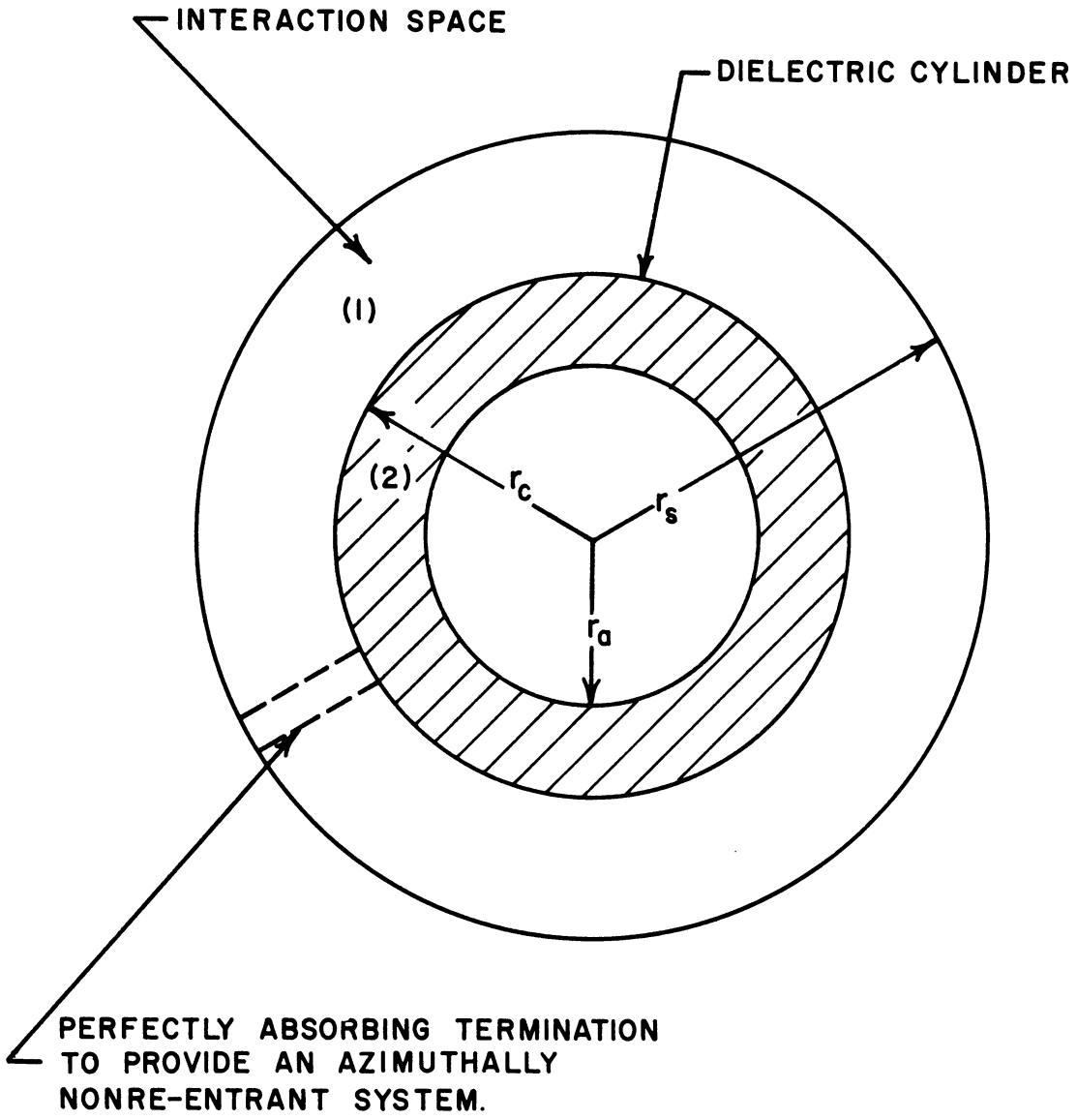

FIG. 2.2 A SIMPLIFIED MODEL OF THE COAXIAL-CYLINDRICAL SLOW-WAVE SYSTEM.

$$v_2 = \frac{1}{\sqrt{\mu_o \epsilon_2}} = \frac{c}{\sqrt{\epsilon'}} \quad , \tag{2.51}$$

where μ_o = permeability of free space in henry/meter,

$\epsilon' = \epsilon_2/\epsilon_o$ = dielectric constant of the medium,

ϵ_o = permittivity of free space in farad/meter,

ϵ_2 = permittivity of the dielectric medium in farad/meter,

$c = (\mu_o \epsilon_o)^{-1/2}$ = free-space velocity of light in meter/second.

Since the dielectric is assumed to be homogeneous and isotropic, the wave phase velocity is given by Eq. 2.51 regardless of the direction of propagation. The use of the simplified model therefore implies the existence of both axial and azimuthal slowing, although only the latter is of importance in E-type devices. While biperiodic transmission lines produce axial as well as azimuthal slowing, other configurations, such as the "vane structure" and the related class of "filter-type" circuits[7], exhibit only azimuthal slowing.

A limitation inherent in the use of the dielectric cylinder as an approximation to the actual slow-wave system is related to the fact that the dielectric, as well as each vertical waveguide wall, is perfectly smooth. Therefore, analyses based on this model account for only one of the infinite number of azimuthal space harmonics present in an actual r-f structure. The constraint is not serious as long as the conditions are such that the electron beam interacts with only one space-harmonic component of the r-f field. This mode of operation may be achieved provided the frequency of the r-f wave is sufficiently removed from the cutoff frequency of the slow-wave structure. However, certain occasions

arise when additional assumptions, made to simplify the analysis, actually imply the occurrence of operation near cutoff*. Under these circumstances it is necessary to exercise care in interpreting the results based on the use of a dielectric slow-wave structure.

The modifications of the r-f fields, that result from the introduction of the slow-wave circuit along the center of the coaxial-cylindrical system, may now be examined. It is typically assumed that the dielectric constant is very much greater than unity, and that the radial thickness $(r_c - r_a)$ is very small. In the region of the dielectric

$$k_{2n}^2 = \left[\omega^2 \mu_o \epsilon_2 - \left(\frac{n\pi}{L}\right)^2\right] > 0 \quad , \tag{2.52}$$

where n is an integer bounded between the limits:

$$-\left(\frac{\omega L}{\pi}\right)\sqrt{\mu_o \epsilon_2} < n < \left(\frac{\omega L}{\pi}\right)\sqrt{\mu_o \epsilon_2} \quad .$$

Since the r-f fields actually travel along the circuit, the above inequality must hold because the condition $k_{2n}^2 < 0$ implies that propagation is cutoff in the slow-wave structure and, consequently, in the entire system. The argument $k_{2n} r$ is therefore a real quantity so that the radial variation of all fields <u>within</u> the dielectric must possess the real Bessel function behavior. The E- and H-modes, for any one of the space harmonics, are then given by Eqs. 2.33-2.38, and Eqs. 2.45-2.50, respectively. When all space harmonics are included, the total

---

* The small-argument approximations to the radial and azimuthal electric field intensities are typically an assumption of this sort. This question is considered further in Appendix C.

fields obtained from the superposition of the E- and H-mode components assume the form

$$E_{z2} = \mathrm{Re} \sum_{n,\beta_o} e^{j\omega t} \cos\left(\frac{n\pi}{L} z\right) A_{n\beta_o} X_{\beta_o}(k_{2n} r) e^{-j\beta_o \theta} \quad , \qquad (2.53)$$

$$H_{z2} = \mathrm{Re} \sum_{n,\beta_o} e^{j\omega t} \sin\left(\frac{n\pi}{L} z\right) jB_{n\beta_o} Z_{\beta_o}(k_{2n} r) e^{-j\beta_o \theta} \quad , \qquad (2.54)$$

$$E_{r2} = \mathrm{Re} \sum_{n,\beta_o} e^{j\omega t} \sin\left(\frac{n\pi}{L} z\right) \left\{ A_{n\beta_o} \left(\frac{-n\pi}{k_{2n} L}\right) X'_{\beta_o}(k_{2n} r) + B_{n\beta_o} \left(\frac{-j\omega\mu_o \beta_o}{k_{2n}^2 r}\right) Z_{\beta_o}(k_{2n} r) \right\} e^{-j\beta_o \theta} \quad , \qquad (2.55)$$

$$E_{\theta 2} = \mathrm{Re} \sum_{n,\beta_o} e^{j\omega t} \sin\left(\frac{n\pi}{L} z\right) \left\{ A_{n\beta_o} \left(\frac{jn\pi\beta_o}{k_{2n}^2 rL}\right) X_{\beta_o}(k_{2n} r) + B_{n\beta_o} \left(\frac{-\omega\mu_o}{k_{2n}}\right) Z'_{\beta_o}(k_{2n} r) \right\} e^{-j\beta_o \theta} \quad , \qquad (2.56)$$

$$H_{r2} = \mathrm{Re} \sum_{n,\beta_o} e^{j\omega t} \cos\left(\frac{n\pi}{L} z\right) \left\{ A_{n\beta_o} \left(\frac{\omega\epsilon_2 \beta_o}{k_{2n}^2 r}\right) X_{\beta_o}(k_{2n} r) + B_{n\beta_o} \left(\frac{jn\pi}{k_{2n} L}\right) Z'_{\beta_o}(k_{2n} r) \right\} e^{-j\beta_o \theta} \quad , \qquad (2.57)$$

$$H_{\theta 2} = \mathrm{Re} \sum_{n,\beta_o} e^{j\omega t} \cos\left(\frac{n\pi}{L} z\right) \left\{ A_{n\beta_o} \left(\frac{-j\omega\epsilon_2}{k_{2n}}\right) X'_{\beta_o}(k_{2n} r) + B_{n\beta_o} \left(\frac{n\pi\beta_o}{k_{2n}^2 rL}\right) Z_{\beta_o}(k_{2n} r) \right\} e^{-j\beta_o \theta} \quad , \qquad (2.58)$$

where $A_{n\beta_o}$ = a constant depending on β_o and n, which is a measure of the space-harmonic amplitude of the associated E-mode wave,

$B_{n\beta_o}$ = a constant depending on β_o and n, which is a measure of the space-harmonic amplitude of the associated H-mode wave,

$$X_{\beta_o}(k_{2n} r) = J_{\beta_o}(k_{2n} r)\, N_{\beta_o}(k_{2n} r_a) - N_{\beta_o}(k_{2n} r)\, J_{\beta_o}(k_{2n} r_a) \quad ,$$

$$Z_{\beta_o}(k_{2n} r) = J_{\beta_o}(k_{2n} r)\, N'_{\beta_o}(k_{2n} r_a) - N_{\beta_o}(k_{2n} r)\, J'_{\beta_o}(k_{2n} r_a) \quad ,$$

2.3.4 The Fields in the Interaction Space. Under typical circumstances the slow circuit waves penetrate the interaction region due to fringing of the r-f fields. In the absence of the circuit such waves could not exist in the adjoining space, as they would then be cutoff. Therefore, the condition which applies to the interaction space must be

$$\left(\omega^2 \mu_o \epsilon_o - \left(\frac{n\pi}{L}\right)^2\right) < 0 \quad .$$

It is convenient to define for region 1 of Fig. 2.2

$$k_{1n} = \sqrt{\left(\frac{n\pi}{L}\right)^2 - \omega^2 \mu_o \epsilon_o} \quad , \qquad (2.59)$$

because the radicand will always be positive. The integer n now lies in the open intervals: $-\infty < -n < -\left(\frac{\omega L}{\pi}\right)\sqrt{\mu_o \epsilon_o}$, $\left(\frac{\omega L}{\pi}\right)\sqrt{\mu_o \epsilon_o} < n < \infty$.

Upon retracing the steps in deriving the component field intensities, it is found that the only change resulting from the definition of k_{1n} according to Eq. 2.59 arises in a modification of Eq. 2.9. In the present case, the differential equation which specifies the radial dependence is

$$R'' + \frac{R'}{r} - \left(k_{1n}^2 + \frac{\beta_o^2}{r^2}\right) R = 0 \quad , \tag{2.60}$$

whose solution is known to be

$$R = F_1 I_{\beta_o}(k_{1n} r) + F_2 K_{\beta_o}(k_{1n} r) \quad , \tag{2.61}$$

where F_1, F_2 = arbitrary constants,

$I_{\beta_o}(k_{1n} r)$ = hyperbolic Bessel function of the first kind with argument $k_{1n} r$ and order β_o,

$K_{\beta_o}(k_{1n} r)$ = hyperbolic Bessel function of the second kind with argument $k_{1n} r$ and order β_o.

Inasmuch as the axial and azimuthal functional dependencies remain unchanged, the field components in the interaction space take the form

$$E_{z1} = \mathrm{Re} \sum_{n,\beta_o} e^{j\omega t} \cos\left(\frac{n\pi}{L} z\right) F_{n\beta_o} V_{\beta_o}(k_{1n} r) e^{-j\beta_o \theta} \quad , \tag{2.62}$$

$$H_{z1} = \mathrm{Re} \sum_{n,\beta_o} e^{j\omega t} \sin\left(\frac{n\pi}{L} z\right) jG_{n\beta_o} Y_{\beta_o}(k_{1n} r) e^{-j\beta_o \theta} \quad , \tag{2.63}$$

$$E_{r1} = \mathrm{Re} \sum_{n,\beta_o} e^{j\omega t} \sin\left(\frac{n\pi}{L} z\right) \left\{ F_{n\beta_o} \left(\frac{-n\pi}{k_{1n} L}\right) V'_{\beta_o}(k_{1n} r) + G_{n\beta_o} \left(\frac{-j\omega\mu_o \beta_o}{k_{1n}^2 r}\right) Y_{\beta_o}(k_{1n} r) \right\} e^{-j\beta_o \theta} \quad , \quad (2.64)$$

$$E_{\theta 1} = \mathrm{Re} \sum_{n,\beta_o} e^{j\omega t} \sin\left(\frac{n\pi}{L} z\right) \left\{ F_{n\beta_o} \left(\frac{jn\pi\beta_o}{k_{1n}^2 rL}\right) V_{\beta_o}(k_{1n} r) + G_{n\beta_o} \left(\frac{-\omega\mu_o}{k_{1n}}\right) Y'_{\beta_o}(k_{1n} r) \right\} e^{-j\beta_o \theta} \quad , \quad (2.65)$$

$$H_{r1} = \mathrm{Re} \sum_{n,\beta_o} e^{j\omega t} \cos\left(\frac{n\pi}{L} z\right) \left\{ F_{n\beta_o} \left(\frac{\omega\epsilon_o \beta_o}{k_{1n}^2 r}\right) V_{\beta_o}(k_{1n} r) + G_{n\beta_o} \left(\frac{jn\pi}{k_{1n} L}\right) Y'_{\beta_o}(k_{1n} r) \right\} e^{-j\beta_o \theta} \quad , \quad (2.66)$$

$$H_{\theta 1} = \mathrm{Re} \sum_{n,\beta_o} e^{j\omega t} \cos\left(\frac{n\pi}{L} z\right) \left\{ F_{n\beta_o} \left(\frac{-j\omega\epsilon_o}{k_{1n}}\right) V'_{\beta_o}(k_{1n} r) + G_{n\beta_o} \left(\frac{n\pi\beta_o}{k_{1n}^2 rL}\right) Y_{\beta_o}(k_{1n} r) \right\} e^{-j\beta_o \theta} \quad , \quad (2.67)$$

where $F_{n\beta_o}$ = a constant depending on β_o and n, which is a measure of the space-harmonic amplitude of the associated E-mode wave,

$G_{n\beta_o}$ = a constant depending on β_o and n, which is a measure of the space-harmonic amplitude of the associated H-mode wave,

$$V_{\beta_o}(k_{1n}r) = I_{\beta_o}(k_{1n}r)\, K_{\beta_o}(k_{1n}r_s) - K_{\beta_o}(k_{1n}r)\, I_{\beta_o}(k_{1n}r_s) \quad ,$$

$$Y_{\beta_o}(k_{1n}r) = I_{\beta_o}(k_{1n}r)\, K'_{\beta_o}(k_{1n}r_s) - K_{\beta_o}(k_{1n}r)\, I'_{\beta_o}(k_{1n}r_s) \quad .$$

2.3.5 Derivation of the Dispersion Relation. The characteristic equation of the smooth waveguide is given by Eq. 2.31 for the E-mode fields, and Eq. 2.43 for the H-mode fields. The usual practice, employed in a study of the higher modes of coaxial-cylindrical systems, is to seek solutions of these characteristic equations by obtaining values of the argument kr for particular choices of β_o. Now since

$$k^2 = (\omega^2 \mu_m \epsilon_m - \gamma^2) \quad ,$$

this is equivalent to finding solutions of γ corresponding to specified values of ω and β_o. Inasmuch as

$$\gamma = \left(\frac{n\pi}{L}\right) \quad ,$$

the analysis leads to the determination of the "waveguide ratio" n/L as a function of the circular propagation constant β_o.

In the design of coaxial-cylindrical systems, the allowed values of β_o are sought for specific choices of the argument kr. This amounts to selecting the "waveguide ratio" n/L in order to obtain a desired set of values of β_o over a prescribed frequency range. It is this latter class of problems that is of importance in selecting a particular configuration of waveguide bend, or E-type device geometry, to meet certain desired operating requirements.

For either of these problems, however, it is apparent that the functional dependence between ω and β_o can be examined for a given

value of the waveguide ratio. A graphical representation of this expression is recognized to be the familiar ω-β diagram of r-f structures[1]. The principal distinction between the results obtained for the smooth waveguide and the widely used periodic structures lies in the fact that the former contains only a single space-periodic component while the latter contains an infinite number. Since the circular propagation constant β_o is related to the linear tangential velocity of the wave at a given radius according to Eq. 2.14, it is also possible to make use of the ω-β diagram for obtaining the dependence of the phase velocity on frequency. A curve of this type is known as a "dispersion relation".

The amplitudes of the various space-harmonic components can be determined explicitly only when the periodic boundary conditions peculiar to a given slow-wave structure are imposed. Certain harmonics may be accentuated while the remaining ones may be suppressed, so that a knowledge of the geometry of a particular r-f circuit must be available before the constants $A_{n\beta_o}$ and $B_{n\beta_o}$ in Eqs. 2.53-2.58, as well as $F_{n\beta_o}$ and $G_{n\beta_o}$ in Eqs. 2.62-2.67, can be specified numerically. In the present case, where the actual structure is replaced by the dielectric cylinder, it is possible to obtain only enough information for plotting the ω-β diagram of one space-periodic component and the associated dispersion relation.

The derivation is carried out under the most general assumption that both the E- and H-mode fields are simultaneously present in the system. The special results applicable to the situation in which either of these modes does not exist can be developed in an analogous manner by setting the appropriate constants to zero.

The boundary conditions used in obtaining the dispersion equation are those for which the radial components of r-f electric and magnetic flux density, as well as the axial and azimuthal components of r-f electric and magnetic field intensity, must be continuous at the dielectric boundary. Stated mathematically, these conditions are:

$$\begin{aligned} E_{r1} &= \epsilon' E_{r2} \quad , \\ E_{\theta 1} &= E_{\theta 2} \quad , \\ E_{z1} &= E_{z2} \quad , \\ H_{z1} &= H_{z2} \quad , \\ \mu_o H_{r1} &= \mu_o H_{r2} \quad , \\ H_{\theta 1} &= H_{\theta 2} \quad . \end{aligned} \qquad (r = r_c) \tag{2.68}$$

Only the first four conditions are necessary in carrying out the desired matching procedure, since there are a total of four unknown constants. These constraints may be applied to Eqs. 2.53-2.58 and Eqs. 2.62-2.67 to obtain

$$\left(\frac{\beta_o}{k_{1n} r_c}\right)^2 \left[\left(\frac{k_{1n}}{k_{2n}}\right)^2 - 1\right]\left[1 - \epsilon'\left(\frac{k_{1n}}{k_{2n}}\right)^2\right]$$

$$= \left[\frac{V'_{\beta_o}\left(k_{1n} r_c\right) Y'_{\beta_o}\left(k_{1n} r_c\right)}{V_{\beta_o}\left(k_{1n} r_c\right) Y_{\beta_o}\left(k_{1n} r_c\right)}\right]\left[1 - \frac{k_{1n}}{k_{2n}}\left(\frac{Y_{\beta_o}\left(k_{1n} r_c\right) Z'_{\beta_o}\left(k_{2n} r_c\right)}{Y'_{\beta_o}\left(k_{1n} r_c\right) Z_{\beta_o}\left(k_{2n} r_c\right)}\right)\right] \cdot$$

$$\cdot \left[\epsilon'\left(\frac{k_{1n}}{k_{2n}}\right)\left(\frac{V_{\beta_o}\left(k_{1n} r_c\right) X'_{\beta_o}\left(k_{2n} r_c\right)}{V'_{\beta_o}\left(k_{1n} r_c\right) X_{\beta_o}\left(k_{2n} r_c\right)}\right) - 1\right] . \tag{2.69}$$

The solution of this equation involves the determination of the allowed values of β_o corresponding to the arguments $k_{1n}r_c$ and $k_{2n}r_c$. For a specific structure the waveguide ratio n/L will be known so that the mathematical process amounts to obtaining the relation between β_o and ω.

2.4 Interpretation of the Results

A study of Eqs. 2.53-2.58 and Eqs. 2.62-2.67 shows that the axial variation of all quantities is specified by eigenfunctions of the form

$$\sin\left(\frac{n\pi}{L}z\right) ,$$

or

$$\cos\left(\frac{n\pi}{L}z\right) ,$$

so that only certain "allowed values" of the above functions can exist. These discrete eigenvalues, corresponding to integral values of n, result from the constraints imposed upon the fields at the perfectly conducting boundaries of the coaxial-cylindrical transmission system.

This sine and cosine description of all fields indicates that a standing wave rather than a traveling wave exists along the z-coordinate. The resulting variation may be thought of as being produced by the superposition of incident and reflected r-f fields advancing in opposing axial directions. That this situation will always prevail in a coaxial-cylindrical system, whose upper and lower axial extremities are terminated at a finite distance by perfectly conducting metal surfaces, was first recognized by Kalähne[13] in two very comprehensive papers. If the height L is increased more cycles of the standing wave pattern are established and the "cutoff" frequency is decreased. In the limit, as L increases indefinitely, the number of cycles increases until the conditions become those of two incident waves traveling in opposite axial directions.

A study of the bounds on n, specified below Eq. 2.52, reveals quantitatively how its range increases with L. This may readily be visualized with the aid of Fig. 2.3, which shows that as L increases, the interval that bounds the range of n for axial propagation in the slow-wave region increases proportionally. The use of structures that exhibit large values of axial slowing, corresponding to large values of ϵ_2, produce a similar effect upon the range of n. The cutoff condition of axial propagation is thus inferred from the requirement that

$$k_{2n}^2 = 0 \quad ,$$

which leads to

$$n \equiv \pm \frac{\omega L}{\pi} \sqrt{\mu_o \epsilon_2} \quad .$$

Integer values of n larger than this magnitude result in imaginary values of k_{2n}, so that the range of n which allows axial propagation in the slow-wave region must lie in the unshaded region of Fig. 2.3. Although the effect of a change of frequency has not been discussed, it obviously exerts the same control over the range of n as a corresponding change in either L or ϵ_2. The important observation to be made is that the range of integer n values is always finite and bounded for any practical structure.

The constraints imposed on n in the interaction region are quite the reverse of those described above. In this case, the ranges of allowed n values must be the ones given in connection with Eq. 2.59, and the cutoff condition

$$k_{1n}^2 = 0 \quad ,$$

yields

$$n \equiv \pm \frac{\omega L}{\pi} \sqrt{\mu_o \epsilon_o} \quad .$$

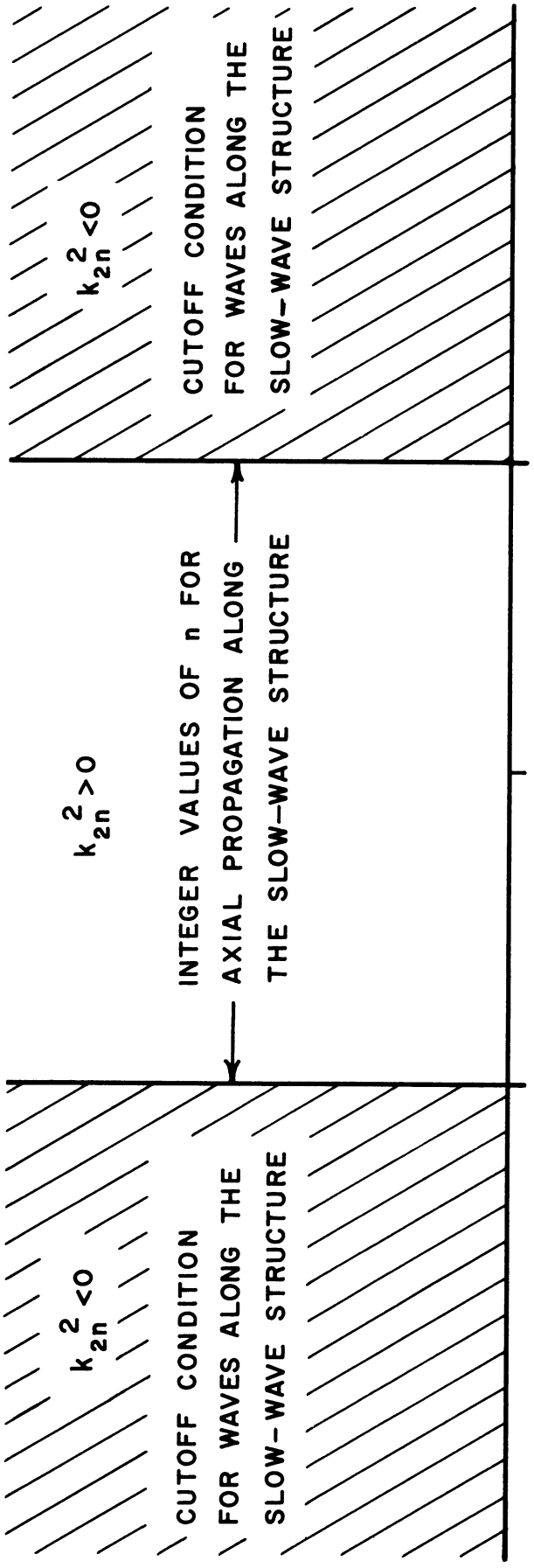

FIG. 2.3 GRAPHICAL REPRESENTATION OF THE RANGE OF n IN THE SLOW-WAVE REGION.

An examination of Fig. 2.4 reveals that an infinite set of positive and negative integer n values, for the cutoff modes in the interaction space, result from the waves present on the r-f circuit. Thus, if the condition is imposed that the circuit fields do not permeate the interaction space in the absence of the slow-wave structure, it follows that the guide height L restricts the cutoff frequency of this space above its operating frequency. The axial eigenvalues for the cutoff modes in the interaction space are then contained in the unshaded regions of the diagram. Under these circumstances a finite and bounded set of wave eigenvalues in the slow-wave region generate a pair-of-sets of infinite eigenvalues in the adjoining free space.

Inasmuch as the propagation conditions for the coaxial-cylindrical, air filled waveguide are fixed by the guide height at a given frequency, it is apparent that the foregoing situation can easily be altered by changing L. If L is sufficiently increased to permit E- or H-mode propagation in the interaction space, the r-f structure then acts as a radiating source which excites strong fields in the adjoining region. The wave axial eigenvalues now lie in the shaded area of Fig. 2.4, and the unshaded regions become the cutoff ranges of n. The diagram appropriate to the interaction region therefore resembles Fig. 2.3, except for a somewhat smaller interval of allowed n values because $\epsilon_0 \ll \epsilon_2$. In this case a finite and bounded set of axial eigenvalues associated with the slow-wave structure generates a set of <u>fewer</u> axial eigenvalues in the interaction region*, and the radial variation of all fields possesses the real Bessel function behavior.

---

* The cutoff frequency of the slow-wave structure will also be reduced by making L larger, thereby causing the unshaded portion of Fig. 2.3 to expand as a result of an increase in the number of permitted axial eigenvalues on the circuit.

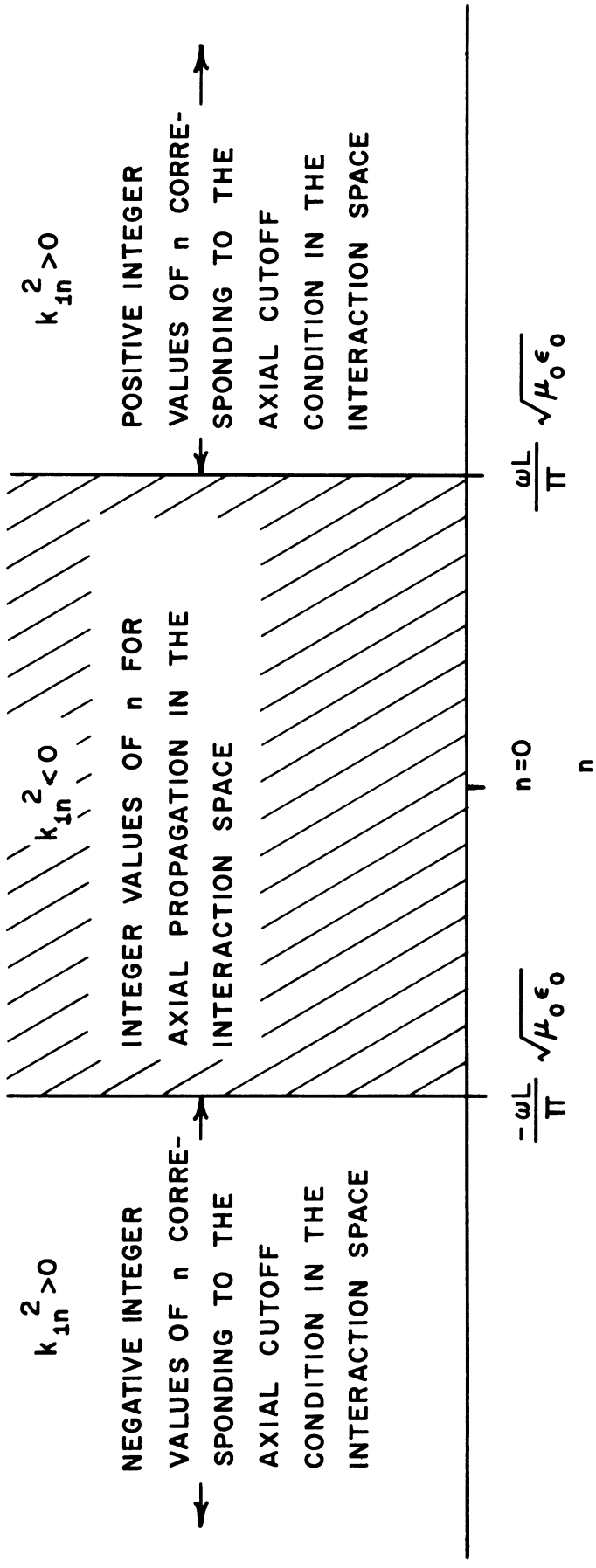

FIG. 2.4 GRAPHICAL REPRESENTATION OF THE RANGE OF n IN THE INTERACTION SPACE.

In view of the fact that the vane-type structure may be considered as a special kind of biperiodic transmission system having only one axial period, the foregoing analysis can easily be extended to this situation. Since no axial slowing is experienced by waves traveling along the vanes, it is evident that the cutoff condition for the vane structure is the same as for the coaxial-cylindrical transmission system. The individual vanes then act as radiators which establish strong fields in the interaction space. The allowed axial eigenvalues of the fields in the interaction space are identical to those in the (azimuthally) slow-wave region, so that the allowed n values for both regions lie in the shaded area of Fig. 2.4. The act of lowering the guide height L to produce cutoff in the interaction region will likewise produce cutoff in the vane structure, and therefore in the entire system. These considerations lead to the conclusion that a finite and bounded set of axial eigenvalues on the r-f structure produces the same set of axial eigenvalues in the interaction region. The radial variation of all fields must again exhibit the real Bessel function behavior.

There is one situation in which propagating fields in the vane structure excite cutoff modes in the interaction region. This condition arises when the guide height is abruptly reduced throughout the interaction space, thereby preventing the generation of the E- or H-mode propagating waves in that region. Under these circumstances the only waves present in the interaction space are the fringing circuit fields, and a finite and bounded set of axial eigenvalues in the circuit region produces an infinite set of positive and negative integer values of n in the adjoining space. The radial behavior of the fields in the interaction region now possesses the hyperbolic Bessel function behavior.

The significant point to be drawn from this discussion is that a finite and bounded set of axial eigenvalues always exists in the slow-wave region, since propagating waves must be present on the circuit, while the number of axial eigenvalues in the interaction space is determined by the relation of the operating frequency to the cutoff frequency of the interaction space. If the height of the guide is such as to suppress propagation of the E- or H-mode waves, only the cutoff modes can exist with their associated infinite sets of positive and negative integer n values and their accompanying hyperbolic Bessel function radial behavior. However, if the guide height is sufficient to permit operation above cutoff, the number of axial eigenvalues in the interaction space must be equal to or less than those in the slow-wave region, and the radial behavior of all fields is of the real Bessel function type.

These facts may be used to provide further insight concerning the derivation of the dispersion relation presented in Section 2.3.5. The investigation employed a dielectric slow-wave structure possessing large axial slowing, since ϵ_2 was assumed to be much greater than ϵ_o. It follows that sets of permissible axial eigenvalues for both the interaction and slow-wave regions lie in the bounded intervals

$$-\frac{\omega L}{\pi}\sqrt{\mu_o \epsilon_2} < -n < -\frac{\omega L}{\pi}\sqrt{\mu_o \epsilon_o} \quad ,$$

$$\frac{\omega L}{\pi}\sqrt{\mu_o \epsilon_o} < n < \frac{\omega L}{\pi}\sqrt{\mu_o \epsilon_2} \quad ,$$

as shown in Fig. 2.5. The analysis thus involves the unstated assumption that only one axial eigenvalue and one value of β_o, admissable to

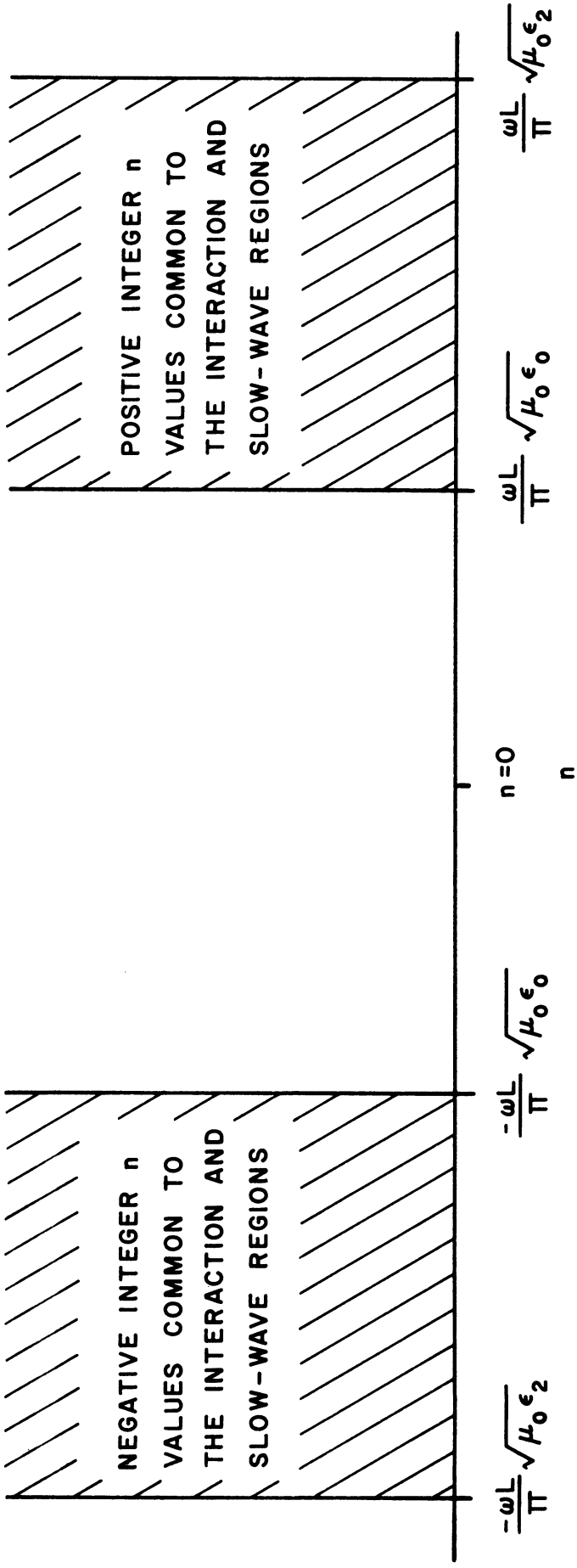

FIG. 2.5 GRAPHICAL REPRESENTATION OF THE RANGE OF n VALUES COMMON TO THE INTERACTION AND SLOW-WAVE REGIONS.

each of these regions, is of importance. This is the step that replaces summation over β_o and n by single expressions. Inspection of this diagram shows that as the axial slowing factor is decreased, i.e., as ϵ_2 approaches ϵ_o, the interval bounding common n values approaches zero. Thus, axially <u>fast</u> propagating circuit fields either produce similar waves in the interaction space having identical axial eigenvalues, or the cutoff modes in the adjoining space possess no integral n values common to the slow-wave region.

The control that the slow-wave structure exerts over the axial velocity of the waves on the circuit leads to further ramifications of the properties of coaxial-cylindrical systems. This may be appreciated by recalling certain characteristics of the cylindrical functions. It is well-known that the Hankel functions are related to the Bessel functions by means of the equations[5]

$$H^{(1)}_{\beta_o}(kr) = J_{\beta_o}(kr) + j\, N_{\beta_o}(kr) \quad , \tag{2.70}$$

$$H^{(2)}_{\beta_o}(kr) = J_{\beta_o}(kr) - j\, N_{\beta_o}(kr) \quad , \tag{2.71}$$

where $H^{(1)}_{\beta_o}(kr)$ = Hankel function of the first kind with argument kr and order β_o,

$H^{(2)}_{\beta_o}(kr)$ = Hankel function of the second kind with argument kr and order β_o.

In view of the linearity of these expressions it is evident that Eqs. 2.53-2.58, which describe the fields in the slow-wave region, might have alternatively been written in terms of the Hankel functions. Inasmuch

as the Bessel function of the first kind $J_{\beta_o}(kr)$ is the cylindrical analogue of the trigonometric cosine, while the Bessel function of the second kind $N_{\beta_o}(kr)$ is the cylindrical analogue of the trigonometric sine, then the Hankel function of the first kind is the cylindrical analogue of the imaginary exponential

$$\epsilon^{jkr} ,$$

while the Hankel function of the second kind is the cylindrical analogue of the imaginary exponential

$$\epsilon^{-jkr} .$$

This correspondence suggests that Eq. 2.70 describes a wave traveling radially inward, while Eq. 2.71 describes a wave traveling radially outward.

The fields in the interaction region, stipulated by Eqs. 2.62-2.67, could likewise have been written in terms of the Hankel functions because

$$I_{\beta_o}(kr) = \frac{(j)^{-\beta_o}}{2}\left[H^{(1)}_{\beta_o}(jkr) + H^{(2)}_{\beta_o}(jkr)\right] , \qquad (2.72)$$

$$K_{\beta_o}(kr) = \frac{\pi}{2}(j)^{\beta_o+1} H^{(1)}_{\beta_o}(jkr) . \qquad (2.73)$$

An examination of these relations suggests that the hyperbolic Bessel function of the first kind $I_{\beta_o}(kr)$ is the circular analogue of the exponential pair

$$\epsilon^{-kr} + \epsilon^{kr} ,$$

and the hyperbolic Bessel function of the second kind $K_{\beta_o}(kr)$ is the circular analogue of

$$\epsilon^{-kr} \quad .$$

Therefore, the function $I_{\beta_o}(kr)$ is the circular analogue of

$$\cosh(kr) \quad ,$$

while the function $K_{\beta_o}(kr)$ is the circular analogue of

$$\cosh(kr) - \sinh(kr) \quad .$$

Accordingly, the hyperbolic Bessel functions may be considered as the circular analogue of "damping functions" whose attenuation increases with radius.

A consideration of these factors leads to the assertion that radially propagating waves accompany axially propagating waves, and that radially attenuating functions accompany axially cutoff modes. While the fields on the slow-wave structure must always be associated with radially and axially propagating waves, the fields in the interaction region may be associated either with radially and axially propagating or attenuating waves, depending upon the relation of the operating frequency to the cutoff frequency of the interaction space.

In contrast to this "permitted set" of axial values, all field components possess an azimuthal variation of the form

$$\epsilon^{-j\beta_o\theta} \quad ,$$

where β_o is the circular propagation constant. Since broadband operation requires the maintenance of synchronism between the spatial angular velocities of the electron beam and r-f wave, then β_o should undergo

changes equal in magnitude to those of ω (see Eq. 2.13). It is therefore necessary to use either an azimuthally nonre-entrant structure having at least one space harmonic whose circular propagation constant varies in this manner, or a re-entrant structure whose space-harmonic amplitudes are distributed over the spectrum such that one component interacts with the beam at every frequency within the band. The helitron employs a structure of the latter form, although the frequency range of the forward-wave amplifier version of this device is known to be quite limited[29]. Somewhat greater bandwidth is attainable from a helitron backward-wave oscillator because the beam velocity can always be adjusted to achieve synchronism with one space-harmonic component throughout the entire band.

An interesting physical interpretation may be applied to the azimuthal component of wave propagation in coaxial-cylindrical systems. As far as azimuthal variations are concerned, the waves may be regarded as propagating along a Riemann surface. Accordingly, each spatial excursion of θ corresponding to 2π electrical radians of $\beta_o\theta$ causes the waves to encounter a "new leaf" of this surface, so that each leaf represents an electrical variation of 2π radians. The total number of leaves required to provide a closed domain of electrical angular values of the fields is equal to the circular propagation constant. Thus β_o is a measure of the number of leaves encompassed in completing a spatial excursion of 2π radians.

The concept may be applied to a large class of azimuthally re-entrant structures. Axially symmetric slow-wave circuits, such as those typically encountered in certain O-type traveling-wave devices, might have radial variations of the form

$$I_{\beta_o}(kr) \quad , \quad K_{\beta_o}(kr) \quad ,$$

where $\beta_o = 0, 1, 2, 3, \ldots$ The circular propagation constant must necessarily be limited to integral values for azimuthally re-entrant structures, since the fields must repeat at spatial angles of $2n\pi$ radians, where n is an integer. When $\beta_o = 0$, no azimuthal variation exists and the foregoing interpretation loses significance. However, the condition that $\beta_o = 1, 2, 3$ implies that one, two, or three leaves, respectively, of the Riemann surface are encountered in executing a spatial excursion of 2π radians. These finite, integral values of β_o make the notion especially clear because in the case of $\beta_o = 2$ the second leaf joins the first along the branch cut $\theta = 0, 4\pi$, while for $\beta_o = 3$ the third leaf joins the first along the branch cut $\theta = 0, 6\pi$. Although the author independently arrived at this interpretation of azimuthal propagation, it was subsequently discovered that Schelkunoff advanced the explanation somewhat earlier[8].

These characteristics of the fields present in the interaction region of coaxial-cylindrical systems raise further questions concerning the generation of an azimuthal component, which is required if a transfer of energy from the electron beam to the r-f wave is to be effective. Inspection of Eqs. 2.62-2.67 reveals that at least one space-harmonic component of either the E- or H-mode waves must differ from zero if $E_{\theta 1}$ is to have a nonzero component, so that an axial r-f electric or magnetic field is required. Waves of this type have been called "complementary modes" to distinguish them from the "principal mode" in which no axial field exists[9]. The principal mode of the coaxial-cylindrical system is composed of a radial r-f electric and an azimuthal r-f magnetic field,

thereby rendering it unsuitable for effective interaction with the electron beam. This is in marked contrast with the helitron structure where the principal mode is capable of producing the required azimuthal electric field component.

A further examination of the field equations in the interaction space reveals that the lowest E-mode field occurs for n = 0, because E_z has the axial variation

$$\cos\left(\frac{n\pi}{L}\,z\right) ,$$

while the lowest H-mode field occurs for n = 1, because H_z varies with z as

$$\sin\left(\frac{n\pi}{L}\,z\right) .$$

However, since E_θ possesses the same axial variation as H_z it follows that the lowest mode for which interaction is possible occurs when n = 1. Field patterns corresponding to several of the lowest eigenvalues for the E- and H-mode fields have been presented by Kalähne[13], and by Marcuvitz[15]. It may be noted that E-mode waves are excited by placing an electric dipole in the interaction space parallel to the axis of the coaxial-cylindrical system, while H-mode waves are excited by placing a magnetic dipole parallel to the same axis.

A novel approach to the study of wave propagation in rectangular waveguides bent into a circle of large radius was presented by Buchholz[11] in 1939. The treatment involves a study of the wave types for which either the electric or magnetic field vector lies entirely in one of the two longitudinal section planes of an initially straight guide. These "longitudinal section waves" are related to the familiar transverse

electric and magnetic waves in such a manner that each of the transverse waves can be resolved into a pair of longitudinal electric and magnetic section waves having the same phase velocity.

While the presence of a slight curvature produces only a minor distortion of this longitudinal-section-wave pair in the region of the bend, the two longitudinal waves now possess different phase velocities. The act of their "slipping through each other" gives rise to a mixed type of propagating wave whose amplitude increases with curvature, rather than the single transverse wave of the straight, rectangular guide. These findings corroborate an important conclusion which follows from the analysis presented in this chapter: When a straight, rectangular waveguide is deformed into a circle, a purely TE or TM wave cannot exist in the curved region even though one or the other of these modes may have been present prior to bending.

2.5 Special Considerations for the Flattened Helix Slow-Wave Structure

The analysis given above is a formal treatment of the "waveguide-type" of slow-wave structures. However, there exists a large class of "helix-type" slow-wave circuits which have received considerable attention because of their importance in O-type traveling-wave devices[7]. Of interest in the design of the small-signal E-type device described in Chapter IV is the flattened helix recently investigated by Johnson[22].

The basic system is modified only to the extent that the helix mandrel is bent into a circle of prescribed radius, instead of being straight. As long as the inter-turn spacing of the helix wire is a small fraction of the radius of curvature of the mandrel, the characteristics of the straight, flattened helix may be considered to apply to

the circular version of the structure. This condition is amply satisfied in the laboratory model.

Since the housing of the experimental E-type device serves only as an evacuated enclosure, the "waveguide modes" exist to a negligible extent. It can also be shown that the fields decay exponentially in the radial and axial directions according to the function[22]

$$\exp\left\{-\frac{\omega x}{(v)_r}\right\} ,$$

where x represents either coordinate variable. For frequencies in the microwave region of the electromagnetic spectrum, the fields very nearly vanish at distances as small as 0.100 inch from the helix surface. Moreover, the axial variation is no longer restricted to a narrow range of selected values. Instead, an essentially plane wave advances along the conducting path of the structure, thereby causing the time variable axial fields to assume all attainable function values at successive intervals. The z-coordinate now possesses a traveling-wave, rather than a standing-wave, character with the result that the electron-wave interaction problem simplifies to a two-dimensional analysis.

2.6 A General Classification of Centrifugal-Focusing Systems

The broad approach of the electromagnetic analysis leads not only to a better understanding of the fields that act on the electron beam of the E-type device, but in addition it permits a wide range of related structures to be viewed as constituents of a general class. In order to accomplish this classification it is desirable to observe that two

basic considerations are involved in the operation of a microwave electron beam tube:

1. The Focusing Mechanism — The electron beam may be caused to follow a specified path by stationary electric or magnetic fields, or by suitable modifications and combinations of them.
2. The r-f Interaction Field — The electron beam encounters an r-f electric field in its flight through the system. This field may propagate along an associated external circuit or along the electron beam itself. Furthermore, the beam may interact with the axial component, or one or more transverse components, of the wave.

The present discussion will be limited to the centrifugal-focusing systems described in the first chapter. In addition, only those electromagnetic fields will be studied that are associated with a circuit external to the beam, since fields arising from energy exchanges within the beam have been excluded from the analysis of this chapter.

Within the framework of these restrictions it is possible to categorize several known devices, in addition to predicting other embodiments that are not presently in existence. The preceding work of this chapter has shown that the helitron may be regarded as a CEF principal mode, azimuthal interaction device, since the electron beam chiefly encounters the azimuthal component of a TEM wave. This wave "sweeps past" the helical ribbon beam at the velocity of light as it absorbs energy, while the electrons are maintained along their proper trajectory by balancing the particle's centrifugal force with a radially-constraining electric field force.

The spiratron is a CEF complementary mode, axial interaction device in which the ribbon beam, following a helical path as in the helitron, interacts with the axial component of the r-f electric field in a coaxial-cylindrical system. Inasmuch as the axial velocity of the beam is small compared to its azimuthal velocity (and very small compared to the free-space velocity of light) it is evident that the r-f structure situated along the inner cylinder must support slow axial waves.

The general class of E-type tubes treated in this dissertation are those of a CEF complementary mode, azimuthal interaction device. It differs from the helitron not only in the electromagnetic field mode, but also by virtue of the fact that the system is azimuthally nonre-entrant. Thus, the electron beam is limited to not more than a single transit and possesses no axial drift velocity. On theoretical grounds, the present device should have a much broader bandwidth than the helitron owing to the use of a relatively nondispersive, flattened helix slow-wave structure. However, the growing-wave gain and power output are likely to be less than that of the helitron in view of the single transit limitation on the beam.

The structure described by Pantell[23] is a CMF complementary mode, azimuthal interaction device, since an axial magnetic field is used to confine the ribbon beam to a helical trajectory similar to the helitron. In this device, also, the electron beam interacts with the azimuthal component of a transverse electric wave. However, the field sweeps past the beam at an axial phase velocity exceeding that of light in free space, as determined by the frequency and mode of the waveguide field. This is necessarily a complementary mode device because the

principal mode cannot propagate in a hollow waveguide. Nevertheless, it should be possible to construct a CMF principal mode, azimuthal interaction device by replacing the radial electric field in the helitron structure with an axial magnetic field. There is serious doubt, however, as to the practicability of such a configuration owing to the magnet weight and power requirements.

Of somewhat more importance is the possibility of constructing another type of CEF complementary mode, azimuthal interaction device. A small, insulated wire could be suspended along the axis of a circular-cylindrical waveguide to provide the necessary radial electric field. A single vertical antenna might be used to excite the TE_{11} mode field, whose azimuthal component absorbs energy from a ribbon beam following a helical path about the axis of the cylinder. Another antenna near the output end of the structure could be used to couple the energy acquired to an external load. There is good experimental evidence to support the feasibility of the device, if it is recalled that this is basically Pantell's structure without a magnetic field. Furthermore, Kline[14] mathematically verified that the field pattern of each complementary mode in the coaxial-cylindrical transmission system approaches the pattern of the corresponding circular-cylindrical waveguide mode as the radius of the center conductor approaches zero. His results also indicate that the field of a given circular-cylindrical waveguide mode is negligibly disturbed by the introduction of a thin inner conductor.

CHAPTER III. THE EQUIVALENT CIRCUIT ANALYSIS

3.1 Introduction

Although the electromagnetic analysis provides a fundamental approach to the determination of the important field components in E-type devices, it is primarily the equivalent circuit analysis that yields quantitative information regarding the waves excited in the presence of an electron beam. The procedure used here consists of ascribing a suitable set of equivalent circuit elements, typically capacitors, inductors and resistors, to the slow-wave structure that supports the azimuthally-propagating r-f wave. In addition, these circuit elements reflect the degree of coupling that exists between the wave and the beam. The electron beam is likewise regarded as an equivalent ring charge situated along a prescribed radius of curvature.

A uniform, unbunched electron beam, passing in the vicinity of the slow-wave structure, is subjected to mechanical forces whose magnitude and orientation result from the electric field intensity of the r-f wave acting on the charged particles constituting the beam. The motion of the stream is therefore "perturbed" from the path it would otherwise follow in the absence of such fields. This modification of the electron's spatial behavior leads to the generation of r-f convection currents whose magnitudes are proportional to the intensity of the electromagnetic fields which produce them. The mathematical description of the convection currents in terms of the associated r-f fields is known as the "ballistic equations".

Alternatively, the fields on the circuit may be thought of as being produced by a density-modulated electron beam passing near the

circuit. The discrete bunches, that result from the grouping of the stream electrons around certain "average velocity" particles, induce fields on the circuit whose frequency and intensity are proportional to the beam current and position relative to the slow-wave structure. The expression which relates the fields produced on the circuit to the r-f convection currents in the electron beam is referred to as the "circuit equation".

Since there is only one beam and one circuit, the circuit and ballistic equations must represent independent functional dependencies between the r-f convection currents and slow-wave fields. The r-f currents and field intensities may therefore be eliminated from these relations to obtain the incremental propagation constants for forward- and backward-wave E-type devices. The growing- and beating-wave gain, and the backward-wave start-oscillation conditions, may then be determined by imposing a specified set of input boundary conditions on the waves described by the propagation constants. Finally, the relations between the convection current in the stream and the fields on the circuit can be used to derive a small-signal estimate of the efficiency of E-type traveling-wave devices.

3.2 The Principal Assumptions Employed in the Equivalent Circuit Analysis

The assumptions employed in the equivalent circuit analysis can be broadly classed as those associated with the r-f structure, which supports (azimuthally) slow electromagnetic waves, and those associated with the electron beam. Although this division is satisfactory for delineating the principal lines of discussion, the mutual character of

the electron-wave interaction phenomenon leads to assumptions of one type affecting those of the other.

Turning first to the r-f structure it will be expedient to consider a biperiodic circuit in which the propagating waves experience both axial and azimuthal slowing. The dimensions of the structure are presumed to be compatible with the small-argument approximation described in Appendix C. Attention will be limited to a study of E-wave cutoff modes in the interaction region, so that the special relations developed in Appendices C and D are applicable. However, the analysis may easily be extended to other situations by deriving suitable expressions from the appropriate relations presented in the last section of Appendix B.

The magnetic field intensity of the wave is ordinarily a small fraction of the r-f electric field intensity magnitude for the slow electromagnetic waves typically encountered in traveling-wave devices[7]. Furthermore, the magnetic field produced by a moving electron stream is negligible compared to the charge fields associated with the particles of the beam, for electron velocities that are small in comparison to the velocity of light[9]. Thus, the principal forces entering into the interaction process are those resulting from static electric fields of the electrons encountering the r-f electric fields of the circuit wave.

The modifications of the fields in the interaction space produced by an energy-carrying electron stream are accounted for by replacing the "cold-circuit" incremental propagation constant by a propagation constant that applies to the region in the presence of the beam. Inasmuch as the electrons are presumed to exhibit azimuthal motion, primarily, the axial propagation constant is considered to be unaffected by the presence of

the electron stream. The slow-wave circuit will also be considered to be lossless, with a suitable loss factor being introduced into the cold-circuit incremental propagation constant. This approximate procedure of accounting for dissipation leads to a simpler circuit equation than would be obtained for the actual circuit involving distributed loss.

The final assumption pertaining to the fields on the circuit involves condition that only the axial eigenvalue corresponding to n=1 is present in the interaction region. In this case the relations derived in Chapter II reveal that at the mid-point of the guide height, where z=L/2, the radial and azimuthal r-f electric field intensities attain their maximum value, while the axial r-f electric field passes through zero. The analysis is therefore materially simplified by treating the behavior of a single electron located at this position, since the absence of an axial r-f electric field limits the study to a two-dimensional investigation (provided the axial component of the space-charge repulsion forces can also be disregarded). Gain computations based on this assumption are likely to represent an upper limit on performance because electrons situated at other axial locations experience an increasing axial and a decreasing azimuthal r-f electric field intensity. However, for the special case of the flattened helix the two-dimensional treatment is applicable to an electron situated at any axial position, as explained in Chapter II.

The assumptions imposed on the nature of the electron beam involve an examination of its behavior in the presence of both d-c and r-f fields. With regard to its steady motion, the electron is considered to possess a linear tangential velocity that is a small fraction of the

velocity of light in free space, over its entire radial extension. Accordingly, nonrelativistic mechanics are suitable for the formulation of the equations of motion. In addition, the ribbon-shaped electron beam is presumed to satisfy the "critical perveance" requirement described by Waters[32,34,35], so that the stream follows a curved path in the interaction region with unvarying radial thickness.

Insofar as the analysis presented in this chapter is concerned, the electron stream may be considered as a Brillouin flow, Eulerian fluid. The Brillouin flow requirement imposes the condition that all electrons move around the center of the system with the same spatial angular velocity, leading to the condition that the stream particles do not slip azimuthally relative to each. Although the present treatment could be extended to include slipping motion, a substantial increase is experienced in the complexity of the mathematical formulation. Nevertheless, it is desirable to obtain some estimate of the effects produced by a slipping electron stream upon the transfer of energy from the beam to the circuit, using the procedure developed here. A brief study of the important effects contributing to this type of motion in E-type devices, and an approximate treatment of the manner in which it alters the growing-wave gain of a small-signal forward-wave amplifier, are considered in the closing section of this chapter.

The Eulerian fluid hypothesis requires only that electron flight lines do not cross, so that the motion of the entire fluid can be characterized in terms of the equations of motion of a single particle[3,5]. The space-charge fields, derived from Poisson's equation to account for bunching of the electron beam under the influence of the velocity-modulating circuit waves, are developed in a manner that is consistent

with the Eulerian constraint, since the electrons are assumed to cluster along parallel trajectories. In addition, the position taken here that bunching occurs principally in the azimuthal direction is consistent with the findings of Wada and Pantell[24,31].

Another important assumption concerning the motion of the electron beam, but one quite distinct from those described above, involves the supposition that the present study is limited to a small-signal analysis. The practical significance of this restriction lies in the fact that all a-c quantities are small in comparison to the d-c or "steady" quantities, so that squares and products of a-c terms may be neglected in relation to their first power. While this linearizing procedure leads to a substantial simplification of the mathematics, it is essential to observe that steady radial or azimuthal motions, arising from sustained electron-wave interaction effects, cannot be treated by this approach. Moreover, large-signal studies also involve the consideration that electron flight lines exhibit numerous crossings, thereby necessitating a complete reformulation of the problem.

The electron beam is therefore considered as a ribbon of extremely small radial extension whose center-of-the-beam-electron radius is r_o. The equations of motion are derived from a Lagrange function for a single particle, consistent with the assumption that electrons at all radial positions encounter the same r-f electric field intensities. The procedure is approximately correct for beams whose radial dimension is a very small fraction of the radial width of the interaction space, but it is otherwise subject to question.

The initial wave amplitudes, which are necessary in the determination of the forward-wave gain and backward-wave oscillation

conditions, are derived on the premise that a match need be achieved at only one level of the input boundary. This approach is strictly correct only for thin beams meeting the requirements of the foregoing paragraph. The matching procedure is also simplified by restricting the treatment to a study of those waves whose velocity of propagation approach the beam velocity, inasmuch as the remaining waves are excited to a negligible extent.

3.3 A Consideration of Unperturbed Motion

An understanding of the ballistic analysis will be facilitated by an examination of the conditions under which an electron can achieve stable motion in the absence of r-f fields. The study is limited to the case of a single electron located at the center-of-the-beam radius r_o. While the present investigation disregards the effects produced by the space-charge repulsion forces, the treatment can be extended to include this consideration through matching solutions of Poisson's equation within the beam and Laplace's equation in the surrounding space[30].

Laplace's equation in cylindrical coordinates takes the form

$$\nabla^2 V = \frac{1}{r} \frac{\partial}{\partial r} \left(r \frac{\partial V}{\partial r} \right)$$

$$= 0 \quad , \tag{3.1}$$

where V designates a scalar potential function of r alone. The boundary conditions are

$$V = V_c \quad \text{at} \quad r = r_c \quad , \tag{3.2}$$

$$V = V_s \quad \text{at} \quad r = r_s \quad , \tag{3.3}$$

where V_c = potential of the circuit measured relative to the cathode in volts,

V_s = potential of the sole electrode measured relative to the cathode in volts,

r_c = radius of the circuit in meters,

r_s = radius of the sole in meters.

Upon applying Eqs. 3.2 and 3.3 to the general solution of Eq. 3.1 the expression for the radial variation of potential may be written

$$V = V_c - (V_c - V_s)\left[\frac{\ell n(r/r_c)}{\ell n(r_s/r_c)}\right] . \qquad (3.4)$$

The radial electric field intensity $E(r)$ is found to be

$$E(r) = -\frac{\partial V}{\partial r} ,$$

$$= \frac{1}{r}\left[\frac{V_c - V_s}{\ell n(r_s/r_c)}\right] . \qquad (3.5)$$

Let it now be assumed that the radial electric field force at r_o just balances the centrifugal force of the electron at the same radius, so that the particle possesses stable motion in the interaction space. This condition may be described mathematically as

$$\frac{mv_o^2}{r_o} + e\,E(r_o) = 0 , \qquad (3.6)$$

where m = mass of the electron in kilograms,

e = negative charge of the electron in coulombs,

v_o = linear tangential velocity of the electron at radius r_o in meters/second,

$E(r_o)$ = radial electric field intensity at radius r_o in volts/meter.

The unperturbed spatial angular velocity of an electron at radius r_o follows directly from Eq. 3.6, after noting that $v_o = \Omega_o r_o$,

$$\Omega_o = \frac{1}{r_o}\sqrt{\frac{\eta(V_c - V_s)}{\ell n(r_s/r_c)}} \quad \text{spatial radians/second} \quad , \tag{3.7}$$

where η is the magnitude of the electron's charge-to-mass ratio in coulomb/kilogram. The importance of this equation is evident from the fact that it relates the equilibrium spatial angular velocity of an electron at a given radius to electrode dimensions and potentials.

One additional relation can be derived from the condition that an electron starting from rest at the cathode gains a kinetic energy equal to its loss in potential energy in falling through a prescribed voltage potential difference. Assuming, as above, that all voltages are measured relative to the cathode, the law of conservation of energy yields for an electron at radius r_o

$$\Omega_o = \frac{1}{r_o}\sqrt{2\eta V_o}$$

$$= \frac{1}{r_o}\sqrt{2\eta\left\{V_c - (V_c - V_s)\left[\frac{\ell n(r_o/r_c)}{\ell n(r_s/r_c)}\right]\right\}} \quad \text{spatial radians/second} \quad , \tag{3.8}$$

where the last result follows from evaluating Eq. 3.4 at r_o. A comparison of Eqs. 3.7 and 3.8 leads to the conclusion that

$$\left(\frac{V_s}{V_c}\right) = \left[\frac{1+2\ \ell n(r_o/r_s)}{1+2\ \ell n(r_o/r_c)}\right] \quad , \tag{3.9}$$

which reveals that the sole-to-circuit voltage ratio necessary to achieve the desired equilibrium motion of an electron at r_o is only a function of the tube geometry. Although this expression was derived on the premise that the space-charge modification of the potential in the interaction space may be neglected, it is a useful approximation for designing E-type devices having small beam currents.

3.4 Treatment of the Electron Beam as an Equivalent Ring Charge

The development of the ballistic equations for the E-type device involves replacing the actual ribbon-shaped electron beam by an equivalent ring charge situated at the center-of-the-beam-electron radius. The substitution is accomplished by first noting that the volume charge density of the beam ρ may be written

$$\rho = \frac{Q_b}{2\pi r_o h \sigma} \text{ coulomb/meter}^3 \quad , \tag{3.10}$$

where Q_b = total charge contained in the beam in coulombs,

h = height of the beam parallel to the z-axis in meters,

σ = radial width of the beam in meters.

The "ring charge density" of the beam τ may likewise be expressed as

$$\tau = \frac{Q_b}{2\pi r_o} \text{ coulomb/meter} \quad , \tag{3.11}$$

where the ring charge is a hypothetical circular line charge located at r_o. The description of the beam in terms of such a circular line charge is a useful approximation which is valid provided

$$\frac{\sigma}{r_o} \ll 1 \quad .$$

This condition is realized to a high degree of accuracy for many E-type devices*. It is clear that the limitation simply requires the radial width of the beam to be a small fraction of the radius of curvature of the center-of-the-beam electron.

A comparison of Eqs. 3.10 and 3.11 indicates that the volume charge density is related to the equivalent line charge density through the simple function

$$\rho = \frac{\tau}{h\sigma} \quad , \tag{3.12}$$

which holds provided the foregoing assumption is satisfied.

3.5 The Space-Charge Fields Produced by Electron Bunching

The fields produced by dense concentrations of electrons result from the bunching that occurs in the presence of the velocity-modulating r-f wave on the circuit. The space-charge fields can be investigated by an examination of Poisson's equation, which takes the following form in cylindrical coordinates

$$\nabla\cdot\overline{E} = \frac{1}{r}\frac{\partial}{\partial r}(rE_r) + \frac{1}{r}\frac{\partial E_\theta}{\partial \theta} + \frac{\partial E_z}{\partial z} \quad ,$$

$$= \rho/\epsilon_o \quad . \tag{3.13}$$

Equation 3.13 involves the assumption that the free-space permittivity also applies to the region containing the beam. The approximation is reasonable for the small-signal devices under study here.

At this point the assumption is introduced that the treatment is limited to a two-dimensional analysis (specifically the radial and

---

* In the experimental device described in Chapter IV this ratio is approximately

$$\frac{\sigma}{r_o} = \frac{1}{45} \quad .$$

azimuthal directions) since the axial electric field vanishes at the mid-point of the guide height. In this case Eq. 3.13 simplifies to the form

$$\frac{\partial}{\partial r}(rE_r) + \frac{\partial E_\theta}{\partial \theta} = \frac{\tau r}{\epsilon_o h \sigma} \quad , \tag{3.14}$$

owing to the relation between line and volume charge densities as given by Eq. 3.12. An examination of the above result shows that the line charge density involves a d-c component, due to the steady azimuthal motion of the beam, and an a-c component due to the space-charge bunching produced by the velocity-modulating r-f waves on the circuit. Accordingly, Eq. 3.14 can be written

$$\frac{\partial}{\partial r}(rE_r) + \frac{\partial E_\theta}{\partial \theta} = (\tau_o + \tau_1)\frac{r}{\epsilon_o h \sigma} \quad , \tag{3.15}$$

where τ_o = d-c component of ring charge density due to the steady motion of the beam in coulomb/meter,

τ_1 = a-c component of ring charge density due to the space-charge bunching of the beam in coulomb/meter.

A study of the left member of Eq. 3.15 reveals that any azimuthal electric field which exists can only result from the azimuthal bunching of the beam, inasmuch as there can be no steady azimuthal field associated with a uniform, unbunched ring charge. However, the radial electric field intensity may, under the most general circumstances, possess a d-c component, due to the unvarying azimuthal current, and an a-c component that results from azimuthal bunching*. If the additional assumption is

---

* It is essential to observe that radial bunching may lead to crossing of electron flight lines and must therefore be excluded from the present treatment.

made that azimuthal bunching of the electron beam generates only an azimuthal electric field, then the radial field produced by the beam results entirely from the uniform component of azimuthal current. Under this restriction Eq. 3.15 can be separated into the pair of equations

$$\frac{\partial}{\partial r}(rE_r^o) = \frac{\tau_o r}{\epsilon_o h\sigma} , \tag{3.16}$$

$$\frac{\partial E_{\theta s}}{\partial \theta} = \frac{\tau_1 r}{\epsilon_o h\sigma} , \tag{3.17}$$

where E_r^o = steady radial electric field intensity produced by the d-c component of azimuthal current in volt/meter,

$E_{\theta s}$ = a-c component of azimuthal electric field intensity produced by azimuthal bunching of the electron beam in volt/meter.

The solution of Eq. 3.16 yields the magnitude of the steady radial electric field intensity arising from the space-charge field of the unmodulated beam. This field, which is a measure of the d-c radial debunching force produced by the individual charges of the electron stream, does not enter into the electron-wave interaction process. Furthermore, a small-signal study of E-type devices is primarily concerned with the radial and azimuthal perturbations of an infinitesimally thin ring charge located at r_o, so that the steady field is of less importance than the alternating azimuthal field described by Eq. 3.17. Interest will therefore be centered on the latter equation in the development of the ballistic relations.

3.6 Derivation of the Ballistic Equations

The equations of motion for an electron revolving about the center of the coaxial-cylindrical system follow from the Lagrange function for a single particle[2]

$$\ddot{r} - r\dot{\theta}^2 = -\eta[E_r + E(r)] \quad , \tag{3.18}$$

$$2\dot{r}\dot{\theta} + r\ddot{\theta} = -\eta(E_\theta + E_{\theta s}) \quad , \tag{3.19}$$

where E_r = radial r-f electric field intensity in volt/meter,

$E(r)$ = static radial electric field intensity which balances the centrifugal force of the electron at radius r in volt/meter,

E_θ = azimuthal r-f electric field intensity in volt/meter,

$E_{\theta s}$ = azimuthal r-f electric field intensity produced by space-charge bunching in volt/meter.

The dots appearing above the quantities in the foregoing equations signify the total time derivatives of these terms. The azimuthal velocity and radial dependence may be expressed in terms of their unperturbed values by means of the relations

$$r = (r_o + \mu) \quad , \tag{3.20}$$

$$\dot{\theta} = \frac{d\theta}{dt} \quad ,$$

$$= (\Omega_o + \nu) \quad , \tag{3.21}$$

where μ = radial perturbation function in meters,

ν = azimuthal velocity perturbation function in spatial radian/second.

It is important to observe that while μ and ν depend on the spatial angle θ, and on time, both of these functions must be independent of radial variations. The condition that

$$\frac{\partial \mu}{\partial r} = 0 \quad ,$$

follows from the Eulerian fluid hypothesis, described in Section 3.2, which prohibits the crossing of electron trajectories. A nonzero rate of change of μ with respect to r implies that electrons at different radial positions experience unequal radial displacements, thereby permitting certain electrons to overtake others*.

The requirement that

$$\frac{\partial \nu}{\partial r} = 0$$

results from the "Brillouin flow" assumption which asserts that the spatial angular velocity of all particles in the electron stream must remain invariant. This stipulation is not as important as the constraint imposed on the radial perturbation function, because variations of ν with changes of r simply indicate the existence of slipping-stream conditions. Although the analysis could still be carried out for a nonzero rate of change of the azimuthal velocity perturbation function with radius (provided that the restriction on μ is still retained in order to assure the validity of the Eulerian fluid hypothesis), the complexity of the mathematical development is correspondingly increased.

---

* This follows from the fact that the electrons at the inside edge of the beam encounter the strongest circuit fields and thus undergo the greatest radial excursion. Since motion of this character leads to intersecting electron trajectories, a zero rate of change of μ with respect to r must be imposed.

The azimuthal velocity and radial perturbation functions are thus dependent only on θ and t, so that upon employing the usual procedure for partial differentiation the equations of motion become

$$(\Omega_o+\nu)\left[(\Omega_o+\nu)\frac{\partial^2\mu}{\partial\theta^2}+\left(\frac{\partial\mu}{\partial\theta}\right)\frac{\partial\nu}{\partial\theta}+\frac{\partial^2\mu}{\partial\theta\partial t}\right]+\left[\frac{\partial^2\mu}{\partial t^2}+\left(\frac{\partial\mu}{\partial\theta}\right)\frac{\partial\nu}{\partial t}+(\Omega_o+\nu)\frac{\partial^2\mu}{\partial\theta\partial t}\right]$$

$$-(r_o+\mu)(\Omega_o+\nu)^2 = -\eta E_r - \frac{(\Omega_o r_o)^2}{r_o+\mu} , \qquad (3.22)$$

$$2(\Omega_o+\nu)\left[(\Omega_o+\nu)\frac{\partial\mu}{\partial\theta}+\frac{\partial\mu}{\partial t}\right]+(r_o+\mu)\left[(\Omega_o+\nu)\frac{\partial\nu}{\partial\theta}+\frac{\partial\nu}{\partial t}\right] = -\eta(E_\theta+E_{\theta s}) . \qquad (3.23)$$

The substitution for $E(r_o+\mu)$, made in the right member of Eq. 3.22, follows from the use of Eqs. 3.5 and 3.7. These expressions may be written in a form for which derivatives do not appear by noting that

$$\frac{\partial f}{\partial\theta} = -j\beta f ,$$

$$\frac{\partial f}{\partial t} = j\omega f ,$$

where f designates a function of θ and time. The $-j\beta$ and $j\omega$ operators are a consequence of the characteristic variation

$$\epsilon^{j(\omega t-\beta_o\theta)} ,$$

that was found to apply to all field components in Chapter II. It is important to observe, however, that the "cold-circuit" circular propagation constant β_o is replaced in the present chapter by the propagation constant β which holds in the presence of an energy-carrying electron beam. Subject to these transformations Eqs. 3.22 and 3.23 can be written as

$$\mu(\Omega_o+\nu)\ (\beta\omega-\Omega_o\beta^2-2\nu\beta^2) + \mu\omega(\Omega_o\beta-\omega+2\nu\beta)$$

$$- (\Omega_o^2\mu+2\Omega_o r_o\nu+\Omega_o^2 r_o+2\Omega_o\mu\nu+r_o\nu^2+\mu\nu^2) + \frac{(\Omega_o r_o)^2}{r_o+\mu} = - \eta E_r \quad , \qquad (3.24)$$

$$2\mu(\Omega_o+\nu)\ (\omega-\beta\Omega_o-\beta\nu) + \nu(r_o+\mu)\ (\omega-\beta\Omega_o-\beta\nu) = j\eta E_\theta - \frac{\eta\tau_1(r_o+\mu)}{\beta\epsilon_o h\sigma} \qquad (3.25)$$

The last term of Eq. 3.25 results from the simplification of Eq. 3.17 through the use of the $-j\beta$ operator.

In addition to these relations there also exists the continuity equation, as well as the radial and azimuthal current equations. The azimuthal current equation has the form

$$I_\theta = (\tau_o + \tau_1)(r_o + \mu)(\Omega_o + \nu) \quad ,$$

$$= - I_o + i_\theta \quad , \qquad (3.26)$$

where

$$I_o = - \Omega_o r_o \tau_o \quad , \qquad (3.27)$$

$$i_\theta = \Omega_o\tau_o\mu + r_o\tau_o\nu + \Omega_o r_o\tau_1 + \tau_o\mu\nu + \Omega_o\mu\tau_1 + r_o\nu\tau_1 + \mu\nu\tau_1 \quad . \qquad (3.28)$$

The radial current equation is given by

$$i_r = (\tau_o + \tau_1)\frac{d}{dt}(r_o + \mu) \quad ,$$

$$= (\tau_o + \tau_1)\left[(\Omega_o + \nu)\frac{\partial\mu}{\partial\theta} + \frac{\partial\mu}{\partial t}\right] \quad ,$$

$$= j\mu(\omega\tau_o - \beta\Omega_o\tau_o - \beta\tau_o\nu + \omega\tau_1 - \beta\Omega_o\tau_1 - \beta\nu\tau_1) \quad . \qquad (3.29)$$

A comparison of Eqs. 3.26 and 3.29 reveals that the azimuthal current has a steady component given by I_o, in addition to the a-c component given by i_θ, whereas the radial current contains only the alternating component. This is a direct consequence of the fact that the steady radial motion of the beam, resulting from interaction with the circuit wave, cannot be accounted for by the present analysis. The steady component of azimuthal current, on the other hand, exists because the electron beam is assumed to enter the interaction region with an initial linear tangential velocity of v_o at radius r_o. The negative sign accompanying I_o in Eqs. 3.26 and 3.27 is necessitated by the unfortunate, but entrenched, notion that current flow is "positive" in the direction opposite to that of electron movement.

The continuity equation has the well-known form[9]

$$\nabla\cdot(\bar{l}_r i_r + \bar{l}_\theta I_\theta) = -\frac{\partial}{\partial t}(\tau_o + \tau_1) \quad , \tag{3.30}$$

which is a mathematical expression of the indestructibility of matter, since the time rate of change of charge flow <u>through</u> any given volume of space must be equal to the negative divergence of the current flow <u>within</u> that volume. In cylindrical coordinates the continuity equation becomes

$$\frac{i_r}{r_o+\mu} + \frac{\partial i_r}{\partial r} + \frac{1}{r_o+\mu}\frac{\partial i_\theta}{\partial \theta} = -\frac{\partial \tau_1}{\partial t} \tag{3.31}$$

because the time rate of change of the steady component of ring charge density τ_o is zero. Furthermore, the second term in the left member of the above equation is also zero in view of the requirement that

$$\frac{\partial \mu}{\partial r} = 0 \quad ,$$

upon recalling the presence of the radial perturbation function μ in every term of Eq. 3.29. Accordingly, the continuity equation assumes the general form

$$\frac{\mu}{r_o+\mu}\left[\tau_o(\omega-\beta\Omega_o) + \tau_1(\omega-\beta\Omega_o) - \beta\tau_o\nu - \beta\nu\tau_1\right] - \frac{\beta}{r_o+\mu}\left[\Omega_o\tau_o\mu + r_o\tau_o\nu + \Omega_o r_o\tau_1 + \tau_o\mu\nu + \Omega_o\mu\tau_1 + r_o\nu\tau_1 + \mu\nu\tau_1\right] = -\omega\tau_1, \quad (3.32)$$

where the appropriate differential operators, and the substitutions for i_θ and i_r from Eqs. 3.28 and 3.29, have been employed.

While the above expressions satisfy the Brillouin flow, Eulerian fluid hypothesis described earlier, they must be simplified further in order to keep the mathematical development within reasonable bounds of complexity. This is accomplished through the use of the small-signal assumption which imposes the condition that all a-c quantities are small in proportion to the d-c or steady quantities, and that squares and products of perturbation functions may be neglected in comparison to the first power of these terms. Within the scope of these limitations the equations of motion and the continuity equation take the form

$$\mu\Omega_o^2\left[(\beta_e-\beta)^2 + 2\right] + \nu(2\Omega_o r_o) = \eta E_r \quad , \quad (3.33)$$

$$\mu 2\Omega_o^2(\beta_e-\beta) + \nu\Omega_o r_o(\beta_e-\beta) + \tau_1\left(\frac{\eta r_o}{\beta\epsilon_o h\sigma}\right) = j\eta E_\theta \quad , \quad (3.34)$$

$$\mu(\beta_e-2\beta) + \nu\left(\frac{-\beta r_o}{\Omega_o}\right) + \tau_1\left[\frac{r_o(\beta_e-\beta)}{\tau_o}\right] = 0 \quad , \quad (3.35)$$

where $\beta_e \triangleq \frac{\omega}{\Omega_o}$ electrical radian/spatial radian. (3.36)

The reduction of Eqs. 3.24, 3.25 and 3.32, to their simplified equivalents involves the approximation

$$\frac{1}{r_o+\mu} = \frac{1}{r_o(1+\mu/r_o)} ,$$

$$\approx \frac{1}{r_o}\left(1 - \frac{\mu}{r_o}\right) , \qquad (3.37)$$

since μ/r_o is assumed to be very much less than unity. Furthermore, the quantity β_e is the analogue of the linear electron phase constant described by Pierce[7], which may be thought of as the circular propagation constant of a disturbance traveling with the same azimuthal velocity as the electron stream. This is a fundamental parameter of E-type devices whose importance will be evident from a careful study of the solutions of the determinantal equation.

Under the small-signal assumption the a-c components of azimuthal and radial current, given by Eqs. 3.28 and 3.29, become

$$i_\theta = \Omega_o\tau_o\mu + r_o\tau_o\nu + \Omega_o r_o\tau_1 , \qquad (3.38)$$

$$i_r = j\tau_o\Omega_o\mu(\beta_e-\beta) . \qquad (3.39)$$

These expressions complete the set of relations necessary for deriving the radial and azimuthal ballistic equations. The details of the procedure are presented below.

The perturbation functions μ, ν and τ_1 are obtained from the solution of Eqs. 3.33-3.35 by means of Cramer's rule[3]. The determinant of the homogeneous system of these equations Δ_s is found to be

$$\Delta_s = \frac{\Omega_o^3 r_o^2}{\tau_o}\left[(\beta_e-\beta)^4 + (\beta_e-\beta)^2(Q-2) + 2Q\left(\frac{\beta_e}{\beta} - 1\right)\right] , \qquad (3.40)$$

where Q is the dimensionless "space-charge" parameter of E-type devices, which is defined as

$$Q \triangleq \frac{\eta\tau_o}{\Omega_o^2\epsilon_o h\sigma} . \qquad (3.41)$$

It is interesting to observe that Q is a negative quantity owing to the fact that the ring charge density τ_o represents the field produced by a uniform beam of electrons. Upon following the customary procedure, the perturbation functions are readily computed

$$\mu = \left(\frac{\eta\Omega_o r_o^2}{\tau_o\Delta_s}\right)\left[E_r\left((\beta_e-\beta)^2 + Q\right) - j2E_\theta(\beta_e-\beta)\right] , \qquad (3.42)$$

$$\nu = \left(\frac{\eta\Omega_o^2 r_o}{\tau_o\Delta_s}\right)\left[E_r\left\{Q\left(\frac{\beta_e}{\beta} - 2\right) - 2(\beta_e-\beta)^2\right\} + jE_\theta(\beta_e-\beta)\left((\beta_e-\beta)^2+2\right)\right] , \qquad (3.43)$$

$$\tau_1 = \frac{\eta\Omega_o r_o}{\Delta_s}\left[-E_r\beta_e(\beta_e-\beta) + jE_\theta(\beta_e-\beta)\left(\beta(\beta_e-\beta)+2\right)\right] . \qquad (3.44)$$

These relations may be used in conjunction with Eqs. 3.38 and 3.39 to obtain the azimuthal and radial ballistic equations,

$$i_\theta = \frac{\eta\tau_o}{\Omega_o}\left[\frac{E_r\left(\frac{Q}{\beta} - (2\beta_e-\beta)\right) + jE_\theta\left(\beta_e(\beta_e-\beta)+2\right)}{(\beta_e-\beta)^3 + (\beta_e-\beta)(Q-2) + \frac{2Q}{\beta}}\right] , \qquad (3.45)$$

$$i_r = \frac{j\eta\tau_o}{\Omega_o}\left[\frac{E_r\left((\beta_e-\beta)^2 + Q\right) - j2E_\theta(\beta_e-\beta)}{(\beta_e-\beta)^3 + (\beta_e-\beta)(Q-2) + \frac{2Q}{\beta}}\right] , \qquad (3.46)$$

The final step in the derivation involves the substitution of the appropriate expression for the radial-to-azimuthal field intensity ratio into the above equations to obtain functions of the form

$$i_\theta/E_\theta \quad ,$$

and

$$i_r/E_r \quad .$$

This can be accomplished with the aid of the relations developed in Appendix C.

The expression for E_r/E_θ appropriate to the small-argument assumption, given by Eq. C.6, and evaluated at the radius of the center-of-the-beam electron, becomes

$$\frac{E_r}{E_\theta} = j\left[\frac{1+(r_s/r_o)^{2\beta_o}}{1-(r_s/r_o)^{2\beta_o}}\right] \quad ,$$

$$= jF_o \quad , \tag{3.47}$$

where F_o is equal to $F(r)$ evaluated at $r = r_o$. This relation may be used in conjunction with Eqs. 3.45 and 3.46 to obtain

$$\frac{i_\theta}{E_\theta} = \frac{j\eta\tau_o}{\Omega_o}\left[\frac{\beta\beta_e(\beta_e-\beta)-F_o\beta(2\beta_e-\beta)+2\beta+F_oQ}{\beta(\beta_e-\beta)^3+\beta(\beta_e-\beta)(Q-2)+2Q}\right] \quad , \tag{3.48}$$

$$\frac{i_r}{E_r} = \frac{j\eta\tau_o}{\Omega_o}\left[\frac{\beta(\beta_e-\beta)^2+\beta Q-\frac{2\beta}{F_o}(\beta_e-\beta)}{\beta(\beta_e-\beta)^3+\beta(\beta_e-\beta)(Q-2)+2Q}\right] \quad . \tag{3.49}$$

It is important to observe that the expressions for E_r and E_θ which appear in the above equations represent the radial and azimuthal r-f

electric field intensities present at the beam. Accordingly, the corresponding fields at the circuit must be multiplied by the appropriate coupling factor when treating the interaction processes occurring at the location of the electron stream.

The ratio of the last two equations is equal to

$$\frac{i_\theta}{i_r} = \frac{1}{jF_o}\left[\frac{\beta\beta_e(\beta_e-\beta)-F_o\beta(2\beta_e-\beta)+2\beta+F_oQ}{\beta(\beta_e-\beta)^2-\frac{2\beta}{F_o}(\beta_e-\beta)+\beta Q}\right] , \qquad (3.50)$$

which can be simplified by introducing approximations applicable to typical E-type devices. It is well known[7], for example, that the small-perturbation analysis involves the consideration that both β and β_o differ from β_e by a very small amount. Furthermore, the numerical value of β_e generally ranges between 25 and 50, so that the assumption

$$\beta_e \gg 1$$

is ordinarily quite accurate. Under these circumstances Eq. 3.47 is very nearly

$$F_o \approx \frac{1+(r_s/r_o)^{2\beta_e}}{1-(r_s/r_o)^{2\beta_e}} , \qquad (3.51)$$

which is approximately equal to -1 for large β_e, since

$$\frac{r_s}{r_o} > 1 .$$

It is also rather interesting to observe that the condition

$$\beta_e \equiv 0 ,$$

corresponding to the complete absence of electrical variations with spatial angle, yields a singular point for the value of F_o, as shown

in Fig. 3.1. The result is not surprising inasmuch as the radial field is the only one which can exist for TEM wave* propagation between coaxial-cylindrical conductors, or with only static fields present. The radial electric field must necessarily be infinitely larger than the azimuthal field in either of these situations.

The final consideration involves the size of the space-charge parameter Q. The computations for the experimental device, presented in Chapter IV, reveal that this quantity lies in the vicinity of -2, so that it is reasonable to assume

$$\beta \approx \beta_e \quad , \qquad F_o = -1 \quad ,$$

$$\beta_e \gg 1 \quad , \qquad Q = -2 \quad .$$

These approximate values may be applied to Eq. 3.50 to obtain

$$\frac{i_\theta}{i_r} \approx j \frac{\beta_e^2}{-2\beta_e} = -j\beta_e/2 \quad . \tag{3.52}$$

It is clear that the a-c component of azimuthal current is much larger than the a-c component of radial current for the range of conditions considered above. The importance of this result pertains to the fact that the azimuthal ballistic equation alone may be employed in the derivation of the circuit and determinantal equations, with only a small order of error arising from the neglect of the radial ballistic equation.

3.7 Derivation of the Circuit Equation

The circuit equation is derived for the most general condition that the relation may be applied to either forward or backward traveling-

---

* The absence of an azimuthal field is accompanied by the absence of an axial field, so that only a plane wave can exist as explained in Chapter II.

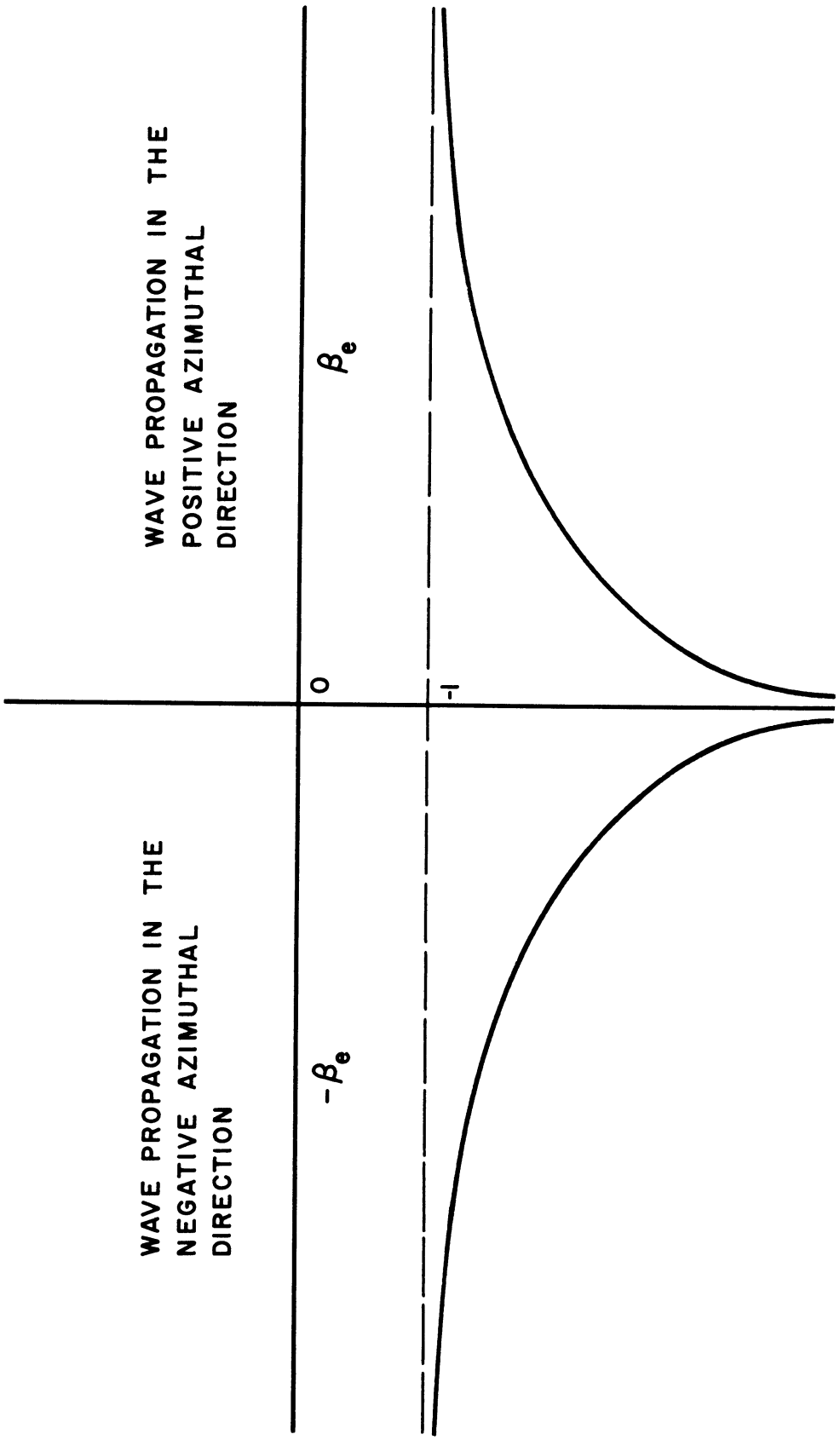

FIG. 3.1 THE VARIATION OF F_0 WITH β_e.

wave devices, by properly selecting the sign of the circuit impedance. A positive sign is associated with the circuit impedance of a forward-wave device, owing to the positive dispersion characteristic that exists when the wave phase and group velocities are uniquely directed[7]. The circuit impedance of a backward-wave device contains a negative sign in consequence of the negative dispersion characteristic resulting from the oppositely directed phase and group velocities of the waves on the r-f structure.

In a recent memorandum Rowe[25] has treated the problem of a sheet beam passing parallel to the face of a biperiodic structure. Expressed in cylindrical coordinates, the general equation for a lossless anisotropic transmission line takes the form

$$\left(v_{o,o}v_{o,1}\frac{Z_{o,o}}{Z_{o,1}}\right)\frac{\partial^2 V(z,\theta,t)}{\partial z^2}+\left(\frac{v_{o,o}}{r_c}\right)^2\frac{\partial^2 V(z,\theta,t)}{\partial \theta^2}$$

$$-\left(1+\frac{v_{o,o}}{v_{o,1}}\frac{Z_{o,o}}{Z_{o,1}}\right)\frac{\partial^2 V(z,\theta,t)}{\partial t^2}=-\frac{v_{o,o}Z_{o,o}}{h\sigma}\frac{\partial^2 \tau_1^*}{\partial t^2}\quad,\qquad(3.53)$$

where $V(z,\theta,t)$ = voltage on the biperiodic structure, which is a function of z, θ and t, in volts,

$v_{o,o}$ = linear tangential phase velocity of the azimuthally-directed wave at the surface of the r-f circuit in meter/second,

$v_{o,1}$ = axial component of the wave phase velocity at the surface of the r-f circuit in meter/second,

$Z_{o,o}$ = azimuthal component of the circuit impedance at the surface of the slow-wave structure in ohms,

$Z_{o,1}$ = axial component of the circuit impedance at the surface of the slow-wave structure in ohms,

τ_1^* = effective a-c component of ring charge density due to space-charge bunching of the beam, which excites fields on the circuit, in coulomb/meter.

The relation between τ_1^* and τ_1, defined by Eq. 3.15, is known to be

$$\tau_1^* = \int_{z=-L/2}^{z=L/2} \int_{r=r_c}^{r=r_s} k_\theta \tau_1 \, dr \, dz \quad , \tag{3.54}$$

where k_θ = azimuthal coupling factor,

r_s = sole radius in meters.

The essential characteristics of the azimuthal coupling factor may be determined by a treatment similar to that employed in the study of the radial-to-azimuthal field ratio presented in Section 3.6. Since β_o is very nearly equal to β_e, the expression for k_θ given by Eq. D.6 of Appendix D becomes approximately

$$k_\theta = \left(\frac{r_o}{r_c}\right)^{\beta_e - 1} \left[\frac{1 - (r_s/r_o)^{2\beta_e}}{1 - (r_s/r_c)^{2\beta_e}} \right] . \tag{3.55}$$

The limiting value of k_θ as β_e approaches infinity is found to be

$$\underset{\beta_e \to \infty}{\text{Lim}} \, k_\theta = \underset{\beta_e \to \infty}{\text{Lim}} \left(\frac{r_o}{r_c}\right)^{\beta_e} \left[\frac{1 - (r_s/r_o)^{2\beta_e}}{1 - (r_s/r_c)^{2\beta_e}} \right] ,$$

$$= 0 \quad . \tag{3.56}$$

Although this evaluation has been carried out for positive values of β_e, corresponding to wave propagation in the positive azimuthal direction, a similar procedure yields the same zero value of k_θ as β_e approaches negative infinity.

The behavior of the azimuthal coupling factor in the vicinity of $\beta_e = 0$ has to be examined more carefully inasmuch as k_θ then assumes the indeterminate form 0/0. The limit may be ascertained in this case through application of the familiar rule

$$\lim_{\beta_e \to 0} k_\theta = \left(\frac{r_c}{r_o}\right) \lim_{\beta_e \to 0} \left[\frac{\frac{d}{d\beta_e}\left(\frac{r_s}{r_o}\right)^{2\beta_e}}{\frac{d}{d\beta_e}\left(\frac{r_s}{r_c}\right)^{2\beta_e}} \right] ,$$

$$= \left(\frac{r_c}{r_o}\right) \left[\frac{\ell n(r_s/r_o)}{\ell n(r_s/r_c)} \right] . \qquad (3.57)$$

The curve of Fig. 3.2 shows clearly that when β_e becomes identically equal to zero the coupling factor depends only on the sole, circuit, and beam radii. For a given set of tube dimensions the highest value of azimuthal coupling factor is thus achieved. However, this represents a rather hypothetical situation since the complete absence of azimuthal variations implies the existence of plane wave propagation between the coaxial-cylindrical conductors. Under these circumstances the interaction of a radial r-f electric field with an azimuthally-directed ribbon beam is negligible.

It is also rather interesting to observe that when $r_o = r_c$ the azimuthal coupling factor approaches unity, independent of the value of β_e, as a study of Eqs. 3.55 and 3.57 reveals. This is to be expected

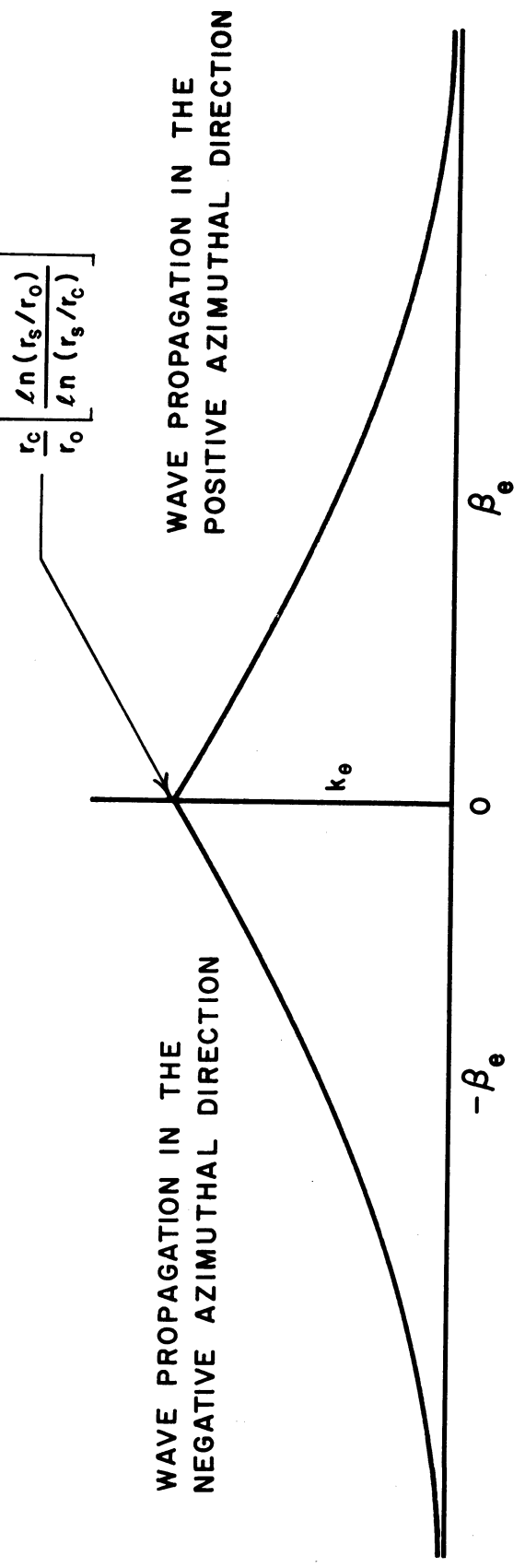

FIG. 3.2 THE VARIATION OF k_e WITH β_e

inasmuch as the center-of-the-beam-electron radius becomes coincident with the circuit radius, thereby providing maximum coupling. This condition can only be approached within practical limits, however, since the more closely the beam is positioned with respect to the circuit the greater is the opportunity for electron interception by the slow-wave structure.

These same equations also show that when $r_o = r_s$ the azimuthal coupling factor vanishes, identically, for all values of β_e. This observation is likewise consistent with the physical situation because the azimuthal component of r-f electric field intensity must approach zero at the surface of the sole electrode, resulting in the complete absence of coupling between the electron beam and the circuit wave.

Although the radial coupling factor k_r does not enter into the computations necessary for the derivation of the circuit equation, according to the method used here, an examination of its behavior provides additional understanding of the relationship between the field and circuit analyses of Chapters II and III. Under the assumption that β_o is very nearly equal to β_e, Eq. D.5 of Appendix D may be written

$$k_r = \left(\frac{r_o}{r_c}\right)^{\beta_e - 1} \left[\frac{1 + (r_s/r_o)^{2\beta_e}}{1 + (r_s/r_c)^{2\beta_e}} \right] . \qquad (3.58)$$

The limiting value of k_r, as β_e approaches positive or negative infinity, is found to be the same as that of k_θ, so that the radial coupling factor vanishes as the magnitude of β_e increases indefinitely. When β_e approaches zero the radial coupling factor approaches r_c/r_o, which is slightly larger than the corresponding limit approached by k_θ (unless

r_o exactly equals r_c). Nevertheless, it is reasonable to expect the general variation of k_r with β_e to exhibit the same overall behavior as that observed in Fig. 3.2.

A study of Eq. 3.58 reveals that when $r_o = r_c$ the unity coupling condition is achieved, since k_r then equals one. The only significant difference between the general characteristics of k_r and k_θ becomes apparent when $r_o = r_s$. In this case k_θ vanishes while the radial coupling factor takes the form

$$k_r = \left(\frac{r_s}{r_c}\right)^{\beta_e - 1} \left[\frac{2}{1 + (r_s/r_c)^{2\beta_e}}\right], \quad (r_o \equiv r_s), \qquad (3.59)$$

which obviously differs from zero. This behavior of k_r is quite consistent with deductions based on a field analysis, since the radial r-f electric field intensity is directed normal to the surface of the sole electrode and need <u>not</u> vanish at that boundary. In fact, the radial coupling factor may approach zero <u>only</u> when r_s approaches infinity, as a study of Eq. 3.59 reveals, because this is the <u>one</u> condition for which the radial r-f electric field intensity vanishes. It follows that the principal difference between k_r and k_θ lies in the nature of their radial variations.

These facts lend additional insight to the evaluation of Eq. 3.54, whose solution must be obtained before the derivation of the circuit equation can be completed. In view of the associated radial integration, the azimuthal coupling factor is only slightly altered by replacing r_o in Eq. D.6 with the general variable r. Upon making this change the expression for τ_1^* assumes the form

$$\tau_1^* = \int_{z=-\frac{h}{2}}^{z=\frac{h}{2}} \int_{r_o-\frac{\sigma}{2}}^{r_o+\frac{\sigma}{2}} \left(\frac{r}{r_c}\right)^{\beta_o-1} \left[\frac{1-(r_s/r)^{2\beta_o}}{1-(r_s/r_c)^{2\beta_o}}\right] \tau_1 \, dr \, dz \quad ,$$

$$= \frac{h\tau_1}{\beta_o r_c^{\beta_o-1}\left(1-(r_s/r_c)^{2\beta_o}\right)} \left[\left(r_o+\frac{\sigma}{2}\right)^{\beta_o} - \left(r_o-\frac{\sigma}{2}\right)^{\beta_o} + \frac{r_s^{2\beta_o}}{\left(r_o+\frac{\sigma}{2}\right)^{\beta_o}} - \frac{r_s^{2\beta_o}}{\left(r_o-\frac{\sigma}{2}\right)^{\beta_o}}\right], \quad (3.60)$$

where the radial and axial limits of integration have been replaced with their values at the extremities of the beam, since the integrals over the remaining regions are zero. The last result in the above equation also involves the assumption that the ring charge density of the electron stream is constant over its radial and axial extensions.

The radial width of the electron beam σ is known to be very small compared to the center-of-the-beam-electron radius r_o. Therefore, when

$$\frac{\sigma}{2r_o} \ll 1$$

the following approximations are found to hold:

$$\left(1+\frac{\sigma}{2r_o}\right)^{\pm\beta_o} \approx 1 \pm \frac{\beta_o\sigma}{2r_o} \quad , \quad (3.61)$$

$$\left(1-\frac{\sigma}{2r_o}\right)^{\pm\beta_o} \approx 1 \mp \frac{\beta_o\sigma}{2r_o} \quad . \quad (3.62)$$

These simplifications may be used in conjunction with Eq. 3.60 to obtain

$$\tau_1^* = \frac{h\tau_1}{\beta_o r_c^{\beta_o - 1}\left(1 - (r_s/r_c)^{2\beta_o}\right)}\left[r_o^{\beta_o}\left(1 + \frac{\beta_o\sigma}{2r_o}\right) - r_o^{\beta_o}\left(1 - \frac{\beta_o\sigma}{2r_o}\right)\right.$$

$$\left. + \left(\frac{r_s^2}{r_o}\right)^{\beta_o}\left\{\left(1 - \frac{\beta_o\sigma}{2r_o}\right) - \left(1 + \frac{\beta_o\sigma}{2r_o}\right)\right\}\right] ,$$

$$= \left(\frac{r_o}{r_c}\right)^{\beta_o - 1}\left[\frac{1 - (r_s/r_o)^{2\beta_o}}{1 - (r_s/r_c)^{2\beta_o}}\right] h\sigma\tau_1 = k_\theta h\sigma\tau_1 \quad . \qquad (3.63)$$

It is interesting to observe that the expression for k_θ given above is identical with the center-of-the-beam azimuthal coupling factor specified by Eq. D.6. It follows that, for ribbon beams whose radial width is a very small fraction of the center-of-beam-electron radius, the circuit fields essentially couple to the center of the radial dimension of the beam.

The ring charge density τ_1 can be related to the azimuthal component of r-f convection current by means of the continuity equation. Upon setting μ equal to zero in Eq. 3.31, so that the current is assumed to be localized to a ring of radius r_o, the desired expression becomes

$$\tau_1 = \frac{\beta i_\theta}{\omega r_o} \quad , \qquad (3.64)$$

in view of the fact that partial derivatives taken with respect to θ and time can be replaced by the $-j\beta$ and $j\omega$ operators, respectively. In addition, the appearance of μ in every term of Eq. 3.29 leads to the restriction that Eq. 3.64 is applicable only to the case in which the radial r-f convection current is zero. This assumption is consistent

with the fact that i_θ is ordinarily much larger than i_r. The preceding equation now takes the form

$$\tau_1^* = \left(\frac{k_\theta h \sigma \beta}{\omega r_o}\right) i_\theta \quad . \tag{3.65}$$

This expression can be used in conjunction with Eq. 3.53, after employing the differential operators

$$\frac{\partial f}{\partial \theta} = - j\beta f \quad ,$$

$$\frac{\partial f}{\partial t} = j\omega f \quad ,$$

$$\frac{\partial f}{\partial z} = - j\gamma f \quad ,$$

to obtain the relation between circuit voltage and the azimuthal current

$$V(z,\theta,t) = \left[\frac{v_{o,o} Z_{o,o} \omega \beta k_\theta}{\left(1 + \frac{v_{o,o}}{v_{o,1}} \frac{Z_{o,o}}{Z_{o,1}}\right)\omega^2 - \left(\frac{\beta v_{o,o}}{r_c}\right)^2 - \left(v_{o,o} v_{o,1} \frac{Z_{o,o}}{Z_{o,1}}\right)\gamma^2} \right] \frac{i_\theta}{r_o} \quad . \tag{3.66}$$

The final step involves the elimination of the azimuthal and axial wave phase velocities from the above expression. The electromagnetic analysis presented in Chapter II may be used to show that

$$v_{o,o} = \left(\frac{\omega r_c}{\beta_o}\right) \quad , \tag{3.67}$$

$$v_{o,1} = \left(\frac{\omega}{\gamma}\right) \quad . \tag{3.68}$$

These relations can be substituted into Eq. 3.66 to obtain the circuit equation

$$V(z,\theta,t) = \left[\frac{\beta_o \beta (k_\theta r_c / r_o) Z_{o,o}}{\beta_o^2 - \beta^2} \right] i_\theta \quad . \tag{3.69}$$

It will be convenient to define the "magnitude of the effective azimuthal interaction impedance" as

$$K \triangleq \left| \frac{k_\theta^2 r_c \, Z_{o,o}}{r_o} \right| \quad . \tag{3.70}$$

The sign of K is positive for forward-wave and negative for a backward-wave device, as explained in the opening paragraph of this section. Therefore, the general circuit equation applicable to both forward- and backward-wave devices may be written

$$V(z,\theta,t) = \pm \left[\frac{K\beta_o \beta}{\beta_o^2 - \beta^2} \right] \frac{i_\theta}{k_\theta} \quad . \tag{3.71}$$

The similarity of this relation to the corresponding forward- and backward-wave circuit equations of the O-type device is apparent[7].

3.8 The Determinantal Equation

The basic relations necessary for the derivation of the determinantal equation are the azimuthal ballistic equation, given by Eq. 3.48, and the circuit equation obtained above. Turning first to a consideration of Eq. 3.48, the azimuthal r-f electric field intensity must be replaced by the voltage $V(z,\theta,t)$. Since the circuit fields have been assumed to be excited primarily by the circular motion of the electron beam, the azimuthal r-f electric field intensity at the center of the beam is related to the circuit voltage according to the expression

$$E_\theta = \frac{-k_\theta}{r_o} \frac{\partial V(z,\theta,t)}{\partial \theta} ,$$

$$= \frac{j\beta k_\theta V(z,\theta,t)}{r_o} . \qquad (3.72)$$

This equation can be substituted into Eq. 3.48 to yield

$$i_\theta = \frac{-\eta \tau_o k_\theta}{\Omega_o r_o} \left[\frac{2\beta^2+\beta^2\beta_e(\beta_e-\beta)-F_o\beta^2(2\beta_e-\beta)+F_oQ\beta}{\beta(\beta_e-\beta)^3+\beta(\beta_e-\beta)(Q-2)+2Q} \right] V(z,\theta,t) . \qquad (3.73)$$

The azimuthal current and circuit voltage can be eliminated from Eqs. 3.71 and 3.73 so as to obtain the secular equation

$$\frac{\pm C^3}{\beta_o^2-\beta^2} \left[\frac{2\beta^3\beta_o+\beta^3\beta_o\beta_e(\beta_e-\beta)-\beta^3\beta_oF_o(2\beta_e-\beta)+F_oQ\beta^2\beta_o}{\beta(\beta_e-\beta)^3+\beta(\beta_e-\beta)(Q-2)+2Q} \right] = 1 , \qquad (3.74)$$

where the upper double-sign preceding C^3 applies to the forward-wave device and the lower sign applies to the backward-wave device. The quantity C is the "gain parameter" whose mathematical definition is

$$C^3 \triangleq K\left(\frac{-\eta\tau_o}{\Omega_o r_o}\right) , \qquad (3.75)$$

in which K is the magnitude of the effective azimuthal interaction impedance prescribed by Eq. 3.70. In view of Eqs. 3.8 and 3.27, the above result can be written

$$C^3 = \frac{KI_o}{2V_o} . \qquad (3.76)$$

Since the quantity

$$\frac{V_o}{I_o}$$

is recognized to be the "beam impedance" of the device[7], it follows that the cube of the gain parameter is equal to the effective interaction impedance divided by twice the beam impedance.

It is appropriate at this point to introduce the incremental propagation constants following the method of Pierce[7]. Thus, the expressions for the circular propagation constants in the presence and in the absence of the electron beam are defined as

$$\beta \triangleq \beta_e(1 + jC\delta) \quad , \tag{3.77}$$

$$\beta_o \triangleq \beta_e[1 + C(b \mp jd)] \quad , \tag{3.78}$$

where b = dimensionless electron injection velocity parameter (mathematically defined below),

d = dimensionless loss parameter of the E-type device,

δ = incremental propagation constant (mathematically defined below).

As with Eq. 3.71, the convention followed in Eq. 3.78 is that the upper double-sign preceding jd applies to the forward-wave device and the lower sign applies to the backward-wave device.

The electron injection velocity parameter b is given by the relation

$$b \triangleq \frac{1}{C}\left(\frac{v_o}{(v_1)_{r_o}} - 1\right) \quad , \tag{3.79}$$

where $(v_1)_{r_o}$ = linear tangential phase velocity of the r-f wave at r_o in the presence of the beam in meter/second*,

---

* In view of Eq. 2.14, this quantity is equal to

$$(v_1)_{r_o} = \omega r_o/\beta \quad ,$$

where ω is the electrical angular velocity of the r-f wave in electrical radian/second.

v_o = linear tangential velocity of the electron beam at r_o in meter/second.

A study of this relation shows that a positive value of b describes the condition for which the electron stream travels faster than the wave, while a negative value of b holds for the case that the beam travels more slowly than the wave. The condition that b = 0 describes the situation for which the spatial angular velocities of the circuit wave and the electron beam at radius r_o are in synchronism. The injection velocity parameter is one of the important independent variables whose magnitude exerts significant influence over the solutions of the determinantal equation.

The incremental propagation constant δ is defined as

$$\delta \triangleq x + jy \quad , \tag{3.80}$$

where x = real part of the incremental propagation constant,

y = imaginary part of the incremental propagation constant.

In view of the characteristic variations which all fields were found to possess in Chapter II, it follows that

$$e^{-j\beta_o\theta} = e^{-j\beta_e\theta(1+bC)} \cdot e^{\pm\beta_e C\theta d} \quad , \tag{3.81}$$

$$e^{-j\beta\theta} = e^{-j\beta_e\theta(1-Cy)} \cdot e^{\beta_e C\theta x} \quad . \tag{3.82}$$

An examination of these expressions shows that a positive value of x yields an exponentially increasing function of the spatial angle θ, associated with growing electromagnetic waves. A negative value of x is associated with waves whose amplitudes exponentially decay with

increasing spatial angle, while a zero value of x indicates the presence of unattenuated waves.

Upon setting x equal to zero, the remaining exponential in Eq. 3.82 leads to

$$\frac{\omega}{\Omega_{w1}} = \frac{\omega}{\Omega_o}(1-Cy) \quad , \tag{3.83}$$

where Ω_{w1} is the spatial angular velocity of r-f wave in the presence of the beam in spatial radian/second.

This relation follows directly from Eq. 3.36, and from the fact that the circular propagation constant in the presence of the beam is equal to the left member of the above equation. Inasmuch as

$$Cy \ll 1 \quad ,$$

the spatial angular velocity of the wave in the presence of the beam becomes

$$\Omega_{w1} = \Omega_o(1+Cy) \quad . \tag{3.84}$$

It is apparent from a study of this expression that $y > 0$ for a wave whose spatial angular velocity exceeds that of an electron at radius r_o, while $y < 0$ for a wave whose spatial angular velocity is less than that of an electron at radius r_o. The condition that y is exactly equal to zero describes the case of synchronism between the wave and electron spatial angular velocities at radius r_o.

The loss parameter d, which appears in Eqs. 3.78 and 3.81, is a pure numeric whose magnitude is either zero or positive, but never

negative. Following the aforementioned convention on the use of the double sign, the last factor in the right member of Eq. 3.81 always involves a negative exponent, whenever d is different from zero. Thus, θ is always a positive quantity for the forward-wave device and a negative quantity for the backward-wave device, so that

$$e^{\pm\beta_e C\theta d} \begin{matrix} < \\ = \end{matrix} 1$$

with the "equals" sign holding only in the special case that either θ or d vanishes.

The small perturbation character of the present analysis imposes certain limitations on the size of the incremental propagation constant and its associated real and imaginary parts. It is found, for example, that over the usual range of operating conditions the magnitude of x lies between 0.5 and 1.0, while the magnitude of y seldom exceeds 10. Likewise, the loss parameter d lies typically between zero and unity. The relative sizes of β_e, C and Q will receive further consideration when a discussion of the numerical results is presented.

The expressions for the circular propagation constants, given by Eqs. 3.77 and 3.78, may now be substituted into Eq. 3.74 to obtain, with a measurable degree of patience and determination,

$$\delta^6(\mp\beta_e^4C^6) + \delta^5(\pm j3\beta_e^4C^5) + \delta^4[C^8\beta_e^3(\beta_e-F_o)(b\mp jd)$$

$$+ C^7\beta_e^3(\beta_e-F_o) \mp C^6\beta_e^4(b\mp jd)^2 \mp 2C^5\beta_e^4(b\mp jd) \pm C^4\beta_e^2(2\beta_e^2+Q-2)]$$

$$+ \delta^3[jC^7\beta_e^2(2+2F_o\beta_e-3\beta_e^2)(b\mp jd) + jC^6\beta_e^2(2+2F_o\beta_e-3\beta_e^2) \pm jC^5\beta_e^4(b\mp jd)^2$$

$$\pm j2C^4\beta_e^4(b\mp jd) \mp j3C^3\beta_e^2(Q-2)] + \delta^2[C^6\beta_e(F_oQ+6\beta_e-3\beta_e^3)(b\mp jd)$$

$$+ C^5\beta_e(F_oQ+6\beta_e-3\beta_e^3) \pm C^4\beta_e^2(Q-2)(b\mp jd)^2 \pm 2C^3\beta_e^2(Q-2)(b\mp jd)$$

$$\pm 2C^2(Q-\beta_e^2(Q-2))] + \delta[jC^5\beta_e(\beta_e^3+2F_o\beta_e^2-6\beta_e-2F_oQ)(b\mp jd)$$

$$+ jC^4\beta_e(\beta_e^3+2F_o\beta_e^2-6\beta_e-2F_oQ) \mp jC^3\beta_e^2(Q-2)(b\mp jd)^2 \mp j2C^2\beta_e^2(Q-2)(b\mp jd)$$

$$\mp j4QC] + [C^4\beta_e(F_o\beta_e^2-2\beta_e-F_oQ)(b\mp jd) + C^3\beta_e(F_o\beta_e^2-2\beta_e-F_oQ)$$

$$\pm 2QC^2(b\mp jd)^2 \pm 4QC(b\mp jd)] = 0 \quad . \tag{3.85}$$

This is the general determinantal equation for E-type traveling-wave devices, in which the upper double-sign applies to the forward-wave device and the lower sign applies to the backward-wave device.

The determinantal equation has been programmed and solved on an IBM-704 digital computer. Extensive solutions of the forward-wave equation are presented in Appendix E, while the corresponding results for the backward-wave equation are given in Appendix G.

Although Eq. 3.85 is the most general expression for the small-signal determinantal equation of forward- and backward-wave E-type devices, its significance can be more readily appreciated through the

introduction of appropriate simplifications. In particular, it will be assumed that*

$$\beta_e \approx 50 \quad , \qquad d = Q = 0 \quad ,$$

$$C \approx 0.05 \quad , \qquad F_o = -1 \quad ,$$

so as to conform to the "reference conditions" discussed in Section 3.11. This choice of parameter values leads to an approximate expression for the determinantal equation having the form

$$\delta^6(\mp\beta_e^2C^4) + \delta^5(\pm j3\beta_e^2C^3) + \delta^4(\pm 2\beta_e^2C^2)(1-bC) \pm j\delta^3C[6+\beta_e^2Cb(2+bC)]$$

$$\pm 4\delta^2(1-bC) + j\delta[\beta_e^2C^2 \pm 2b(2+bC)] - \beta_eC(1+bC) \approx 0 \quad . \qquad (3.86)$$

It is interesting to observe that the presence of β_e in Eqs. 3.85 and 3.86 points to a fundamental difference between E- and O-type tubes, since no similar quantity arises in the determinantal equation of the latter device[7]. The influence which this parameter exerts over the behavior of the E-type performance characteristics will receive further attention in Section 3.11, where its physical consequences are examined in detail.

3.9 The Input Boundary Problem

In order to investigate the growing- and beating-wave gain characteristics of the forward-wave E-type device, as well as the start-oscillation conditions of the backward-wave device, it is necessary to

---

* The numerical values of β_e and C given here are assumed to designate the centers of the regions in which these parameters lie.

determine the initial wave amplitudes set up at the input boundary. The problem can be uniquely formulated only when as many constraints are imposed as there are waves to be matched at the entrance to the interaction region. Since the solution of the determinantal equation involves six roots, each of which may possess real and imaginary parts[3], a total of six waves are excited by an energy-carrying electron beam. Only four of these waves are found to be important, however, as a careful examination of the numerical results indicates.

It is therefore essential to prescribe only four independent conditions which must be satisfied at the input. These are:

1. The total circuit voltage applied at the input is equal to the sum of the circuit voltages associated with each wave.
2. The total azimuthal convection current is zero at the input.
3. The total azimuthal velocity variation of the electron beam is zero at the input.
4. The total radial variation of the electron beam is zero at the input.

Stated mathematically, these conditions become at $\theta = 0$ and $r = r_o$

$$\sum_{n=1}^{4} V_n = V_{RO} \quad , \tag{3.87}$$

$$\sum_{n=1}^{4} i_{\theta n} = 0 \quad , \tag{3.88}$$

$$\sum_{n=1}^{4} v_n = 0 \quad , \tag{3.89}$$

$$\sum_{n=1}^{4} \mu_n = 0 \quad , \tag{3.90}$$

where V_{RO} = total voltage applied to the r-f circuit at $\theta = 0$,

V_n = the amplitude of the circuit voltage of the nth wave at $\theta = 0$ and $r = r_o$ in volts,

$i_{\theta n}$ = the amplitude of the azimuthal convection current of the nth wave at $\theta = 0$ and $r = r_o$ in amperes,

ν_n = the amplitude of the azimuthal velocity perturbation of the nth wave at $\theta = 0$ and $r = r_o$ in spatial radians/second,

μ_n = the amplitude of the radial perturbation of the nth wave at $\theta = 0$ and $r = r_o$ in meters.

It is apparent that the summation over the four desired waves, as indicated in the above equations, must be carried out in such a manner as to exclude the remaining two. This is easily accomplished through appropriate programming instructions supplied to the computer.

The general form of the nth component of the above perturbation expressions can be obtained by substituting

$$\beta_n = \beta_e(1 + jC\delta_n) \qquad (n + 4 \equiv n) \quad , \tag{3.91}$$

into Eqs. 3.42, 3.43 and 3.73, thus yielding

$$i_{\theta n}\left(\frac{-\Omega_o r_o}{\eta \tau_o k_\theta \beta_e}\right) = C_{\theta n} V_n \quad , \tag{3.92}$$

$$\nu_n\left(\frac{-\Omega_o r_o^2}{\beta_e^2 \eta k_\theta}\right) = C_{\nu n} V_n \quad , \tag{3.93}$$

$$\mu_n \begin{pmatrix} -\Omega^2 r_o \\ \beta_e^2 \eta k_\theta \end{pmatrix} = C_{\mu n} V_n \quad , \tag{3.94}$$

where the coefficients $C_{\theta n}$, $C_{\nu n}$ and $C_{\mu n}$ are given by Eqs. 3.95-3.97, which appear on the following page.

The input boundary conditions, given by Eqs. 3.87-3.90, can now be expressed using these coefficients in the compact form of matrix algebra

$$\begin{Vmatrix} V_{RO} \\ 0 \\ 0 \\ 0 \end{Vmatrix} = \begin{Vmatrix} 1 & 1 & 1 & 1 \\ C_{\theta 1} & C_{\theta 2} & C_{\theta 3} & C_{\theta 4} \\ C_{\nu 1} & C_{\nu 2} & C_{\nu 3} & C_{\nu 4} \\ C_{\mu 1} & C_{\mu 2} & C_{\mu 3} & C_{\mu 4} \end{Vmatrix} \cdot \begin{Vmatrix} V_1 \\ V_2 \\ V_3 \\ V_4 \end{Vmatrix} \quad . \tag{3.98}$$

The inverse of the C-matrix leads to the desired set of initial wave amplitudes. Thus,

$$\begin{Vmatrix} \left(\frac{V_1}{V_{RO}}\right) \\ \left(\frac{V_2}{V_{RO}}\right) \\ \left(\frac{V_3}{V_{RO}}\right) \\ \left(\frac{V_4}{V_{RO}}\right) \end{Vmatrix} = \begin{Vmatrix} D_{11} & D_{12} & D_{13} & D_{14} \\ D_{21} & D_{22} & D_{23} & D_{24} \\ D_{31} & D_{32} & D_{33} & D_{34} \\ D_{41} & D_{42} & D_{43} & D_{44} \end{Vmatrix} \cdot \begin{Vmatrix} 1 \\ 0 \\ 0 \\ 0 \end{Vmatrix} \quad , \tag{3.99}$$

$$C_{\theta n} = \frac{\beta_e(2-F_o\beta_e)(1-C^2\delta_n^2)+2(\beta_e-F_o)(\beta_eC\delta_n)^2+QF_o+j\left\{2\beta_eC\delta_n(2-F_o\beta_e)+\beta_e^2C\delta_n(F_o-\beta_e)(1-C^2\delta_n^2)+QF_oC\delta_n\right\}}{Q\left\{2+(\beta_eC\delta_n)^2-j\beta_e^2C\delta_n\right\}-\left(2+(\beta_eC\delta_n)^2\right)\left\{(\beta_eC\delta_n)^2-j\beta_e^2C\delta_n\right\}}, \tag{3.95}$$

$$C_{\nu n} = \frac{\beta_eC\delta_n\left\{2C\delta_n\left(2-(\beta_eC\delta_n)^2\right)+2F_o\beta_eC\delta_n(1-C^2\delta_n^2)\right\}+QF_o(2C^2\delta_n^2-1)+j\left\{(\beta_eC\delta_n)^2+C^2\delta_n^2\left(2-(\beta_eC\delta_n)^2\right)+4F_o\beta_eC^2\delta_n^2-3QF_oC\delta_n-2\right\}}{\beta_e^3C^2\delta_n^2(1+jC\delta_n)\left(2+(\beta_eC\delta_n)^2\right)-Q\beta_eC\delta_n\left\{\beta_e^2C\delta_n+j\left(2+(\beta_eC\delta_n)^2\right)\right\}}, \tag{3.96}$$

$$C_{\mu n} = \frac{QF_o(1-C^2\delta_n^2)-\beta_eC^2\delta_n^2\left\{4+F_o\beta_e(1-C^2\delta_n^2)\right\}+j2C\delta_n\left\{QF_o+\beta_e-\beta_eC^2\delta_n^2(1+F_o\beta_e)\right\}}{\beta_e^3C^2\delta_n^2(1+jC\delta_n)\left(2+(\beta_eC\delta_n)^2\right)-Q\beta_eC\delta_n\left\{\beta_e^2C\delta_n+j\left(2+(\beta_eC\delta_n)^2\right)\right\}}. \tag{3.97}$$

so that

$$\begin{Vmatrix} D_{11} \\ D_{21} \\ D_{31} \\ D_{41} \end{Vmatrix} = \begin{Vmatrix} \left(\frac{V_1}{V_{RO}}\right) \\ \left(\frac{V_2}{V_{RO}}\right) \\ \left(\frac{V_3}{V_{RO}}\right) \\ \left(\frac{V_4}{V_{RO}}\right) \end{Vmatrix} . \qquad (3.100)$$

The D-matrix is the symbolic form of the desired inverse of the C-matrix, while the elements D_{11}, ..., D_{41} are the initial wave amplitudes appropriate to the stipulated boundary conditions. The real and imaginary parts of the D-elements are given by

$$D_{n1} = u_{n1} + jv_{n1} , \qquad (3.101)$$

where u_{n1} = real part of the initial amplitude of the nth wave,

v_{n1} = imaginary part of the initial amplitude of the nth wave.

The complexity of computer programming, and the required amount of machine time, can be significantly decreased by employing approximate forms of the coefficients $C_{\theta n}$, $C_{\nu n}$ and $C_{\mu n}$, suitable to the parameter ranges typically encountered. Upon making the assumption that

$$\beta_e \gg 1 , \quad F_o = -1 , \quad |\delta_n| \approx 1 ,$$

$$C \ll 1 , \quad Q \approx -2 ,$$

the expressions for the coefficients take the approximate form

$$C_{\theta n} = \frac{1-j\beta_e C\delta_n}{2Q+j\beta_e^2 C\delta_n\left[2-Q+(\beta_e C\delta_n)^2\right]} , \qquad (3.102)$$

$$C_{\nu n} = \frac{Q-2(\beta_e C\delta_n)^2+j\beta_e C\delta_n\left\{(\beta_e C\delta_n)^2-2\right\}}{\beta_e^3 C^2\delta_n^2\left[2-Q+(\beta_e C\delta_n)^2\right]} , \qquad (3.103)$$

$$C_{\mu n} = \frac{Q-(\beta_e C\delta_n)^2-j2\beta_e C\delta_n}{\beta_e^3 C^2\delta_n^2\left[2-Q+(\beta_e C\delta_n)^2\right]} . \qquad (3.104)$$

The relations given by Eqs. 3.102-3.104 have been programmed with the quantities β_e, C, Q, δ_n regarded as input data. The computation of these expressions, in conjunction with an associated matrix inversion sub-routine, leads to the initial wave amplitudes prescribed by Eqs. 3.100 and 3.101.

Finally, the initial wave amplitudes may be used to obtain the small-signal gain of the E-type device by means of the formula

$$\text{Gain (db)} = 10 \log_{10} \left| \sum_{n=1}^{4} \epsilon^{\Phi x_n} \left\{ u_{n1}\cos \Phi y_n - v_{n1}\sin \Phi y_n + j\left(v_{n1}\cos \Phi y_n + u_{n1}\sin \Phi y_n \right) \right\} \right|^2 , \qquad (3.105)$$

where $\Phi \triangleq \beta_e C\theta$ electrical radians,

θ = spatial angle in spatial radians.

The significance of the definition selected for the angle Φ can be understood from a study of the relations previously developed for β_e, b, and the spatial angular velocity of the r-f wave. Thus,

$$\Phi = 2\pi C \left(\frac{f\theta}{\Omega_o}\right) , \tag{3.106}$$

where f = frequency of the r-f wave in electrical cycles/second,

Ω_o = unperturbed spatial angular velocity of the center-of-the-beam electron in spatial radians/second.

The linear tangential velocity of the r-f wave at radius r_o, in the presence of the electron beam, is equal to

$$(v_1)_{r_o} = \Omega_{w1} r_o , \tag{3.107}$$

where Ω_{w1} is spatial angular velocity of the r-f wave in the presence of the beam. Upon substituting Eq. 3.107 into 3.79 it follows that

$$\Omega_o = \Omega_{w1}(1 + bC) , \tag{3.108}$$

since $v_o = \Omega_o r_o$. In addition, a fundamental relation for circularly-propagating waves has the form*

$$\Omega_{w1} = f\theta_g , \tag{3.109}$$

where θ_g is <u>spatial</u> "wave angle" corresponding to 2π <u>electrical radians</u> of the r-f wave in the presence of the beam.

---

* This expression is the circular analogue of the relation between phase velocity, frequency and wavelength of systems involving rectilinear electromagnetic propagation.

Finally, Eqs. 3.108 and 3.109 can be used in conjunction with Eq. 3.106 to obtain

$$\Phi = \beta_e C\theta \quad ,$$

$$= 2\pi C N_s \quad , \tag{3.110}$$

in which N_s is given by the general relation

$$N_s = N(1+bC)^{-1} \quad , \tag{3.111}$$

and

$$N = \theta/\theta_g \quad . \tag{3.112}$$

The quantity N therefore specifies the number of "wave angles" contained in a total spatial angle of θ radians. Clearly, the electrical angle Φ is proportional to the total number of wave angles along the r-f structure and to the gain parameter.

The same gain relation, given by Eq. 3.105, is employed in the study of both forward- and backward-wave devices. The details of its implementation in the solution of problems appropriate to each type of traveling-wave device are described more thoroughly in the following section pertaining to the computer program. Numerical results for the forward-wave device appear in Appendix F, while those of the backward-wave device are presented in Appendix H.

3.10 The Computer Program for the Small-Signal E-Type Device

The purpose of this section is to briefly describe the important features of the digital computer program for the small-signal E-type device. The program, which is written in the MAD (Michigan Algorithm

Decoder) computer language, is capable of treating the following classes of problems:

1. Computation of the incremental propagation constants of forward- and backward-wave E-type traveling-wave devices.
2. Computation of the initial wave amplitudes of forward- and backward-wave E-type traveling-wave devices.
3. Computation of the growing- and beating-wave gain of forward-wave E-type devices.
4. Computation of the gain and start-oscillation characteristics of backward-wave E-type devices.

The code name for this program is known as TWEET: Traveling-Wave Electrostatic E-Type. Although a flow diagram of the TWEET program is presented in Fig. 3.3, it must be emphasized that the configuration shown is greatly simplified so as to convey only the major divisions of computation involved in the processing of data.

The data supplied to the computer includes the parameters β_e, C, d and Q, with F_o set to -1, and the independent variables b and Φ. In addition, a binary instruction is provided to designate computation in either the forward- or backward-wave mode. All data except Φ are then used in computing the coefficients of the sixth-order determinantal equation polynomial. The roots of this equation are the real and imaginary parts of the desired incremental propagation constants. Although all six propagation constants are read out as part of the problem solution, only the four sets known to be important in affecting the input match are retained in computing the coefficients $C_{\theta n}$, $C_{\nu n}$ and $C_{\mu n}$

If the initial decision involved the forward-wave problem, the gain is obtained by supplying the independent variable Φ and the four

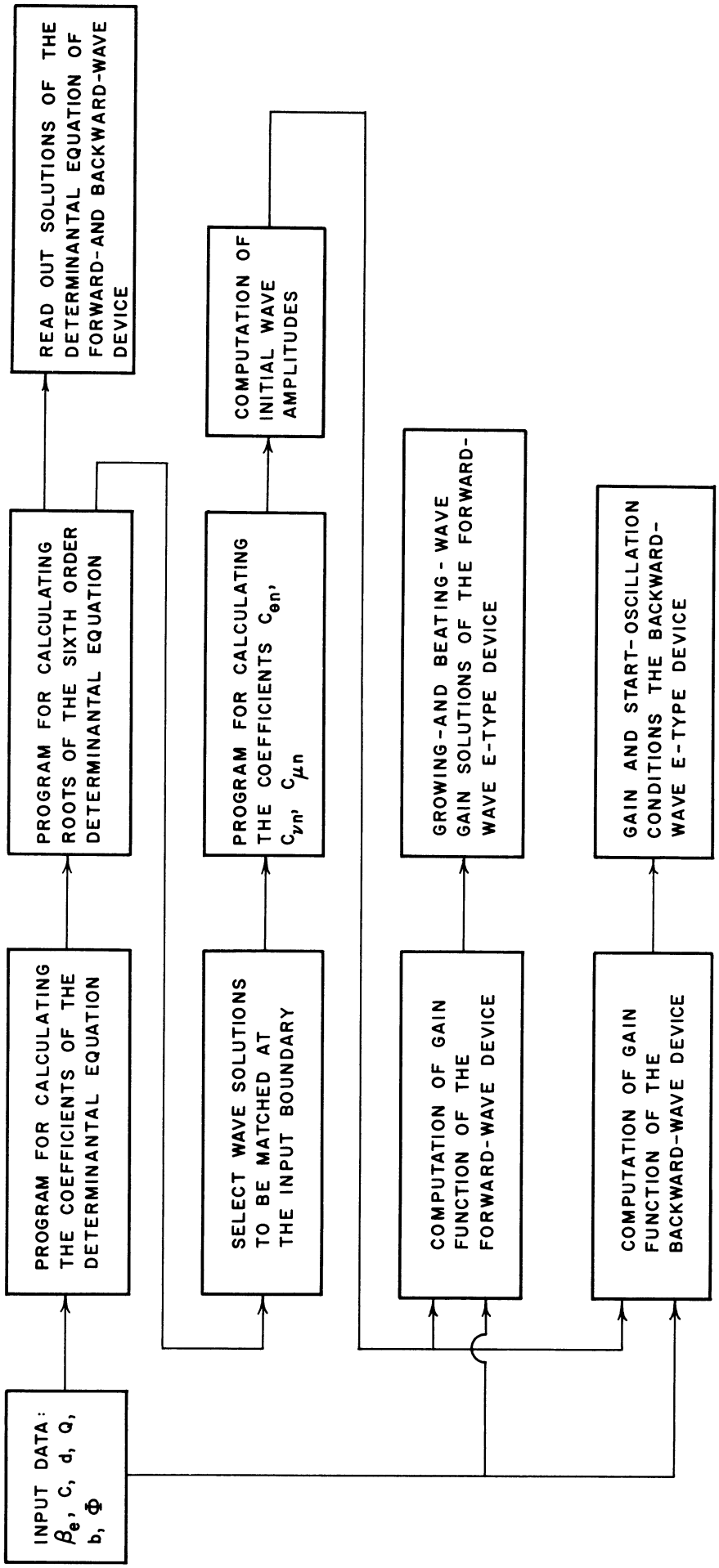

FIG. 3.3 THE FLOW DIAGRAM FOR THE TWEET PROGRAM.

sets of initial wave amplitudes to the appropriate gain computation. The output then represents the gain in terms of the electrical angle Φ, the parameters β_e, C, d, Q and the independent variable b. If the initial decision involved the backward-wave device, its gain is found by supplying similar information to the proper computation function. Since backward-wave gain is known to result from beating of the separate waves[7], such a gain-versus-angle plot may be expected to exhibit the customary cyclical variation.

The start-oscillation condition may be thought of in terms of a backward-wave amplifier possessing infinite gain. The solution of this problem differs from the simpler case described above, however, because only particular choices of the independent variables b and Φ leads to infinite values of backward-wave gain.

3.11 Interpretation of the Results

The graphical representation of the digital computations appearing in Appendices E-H constitute the solution to the small-signal E-type forward- and backward-wave devices. The extremely wide range of device parameters over which these results have been examined has shed considerable light on those conditions that may reasonably be expected to prevail in a working model of this electron beam tube.

3.11.1 The Forward-Wave Propagation Constants. The real and imaginary parts of the incremental propagation constants of the small-signal forward-wave E-type device are presented in Appendix E. A study of Fig. E.1 reveals that in the absence of loss and space charge, for which $Q = d = 0$, the real parts possess a dependency on the relative electron injection velocity parameter b that resembles the one found in

O-type devices[7]. Thus x_1, which is greater than zero, is associated with the wave that exponentially increases with increasing spatial angle, while x_2 is associated with the exponentially decreasing wave. Some unusual features of the E-type device are apparent, however, from a close inspection of the computed results.

It may be noted that for the arbitrarily selected "reference conditions"

$$\beta_e = 50 \quad , \quad d = 0 \quad , \quad (x_1)_{max} = 0.6234 \quad ,$$

$$C = 0.05 \quad , \quad Q = 0 \quad ,$$

the maximum value of x_1, which occurs when the spatial angular velocity of the electron beam and the r-f wave are in synchronism, is smaller than for the corresponding conditions

$$C = 0.05 \quad , \quad d = 0 \quad ,$$

$$QC = 0 \quad , \quad (x_1)_{max} = 0.88768 \quad ,$$

of the O-type device[7]. Since the (positive) real part of the incremental propagation constant is a measure of the "gain rate", or gain per unit spatial angle, it is reasonable to conclude that under comparable conditions the growing-wave gain of the E-type device is likely to be less than that of the O-type. It is essential to emphasize, however, that this assertion is valid only when made in regard to a specific set of β_e values. An increase of β_e, with all other parameters held fixed, leads to a maximum value of x_1 for the E-type device which more nearly approaches that of O-type, as an inspection of Fig. E.10 reveals. This peculiar characteristic that causes the gain of the E-type device to depend upon the magnitude of β_e will receive considerable attention later.

Further comparison indicates that whereas x_1 and x_2 asymptotically approach zero as b decreases beyond bound for the O-type device possessing no loss or space charge, the results obtained here show that x_1 and x_2 always vanish for a finite, negative value of b. It follows that, even in the absence of loss and space charge, there exists a "low velocity limit" for the electron stream in E-type devices below which growing-wave gain cannot exist. The customary "high velocity limit" is clearly in evidence since x_1 and x_2 vanish for a finite, positive value of b. This property closely parallels the comparable behavior of the O-type device.

The associated imaginary parts of the incremental propagation constants are presented in Figs. E.2-E.7. The "cold-circuit wave phase velocity" appearing in these graphs can be verified mathematically in the following manner. The relative injection velocity parameter, defined by Eq. 3.79, may alternatively be written in the form

$$b = \frac{1}{C}\left(\frac{\Omega_o}{\Omega_{w1}} - 1\right) , \tag{3.113}$$

since

$$v_o = \Omega_o r_o ,$$

and

$$(v_1)_{r_o} = \Omega_{w1} r_o .$$

Furthermore, the expression for the imaginary part of the incremental propagation constant may be obtained from Eq. 3.83

$$-y = \frac{1}{C}\left(\frac{\Omega_o}{\Omega_{w1}} - 1\right) . \tag{3.114}$$

A comparison of Eqs. 3.113 and 3.114 shows that

$$y = -b \quad , \tag{3.115}$$

from which it is apparent that the cold-circuit wave phase velocity must be a straight line function passing through the origin of the y-b coordinate system at an angle of -45 degrees.

The designation of the incremental propagation constants has been made in such a manner as to facilitate comparisons with corresponding solutions to the O-type determinantal equation. Thus, y_1 and y_2 resemble their O-type counterparts (some differences are also in evidence, as will be subsequently explained) as do their corresponding real parts x_1 and x_2, respectively. Moreover, the wave identified with the imaginary part y_3 exhibits the identical behavior in E-type as that of O-type devices, although the one associated with y_4 shows no similarity to corresponding phenomena in O-type tubes. It will also be noted that only four of the six sets of incremental propagation constants are presented in these diagrams. An extremely wide range of digital computer results have shown that, under all circumstances applicable to both forward- and backward-wave devices, the remaining two incremental propagation constants are accurately given by

$$\delta_5 = j\left(\frac{1}{C}\right) \quad , \tag{3.116}$$

$$\delta_6 = \pm d + j\left(b + \frac{2}{C}\right) \quad , \tag{3.117}$$

where the upper double-sign preceding d in the last relation applies to the forward-wave device, and the lower sign applies to the backward-wave device. Upon substituting these expressions into Eq. 3.77 the

azimuthal propagation constants in the presence of the electron stream become

$$\beta_5 = \beta_e \left[1 + jC \left(\frac{j}{C} \right) \right] ,$$

$$= 0 , \qquad (3.118)$$

$$\beta_6 = \beta_e \left[1 + jC \left\{ \pm d + j \left(b + \frac{2}{C} \right) \right\} \right] ,$$

$$= - \beta_e (1 + bC \mp jCd) . \qquad (3.119)$$

In view of the known azimuthal variation of all fields in the presence of the beam

$$e^{\mp j\beta\theta} ,$$

these results lead to interesting conclusions. The fact that β_5 is zero implies that the wave associated with the incremental propagation constant δ_5 possesses no azimuthally-oriented propagation and is thus constrained to exhibit only radial motion, if any (no assertations can be made in regard to its axial motion since the analysis has been restricted to a two dimensional treatment, as explained in the opening sections of this chapter). It has accordingly become convenient to designate this as the "radial wave".

A study of Eq. 3.119 shows that the wave associated with the incremental propagation constant δ_6 possesses an azimuthal phase delay that numerically increases in the direction <u>opposite</u> to the remaining four waves exhibiting azimuthal propagation. This wave, which arises on the r-f circuit from the charge-induction fields of the electron beam,

is identified* as the "backward wave". It is essential to have a clear conception of the term "backward wave" used here, so that it may readily be distinguished from the phenomena occurring in backward-wave devices. The latter designation applies to that negative dispersion property of the slow-wave circuit by virtue of which the wave phase and group velocities are oppositely directed. Inasmuch as both the radial and backward waves are far out of synchronism with the spatial angular velocity of the beam, these disturbances are excited to a negligible extent as compared to the remaining waves and may therefore be dropped from further consideration.

Turning now to a detailed investigation of the imaginary parts of the incremental propagation constants, a study of Figs. E.1 and E.2 shows that y_1 and y_2 possess the same value over the range of b for which x_1 and x_2 differ from zero. For values of b lying beyond this interval, y_1 and y_2 assume separate and distinct values. At large negative values of b, in the region where the real parts of the propagation constants vanish, y_1 approaches zero while y_2 approaches the complex conjugate of y_4. The significance of a vanishing value of y_1 can be inferred from a study of Eq. 3.114 which yields

$$\Omega_{w1} = \Omega_o \quad ,$$

so that the angular velocity of the associated wave approaches that of the electron beam. Disturbances of this character which propatate along the electron stream are known[7] as "space-charge waves".

---

* The reader is especially cautioned <u>not</u> to regard the source of this wave as arising from reflections occurring at a mismatched output transducer. The wave actually results from the negative azimuthal propagation predicted by the "second solution" of the one-dimensional wave equation (the θ-dimension). It therefore appears regardless of the state of the output match, although reflections may contribute additional components.

Inasmuch as Eq. 3.114 reveals that y is positive for a wave whose spatial angular velocity is greater than the unperturbed velocity of the electron stream, and negative for a wave whose spatial angular velocity is less than that of the beam, it follows that y_2 is a "fast" and y_4 is a "slow" space-charge wave. By the same reasoning, y_1 is a "synchronous" space-charge wave. Thus, in the range of large negative values of b, for which the electron stream spatial angular velocity is much less than that of an undisturbed circuit wave, three space-charge waves exist. One of these possesses the same spatial angular velocity as the unperturbed electron stream, and the remaining two represent disturbances traveling slightly faster and slower than the beam. In this same range of b values the phase velocity of the wave identified with the imaginary part of the incremental propagation constant y_3 asymptotically approaches the cold-circuit wave phase velocity line shown in Fig. E.2. This "circuit wave" character, which y_3 thus acquires, is a basic property of the wave that propagates on the r-f structure, with a modification resulting from the nonsynchronous beam[7].

At sufficiently large positive values of b, for which the real parts of the incremental propagation constants vanish, the imaginary part y_2 approaches -b, while y_4 approaches zero. A careful study of the graphical results also shows that y_3 and y_1 not only become complex conjugates, but in addition they asymptotically approach the same positive and negative values as do y_2 and y_4 at large negative values of b. Thus, y_3 and y_1 are the fast and slow space-charge waves and y_2 is the circuit wave in the range of b for which the spatial angular velocity of the beam is much greater than that of the r-f wave. In this case y_4 becomes the synchronous space-charge wave, whose spatial angular velocity

approaches coincidence with the beam. The consistency of this basic behavior is evident from a study of all curves for which the loss parameter d vanishes. Before proceeding with an examination of the specific modifications produced by the parameters β_e, C and Q, however, it is appropriate to consider the significance of these results in light of other traveling-wave devices.

Although these solutions bear a resemblance to the O-type incremental propagation constants, several features distinguish the present results. The most important of these pertain to the behavior of the real and imaginary parts of the incremental propagation constants in the range of negative b values. The fact that there always exists a low velocity limit for the spatial angular velocity of the electron beam, below which growing-wave gain cannot occur in the absence of space charge, is a property more closely related to M- than O-type devices. It must be emphasized, however, that this and subsequent comparisons are valid only when thin, nonslipping-stream beams are considered, since the incremental propagation constants of M-type devices undergo marked changes when slipping-stream motion exists. Moreover, the analysis of E-type devices presented in this dissertation is rigorously correct only for thin beams, as explained in the opening sections of the chapter.

The second characteristic of the present results which resembles the behavior of M-type devices is the fact that, over a portion of the range of b for which x_1 and x_2 differ from zero, the imaginary parts y_1 and y_2 are greater than zero. Within this range of relative injection velocity values the growing- and declining-waves travel faster than the electron beam which creates them. In the absence of space charge no

such property is associated with the operation of O-type devices[7] although it occurs in M-type tubes.

While these observations reveal a distinct similarity between E- and M-type devices, final judgment concerning the proper classification of E-type traveling-wave tubes must be reserved until radial and azimuthal energy exchanges are studied in the next section of this chapter. Furthermore, the E-type device appears to have distinctive properties all its own. Some of these will become apparent from the ensuing discussion, but the existence of y_4 can be cited at this point. It is unlikely that this slow space-charge wave, whose azimuthal velocity approaches the spatial angular velocity of the electron beam at large positive values of b, is produced by purely azimuthal interactions, since no similar wave is found in O-type devices. Such a wave might result from the azimuthally-periodic character of the radial r-f fields, or from the combined effects of the radial and azimuthal r-f fields. The complexity of the mathematics makes it rather difficult to distinguish which of these sources account for its origin. Nevertheless, the presence of this wave gives rise to three space-charge waves at the extremes of the velocity range, rather than the customary two of O-type devices.

Upon returning to a consideration of the specific modifications of the incremental propagation constants produced changes of β_e, C, Q and d, attention will first be devoted to a study of the space-charge parameter. It should be noted that a nonzero value of Q refers to the condition in which the a-c space-charge field of the beam alters the waves propagating in the interaction region. A vanishing value of the space-charge parameter implies that energy transformations between the

electron beam and the r-f wave are being examined under the condition that the fields of the beam do not alter these energy exchanges.

The fact that the space-charge parameter is a negative quantity, according to Eq. 3.41, is in contrast to the O-type device[7], where the comparable QC parameter is always positive. Moreover, Pantell obtained a negative expression for the space-charge parameter associated with the helitron backward-wave oscillator[24]. The physical interpretation of this sign change points to another distinction between E- and O-type traveling-wave tubes.

An electron subjected to the linear motion encountered in O-type tubes is accelerated in a direction opposite to that of the applied electric field, so that space-charge forces tend to debunch such an electron stream. However, the circular motion of the beam in E-type devices is such that an azimuthal space-charge field, which tends to decelerate an electron and thereby decrease its radius of rotation, results in an increase in the electron's spatial angular velocity*. Thus, the azimuthal acceleration of an electrostatically-focused electron is in the same direction as the azimuthal electric field, so that space-charge forces tend to increase bunching in the beam of E-type tubes. As compared to the O-type device, this behavior may be likened to rectilinear motion of a hypothetical particle possessing either positive charge or negative mass.

The most significant effects produced by a small increase in the space-charge parameter are a reduction of the maximum value of x_1,

---

* This point is treated more thoroughly in Section 3.13.1, where it is shown that the spatial angular velocity of the particle must increase with decreasing radius, if equilibrium between the centrifugal and radial electric field forces is to be preserved.

occurring near b = 0, and a decrease in the negative value of b for which growing-wave gain ceases (which occurs at x = 0). Thus, a comparison of the solutions for Q = 0 and Q = -0.20 in Fig. E.1 reveals that the same overall shape of the x-versus-b curve is retained. A study of Figs. E.2 and E.3 shows that the positive value which y_2 approaches at large negative values of b, and y_3 approaches at large positive values of b, increases with space charge. The negative value which y_4 and y_1 approach at large negative and positive values of b, likewise, increases under these circumstances. It follows that the velocities of the fast and slow space-charge waves depart further from the beam angular velocity as Q assumes increasing negative values.

Further increases in the magnitude of Q lead to rather marked changes in the x-versus-b curve, as Fig. E.1 reveals. Not only does the negative value of b for which growing-wave gain ceases become smaller, but the maximum value of x_1, near b = 0, also decreases significantly. This is clearly shown in the solutions for Q = -2 and Q = -3. The maximum positive value of b for which growing-wave gain ceases is also observed to increase with more negative values of Q. The most interesting feature of these results, however, is associated with the "pattern dimpling" occurring in the region near b = 0. The progressive increase in the size of the dimples with increasing Q eventually leads to "pattern splitting", such that two "islands" of growing-wave gain may be identified with the solutions for Q = -15. It will be noted that, under all circumstances involving large negative values of Q, the x-versus-b curve shrinks about the origin after reaching a maximum value slightly to the left of b = 0. The portion of this curve lying to the right of the origin, which arises out of the splitting behavior, is

initially large and closely situated to the region surrounding the origin. Additional increases of Q not only result in a reduction of the x-versus-b curve near b = 0, but also, a reduction in the height and width of the separated elliptical portion on the right. Simultaneously, this separated ellipse moves out along the b-axis, finally diminishing to a single point as Q approaches minus infinity. In the presence of intense space-charge fields E-type devices are thus charac terized by islands of growing-wave gain, for which the real parts of the incremental propagation constants differ from zero, separated by regions where the real parts vanish. This is a distinctive property not found in either M- or O-type traveling-wave tubes[7].

The variation of the real parts of the incremental propagation constants acquires further significance when the imaginary parts, presented in Figs. E.2-E.7, are examined. At relatively small values of Q the intersection of the curve y_4 with the common curve y_1, y_2 is nearly perpendicular, as Figs. E.2-E.4 show. However, successive increases in Q cause the portion of the y_4-curve to the left of the vertical axis to move downward, while the portion to the right moves upward. In addition, Figs. E.5 and E.6 show that the slope of the y_4-curve approaches that of y_1, y_2 in the region of intersection, as the space-charge parameter increases. Upon studying Fig. E.1 carefully, it is found that this is precisely the range of b values for which dimpling becomes pronounced. Still larger values of Q lead to separate intervals where y_1 and y_2, and then y_2 and y_4, have common values, as shown in Fig. E.7. Each of these "common value ranges" is associated with nonvanishing real parts, where the pattern splitting phenomena of Fig. E.1 is observed. It should also be noted that the positions of y_1 and

y_4 interchange in the region to the right of the vertical axis when intense space-charge fields are present.

It is important to emphasize that the overall behavior of the incremental propagation constants do not result from the absolute size and change of a given tube parameter, such as β_e, C, d or Q, but rather from its size and change in relation to the remaining parameters. This fact may be appreciated from a study of Figs. E.16-E.22 where the propagation constants are examined over the same range of Q values with β_e and d unchanged, but with the size of C doubled. In the absence of space charge the maximum value of x_1 now increases, as a comparison of Figs. E.1 and E.16 reveals. Furthermore, the range over which growing-wave gain exists now extends to larger negative values of b. Although the curves possess the same general shape as in the case of C = 0.05, no pattern slipping can be found in Fig. E.16, and dimpling occurs only for the largest negative value of Q appearing in that graph. The intensity of the space-charge field necessary to produce complete separation of the pattern into two regions of growing-wave gain is quite large, indeed, for C = 0.10.

A study of the imaginary parts, presented in Figs. E.17-E.22, provides some indication of the differences in the behavior of the propagation constants produced by changes of the gain parameter C. An examination of Figs. E.2 and E.17 shows that as C is increased the curves y_1, y_2 and y_4 move toward the b-axis in the range of negative b values, while the curves y_1, y_3 and y_4 move toward the same axis in the range of positive b values. An increase in Q causes these curves to move away from this axis again, but even when Q = -15 (and C = 0.10) the departure is only about half of that found for the same value of Q when C = 0.05.

Accordingly, the velocity of the fast and slow space-charge waves more nearly approaches the spatial angular velocity of the electron beam as C is increased for a fixed value of Q. Conversely, the velocity of these space-charge waves departs further from the beam velocity as the magnitude of Q is increased while C is held fixed. It follows, therefore, that the slope of the y_4-curve in Figs. E.17-E.22 never quite approaches that of y_1, y_2 in the region of their intersection, for the range of Q values plotted. The pattern splitting found in Fig. E.1 is consequently not observed in Fig. E.16, where the size of the gain parameter has been doubled.

Although these results indicate the manner in which the propagation constants depend upon the parameters Q and C, the same curves may be used to describe the effects produced by changes of the gain parameter alone. A comparison of Figs. E.1 and E.16 (for the case that Q = 0) with Fig. E.8 reveals that the pattern splitting behavior observed with large values of Q also occurs with very small values of C. Thus, when C is reduced to 0.01 the x-versus-b curve divides into two elliptical shaped regions, one of which surrounds the origin and the other situated along the positive b-axis. As C approaches zero the stationary portion collapses to a single point at the origin, while the ellipse lying on the positive b-axis simultaneously shrinks and moves outward, finally vanishing to a single point at infinity. The behavior of the y_1, y_2- and y_4-curves in the region of common values of y_1 and y_2, and of y_2 and y_4, is similar for the small C and large Q cases, as a study of Figs. E.7 and E.9 shows. Likewise, the spatial angular velocity of the fast and slow space-charge waves departs further from the beam velocity as the gain parameter C is reduced in size.

It is interesting to observe that in addition to this novel pattern splitting behavior, which appears to be uniquely associated with E-type devices, its existence always results in a maximum value of x_1 (associated with the ellipse surrounding the origin) at $b = 0$. It follows that, under pattern splitting conditions, the growing-wave gain will always attain one of its maximum values, as a function of b, when the spatial angular velocity of the r-f wave is in synchronism with the electron beam. The relation between the spatial angular velocities of the electron beam and the r-f wave necessary to attain the second growing-wave gain maximum depends upon the location of the separated ellipse along the positive b-axis.

In addition to the pattern splitting behavior occurring at small values of C and large negative values of Q, the E-type device possesses another unusual property. A study of Figs. E.10-E.15, and E.23-E.25, shows that the small-signal incremental propagation constants also depend upon the size of the circular propagation constant of the electron beam β_e. The size of $(x_1)_{max}$ and the negative value of b at which the real parts vanish are observed to increase with β_e, as an examination of the curves $\beta_e = 75$ in Fig. E.10, and $Q = 0$ in Fig. E.1, reveals. Furthermore, Figs. E.10 and E.13 show that the x-versus-b curve undergoes pattern dimpling, and finally splitting, when β_e decreases. The separation of the real parts into two elliptical shaped regions, one of which surrounds the origin and the other situated along the positive b-axis, is much like that existing in the presence of large Q and small C. The general behavior of the imaginary parts of the incremental propagation constants also follows the trend previously noted when pattern splitting of the real parts occurs. Thus, Figs. E.11, E.12, E.14 and E.15 show

that the velocity of the fast and slow space-charge waves departs further from the spatial angular velocity of the electron beam as β_e is made smaller. The regions of b where y_1 and y_2, and then y_2 and y_4, have common values are shown clearly by these curves.

The fact that the propagation constants do not depend upon the absolute size and change of β_e but, instead, upon its size and change in relation to the remaining parameters is brought out by a study of Figs. E.23-E.25. No pattern dimpling of the x-versus-b curve occurs for $\beta_e = 25$ and $C = 0.10$, although it is clearly in evidence for $\beta_e = 25$ and $C = 0.05$ as noted above. When β_e is reduced to 5, however, the change is large enough to produce complete splitting even for $C = 0.10$. Nevertheless, Figs. E.13 and E.23 show that the maximum value of x_1 for the two ellipses is larger, and the separation between the ellipses is smaller, when C is doubled in magnitude (with $\beta_e = 5$). The behavior of the imaginary parts of the incremental propagation constants in the presence and absence of splitting, with large C, follows the foregoing trend, as Figs. E.24 and E.25 reveal.

Although the exact nature of the control exerted over the incremental propagation constants by the space-charge and gain parameters is somewhat different as compared to O-type devices, the general condition is satisfied that the growing-wave gain is degraded by an increase in (the negative value of) Q and a reduction of C. While other types of traveling-wave tubes exhibit comparable properties, apparently the E-type device is the only one whose gain depends on β_e. It is appropriate, therefore, to examine its specific consequences.

Since a study of Eq. 3.78 shows that β_e ordinarily differs from β_o by a small amount, then β_e is very nearly equal to the number of

"leaves" of the Riemann surface associated with the azimuthal wave propagation explained in Chapter II. Accordingly, the condition that β_e must be sufficiently large to produce a desired amount of growing-wave gain in a given spatial angle (which follows from the analysis of the present chapter) is equivalent to the requirement that many leaves of the surface should be encountered during azimuthal propagation.

The dependence of the growing-wave gain upon the size of β_e acquires further significance when this parameter is related to the physical dimensions of the system geometry. Thus, Eq. 3.36 may be written in the alternative form

$$\beta_e = \pi\sqrt{\frac{2}{\eta}}\left(\frac{fr_o}{\sqrt{V_o}}\right) \text{ electrical radian/spatial radian} \quad . \qquad (3.120)$$

This relation shows that β_e can be increased by an increase in the operating frequency or the radius of the center-of-the-beam electron, or by a decrease in the beam potential. Attempts to raise β_e through an increase in frequency or a decrease in beam potential are not considered as desirable methods of control, since the lowest operating frequency and largest power output are restricted by these prerogatives. Customarily, the designer prefers to set these specifications on the basis of the intended application of the device.

The only remaining method of increasing β_e, then, involves the use of a tube employing a large center-of-the-beam-electron radius*.

---

* It is essential to observe that this change of beam radius requires a corresponding change of circuit radius in order to preserve the beam-to-circuit coupling. If this precaution is not observed, the gain parameter may be so reduced by a decrease of coupling as to seriously degrade the gain of the device.

However, it has been shown by Waters[35] that a ribbon-shaped electron beam requires very critical launching conditions at the entrance to the interaction region as the center-of-the-beam radius is made larger. Under typical operating conditions, stable motion of the electron stream in the interaction region can only be obtained when relatively small beam radii are employed. The designer is thus confronted with the conflicting requirements of maintaining a small beam radius in order to insure stable electron motion and, simultaneously, using a radius sufficiently large to provide adequate growing-wave gain. It is essential to emphasize that this control which β_e (and therefore the beam radius) exerts over the growing-wave gain of the E-type device is far more subtle than the simple fact that a larger circuit radius provides a greater length of arc on which more turns of a helix can be wound (assuming that the flattened helix is being used), so that a greater electrical length is contained in the same spatial angle. Much more important is the consideration that β_e exerts a control over x_1, which is proportional to the gain per unit spatial angle, that is very similar to the gain parameter C. Thus, an extremely small center-of-the-beam-electron radius in E-type devices leads to a degradation of growing-wave gain that can be compared to the use of a very small gain parameter. These facts are strongly in evidence from a study of the graphical results presented in Appendices E and F.

Since these considerations show that the upper limit on the size of β_e, and therefore the gain per unit spatial angle, is controlled chiefly by the required stability of the beam, a large overall gain appears to be attainable in only two possible ways:

1. A relatively small center-of-the-beam-electron radius can be employed to insure stable electron motion, but the device could be constructed as an azimuthally re-entrant system so as to permit the ribbon-shaped helical beam to drift axially. Adequate gain could then be achieved by allowing the beam to execute a large number of spatial cycles as it advances parallel to the axis of the system. This idea is embodied in the helitron[24,31,38], in the invention of Pantell[23], and in the device proposed in the closing section of Chapter II.
2. It may be possible to achieve a large overall gain in an azimuthally nonre-entrant E-type device by retaining the same basic geometry as in Fig. 1.1. Since this would require the use of a large value of β_e, and beam radius, it becomes necessary to provide some means for stabilizing the beam. One method might involve the use of a "segmented sole", whose adjacent segments are connected to different values of d-c voltage. The purpose of this embodiment, which resembles as O-type periodic-electrostatically-focused device deformed into a circle, is to provide a "periodic perturbation" on the circular motion of the beam and thereby obtain the needed control.

The determinantal equation solutions for the condition that loss exists in the absence of space charge are presented in Figs. E.26-E.29, where d has the values of 0.25 and 0.50. A study of the imaginary parts appearing in Figs. E.27 and E.29 shows that the general shapes of these curves are very similar to their counterparts in the lossless case of Fig. E.2. Moreover, these propagation constants undergo only a relatively

small change when the loss is increased from 0.25 to 0.50, as a comparison of Figs. E.27 and E.29 shows. The only notable exception appears to be the fact that, in the presence of loss, the functions y_1 and y_2 do not collapse to a single curve in a small region around the origin.

It is primarily the real parts of the incremental propagation constants that undergo significant changes when finite loss exists, as a study of Figs. E.1, E.26 and E.28 reveals. In this case the real parts no longer form a closed curve symmetrical about the b-axis but, instead, take the shape appearing in Figs. E.26 and E.28. Furthermore, the waves associated with the propagation constants δ_3 and δ_4 now possess the real parts x_3 and x_4, respectively. A study of Eq. 3.117 shows that the wave associated with the propagation constant δ_6 acquires an unvarying real part, whose magnitude is equal to d, in the presence of loss. The radial wave possesses no attenuation, even in the presence of loss, as Eq. 3.116 shows. This is to be expected owing to its absence of azimuthal motion.

An examination of Fig. E.1 (for the case that Q = 0) and Figs. E.26 and E.28 shows that loss reduces the maximum (positive) value of x_1 and increases the maximum (negative) value of x_2. Thus, the gain of the increasing wave is reduced, while the attenuation of the decreasing wave is increased. In addition, the wave associated with δ_3, that is unattenuated in the lossless case, now decreases with increasing spatial angle. Although these characteristics resemble phenomena found in O-type devices[7], the E-type traveling-wave tube possesses the unusual feature that the wave associated with δ_4 has a positive real part. This

implies that the addition of loss produces a growing-wave component not present when d = 0.

It is interesting to observe that the magnitudes of the maximum values of x_1 and x_2 occur near b = 0 where the spatial angular velocity of the electron beam and the r-f wave are in synchronism. Thus, the largest value of growing-wave gain should occur in this region for a specified value of loss. The gain component contributed by x_4, however, attains its largest value near b = 1, where the spatial angular velocity of the beam exceeds that of the r-f wave. In spite of the increase of x_4 with loss the overall gain decreases owing to the large changes of x_1 and x_2, as the curves presented in Appendix F reveal. At large values of b the attenuation of the circuit wave (given by x_3 at negative values of b, and by x_2 at positive values of b) approaches the attenuation in the absence of the beam, while the attenuation of the remaining waves vanishes.

The effect of introducing loss and space charge, simultaneously, may be determined from a study of Figs. E.30-E.33. While the general configuration of the real and imaginary parts of the propagation constants are similar to the corresponding curves involving loss but no space charge, certain obvious changes may be observed. The curve y_4, for example, becomes more nearly straight and parallel to the b-axis with increasing space charge, as Figs. E.31 and E.33 show. Furthermore, y_4 is displaced further downward and y_2 is displaced further upward at large negative values of b. At large positive values of b the curve y_3 is displaced further upward, equal in magnitude to the displacement of y_4. Since the displacement is the same in both figures, where the space charge is held fixed and the loss is permitted to vary, the

velocity of the fast and slow space-charge waves appears to depend upon the magnitude of Q, but not upon d. A comparison of these graphs with Fig. E.6, where Q has the same value as Figs. E.31 and E.33, but d = 0, supports this assertion. Inasmuch as y_1 is very nearly zero over a large range of b values, this space-charge wave travels at a spatial angular velocity close to that of the beam. In the vicinity of synchronism between the electron beam and the r-f wave, however, a slight change in y_1 may be noted. For a beam velocity slightly slower than the r-f wave the wave associated with y_1 travels slightly faster than the beam, while for a beam velocity slightly faster than the r-f wave the y_1-wave travels slightly slower than the electron stream velocity.

The real parts of the incremental propagation constants exhibit the same general behavior in the presence of loss and space charge as they do when Q = 0. Thus, the attenuation of the circuit wave (given by x_3 at large negative values of b, and by x_2 at large positive values of b) approaches the loss in the absence of the electron stream, while the attenuation of the remaining waves approaches zero at these extreme ranges of b. In addition, the magnitudes of the maximum values of x_1 and x_2 decrease as compared to their zero-space-charge quantities. It is also interesting to observe in Figs. E.30 and E.32 that the maximum value of x_4 increases, and shifts slightly to the right, as space charge is increased in the presence of loss. Moreover, increasing the loss alone, for a fixed value of space charge, leads to a reduction in the maximum value of x_4, so that the growing-wave gain contribution produced by the wave δ_4 (in the presence of loss) would appear to more directly result from space charge than from loss. These curves suggest that the

component of gain due to δ_4 could be maximized by using relatively large space charge and small loss.

3.11.2 The Forward-Wave Gain Solutions. The gain in decibels is plotted versus the electrical angle Φ for the forward-wave device solutions appearing in Appendix F. These curves exhibit considerable rounding in the vicinity of $\Phi = 0$, where the initial amplitudes of all four waves are significant. The gain at any point in this region is determined by the manner in which these waves vectorially combine. At large electrical angles, however, the wave whose amplitude exponentially increases with spatial angle predominates, so that the gain function approaches the characteristic straight line variation.

It is of interest to examine the initial loss which results from exciting the four individual waves at the input boundary*. For the particular conditions

$$\beta_e = 50 \quad , \quad b = 0 \quad , \quad Q = 0 \quad ,$$

$$C = 0.05 \quad , \quad d = 0 \quad ,$$

these four waves have the following complex values at $\theta = 0$:

$$u_{11} + jv_{11} = 0.427128 + j0.029554, \quad u_{31} + jv_{31} = 0.23116 + j0,$$

$$u_{21} + jv_{21} = 0.427128 - j0.029554, \quad u_{41} + jv_{41} = -0.085416 + j0.$$

The initial loss for the growing-wave is given by[7]

---

* The radial and backward waves are neglected in this computation, since their amplitudes are small in comparison to the remaining four waves.

Growing-Wave Initial Loss =

$$20 \log_{10} \frac{\sqrt{u_{11}^2 + v_{11}^2}}{\sqrt{(u_{11} + u_{21} + u_{31} + u_{41})^2 + (v_{11} + v_{21} + v_{31} + v_{41})^2}} \text{ db} ,$$

whose value in the present case is equal to -7.36 db. The magnitude of this loss, which must be added to the computed amplification to obtain the "electronic gain" associated with the growing wave, is observed to be slightly smaller than the value of -9.54 db that the O-type tube exhibits for small C, and no loss or space charge, at synchronism.

The influence of β_e upon the growing-wave gain is shown in Fig. F.1, for the condition of no loss or space charge, with the spatial angular velocity of the electron beam and r-f wave in synchronism. Although the degradation in gain produced by a reduction of β_e is apparent, the effect becomes more pronounced as β_e is made smaller. Thus, a decrease of β_e from 50 to 25 leads to a gain decrement of more than three times that found when β_e is reduced from 75 to 50, at an electrical angle of 500 degrees.

The control which the gain parameter C exerts over the growing-wave gain, for a fixed value of β_e with no loss or space charge, and for synchronism between the spatial angular velocities of the electron beam and r-f wave, is shown in Fig. F.2. It may be observed here, also, that the reduction of gain resulting from a decrease of C becomes more significant as the gain parameter is made progressively smaller.

The reduction of growing-wave gain produced by a finite, nonzero circuit loss in the absence of space charge may be determined from a study of Fig. F.3, when the spatial angular velocities of the electron

beam and r-f wave are in synchronism. At small electrical angles, negative gain values are seen to prevail when loss is present, since energy transformations from the electron beam to the r-f wave are insufficient to overcome the resulting attenuation. As the loss is increased, the maximum negative value to which the gain decreases is observed to become greater. Furthermore, a greater electrical angle is required before the zero (db) gain level is reached, since the electron beam must interact with the r-f wave over a larger spatial angle to compensate for the increased loss. At large electrical angles the growing-wave predominates, so that the customary straight line gain function is obtained. The gain decrement resulting from an increase of loss is nearly proportional to the amount of loss introduced, over the range of values presented in these curves.

The effect of space charge on growing-wave gain is shown in Fig. F.4, for the case of no loss and synchronism between the spatial angular velocities of the electron beam and r-f wave. The results are similar to those of Figs. F.1 and F.2, where β_e and C are permitted to vary, since the gain function starts at zero db and never assumes negative values. The curvature observed at small electrical angles results, as before, from the vector addition of all four waves, each of whose amplitudes are significant in this region. At large electrical angles the gain curve approaches the usual straight line function associated with the dominance of the growing-wave. A study of this figure shows that the gain decrement is nearly proportional to the magnitude of Q within the plotted range of values.

Although the foregoing results have demonstrated how the growing-wave gain is affected by isolated changes of each tube parameter, a

practical E-type amplifier would normally operate with finite amounts of β_e, C, d and Q. It is of interest, therefore, to estimate the performance characteristics obtainable for fixed values of β_e and C, and varying amounts of loss and space charge. The gain reduction produced by an increase of loss, with Q = -5, is seen from Fig. F.5 to be much more severe than when no space charge exists, as in Fig. F.3. For the relatively small loss value of d = 0.25, the gain function resembles the zero-space-charge case, although the electrical angle over which it is less than zero db and the maximum negative value which it attains are now substantially increased. The introduction of greater loss, d = 0.50, leads to a large undulatory region in which the gain function finally reaches the zero db level at the large angle of 700 electrical degrees.

The gain reduction produced by increasing space charge at two fixed values of loss can be determined from a study of Figs. F.6 and F.7. When these curves are compared to the decrease of gain arising from an increase of space charge alone, as shown in Fig. F.4, it is apparent that the presence of loss is responsible for the negative gain values observed. It is also clear that if the space charge is increased, while the nonzero loss is held fixed, the electrical angle spanning the negative gain interval, as well as the maximum negative gain value, increases. This behavior prevails as the loss is increased, with the gain degradation becoming more pronounced for greater loss. The severity of these conditions may be further appreciated from a study of Fig. F.8, where the gain obtained for Q = d = 0 is compared to two situations involving the combined affects of loss and space charge.

The effect of the relative injection velocity parameter b on the gain characteristics of the E-type forward-wave device may be determined from a study of Figs. F.9-F.12, which apply to the condition of no loss and small space charge. The real and imaginary parts of the associated incremental propagation constants are given in Figs. E.1 (for Q = -0.20) and E.2. At large negative values of b, where the real parts vanish, the net gain at any spatial angle depends on the vector sum of all four waves. The net gain may therefore be positive (indicating amplification) or negative (indicating attenuation), depending upon the "constructive" or "destructive" interference produced by the four component waves. A plot of gain in db versus the electrical angle Φ exhibits the spatial beating pattern evident in Figs. F.9 and F.10. These figures show that the amplitude of the beats increases with both the electrical angle and the relative injection velocity parameter, as the b value is approached for which x_1 just vanishes. Thus, the beating-wave gain (examined at an electrical angle corresponding to one of the maximum positive excursions of the gain function) is observed to rise as b assumes the sequence of values -6, -5.5, -5, -4.5, in Figs. F.9 and F.10.

Although Fig. E.1 shows that a nonzero value of x exists at b = -3.5, the corresponding gain plot appearing in Fig. F.11 exhibits considerable spatial beating. However, the amplitudes of these excursions are observed to exponentially increase with electrical angle. A similar behavior may be noted for b = -2.5, though the adjacent "cycles" have widely different maximum values. When b = -1.5 only one such cyclical variation can be distinctly identified, but substantial curvature of the gain function is apparent. The significant point to be drawn from this study is that the transition from beating- to growing-

wave gain is gradual, with the spatial beating phenomena existing well within the range of nonvanishing values of x. The distinction between growing- and beating-wave gain therefore has meaning only in a relative sense over the range of negative b values examined here.

In contrast to this behavior, the gain function possesses a linear spatial variation when b is equal to or greater than zero. An examination of the upper set of curves in Fig. F.12 shows that the growing-wave gain is largest when b = 0, corresponding to synchronism between the spatial angular velocities of the electron beam and r-f wave, and steadily decreases as b assumes the successive values 0.5, 1.0, 1.5. When these results are compared to the x-versus-b dependency for Q = -0.20 in Fig. E.1, it becomes apparent that the decrease of growing-wave gain with an increase of b is due to the reduction of the positive real part of the propagation constant caused by this same change of b. A comparison of Figs. E.1 and F.12 reveals, however, that growing-wave gain still exists in the region of b = 1.5 where x_1 is rapidly approaching zero.

When b assumes still larger values, the growing-wave character is completely absent from the gain function, as a study of the lower set of curves in Fig. F.12 reveals. Moreover, the amplitudes of the spatial beats, to which the gain function now reverts, decreases as b takes on the successive values 1.75, 2.00, 2.50. Although the transition from growing- to beating-wave gain is much more distinct in this case, as compared to the beating-to-growing-wave change observed over the range of negative b values, the condition is still satisfied that the amplitudes of spatial beats increase as the b value at which $x_1 = 0$ is approached.

The last set of gain curves appearing in Fig. F.13 apply to the same tube parameters as employed in the above computations, with the one exception that the space-charge parameter is chosen sufficiently large so as to produce marked dimpling in the x-versus-b curves of Fig. E.1. The fact that the largest value of x_1 no longer occurs at synchronism between the spatial angular velocities of the electron beam and the r-f wave readily explains the observed behavior. The relative injection velocity values lying near the peaks of the x-versus-b curve in Fig. E.1, equal to -0.25 and 1.05, lead to larger amounts of growing-wave gain in Fig. F.13 than the synchronism case of b = 0. In fact, the value of x_1 at b = 1.375 is only slightly greater than at b = 0, but the associated gain curve clearly exceeds that of the synchronism case. However, the condition b = 0.375, near the dimple in the x-versus-b curve, yields a growing-wave gain value less than for b = 0. The spatial beating phenomena associated with the vanishing real parts occurring at b = 2.375 is clearly in evidence.

3.11.3 The Backward-Wave Propagation Constants. The real and imaginary parts of the small-signal backward-wave propagation constants are presented in Appendix G. Although the total number of solutions are somewhat less than for the corresponding forward-wave case, the range of parameter variations have been chosen over sufficiently wide limits so that the important characteristics may be readily identified.

The determinantal equation solutions applicable to the previously selected reference conditions

$$\beta_e = 50 \quad , \quad d = 0 \quad ,$$

$$C = 0.05 \quad , \quad Q = 0 \quad ,$$

appear in Figs. G.1 and G.2. It may be noted that in the absence of loss and space charge the real parts of the propagation constants resemble their forward-wave counterparts, with the exception that the closed curve is now reversed in relation to the ordinate b = 0. Thus, the low velocity limit for the electron stream, below which the real parts of the propagation constants vanish, is much nearer to the synchronous velocity (b = 0), while the high velocity limit extends to larger positive values of b than for the forward-wave device. However, the maximum value of x_1 still occurs near b = 0, where the spatial angular velocities of the electron beam and r-f wave are in synchronism.

This reversal of the x-versus-b curve in the backward-wave solutions, as contracted to the forward-wave case, may be compared to the direction of power flow (and group velocity) in the two devices. The electron stream and r-f wave phase front advance in the assumed positive azimuthal direction for both types of traveling-wave tubes, but power flows in the positive azimuthal direction for the forward-wave device and in the negative azimuthal direction for the backward-wave device. In view of the oppositely-directed group velocity associated with backward-wave tubes, the positive real part of the propagation constant x_1 leads to a dimunition of energy in the negative azimuthal direction, while the negative real part x_2 leads to an increase of energy in the same direction.

The explanation presented in Section 3.11.1, which asserted that x_1 is associated with the increasing wave and x_2 with the decreasing wave, is consistent with the present discussion owing to the power-flow direction in forward-wave devices. In the absence of loss the energy increase acquired by one of these waves is just balanced by the energy

decrease of the other (for both forward- and backward-wave devices), since the magnitudes of x_1 and x_2 are then equal at each value of b which yields nonvanishing real parts. Although the net change of energy is zero for the two classes of traveling-wave tubes (when no circuit loss exists), amplification may take place by either a growing- or beating-wave process in the forward-wave device, whereas only beating-wave amplification exists in backward-wave tubes[7].

The imaginary parts of the backward-wave propagation constants are interchanged in comparison to their forward-wave equivalents, as a study of Figs. E.2 and G.2 reveals. At large negative values of b, for which the spatial angular velocity of the electron beam is much less than that of the r-f wave, the imaginary parts y_2 and y_3 are associated with the fast and slow space-charge waves. In this case y_4 distinguishes the synchronous space-charge wave, whose spatial angular velocity coincides with the unperturbed beam velocity, while the circuit wave is identified by y_1. When the spatial angular velocity of the electron beam is much greater than that of the r-f wave, corresponding to large positive values of b, the imaginary parts y_2 and y_4 are associated with the fast and slow space-charge waves. In this same range of b values y_1 becomes the synchronous space-charge wave while y_3 becomes the circuit wave. Over the region of electron velocities for which x_1 and x_2 differ from zero the corresponding imaginary parts coalesce to a single curve, in the absence of loss. This property is shared by the propagation constants of both forward- and backward-wave devices.

A substantial reduction in the magnitude of the gain parameter leads to the propagation constant behavior shown in Figs. G.3 and G.4.

It is immediately evident that important differences can be distinguished from the corresponding forward-wave solutions appearing in Fig. E.8. In the present case the real parts form an ellipse whose dimensions decrease, and whose position shifts to the left along the negative b-axis, as C approaches zero. This leftward shift of the separated ellipse is opposite to that observed under comparable conditions in the forward-wave device. Furthermore, a careful examination of the backward-wave solutions shows that no portion of the x-versus-b curve surrounds the origin, as the separated ellipse moves out along the negative b-axis. Thus, nonvanishing real parts of the incremental propagation constants cannot be found near b = 0, where the spatial angular velocities of the electron beam and r-f wave are synchronism, for small-C backward-wave E-type devices.

The imaginary parts of the incremental propagation constants, shown in Fig. G.4, are similar in appearance to those of the reference conditions in Fig. G.2. However, the velocities of the fast and slow space-charge waves (given by y_2 and y_3 at large negative values of b, and by y_2 and y_4 at large positive values of b) depart further from the unperturbed velocity of the beam. In addition, the synchronous space-charge wave (given by y_4 at large negative values of b, and by y_1 at large positive values of b) now approaches coincidence with the beam angular velocity at smaller magnitudes of b. The interval over which y_1 and y_2 possess a common value is much more restricted, in accord with the range of nonzero real parts shown in Fig. G.3. The circuit wave (represented by y_1 at large negative values of b, and by y_3 at large positive values of b)retains substantially the same behavior.

When the gain parameter is doubled, with β_e, d and Q held fixed at their reference values, the propagation constants take the form shown in Figs. G.5 and G.6. A comparison of these solutions with the corresponding results of the forward-wave case, appearing in Figs. E.16 (with Q = 0) and E.17, shows clearly that the x-versus-b curve of the backward-wave device cannot be obtained, in general, by a simple rotation of the associated forward-wave curve about the ordinate b = 0. Thus, when C is increased the range of b over which nonvanishing real parts are found is much greater for the backward- than the forward-wave device. The general behavior of the imaginary parts is consistent with this basic pattern, since the wide range of b values over which y_1 and y_2 lie along a single curve is to be expected in view of the large interval spanning the nonzero real parts. In addition, an increase in the gain parameter causes y_2, y_3 and y_4 to move toward the b-axis for negative values of b, while y_1, y_2 and y_4 move toward the same axis at positive values of b. Accordingly, the fast and slow space-charge waves depart less from the spatial angular velocity of the beam as C increases, and the synchronous space-charge wave approaches coincidence with the beam velocity at smaller magnitudes of b.

The propagation constants presented in Figs. G.7 and G.8, where β_e is greatly reduced, possess characteristics similar to those resulting from the use of a small gain parameter. Comparable backward-wave start-oscillation characteristics can therefore be anticipated when either β_e or C is subjected to appropriate changes, as verified by the numerical results of Appendix H. It follows that both the growing-wave gain of the forward-wave amplifier and the start-oscillation

conditions of the backward-wave oscillator are affected by the radius of curvature of the ribbon beam in E-type traveling-wave tubes.

When Q assumes the large negative value of -15, with all other parameters remaining fixed, the propagation constants take the form shown in Figs. G.9 and G.10. These results are seen to resemble those obtained when C is very small, as in Figs. G.3 and G.4, or when β_e is small, as in Figs. G.7 and G.8. Thus, the control exerted over the real and imaginary parts of the propagation constants is essentially the same whether β_e or C decreases, or Q increases to a large negative value. In each of these situations the real parts form a closed curve, usually elliptical in shape, whose size and location along the negative b-axis depends upon the relative magnitudes of the parameters involved. Accordingly, nonvanishing real parts may be generated only when the relation between the spatial angular velocities of the electron beam and the r-f wave are such as to yield b values spanning the region occupied by the ellipse.

The imaginary parts associated with the fast and slow space-charge waves are observed to move farther from the b-axis, while the imaginary parts associated with the synchronous space-charge waves move closer to this axis, when the above conditions exist. The velocities of the fast and slow space-charge waves are therefore seen to depart further from the spatial angular velocity of the beam, and the velocity of the synchronous space-charge wave approaches coincidence with the beam angular velocity at smaller absolute values of b, as β_e or C decreases, or Q increases, in magnitude.

A simultaneous increase in the magnitudes of Q and C has the effect of partially cancelling the changes in the propagating constants

which would be produced by either one of these parameters varying independently. This is shown clearly in the curves of Figs. G.11 and G.12 where β_e and d retain their reference values, but C is doubled and Q is now equal to -15. In this case a large range of b no longer exists for which nonvanishing real parts occur, although it is clearly in evidence when only C is increased, as in Fig. G.5. Likewise, the x-versus-b curve does not have the elliptical shape, displaced along the negative b-axis, as it does when Q alone assumes the large negative value shown in Fig. G.9. A study of the imaginary parts presented in Fig. G.12 reveals that the departure of y_2 and y_3 from the b-axis at large negative values of b, and the departure of y_2 and y_4 from this same axis at large positive values of b, is less than when the magnitude of Q is independently increased, as in Fig. G.10. Thus, the velocities of the fast and slow space-charge waves now depart from the beam angular velocity to a lesser extent than if the magnitude of Q is independently increased. However, the departure is greater than if C alone is increased, as a study of Fig. G.6 reveals.

The change that the propagation constants undergo when loss is introduced can be determined from a study of Figs. G.13-G.16. The first two of these curves pertain to the case in which β_e, C and Q retain their reference values and d is set equal to 0.50. An examination of Fig. G.13 shows that the circuit wave (given by x_1 at large negative values of b, and by x_3 at large positive values of b) acquires a positive real part whose magnitude is equal to the loss in the absence of the electron stream, while the real parts of the remaining waves approach zero at these extreme ranges of b. The sign reversal of x_1 and x_3 at large negative and positive values of b, as compared to the corresponding

forward-wave case involving x_3 and x_2 in Fig. E.28, is to be expected in view of the oppositely-directed power flow in backward-wave case. Accordingly, the positive real parts associated with these waves now represent attenuation, as explained earlier in this section. It is also interesting to observe that the sign of the real part of the backward-wave undergoes the change indicated by Eq. 3.117. However, the radial wave, described by Eq. 3.116, possesses no real part owing to a complete absence of azimuthally-oriented propagation.

The magnitudes of x_1, x_2 and x_4 are observed to reach their maximum values near b = 0, where the spatial angular velocities of the electron beam and r-f wave are in synchronism. The maximum values of x_1 and x_4 are seen to be larger, while that of x_2 is smaller, than for the lossless case shown in Fig. G.1. The addition of loss therefore increases the attenuation of these waves whose energy flows opposite to the assumed positive azimuthal direction.

The behavior of the imaginary parts of the propagation constants in the presence of loss is shown in Fig. G.14. A comparison of these curves with the corresponding results for the lossless case of Fig. G.2 reveals that the same general characteristics prevail. The principal differences consist of a slight change in the shape of the y_2-curve, particularly near b = -1, and the separate values which y_1 and y_2 possess, except in their region of intersection. However, the limits which y_2 and y_3 approach at large negative values of b, and which y_2 and y_4 approach at large positive values of b, are substantially the same as in the lossless case. The velocities of the fast and slow space-charge waves are thus unaffected by the addition of loss. This conclusion is in agreement with the findings of the forward-wave case.

An increase in the gain parameter, with β_e, d and Q unchanged from their above values, leads to the behavior shown in Figs. G.15 and G.16. While the magnitude of x_1 attains the same maximum value as in Fig. G.13, the magnitude of x_2 increases and x_4 decreases. The gain parameter thus appears to exert some control over the attenuation of these waves. However, the circuit wave (given by x_1 at large negative values of b, and by x_3 at large positive values of b) still acquires a positive real part (which corresponds to attenuation in the backward-wave device) equal in magnitude to the loss produced in the absence of electrons. It is also interesting to observe that x_1 and x_3 asymptotically approach zero, in the region where $b > 0$, much more slowly than when $C = 0.05$.

The imaginary parts of the propagation constants, shown in Fig. G.16, possess essentially the same overall behavior as when $C = 0.05$. However, the positive and negative values which y_2 and y_3 approach at large negative values of b, and which y_2 and y_4 approach at large positive values of b, are observed to decrease as C is made larger. The velocities of the slow and fast space-charge waves now depart less from the spatial angular velocity of the electron beam. A comparison of these curves with Fig. G.6, where β_e, C and Q have the same values but $d = 0$, shows that the gain parameter is chiefly responsible for this control over the angular velocity of the space-charge waves.

3.11.4 The Start-Oscillation Characteristics. The procedure for finding the start-oscillation conditions using the IBM-704 digital computer was explained in connection with the TWEET program in Section 3.10. Once the lowest order combinations of b_{so} and Φ_{so} have been

found, which satisfy the start-oscillation requirements for a given set of tube parameters, the "CN_s length" at oscillation may be obtained from Eq. 3.110,

$$(CN_s)_{so} = \frac{\Phi_{so}}{2\pi} , \qquad (3.121)$$

where $(CN_s)_{so}$ = start-oscillation length,

Φ_{so} = electrical angle at start-oscillation in radians.

The quantities b_{so} and Φ_{so} (where the subscript "so" designates the start-oscillation values) have been tabulated in Appendix H, together with the incremental propagation constants employed in the input boundary problem, as a function of the various tube parameters.

A simple expression for the start-oscillation current can be derived under the assumption that the "critical perveance" conditions apply to the ribbon-shaped electron beam. In view of Eq. 3.76, the beam current at oscillation can be written

$$I_{so} = \frac{2C^3 V_{so}}{K} , \qquad (3.122)$$

where I_{so} = start-oscillation current in amperes,

V_{so} = beam potential at oscillation in volts,

K = magnitude of the effective interaction impedance of the backward-wave mode in ohms.

It should be noted that the value of the gain parameter C employed in the above equation must satisfy the start-oscillation relation given by Eq. 3.121. Thus C, β_e, Q and d are chosen as independent parameters and the digital computer is used to obtain the corresponding solutions b_{so}

and Φ_{so}. The value of C in Eq. 3.122 is therefore related to a specific electrical length at which backward-wave oscillations are sustained.

The "critical perveance" P_c for which no rippling occurs is known to be[32,34,35]

$$P_c = \frac{21 \cdot 10^{-6} h\sigma}{r_o^2} \quad . \tag{3.123}$$

Since this condition is presumed to hold, the starting voltage and current are related by the expression

$$V_{so} = \left(\frac{I_{so}}{P_c}\right)^{2/3} \quad . \tag{3.124}$$

Equations 3.123 and 3.124 may be used in conjunction with Eq. 3.122 to obtain

$$I_{so} = \left[1.814 \cdot 10^{10} \left(\frac{r_o^2}{h\sigma}\right)^2 \left(\frac{C^3}{K}\right)^3\right] \text{amperes} \quad . \tag{3.125}$$

If the parameters are assumed to have the specific set of values

$$C = 0.06 \quad , \quad r_o = 0.541" \quad , \quad d = 0.012" \quad ,$$

$$K = 20 \text{ ohms} \quad , \quad h = 0.500" \quad ,$$

then the starting current is found to be

$$I_{so} = 0.544 \text{ milliamperes} \quad .$$

The voltage tuning curve may also be investigated with the aid of the previously developed theory. To this end, Eq. 3.79 is first rewritten as

$$\sqrt{2\eta V_o} = \frac{2\pi f r_o}{\beta}(1+bC) \quad , \tag{3.126}$$

since

$$\Omega_o r_o = \sqrt{2\eta V_o} \quad , \tag{3.127}$$

and

$$(v_1)_{r_o} = \Omega_{w1} r_o \quad ,$$

$$= \left(\frac{\omega}{\beta}\right) r_o \quad . \tag{3.128}$$

The expression for β, given by Eq. 3.77, may be substituted into Eq. 3.126 to obtain the relation

$$V_o = \frac{2}{\eta}\left(\frac{\pi r_o}{\beta_e}\right)^2 \left| \frac{1+bC}{1+jC\delta} \right|^2 f^2 \quad . \tag{3.129}$$

This equation shows that the voltage-versus-frequency dependency is a parabolic curve, symmetric about the voltage axis. If V_o is explicitly interpreted to be the start-oscillation voltage, then Eq. 3.129 becomes

$$V_{so} = \frac{2}{\eta}\left(\frac{\pi r_o}{\beta_e}\right)^2 \left| \frac{1+b_{so}C}{1-Cy+jCx} \right|^2 f^2 \quad , \tag{3.130}$$

where b_{so} = the value of b at which oscillation begins, as obtained from the computer solutions,

C = the value of the gain parameter satisfying the start-oscillator length given by Eq. 3.121,

x = real part of the incremental propagation constant at oscillation,

y = imaginary part of the incremental propagation constant at oscillation.

Since C, as used in the above equation, is related to the electrical angle Φ_{so} at which oscillations arise for a prescribed set of values of β_e, Q and d, then the start-oscillation voltage derived here actually involves the solutions b_{so} and Φ_{so} provided by the computer. An examination of these expressions shows that a two-to-one change in frequency requires a four-to-one change in voltage. This characteristic of the class of E-type backward-wave devices studied here is the same as for O-type tubes.

Turning now to a consideration of the numerical results presented in Appendix H, it may first be noted that b_{so} increases and Φ_{so} decreases as C is made larger in the absence of loss and space charge. Thus, if $\beta_e = 50$ and $Q = d = 0$, the electrical angle decreases by 55 percent and the relative injection velocity increases to more than fourteen times its initial value when C changes from 0.01 to 0.10. A comparable behavior is observed when C, d and Q are held fixed at their reference values and β_e is allowed to increase from 10 to 50. A five-to-one increase in β_e is therefore seen to yield approximately the same starting conditions as a ten-to-one increase in C. These results confirm the assertion made in Section 3.11.3 that the radius of the center-of-the-beam electron exerts an important influence over the start-oscillation characteristics of E-type backward-wave devices.

The introduction of space charge, with $\beta_e = 50$, $C = 0.05$ and $d = 0$, increases b_{so} and Φ_{so} as compared to their zero-space-charge values. A change of Q from 0 to -5 increases b_{so} approximately 50 percent, while Φ_{so} increases nearly 4.5 times. The addition of loss slightly decreases b_{so} and increases Φ_{so} as a study of the conditions for $\beta_e = 50$, $C = 0.05$, $Q = 0$ and $d = 0, 0.5$ reveals.

The last set of numerical results were obtained for parameter values that could apply to the experimental E-type device described in Chapter IV. Although that tube is intended to function as an amplifier, it was thought to be of interest to predict the starting conditions for a backward-wave oscillator operating under similar circumstances. The structure length would then be $(CN_s)_{so} = 0.781$, from which it follows (for the specified value of C) that the number of wave angles at oscillation becomes

$$(N)_{so} = \frac{(CN_s)_{so}}{C}(1+bC) = 14.2 \quad .$$

The start-oscillation voltage can be computed with the aid of Eq. 3.130. At an operating frequency of 5000 mcs, the parameter values

$$\beta_e = 23 \quad , \quad r_o = 0.541" \quad , \quad b_{so} = 1.543 \quad ,$$

$$x = 0 \quad , \quad y = 1.378 \quad ,$$

lead to a required beam voltage of

$$V_{so} = 1020 \text{ volts} \quad .$$

It is of interest to compare the starting conditions of E-type to the similar characteristics of O-type devices. However, the differences in the definitions of the gain and space-charge parameters for each of these tubes should be recalled, since C^3 is defined as one-fourth the circuit impedance divided by the beam impedance for O-type tubes[7], whereas the corresponding quantity is twice as large for the E-type device (see Eq. 3.76). Likewise, the comparisons are restricted to the largest value of the β_e parameter (recorded in Table H.1) for

E-type tubes, since this case more closely approaches that of the O-type solutions.

The data for the O-type backward-wave oscillator was taken from a report by Rowe and Sobol[39], which will soon be published in the IRE Professional Group Transactions on Electron Devices. Though the numerical results for the two classes of traveling-wave tubes may not represent exact equivalents, the entries appearing in Table 3.1 have chosen to conform as closely as possible.

While a study of these results reveals evident differences between the starting conditions of E- and O-type tubes, it may be observed that b_{so} increases and Φ_{so} decreases as C is made larger for both devices, in the absence of loss and space charge. The introduction of loss or space charge, at a fixed value of C, also produces corresponding changes in the starting conditions of E- and O-type devices (as compared to their lossless, zero-space-charge values). However, the start-oscillation characteristics of E-type tubes appear to be much more sensitive to a given change of parameters than their O-type counterpart, as a study of the large increase of Φ_{so} with space charge indicates.

3.12 A Small-Signal Efficiency Estimate of E-Type Devices

An adequate theoretical prediction of power output and efficiency can only be obtained through the use of a large-signal, nonlinear analysis. However, the extreme complexity of such an approach makes it very desirable to utilize the small-signal linearized study in estimating these characteristics of E-type devices, so that some basis exists for a comparison with other traveling-wave tubes. The treatment presented here resembles the method originally used by Pierce[7], but slightly

Table 3.1 Comparison of E- and O-Type Starting Conditions*

E-Type Oscillator ($\beta_e = 50$)					O-Type Oscillator				
C	Q	d	b_{so}	Φ_{so} (radians)	C	QC	d	b_{so}	Φ_{so} (radians)
0.01	0	0	0.074121	4.288002	0.02	0	0	1.537	1.94
0.05	0	0	0.968852	2.477898	0.05	0	0	1.559	1.89
0.10	0	0	1.048689	2.369385	0.08	0	0	1.580	1.84
0.05	-5	0	1.316758	11.156832	0.05	0.20	0	1.593	2.01
0.05	0	0.5	0.812274	3.330374	0.05	0	0.5	1.375	2.32

* Note that although $C_{\text{E-Type}} = \sqrt[3]{2}\ C_{\text{O-Type}}$, the nearest available O-type values are tabulated.

modified since the azimuthal r-f convection current of the ribbon-shaped beam is employed in the computation of energy transfer to both the radial and azimuthal r-f electric field components.

It is appropriate to first examine the relative magnitudes of the average power transferred to the r-f wave as a result of the radial and azimuthal convection currents encountering the circuit fields. The ratio of the average radial-to-azimuthal power delivered to the r-f wave is given by

$$\frac{P_r}{P_\theta} = \frac{\left|E_{r\ max}\right| \cdot \left|i_{r\ max}\right|}{\left|E_{\theta\ max}\right| \cdot \left|i_{\theta\ max}\right|} \quad , \tag{3.131}$$

where P_r = average radial power transferred to the wave,

P_θ = average azimuthal power transferred to the wave,

$E_{r\ max}$ = maximum value of radial r-f electric field intensity,

$E_{\theta\ max}$ = maximum value of azimuthal r-f electric field intensity,

$i_{r\ max}$ = maximum value of radial convection current,

$i_{\theta\ max}$ = maximum value of azimuthal convection current.

In view of Eq. 3.47, and the fact that $F_o = -1$ for the E-type devices studied here, it follows that

$$\frac{P_r}{P_\theta} = \left|\frac{i_{r\ max}}{i_{\theta\ max}}\right| \quad . \tag{3.132}$$

It was shown in Eq. 3.52 that the azimuthal-to-radial r-f convection currents are in the ratio of $\beta_e/2$. Accordingly, the above expression reduces to

$$\frac{P_r}{P_\theta} \approx \frac{2}{\beta_e} \quad , \tag{3.133}$$

and since β_e is typically 25 or larger the conclusion follows at once that the power contributed to the r-f wave by radial beam motion is probably not greater than 8 percent of that transferred by the azimuthal component of interaction. The radial power may therefore be neglected from computations of efficiency, with the introduction of only a small degree of error.

The average value of azimuthal power may alternately be expressed in the form

$$P = \frac{\left|V_{\theta\ eff}\right|^2}{K} = \frac{\left|V_{\theta\ max}\right|^2}{2K} , \qquad (3.134)$$

where $V_{\theta\ eff}$ = effective value of the azimuthal component of r-f voltage at the beam,

$V_{\theta\ max}$ = maximum value of the azimuthal component of r-f voltage at the beam.

The maximum value of azimuthal electric field intensity at the beam $E_{\theta\ max}$ is related to $V_{\theta\ max}$ according to the expression

$$E_{\theta\ max} = \frac{-1}{r_o} \frac{\partial V_{\theta\ max}}{\partial \theta} = \frac{j\beta V_{\theta\ max}}{r_o} . \qquad (3.135)$$

Upon substituting Eq. 3.135 into 3.134 the azimuthal power becomes

$$P_\theta = \left|\frac{E_{\theta\ max} r_o}{j\beta}\right|^2 \cdot \left(\frac{1}{2K}\right) . \qquad (3.136)$$

The maximum value of the azimuthal electric field intensity may be obtained from Eq. 3.48,

$$E_{\theta\ max} = \frac{-j\Omega_o}{\eta\tau_o}\left[\frac{\left(2+(\beta_e C\delta)^2\right)\left(Q-(\beta_e C\delta)^2\right)+j\beta_e^2 C\delta\left(2-Q+(\beta_e C\delta)^2\right)}{\beta_e(2-F_o\beta_e)+(\beta_e C\delta)^2(\beta_e-F_o)+F_oQ+j\beta_e C\delta(2-\beta_e^2)}\right] i_{\theta\ max} \ , \tag{3.137}$$

where the circular propagation constant in the presence of the beam β has been replaced by

$$\beta = \beta_e(1+jC\delta) \ .$$

Following the approach used by Pierce[7], it will be assumed that the ratio of the maximum value of the fundamental component of azimuthal convection current to the d-c or average value is given by

$$\alpha = \left|i_{\theta\ max}\right| \Big/ I_o \ , \tag{3.138}$$

where α is bounded by the limits

$$1 \leq \alpha \leq 2 \ .$$

Equations 3.137 and 3.138 may be used in conjunction with Eq. 3.136 to obtain

$$P_\theta = \frac{\alpha^2 V_o I_o}{\beta_e^2 C^3}\left|\frac{1}{(1+jC\delta)}\right|^2 \cdot \left|\left[\frac{\left(2+(\beta_e C\delta)^2\right)\left(Q-(\beta_e C\delta)^2\right)+j\beta_e^2 C\delta\left(2-Q+(\beta_e C\delta)^2\right)}{\beta_e(2-F_o\beta_e)+(\beta_e C\delta)^2(\beta_e-F_o)+F_oQ+j\beta_e C\delta(2-\beta_e^2)}\right]\right|^2 , \tag{3.139}$$

inasmuch as

$$\left|\frac{-\Omega_o r_o \alpha I_o}{\eta\tau_o}\right|^2 \cdot \left(\frac{1}{2K}\right) = \frac{\alpha^2 V_o I_o}{C^3} \ .$$

The efficiency is therefore equal to the expression given by Eq. 3.140 on the following page.

The assumptions that

$$\beta_e \gg 1 , \qquad F_o = -1 ,$$

$$|C\delta| \ll 1 , \qquad |Q| \approx 2 ,$$

lead to the simplification

$$\eta_\theta \approx \frac{\alpha^2}{\beta_e^6 C^3} \left| \frac{2Q+j\beta_e^2 C\delta\left(2-Q+(\beta_e C\delta)^2\right)}{1-j\beta_e C\delta} \right|^2 . \tag{3.141}$$

It will be recalled that the growing wave is the one whose real part x_1 is greater than zero, and that this wave increases exponentially with the spatial angle θ. Accordingly, the incremental propagation constant

$$\delta_1 = x_1 + jy_1 ,$$

may be substituted into Eq. 3.141 to obtain

$$\eta_\theta = \frac{\left(2Q+y_1\left\{\beta_e^4 C^3(y_1^2-3x_1^2)-\beta_e^2 C(2-Q)\right\}\right)^2+x_1^2\left(\beta_e^4 C^3(x_1^2-3y_1^2)+\beta_e^2 C(2-Q)\right)^2}{\left\{1+2\beta_e Cy_1+\beta_e^2 C^2(x_1^2+y_1^2)\right\}\left(\beta_e^6 C^3/\alpha^2\right)} \tag{3.142}$$

Still further simplification may be achieved by making use of information already available from other traveling-wave tubes. It is known, for example, that the maximum efficiency of O-type devices occurs for a positive value of b slightly larger than that for which x_1 becomes zero. Furthermore, space charge exerts only a relatively minor influence

$$\eta_\theta = \frac{P_\theta}{V_o I_o} \quad ,$$

$$= \frac{\alpha^2}{\beta_e^2 C^3} \cdot \left| \frac{\left(2+(\beta_e C\delta)^2\right)\left(Q-(\beta_e C\delta)^2\right)+j\beta_e^2 C\delta\left(2-Q+(\beta_e C\delta)^2\right)}{(\beta_e C\delta)^2(2\beta_e-F_o)+2\beta_e(1-C^2\delta^2)+F_o(Q-\beta_e^2)+jC\delta\left\{\beta_e(4-F_o\beta_e-\beta_e^2)+F_oQ+(\beta_e C\delta)^2(\beta_e-F_o)\right\}} \right|^2 \cdot$$

(3.140)

over efficiency as compared to the remaining parameters of the O-type traveling-wave device. If at least comparable behavior of E-type devices might be anticipated, Q and x_1 may be set to zero in the foregoing equation to obtain

$$\eta_\theta = \frac{\alpha^2 y_1^2}{\beta_e^2 C}\left[\frac{(\beta_e C y_1)^4 - 4(\beta_e C y_1)^2 + 4}{1 + 2\beta_e C y_1 + (\beta_e C y_1)^2}\right] . \qquad (3.143)$$

While Eq. 3.143 is the simplest form which the efficiency may take (without invoking serious error by the further neglect of terms) for the typically encountered ranges of β_e and C, a special reduction may be obtained by proceeding to the "asymptotic form". Thus, the limiting value of η_θ may be explored as β_e <u>alone</u> is permitted to increase without limit, so that

$$\lim_{\beta_e \to \infty} \eta_\theta = \lim_{\beta_e \to \infty} \frac{\alpha^2 y_1^2}{\beta_e^2 C}\left[\frac{(\beta_e C y_1)^4 - 4(\beta_e C y_1)^2 + 4}{1 + 2\beta_e C y_1 + (\beta_e C y_1)^2}\right] = \alpha^2 y_1^4 C . \qquad (3.144)$$

A proper appreciation of this result, which resembles a similar expression for O-type devices, can only be acquired from a study of the physical circumstances which render the limit valid. In view of Eqs. 3.70, 3.75 and 3.76, the gain parameter C takes the form

$$C = \sqrt[3]{\left|\frac{k_\theta^2 r_c Z_{o,o}}{r_o}\right| \frac{I_o}{2V_o}} . \qquad (3.145)$$

Moreover, it was shown previously that k_θ approaches zero as the absolute value of β_e increases beyond bound. Consequently,

$$\lim_{\beta_e \to \infty} C \equiv 0$$

so that the limiting process indicated above leads to the existence of the indeterminate form

$$0 \cdot \infty$$

which appears in both the numerator and denominator of Eq. 3.144. The only condition for which k_θ is <u>independent</u> of β_e is that holding when

$$r_o = r_c \quad ,$$

as discussed previously in connection with Fig. 3.2. It follows that the limit process leading to Eq. 3.144 is strictly valid only for this hypothetical case of maximum beam-to-circuit coupling. However, the asymptotic form of efficiency is probably applicable to actual tubes because the beam is customarily positioned as close to the circuit as physical circumstances permit. For example, in the experimental device described in Chapter IV

$$\frac{r_o}{r_c} = 1.02 \quad ,$$

so that the foregoing efficiency expression would appear to be useable.

The limit process employed above also involves the consideration that y_1 is <u>independent</u> of changes in β_e. However, a study of the numerical results presented in Appendix E reveals that y_1 decreases when either β_e or C increases. If the "tight" beam-to-circuit coupling condition is assumed to hold, then C remains substantially constant, and it is found that β_e increases much more rapidly than y_1 decreases. Under these circumstances, the asymptotic form of the efficiency equation is a legitimate approximation.

Several computations have been carried out in order to ascertain probable numerical values of efficiency that may be expected. First, the data

$$\beta_e = 50 \quad , \quad b = 0 \quad , \quad x_1 = 0.560135 \quad ,$$
$$C = 0.05 \quad , \quad d = 0 \quad , \quad y_1 = -0.268522 \quad ,$$
$$Q = -1.00 \quad , \quad \alpha = 1.2 \quad ,$$

were applied to Eq. 3.142, with the result that

$$\eta_\theta = 5.72 \text{ percent} \quad .$$

Next, the conditions

$$\beta_e = 50 \quad , \quad b = 1.50 \quad , \quad x_1 = 0 \quad ,$$
$$C = 0.05 \quad , \quad d = 0 \quad , \quad y_1 = -1.25 \quad ,$$
$$Q = 0 \quad , \quad \alpha = 1.2 \quad ,$$

were used in conjunction with the asymptotic form of efficiency, Eq. 3.144 to obtain

$$\eta_\theta = 17.55 \text{ percent} \quad .$$

It will be noted that the selections of β_e, C, Q, b and d fix the values of x_1 and y_1 which are the corresponding solutions of the determinantal equation. The choice of $\alpha = 1.2$ is based on experienced estimates from similar studies of O-type devices.

The most significant conclusion to be drawn from this investigation is that the efficiency of the E-type device is comparable to that achieved in O-type traveling-wave tubes. The similarity between the two devices is particularly striking because:

1. The fact that the radial convection current and power are small fractions of their azimuthal counterparts implies that the

E-type interaction phenomena are chiefly azimuthally-oriented. Thus, the energy transformations taking place in the z-direction of O-type devices are replaced by corresponding transformations in the θ-direction of E-type devices.

2. The asymptotic form of the efficiency of E-type devices, given by Eq. 3.144, bears a strong resemblance to a similar expression obtained for O-type traveling-wave tubes[7]. In each case, the efficiency is directly proportional to the gain parameter C.

3. The range of numerical values of efficiency computed above for the E-type device fall within the general limits obtained with O-type traveling-wave tubes.

3.13 Slipping-Stream Motion in E-Type Traveling-Wave Devices

3.13.1 The Origin of Slipping-Stream Motion. The behavior of a ribbon-shaped beam passing between the coaxial-cylindrical conductors of an E-type traveling-wave device is such that electrons located at different radial positions possess unequal angular velocities. Since this condition clearly violates the Brillouin flow hypothesis used in the formulation of the ballistic equations, it is essential to examine the sources of this motion in which electrons slip past each other azimuthally.

The nature of the slipping-stream motion in E-type devices may be examined by an approach similar to that presented by Waters[35]. The development is carried out by noting that Poisson's equation for a ribbon-shaped beam in the presence of only a static radial electric field may be written

$$\frac{1}{r}\ \frac{d}{dr}\left(r\ \frac{dV}{dr}\right)\ =\ -\ \frac{\rho_o}{\epsilon_o}\quad , \tag{3.146}$$

where ρ_o is the steady component of volume charge density of the beam in coulomb/meter^3. If it is assumed that ρ_o is independent of the radius, then a first integral of this equation leads to

$$r\left(\frac{dV}{dr}\right)\ =\ C_1\ -\ \frac{\rho_o r^2}{2\epsilon_o}\quad , \tag{3.147}$$

where C_1 is a constant of integration. Upon recalling that the dynamic equilibrium condition requires the centrifugal force of the revolving electron to be balanced, at any radial position, by an equal and opposite radial electric field force it follows that

$$\frac{mv^2}{r}\ =\ -\ eE(r)\quad , \tag{3.148}$$

where v is linear tangential velocity of the electron at radius r in meter/second. In view of Eq. 3.5, and as a consequence of the principle of conservation of energy

$$v^2\ =\ 2\eta V\quad , \tag{3.149}$$

Equation 3.147 becomes

$$2V\ =\ \frac{\rho_o r^2}{2\epsilon_o}\ -\ C_1\quad . \tag{3.150}$$

The condition that

$$V\ =\ V_o\quad ,\qquad \text{when}\qquad r\ =\ r_o\quad ,$$

yields for the constant of integration

$$C_1\ =\ \frac{\rho_o r_o^2}{2\epsilon_o}\ -\ 2V_o\quad . \tag{3.151}$$

This expression may be substituted into Eq. 3.147 to obtain after integrating with respect to r

$$V = C_2 - \frac{\rho_o r^2}{4\epsilon_o} + \left(\frac{\rho_o r_o^2}{2\epsilon_o} - 2V_o\right) \ell n\ r \quad , \tag{3.152}$$

where C_2 is another constant of integration. The same condition can be employed in its evaluation as was used for C_1, so that

$$C_2 = V_o + \frac{\rho_o r_o^2}{4\epsilon_o} - \left(\frac{\rho_o r_o^2}{2\epsilon_o} - 2V_o\right) \ell n\ r_o \quad , \tag{3.153}$$

and the general expression for potential variation across the beam becomes

$$V = V_o + \frac{\rho_o}{4\epsilon_o}(r_o^2 - r^2) + \left(2V_o - \frac{\rho_o r_o^2}{2\epsilon_o}\right) \ell n \left(\frac{r_o}{r}\right) \quad . \tag{3.154}$$

The spatial angular velocity of an electron at any arbitrary radius is given by

$$\Omega_r = \frac{1}{r}\sqrt{2\eta V} \quad , \tag{3.155}$$

which is seen to vary as the square root of the beam potential.

The following definitions may now be introduced:

V_1 = d-c potential at the <u>outside</u> edge of the beam in volts,

V_2 = d-c potential at the <u>inside</u> edge of the beam in volts,

r_1 = radius of the <u>outside</u> edge of the beam in meters,

r_2 = radius of the <u>inside</u> edge of the beam in meters.

The radii at the outer and inner edges of the beam may be written

$$r_1 = r_o(1 + \sigma/2r_o) \quad , \tag{3.156}$$

$$r_2 = r_o(1 - \sigma/2r_o) \quad . \tag{3.157}$$

These expressions may be applied to Eq. 3.154 to obtain

$$V_1 = V_o - \frac{\rho_o r_o^2}{4\epsilon_o}\left(\frac{\sigma}{r_o} + \left(\frac{\sigma}{2r_o}\right)^2\right) + \left(\frac{\rho_o r_o^2}{2\epsilon_o} - 2V_o\right) \ell n \left(1 + \frac{\sigma}{2r_o}\right) \quad , \tag{3.158}$$

$$V_2 = V_o + \frac{\rho_o r_o^2}{4\epsilon_o}\left(\frac{\sigma}{r_o} - \left(\frac{\sigma}{2r_o}\right)^2\right) + \left(\frac{\rho_o r_o^2}{2\epsilon_o} - 2V_o\right) \ell n \left(1 - \frac{\sigma}{2r_o}\right) \quad . \tag{3.159}$$

In view of the fact that

$$\frac{\sigma}{2r_o} \ll 1 \quad ,$$

the series expansion for the natural logarithm function is given by

$$\ell n \left(1 \pm \frac{\sigma}{2r_o}\right) = \left(\pm \frac{\sigma}{2r_o}\right) - \frac{1}{2}\left(\pm \frac{\sigma}{2r_o}\right)^2 + \frac{1}{3}\left(\pm \frac{\sigma}{2r_o}\right)^3 - \frac{1}{4}\left(\pm \frac{\sigma}{2r_o}\right)^4 + \cdots \quad . \tag{3.160}$$

This equation may be used in conjunction with Eqs. 3.158 and 3.159 to yield

$$V_1 = V_o\left[1 - \frac{\sigma}{r_o}\left\{1 - \frac{1}{2}\left(\frac{\sigma}{2r_o}\right) + \frac{1}{3}\left(\frac{\sigma}{2r_o}\right)^2 - \frac{1}{4}\left(\frac{\sigma}{2r_o}\right)^3 + \cdots\right\}\right]$$

$$- \frac{\rho_o \sigma^2}{8\epsilon_o}\left[1 - \frac{1}{3}\left(\frac{\sigma}{2r_o}\right) + \frac{1}{4}\left(\frac{\sigma}{2r_o}\right)^2 - \frac{1}{5}\left(\frac{\sigma}{2r_o}\right)^3 + \cdots\right] \quad , \tag{3.161}$$

$$V_2 = V_o \left[1 + \frac{\sigma}{r_o} \left\{ 1 + \frac{1}{2}\left(\frac{\sigma}{2r_o}\right) + \frac{1}{3}\left(\frac{\sigma}{2r_o}\right)^2 + \frac{1}{4}\left(\frac{\sigma}{2r_o}\right)^3 + \cdots \right\} \right]$$

$$- \frac{\rho_o \sigma^2}{8\epsilon_o} \left[1 + \frac{1}{3}\left(\frac{\sigma}{2r_o}\right) + \frac{1}{4}\left(\frac{\sigma}{2r_o}\right)^2 + \frac{1}{5}\left(\frac{\sigma}{2r_o}\right)^3 + \cdots \right] . \quad (3.162)$$

These results reveal several interesting facts concerning the potential variation within the ribbon-shaped electron beam. It may first be noted that when $\sigma \to 0$,

$$V_1 = V_2 = V_o ,$$

so that the beam potential possesses the single value of an electron at radius r_o. This is certainly to be expected because in this case the radial width is zero, and the potential becomes identical with that of the center-of-the-beam electron.

It next becomes apparent that the first term in the right members of each of the above equations accounts for the potential variation across the beam resulting from the condition that the electron's centrifugal force is balanced, at any radial position, by an equal and opposite radial electric field force. This term is therefore identified with the "force equilibrium constraint".

The second term in the right members of each of these equations accounts for the potential variation across the beam due to the space-charge field associated with the stream electrons. Clearly, the potential variation reduces to that imposed by the force equilibrium constraint when the space-charge field vanishes.

The relative importance of each of these contributions to potential variation may be more readily determined by introducing one

additional transformation to simplify the coefficients preceding the expressions in the brackets associated with the second terms of Eqs. 3.161 and 3.162. In view of Eqs. 3.12, 3.27 and 3.123 it follows that

$$\rho_o = \frac{-21\cdot 10^{-6} V_o}{r_o^2 \sqrt{2\eta}} \quad , \tag{3.163}$$

so that Eqs. 3.161 and 3.162 take the form

$$V_1 = V_o \left[1 - \frac{\sigma}{r_o} \left\{ 1 - \frac{1}{2}\left(\frac{\sigma}{2r_o}\right) + \frac{1}{3}\left(\frac{\sigma}{2r_o}\right)^2 - \frac{1}{4}\left(\frac{\sigma}{2r_o}\right)^3 + \ldots \right\} \right.$$

$$\left. + \frac{1}{2}\left(\frac{\sigma}{r_o}\right)^2 \left\{ 1 - \frac{1}{3}\left(\frac{\sigma}{2r_o}\right) + \frac{1}{4}\left(\frac{\sigma}{2r_o}\right)^2 - \frac{1}{5}\left(\frac{\sigma}{2r_o}\right)^2 + \ldots \right\} \right] \quad , \tag{3.164}$$

$$V_2 = V_o \left[1 + \frac{\sigma}{r_o} \left\{ 1 + \frac{1}{2}\left(\frac{\sigma}{2r_o}\right) + \frac{1}{3}\left(\frac{\sigma}{2r_o}\right)^2 + \frac{1}{4}\left(\frac{\sigma}{2r_o}\right)^3 + \ldots \right\} \right.$$

$$\left. + \frac{1}{2}\left(\frac{\sigma}{r_o}\right)^2 \left\{ 1 + \frac{1}{3}\left(\frac{\sigma}{2r_o}\right) + \frac{1}{4}\left(\frac{\sigma}{2r_o}\right)^2 + \frac{1}{5}\left(\frac{\sigma}{2r_o}\right)^2 + \ldots \right\} \right] \quad . \tag{3.165}$$

These relations show at once that, since

$$\frac{\sigma}{r_o} \ll 1 \quad ,$$

the potential variation across the beam resulting from the space-charge fields produced by the stream electrons is only a small fraction of that associated with the force equilibrium constraint. Thus, the <u>important</u> source of steady potential variation across the beam is imposed by the maintenance of dynamic equilibrium at any radial position, so that the electron's centrifugal force is opposed by an equal-magnitude

radial electric field force. In view of Eq. 3.155 it follows that the spatial angular velocity of any stream electron varies in proportion to the square root of the potential variation arising from the dynamic equilibrium condition.

If it is now assumed that terms in σ/r_o may be neglected for squares and higher powers, the spatial angular velocity of electrons situated at the outside and inside edges of the beam become

$$\Omega_1 = \frac{1}{r_1}\sqrt{2\eta V_1} \ ,$$

$$\approx \frac{1}{r_o + \frac{\sigma}{2}}\sqrt{2\eta V_o\left(1 - \frac{\sigma}{r_o}\right)} \ , \qquad (3.166)$$

$$\Omega_2 = \frac{1}{r_2}\sqrt{2\eta V_2} \ ,$$

$$\approx \frac{1}{r_o - \frac{\sigma}{2}}\sqrt{2\eta V_o\left(1 + \frac{\sigma}{r_o}\right)} \ , \qquad (3.167)$$

where Ω_1 = spatial angular velocity of an electron at the <u>outside</u> edge of the beam in spatial radians/second,

Ω_2 = spatial angular velocity of an electron at the <u>inside</u> edge of the beam in spatial radians/second.

In view of Eq. 3.8, the spatial angular velocities of the electrons at the outside and inside edges of the beam take the approximate forms

$$\Omega_1 \approx \Omega_o\left(1 - \frac{\sigma}{r_o}\right) \ , \qquad (3.168)$$

$$\Omega_2 \approx \Omega_o \left(1 + \frac{\sigma}{r_o}\right) . \qquad (3.169)$$

These results show that the spatial angular velocity of an electron at the inside edge of the beam is just as much greater than that of the center-of-the-beam electron as an electron at the outside edge of the beam is less than that of the center-of-the-beam electron, when the radial width of the stream is a small fraction of r_o. The spatial angular velocity of the electrons is thus seen to increase as the inside edge of the beam is approached.

Although this study of slipping-stream motion in E-type devices was confined to an investigation of the effects produced by the "steady forces", it is also reasonable to expect the existence of another cause of this behavior. Since the intensity of all r-f fields decrease rapidly with increasing radius, as the examination of the radial and azimuthal coupling factors has revealed, electrons at the inside edge of the beam encounter a much stronger retarding field when they transfer energy to the circuit wave than those at the outside edge. Accordingly, the inside-edge electrons tend to have their spatial angular velocity reduced more than those at the center and outside edges of the beam. However, in a small-signal study all a-c variations are assumed to be negligible as compared to the unvarying quantities, so that slipping-stream motion resulting from favorable electron-wave energy transformations is likely to be a small fraction of that resulting from the force equilibrium constraint. The position is therefore taken that the space-charge and r-f fields modify the spatial angular velocity of the electrons very little relative to the variation imposed by the dynamic equilibrium condition.

3.13.2 An Approximate Method of Calculating Slipping-Stream Gain. The procedure employed here to account for the effect produced on the growing-wave gain of a small-signal E-type forward-wave amplifier by slipping-stream motion involves an examination of the manner in which energy transformations between the electron beam and the circuit wave are modified by this variation of spatial angular velocity. The method disregards energy exchanges resulting from the motion of electrons with respect to each other.

The radial extension of the ribbon beam is divided into two segments of equal width, such that all electrons contained within either segment have the same spatial angular velocity, but the angular velocity of the segments differ. This is equivalent to dividing the actual slipping electron stream into two Brillouin flow beams whose spatial angular velocities at the outside and inside edges are given by Eqs. 3.168 and 3.169, respectively.

Each portion of the beam is assumed to interact independently with the wave on the r-f circuit, so that the presence of the remaining segment is ignored when the gain contribution of a given division of the stream is being determined. Furthermore, the computations are carried out by disregarding the change of beam-to-circuit coupling resulting from the radial disposition of the two regions. Accordingly, only spatial angular velocity variations, and not radial differences, will be considered in the ensuing calculations.

The expressions for β_e, Q and b for the outside and inside portions of the beam are computed with the aid of Eqs. 3.168 and 3.169. The results of these substitutions appear below, with the appropriate

subscripted values corresponding to the associated segments of the stream, whereas unsubscripted quantities refer to the entire nonslipping-stream beam.

1. Outside Segment:

$$\beta_{e1} = \frac{\omega}{\Omega_o\left(1 - \frac{\sigma}{r_o}\right)} \approx \beta_e\left(1 + \frac{\sigma}{r_o}\right) , \tag{3.170}$$

$$Q_1 = \frac{\eta\tau_o/2}{\Omega_o^2\left(1 - \frac{\sigma}{r_o}\right)^2 \epsilon_o h\sigma/2} \approx Q\left(1 + \frac{2\sigma}{r_o}\right) , \tag{3.171}$$

$$b_1 = \frac{1}{C}\left[\frac{\Omega_o}{\Omega_{w1}}\left(1 - \frac{\sigma}{r_o}\right) - 1\right] = b - \frac{1}{C}\left(\frac{\Omega_o}{\Omega_{w1}}\right)\frac{\sigma}{r_o} . \tag{3.172}$$

2. Inside Segment:

$$\beta_{e2} = \frac{\omega}{\Omega_o\left(1 + \frac{\sigma}{r_o}\right)} \approx \beta_e\left(1 - \frac{\sigma}{r_o}\right) , \tag{3.173}$$

$$Q_2 = \frac{\eta\tau_o/2}{\Omega_o^2\left(1 + \frac{\sigma}{r_o}\right)^2 \epsilon_o h\sigma/2} \approx Q\left(1 - \frac{2\sigma}{r_o}\right) , \tag{3.174}$$

$$b_2 = \frac{1}{C}\left[\frac{\Omega_o}{\Omega_{w1}}\left(1 + \frac{\sigma}{r_o}\right) - 1\right] = b + \frac{1}{C}\left(\frac{\Omega_o}{\Omega_{w1}}\right)\frac{\sigma}{r_o} . \tag{3.175}$$

It is important to observe that the gain parameters associated with the two segments of the beam have the same magnitude as that of the entire nonslipping-stream beam. This may be verified by first recalling

that the magnitude of the effective interaction impedance is inversely proportional to the azimuthal r-f power transferred to the beam, according to Eq. 3.136. Thus, if the power delivered to the wave on the circuit is assumed to result from equal contributions of the two portions of the beam, it follows that*

$$K_1 = K_2 = \frac{1}{2(P_\theta/2)}\left|\frac{E_{\theta\ max}\, r_o}{j\beta}\right|^2 = 2K \quad . \tag{3.176}$$

This relation may be used in conjunction with Eq. 3.76 to obtain

$$C_1 = C_2 = \sqrt[3]{\frac{2K(I_o/2)}{2V_o}} = C \quad , \tag{3.177}$$

so that the same gain parameter applies to each portion of the stream as to the entire nonslipping-stream beam. A careful consideration of this line of reasoning shows clearly that if the division had been made into n similar beams, each possessing a specific value of spatial angular velocity, the gain parameter associated with each segment would be the same as for the entire Brillouin flow beam.

These parameters can be supplied to the digital computer to obtain the determinantal equation solutions. The resulting roots may then be used in the computation of the initial wave amplitudes and the growing-wave gain associated with the two segments of the beam. If the assumption is made that the electrical angle Φ is chosen sufficiently large

---

* It is important to observe that the <u>same</u> values of $E_{\theta\ max}$ and r_o apply to both segments of the beam, in view of the assumption of a constant beam-to-circuit coupling. Therefore, the model treated here actually presumes that the two Brillouin flow beams are spatial superimposed, but otherwise independent. The requirement that the beam-to-circuit coupling must change implies that <u>both</u> $E_{\theta\ max}$ and r_o would likewise change for the two segments, thereby materially complicating the analysis.

so that only the growing-wave predominates, then the complex gain vector is found from Eq. 3.105 to be

$$\zeta = |\zeta| e^{j\Psi} \quad , \tag{3.178}$$

where

$$|\zeta| = \text{Inverse-Log}_{10}\left[\frac{\text{Gain (db)}}{20}\right] \quad , \tag{3.179}$$

$$\Psi = \text{Inverse-Tangent}\left[\frac{v_{11}\cos\Phi y_1 + u_{11}\sin\Phi y_1}{u_{11}\cos\Phi y_1 - v_{11}\sin\Phi y_1}\right] \quad . \tag{3.180}$$

All of the quantities necessary for carrying out the computation indicated above may be obtained from the digital computer. Therefore, if the complex vector which determines the growing-wave gain for each segment of the beam is ascertained by this procedure, and if the components are then properly added, the result is found to be

$$\zeta_{ss} = |\zeta_1| e^{j\Psi_1} + |\zeta_2| e^{j\Psi_2} \quad , \tag{3.181}$$

where ζ_{ss} = slipping-stream gain vector,

$|\zeta_1|$ = magnitude of the gain vector associated with the outside segment of the beam,

$|\zeta_2|$ = magnitude of the gain vector associated with the inside segment of the beam,

Ψ_1 = angle associated with the vector ζ_1,

Ψ_2 = angle associated with the vector ζ_2.

In view of the relation between the exponential and trigonometric functions, the slipping-stream gain may be written in the form

$$\text{Slipping-Stream Gain (db)} = 10 \operatorname{Log}_{10} \left| \left\{ |\zeta_1| \cos\Psi_1 + |\zeta_2| \cos \Psi_2 \right\}^2 + \left\{ |\zeta_1| \sin\Psi_1 + |\zeta_2| \sin\Psi_2 \right\}^2 \right| . \qquad (3.182)$$

The accuracy of the computation can be improved by dividing the beam into a larger number of radial segments, since the spatial angular velocity difference between adjacent divisions would then be smaller. In the limit, as an infinite number of segments are taken, the spatial angular velocity variation between adjacent divisions vanishes, so that the conditions revert to those of a uniform angular velocity variation across the beam.

3.13.3 A Numerical Example. The computations are carried out using the following set of parameter values which apply to the entire Brillouin flow beam:

$\beta_e = 50$, $Q = -2.00$, $d = 0$, $\Phi = 550$ electrical degrees.

$C = 0.05$, $b = 0$, $\frac{\sigma}{r_o} = 0.02$,

This data is used in conjunction with the relations derived in the previous section to obtain the corresponding quantities associated with the outside and inside segments of the beam. The results appear in Table 3.2.

Table 3.2 Quantities Employed in the Slipping-Stream Gain Calculation

Electron Phase Constant	Gain Parameter	Space-Charge Parameter	Injection Velocity Parameter	Electrical Angle (Degrees)
$\beta_{e1} = 51$	$C_1 = 0.05$	$Q_1 = -2.08$	$b_1 = -0.40$	$\Phi_1 = 561$
$\beta_{e2} = 49$	$C_2 = 0.05$	$Q_2 = -1.92$	$b_2 = 0.40$	$\Phi_2 = 539$

Table 3.3 Numerical Solutions for the Growing-Wave Gain Associated with the Two Segments of the Beam

Segment	x_1	y_1	u_{11}	v_{11}	Vector Modulus	Vector Angle
Outside	0.503241	-0.067849	0.364367	0.201688	$\lvert\zeta_1\rvert=57.6$	$\Psi_1=-9.10°$
Inside	0.466349	-0.514259	0.589980	-0.011640	$\lvert\zeta_2\rvert=47.2$	$\Psi_2=81.67°$

The slipping-stream gain is computed from Eq. 3.182 using the last two columns of the data tabulated above. In addition, the thin beam gain for the entire Brillouin flow beam is read from Fig. F.4. The gains obtained for the slipping- and nonslipping-stream beams are recorded below.

Table 3.4 Numerical Results of the Gain Computation

Thin Beam Gain Obtained from Fig. F.4 = 35.5 db.

Slipping-Stream Gain Obtained from Eq. 3.182 = 33.5 db.

While the slipping-stream gain loss is found to be two db, according to the procedure used here, the method can only be considered approximate, since the spatial angular velocity of the electrons varies

uniformly across the radial extension of the beam. Moreover, the beam-to-circuit coupling has been disregarded, as explained in Section 3.13.2, although it may vary appreciably in a given physical situation.

CHAPTER IV. THE EXPERIMENTAL SMALL-SIGNAL E-TYPE TRAVELING-WAVE AMPLIFIER

4.1 Introduction

The small-signal analysis presented in the previous chapter has served to provide a general understanding of the electron-wave interaction phenomena in E-type devices and its important consequences. It is the purpose of this chapter to describe the design and performance characteristics of an experimental small-signal amplifier.

The factors influencing the selection of the slow-wave circuit are discussed in connection with preliminary laboratory investigations made on several prototype structures. The knowledge acquired from this study was then used as a starting point in the design of the actual small-signal amplifier. This, together with a consideration of the design requirements imposed upon the ribbon beam and its spatial extension in order to achieve dynamic equilibrium, leads to specifications for the geometry of the electron gun and of the interaction region. The results of the analytical study are also invoked at this point so that a suitable compromise between several conflicting factors may be achieved. In addition, the work permits the prediction of the theoretical performance characteristics for the experimental device. Finally, the results of cold- and hot-test measurements made on the actual tube are presented for comparison.

4.2 Choice of the Slow-Wave Circuit

A number of biperiodic, filter- and helix-type slow-wave structures were considered with a view toward their use in the small-signal

E-type forward-wave amplifier. The factors of bandwidth, surface impedance, ease of construction, and compatability with other design requirements, led to the selection of the flattened helix[22] as the preferred r-f circuit. Though its power handling ability is limited, this is not a severe restriction in the intended small-signal application. The mechanical and electrical characteristics of two flattened helices, wound on a straight polystyrene mandrel and designed for operation over the frequency range of 3.95-5.85 kmc, are recorded below.

Table 4.1 Mechanical Characteristics of the Flattened Helix

Helix Model	Wire Diameter (Inch)	Pitch Factor (Inch/Turn)	Mandrel Height (Inch)	Mandrel Width (Inch)	Helix Length (Inch)
No. 1	0.012	0.0625	0.375	0.0625	5.00
No. 2	0.008	0.0833	0.500	0.080	5.00

Table 4.2 Computed Electrical Characteristics of the Flattened Helix

Frequency, kmc	Surface Impedance, Ohms	Wave Slowing Factor	Synchronous Beam Potential, Volts
	Helix No. 1		
3.95	83.5	1/16.4	950
5.85	58.8	1/16.23	972
	Helix No. 2		
3.95	81.2	1/16.5	944
5.85	51.0	1/16.1	988

Table 4.3 Measured Electrical Characteristics of the Flattened Helix

	Helix No. 1	
Frequency, kmc	Wave Slowing Factor	Wave Slowing Factor
3.95	1/13.8	1/13.5
5.85	1/12.9	1/13.5
Frequency, kmc	Input VSWR	Input VSWR
5.00	1.26:1	1.18:1

The "wave slowing factor" appearing in Tables 4.2 and 4.3 refers to the ratio of the wave phase velocity along the helix to the velocity of light in free space, and the "synchronous beam potential" designates the d-c voltage required to accelerate the beam up to this phase velocity. It is desirable in an amplifier to maintain the slowing factor as nearly constant with frequency as possible, so that broadband interaction may be achieved. The actual procedure for measuring this quantity involves the use of a moving probe which samples the r-f wave along the helix. The slowing factor is found to be equal to the ratio of the structure wavelength to the free-space wavelength of the r-f wave.

The results show that, while some disparity between the computed and measured slowing factors exists, its frequency variation is relatively small. This nondispersive behavior indicates that the flattened helix is suited to broadband amplifier operation. The fact that the observed slowing factor was slightly less than the computed value simply indicates that the synchronous beam potential must be increased a small amount.

The surface impedance, which is a measure of the intensity of the r-f fields at the edge of the slow-wave structure, is a rather

difficult quantity to measure. However, the large computed value of some 50 to 80 ohms indicates that the flattened helix should be capable of yielding adequate small-signal amplification. An impedance reduction of as much as 50 percent at the location of the beam would still permit useful signal gain to be achieved, since traveling-wave interaction impedances are known to have a minimum useful value in the range of some tens of ohms[7].

The input VSWR recorded in Table 4.3 was measured with the output section of the flattened helix match terminated. Although this very good input match was not realized over the entire band, experimental results indicate that a nearly perfect match can be obtained at a single frequency without the use of auxiliary components. Furthermore, an input VSWR of less than 2:1 was measured over a bandwidth as large as 400 mcs surrounding the midband frequency of 5000 mcs for both helices. It is reasonable to expect that a very low input VSWR could be achieved over the entire band by means of suitable matching devices, since similar procedures have been found to be very successful in O-type traveling-wave tubes.

On the basis of these computed and measured characteristics it was concluded that the structure would adequately serve the required purposes of a slow-wave circuit for the small-signal amplifier. The only change necessitated by its use in the E-type device would be that resulting from the circular geometry of the tube. Thus, the helix must be wound on a circular, rather than a straight, mandrel of square cross section. However, the radius of curvature is thought to be sufficiently large so that the impedance and dispersion characteristics are not seriously altered by this change of shape.

4.3 The Design of the Small-Signal Amplifier

Once the slow-wave structure has been selected it is possible to concentrate attention on the mechanical and electrical conditions which must be satisfied in order to achieve stable electron motion. The investigations carried out by Waters[32,34,35] have shown that the following restrictions must be met in the design of the ribbon beam for an E-type device:

1. The radius of the center-of-the-beam electron must be small, preferably less than one inch, in order to obtain adequate electrostatic restraining forces.
2. The ribbon beam must enter the interaction region as nearly tangential to the circle of radius r_o as possible to prevent severe radial rippling of the electron stream.
3. The dimensions of the electron stream must bear the proper relation to the critical perveance, as described in Section 3.11.4, in order to minimize rippling.

In addition, it was shown that the sole and circuit voltages must satisfy Eq. 3.9 in order to obtain stable beam motion.

Although the foregoing requirements serve to fix the stability conditions on the electron beam, the consequences of the small-signal analysis impose still further constraints if reasonable values of signal amplification are to be realized. The most important of these are:

1. The radius of the center-of-the-beam electron should be as large as possible in order to make β_e, and therefore the gain per unit spatial angle, as large as possible.
2. The radius of the inside edge of the beam should be situated as close to the r-f structure as possible so as to achieve

the largest possible value of beam-to-circuit coupling. This increases the gain parameter C and, therefore, the gain per unit spatial angle.

3. The axial height of the flattened helix should not be made too large if impractically small values of surface impedance, and therefore gain, are to be avoided.

A careful examination of the full range of requirements imposed by the beam stability and effective electron-wave interaction constraints reveals several conflicting stipulations. The first, and perhaps most serious, of these arises from the small radius condition necessary to insure adequate "beam stiffness" and the large radius needed to achieve acceptable gain*. For the frequency range of the device under investigation, it appears that a reasonable compromise between gain and beam stiffness can be achieved for a center-of-the-beam-electron radius of approximately one-half inch.

Another difficulty arises from the requirement that the electron stream should be situated as close to the circuit as possible to maintain a high beam-to-circuit coupling, while too close a spacing leads to excessive interception of the beam current by the helix. In addition, an improperly launched beam, or one not meeting the critical perveance condition, may exhibit severe rippling, thereby leading to intolerable amounts of electron interception. The net effect of this condition will not only result in a loss of small-signal gain, but also over-heating,

---

* Dr. Waters has defined "beam stiffness" in terms of the maximum radial excursion which a given electron of the beam undergoes for a specified initial radial velocity component. Thus, the larger the excursion the smaller is the beam stiffness, and conversely. The beam stiffness of an E-type device is found to be inversely proportional to the radius.

and in some cases complete burn out, of the slow-wave circuit. A careful examination of the problem reveals that the spacing between the center of the beam and the surface of the r-f structure should be of the order of 0.012 inch, and that the beam should be designed to satisfy the critical perveance requirement. Furthermore, three "launch electrodes" are located along the circuit radius between the electron gun and the entrance to the interaction space so that the required beam "entrance conditions" can be adjusted electronically after all efforts have been made to properly inject the ribbon beam by mechanical means. The total transit angle of the beam from the electron gun to the collector amounts to a spatial excursion of 225 degrees.

One final consideration pertains to the height of the ribbon beam parallel to the axis of the cylindrical system. A study of the critical perveance relation shows that the beam current (and therefore r-f power output) increases directly with beam height. However, if all helix dimensions except the height are held constant, it is found that the surface impedance and gain decreases as h increases. On the basis of the results presented in Section 4.2 the beam height was chosen to be 0.500 inch.

The electron gun used in this tube consists of a three-electrode electrostatic lens, such as the type described by Pierce[6], and a "mask electrode" placed in front of the electron emitting surface. The latter element, which serves to delineate the 0.500 inch x 0.012 inch cross-sectional dimensions of the beam, is situated at the "entrance pupil" of the lens system in order to produce a sharp focusing action. The "exit pupil" of the electrostatic lens lies in the interaction region near the spatial angle at which the r-f circuit begins. The maximum

accelerating voltage for the electron gun is of the order of 1000 volts, consistent with a design slowing factor of the r-f wave equal to one-sixteenth of the velocity of light along the flattened helix. The d-c beam current is approximately 14 milliamperes.

The mechanical and electrical characteristics of the small-signal forward-wave amplifier are summarized in the accompanying tables. In addition, the last table provides a display of the values β_e, C and Q, over the frequency range 3.95-5.85 kmc. A set of "midband parameters", that are used in conjunction with the theoretical analysis to predict the performance characteristics, are also presented.

Table 4.4 Mechanical Characteristics of the Amplifier Flattened Helix

Mandrel Height (Inch)	Mandrel Width (Inch)	Mandrel Radius (Inch)	Mandrel Spatial Angle (Degrees)	Molybdenum Helix Tape	Helix Pitch Factor (Inch/Turn)
0.550	0.040	0.515	170	0.015 inch x 0.005 inch	1/13.2

Table 4.5 Computed Electrical Characteristics of the Amplifier Flattened Helix

Frequency, kmc	Surface Impedance, Ohms	Effective Interaction Impedance, Ohms	Wave Slowing Factor	Synchronous Beam Potential, Volts
3.95	104	51	1/15.25	1100
5.00	77	30.8	1/15.76	1030
5.85	57.4	18.7	1/16	1000

Table 4.6 Mechanical and Electrical Characteristics of the Small-Signal Amplifier

r_c = radius to outside edge of slow-wave circuit = 0.530 inch

r_o = radius of the center-of-the-beam electron = 0.541 inch

r_s = radius to inside edge of sole electrode = 0.688 inch

h = height of the beam parallel to the cylindrical axis = 0.500 inch

σ = unrippled radial width of the electron beam = 0.012 inch

P_c = critical perveance of the beam for no rippling = 0.43 micropervs

V_H = d-c potential of flattened helix = 0 volts

V_{L3} = d-c potential of launch electrode adjacent to helix = -6 volts

V_{L2} = d-c potential of center launch electrode = -16 volts

V_{L1} = d-c potential of launch electrode adjacent to electron gun = -31 volts

V_4 = d-c potential of final electrode of electron gun = -46 volts

V_3 = d-c potential of third electrode of electron gun = -713 volts

V_2 = d-c potential of second electrode of electron gun = -46 volts

V_1 = d-c potential of mask electrode = -900 volts

V_f = d-c potential of filament = -1046 volts

V_s = d-c potential of sole electrode = -523 volts

V_c = d-c potential of collector electrode = -20 volts

I_o = d-c current in electron beam = 13.68 milliamperes

W_o = d-c power of electron beam = 13.68 watts

J_o = current density of electron beam = 352 ma/cm^2

J_s = required emission current density from filament = 1 $ampere/cm^2$

T_o = estimated operating temperature of tungsten filament = 2400° C

Table 4.7 Small-Signal Parameters of the E-Type Forward-Wave Amplifier

Frequency, kmc	β_e	C	Q	d
3.95	18.4	0.074	-2.00	0 to 1
5.00	23.0	0.060	-2.00	0 to 1
5.85	27.6	0.050	-2.00	0 to 1
	"Midband" Parameters Used in the Theoretical Predictions			
	23	0.06	-2.0	0 to 1

The general features of the small-signal amplifier are shown in the photograph of Fig. 4.1. A discussion of the theoretical performance characteristics, obtained by supplying the parameters listed in the foregoing table to the TWEET program, is presented in the next section.

4.4 Theoretical Predictions for the Small-Signal Amplifier

The theoretical predictions for the experimental forward-wave amplifier constructed in this laboratory are presented in Appendix I. In view of the extensive discussion of the small-signal solutions presented in Section 3.11, the purpose of this section is to describe the propagation constants and gain characteristics of the experimental device. Since typical values of the tube parameters can be estimated within reasonable limits of accuracy, except for loss, computations were made over fairly wide limits of d.

The incremental propagation constants which apply to the lossless case are shown in Fig. I.1. The observed "pattern splitting" of the real parts is probably due to the combined effects of the relatively small size of β_e and large size of Q, since the gain parameter is sufficiently

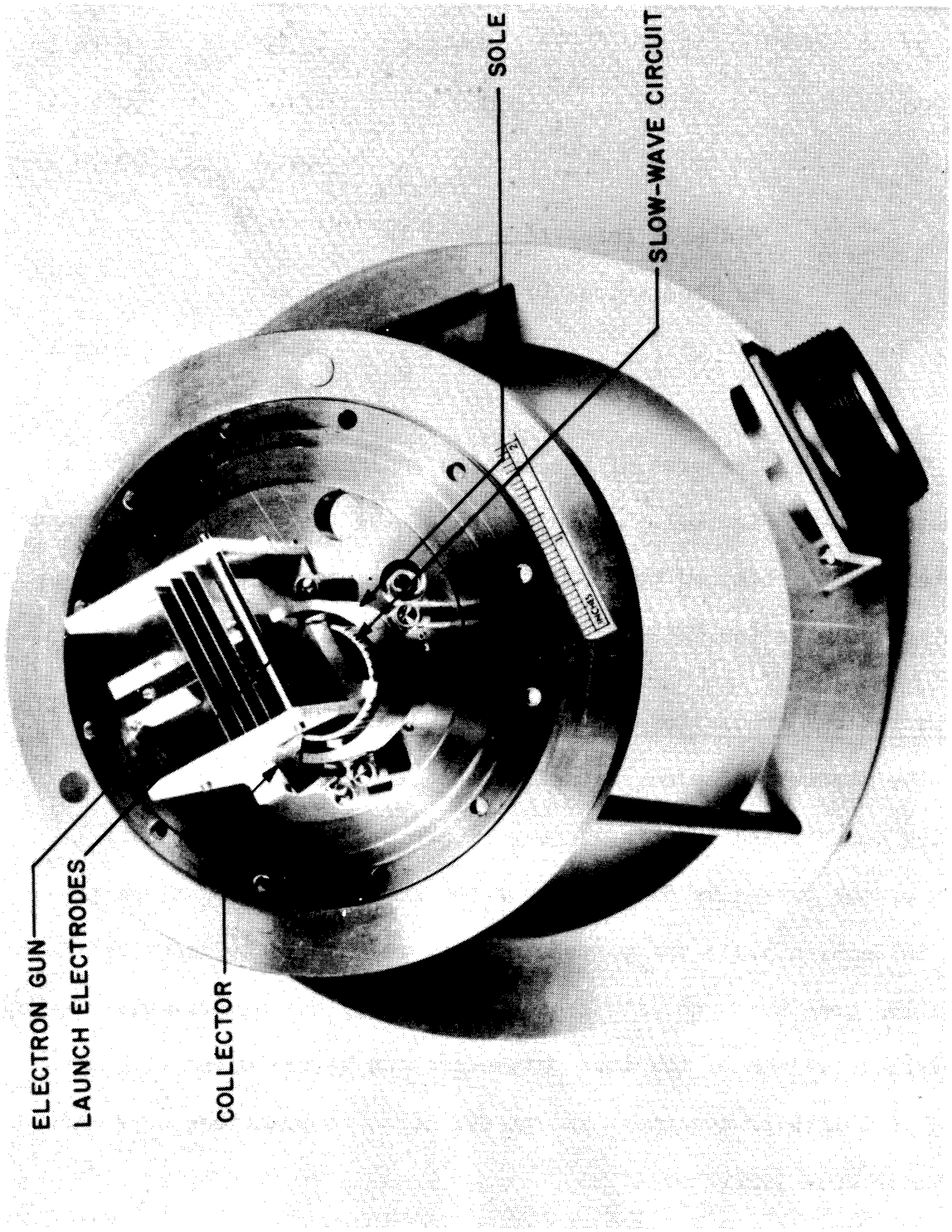

FIG. 4.1 EXPERIMENTAL E-TYPE TRAVELING-WAVE AMPLIFIER.

large as to discount its influence. The two ellipses associated with the x-versus-b curve are closely situated as a result of the fact that splitting takes place for parameter values not far removed from those of the experimental tube. The major axis of the ellipse surrounding the origin is seen to be only slightly larger than its separated counterpart to the right, just as would be expected from a consideration of their proximity along the b-axis.

A study of the imaginary parts reveals that y_2 and y_4 represent the fast and slow space-charge waves at large negative values of b. In this same region, y_3 becomes the circuit wave while y_1 becomes the synchronous space-charge wave. The coalescing of curves y_1 and y_2, and then y_2 and y_4, in the vicinity of the origin, coincides with the range of b values for which nonvanishing real parts exist. At large positive values of b, the imaginary parts y_3 and y_4 are identified with the fast and slow space-charge waves, while y_1 and y_2 become associated with the synchronous space-charge and circuit waves, respectively. Since this basic pattern is unchanged for all values of loss, other than the fact that the curves do not coalesce when d is nonzero, the imaginary parts will receive no further attention. It is nevertheless interesting to observe, from a study of Figs. I.1-I.7, that the values which y_2 and y_4 approach at large negative values of b, and which y_3 and y_4 approach at large positive values of b, are such that the velocities of the fast and slow space-charge waves are independent of the circuit loss, in good agreement with the findings in Chapter III.

For the relatively small loss value which exists when d = 0.010, the real parts take the form shown in Fig. I.2. The circuit wave (given

by x_3 at large negative values of b, and by x_2 at large positive values of b) acquires a negative real part whose magnitude is equal to the loss in the absence of the beam. Precisely the same behavior exists when d assumes the successive values 0.050, 0.100, 0.500 and 1.00, as a careful examination of Figs. I.3-I.6 reveals. Perhaps the most interesting feature of these curves is the manner in which the loss parameter influences the magnitudes of x_1, x_2 and x_4, in the vicinity of b = 0, where they attain their maximum values. Successive increases of d leads to a reduction in the magnitudes of x_1 and x_4, which are associated with exponentially growing-waves, and to an increase in the magnitude of x_2, which is associated with the exponentially decaying wave. The behavior of the radial and backward waves is accurately described by Eqs. 3.116 and 3.117, in both the presence and absence of loss.

The gain characteristics of the experimental forward-wave amplifier are shown in Figs. I.8-I.12. A careful study of Fig. I.1 shows that the real parts of the propagation constants just vanish at b = -1.2, 0.80, 2.20. The numerical solutions of the gain function appearing in Fig. I.8 indeed verify that only beating-wave gain is possible at these electron injection velocities. The largest gain occurs for b = 2.20 at an angle of 500 electrical degrees, where it reaches a value of 7.5 db.

The results appearing in Figs. I.9-I.12 show, however, that the customary growing-wave gain is strongly in evidence at b = 0, 1.5, near the maxima of the x-versus-b curves. A successive increase of loss results in a continuing decrease of gain at each of these values of b. A comparison of Figs. I.9 and I.10 with the x-versus-b curves shows that the growing-wave gain occurring near b = 0 is due principally to the wave δ_1, while the growing-wave gain observed near b = 1.5 is due to δ_4.

Since the amplitude of x_1 is greater than that of x_4, the growing-wave gain produced near b = 0 always exceeds that near b = 1.5, for a given value of loss. When the loss becomes very large, as in Figs. I.11 and I.12, the gain is severely degraded. Therefore, care must be taken to avoid the use of excessive amounts of attenuating materials (such as aquadag), which are sometimes applied to the r-f structure in order to minimize spurious oscillations caused by reflections from a mismatched output transducer.

An examination of Fig. I.9 reveals that the growing-wave gain at an angle of 500 electrical degrees lies between 20 and 25 db, depending on the loss. Since this is more than three times the beating-wave gain obtained at the same electrical angle when b = 2.20, it was decided to construct the device as a growing-wave rather than a beating-wave amplifier.

A total of fifteen turns of the helix will be available for receiving a continuing transfer of energy from the electron beam. Since the mean height and width of the flattened helix are 0.565 inch and 0.045 inch, respectively, the total wire length is

$$\text{Total length of helix wire} = 30\,(0.565 + 0.045)$$

$$= 18.30 \text{ inches.}$$

The wavelength at an operating frequency of 5000 mcs is equal to

$$\lambda_{5\text{kmc}} = \left(\frac{3\cdot 10^{10} \text{ cm/sec}}{5\cdot 10^{9} \text{ cps}}\right) \quad \frac{1}{2.54 \text{ cm/inch}}$$

$$= 2.36 \text{ inches.}$$

The electrical length of the helix is approximately

$$N = \frac{18.3}{2.36} = 7.75 \text{ "wave angles".}$$

For the synchronism case, b = 0, so that Eq. 3.111 simplifies to

$$N_s = N.$$

Therefore, the electrical angle Φ, given by Eq. 3.110, becomes

$$\Phi = \left[360\ (0.06)\ 7.75\right] = 167 \text{ degrees.}$$

The curves of Fig. I.9 show that the growing-wave gain corresponding to this electrical angle is approximately 4.5 db, in the absence of loss. In view of this relatively small level of amplification it has been decided not to apply any loss coating to the r-f structure.

It has occurred to the writer that an interesting test of the theory would be possible from the theoretical predictions obtained here. Since growing-wave gain is obtained at b = 0, 1.50, and beating-wave gain occurs at b = 0.80, it would appear that by changing the relative injection velocity a "growing-beating-growing-wave" behavior should be observable. Unfortunately, this change of electron velocity also requires a simultaneous change of the equilibrium potential applied between the sole and slow-wave circuit, as well as several electrode potentials of the electron gun*. For practical reasons, therefore, it might be a rather difficult task to accomplish, and no provision for it has been made in the existing device. Nevertheless, an investigation of this sort affords a novel approach to experimental support of the analysis.

---

* These changes also require a simultaneous adjustment of the beam current if the critical perveance conditions, which minimize rippling, are to be maintained. If the current is required to increase to large proportions, emission density limitations may be imposed by the electron source.

4.5 Experimental Results

The cold-test measurements made on the experimental amplifier involve a determination of the reflection and insertion loss characteristics of the r-f structure. The input VSWR, observed with the output match terminated, and the output VSWR, observed with the input match terminated, are plotted as a function of frequency in Fig. 4.2. The input and output r-f connections to the flattened helix were adjusted to produce a minimum standing wave ratio at a frequency near 5000 mcs by means of a line-above-ground transmission system. Since this particular feed system possesses a limited bandwidth, the VSWR observed at other frequencies increases appreciably above its midband value. Nevertheless, the VSWR measured at both the input and output terminals does not exceed 2.5 to 1 in a 400 mcs region surrounding the center frequency of 5000 mcs. It should also be noted that these results include the reflection characteristics of the type-N connectors attached to the external coaxial transmission line. Independent measurements made by the author and his associates have shown that the connectors used here exhibit standing wave ratios as large as 3 to 1 as the X-band frequency range is approached.

The cold-circuit insertion loss characteristics shown in Fig. 4.3 were obtained by the r-f substitution procedure. This measurement technique, which is known for its accuracy since the results are independent of the detector response law associated with the read-out device, makes use of a calibrated variable r-f attenuator. The attenuator is adjusted to provide a convenient signal level on the oscilloscope with the slow-wave circuit inserted in the test network. The slow-wave circuit is subsequently removed and the attenuator is sufficiently increased to

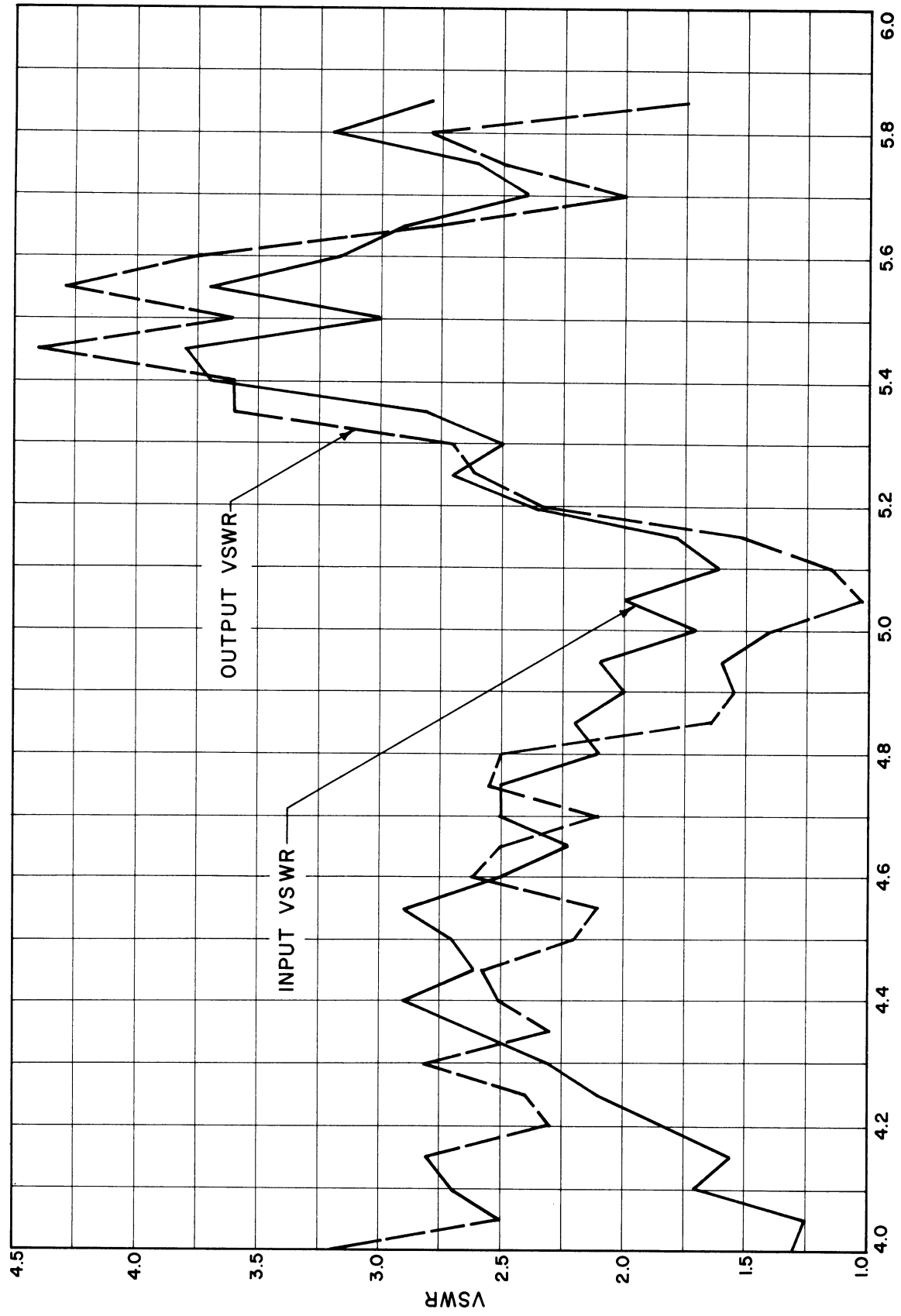

FIG. 4.2 VSWR MEASUREMENTS ON AMPLIFIER FLATTENED HELIX.

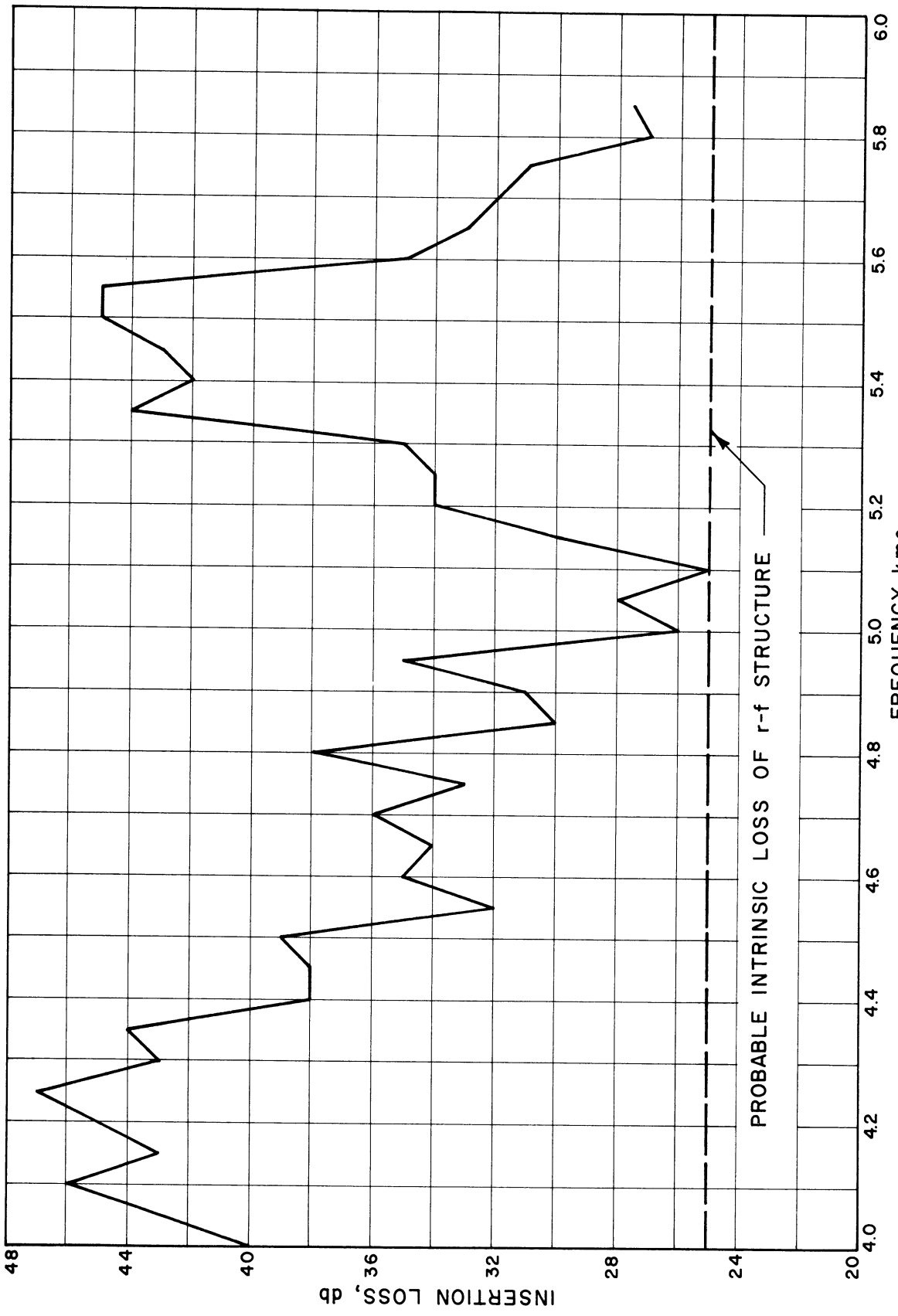

FIG. 4.3 INSERTION LOSS CHARACTERISTICS OF THE AMPLIFIER FLATTENED HELIX.

return the signal to its former level. The difference in attenuator readings then represents the insertion loss of the flattened helix.

A careful examination of this figure shows that its overall shape resembles that of Fig. 4.2. In those regions of the r-f spectrum where the standing wave ratio is small the insertion loss also decreases, and as the VSWR increases the loss similarly rises. This behavior is to be expected because the measured insertion loss results from an "intrinsic component", that is associated with the energy dissipated in the structure, and a "reflection component", that accounts for wave reflections from mismatched input and output terminations. Since the minimum VSWR and insertion loss occur at a frequency near 5100 mcs, the intrinsic loss is estimated to be approximately 25 db, as shown in Fig. 4.3. The importance of achieving a good match is clearly evident from this curve, inasmuch as large reflections lead to an insertion loss that is almost twice the intrinsic loss near the edges of the frequency band.

The unusually high value of intrinsic loss found here has led to an investigation of the factors contributing to its presence. Among the potential sources of dissipative loss are the following:

1. Resistive Losses — These result from the attenuation produced when the wave encounters the ohmic resistance of the helix wire. However, a careful set of measurements made on the structure reveals that the d-c resistance of the flattened helix is only four ohms, which is not likely to produce the large value of loss observed.
2. Radiation Losses — These result from energy escaping directly from the r-f transmission system connected to the ends of the helix, as well as radiation from the individual turns of the

helix itself. The fact that much larger standing wave ratios were observed near the band extremities for the two flattened helices wound on the straight polystyrene mandrels (described in Section 4.2) suggests that radiation from the individual turns of the helix is probably small. There is the possibility, however, that radiation from the line-above-ground feed system connected to the amplifier flattened helix might contribute to the observed intrinsic loss, since the ground plane does not completely surround the center conductor. The coaxial feed system used in the test helices avoids this problem, inasmuch as the center wire is completely shielded by the outer conductor.

3. Dielectric Losses — These result from the energy absorbed by the dielectric mandrel in the presence of a high frequency r-f field. While the loss tangent of polystyrene is known to be low over the 3.95-5.85 kmc frequency band, the characteristics of the ceramic mandrel are not known. The decision to use the ceramic material was based on the assumption that <u>each</u> of the wide faces would be undercut 0.015 inches. However, the danger of breakage during machining was found to be so great as to warrant an undercut of not more than 0.010 inches on the outside face <u>only</u> of the mandrel. Thus, both increased dielectric loading, which results in a larger wave slowing factor and a smaller surface impedance, and greater dielectric lossless are produced by this physical limitation. An independent set of measurements carried out with a flattened helix wound on a similar ceramic mandrel confirms the premise that dielectric losses are chiefly responsible for the large intrinsic loss (a coaxial feed system

was used to minimize direct radiation from the center conductor of the transmission line).

Aside from these considerations another possible source of difficulty was investigated. Since the E-type device requires the presence of a static radial electric field to balance the centrifugal force of the revolving electrons in order to maintain dynamic equilibrium, it is necessary to provide a d-c return between the helix and the housing. A small, round helix was employed to provide a low resistance connection to the source voltage while yielding a high impedance for the r-f signal. Several of these "r-f chokes" were constructed and installed for test. It was found that a 0.080 inch diameter helix, one inch long and containing 64 turns, produced the largest value of r-f impedance.

In spite of the reduced insertion loss afforded by an investigation of the choke design, it is apparent that a low impedance r-f choke cannot be solely responsible for the results observed. If this were the case, then the insertion loss would have been due almost entirely to the reflection component, with the intrinsic loss being very small. Under these circumstances the slow-wave structure is characterized by extremely large reflections, which were not observed, and the small standing wave ratio obtained at 5.1 kmc could not exist. It follows that the most important source of cold-circuit loss is that associated with the dielectric properties of the ceramic mandrel. The recommendation made in Chapter V, concerning a modification of the mandrel in order to raise the helix surface impedance, should substantially reduce the intrinsic loss of the slow-wave circuit.

The beam transmission characteristics of the experimental E-type device are shown in Fig. 4.4. The three curves appearing in this figure have the following significance:

1. Overall Beam Transmission — This refers to the ratio of the collector current to the total current transmitted beyond the mask electrode. The quantity therefore accounts for the current intercepted by the electron gun and launch electrodes, as well as that falling on the helix and sole. The most severe restrictions are thus imposed by this description of beam transmission. In addition, the electrons involved in this computation are required to travel over the longest spatial distance in order to arrive at the collector.
2. Beam Transmission through Entire Drift Space — This refers to the ratio of the collector current to the current leaving the electron gun. It therefore represents a less severe description of beam transmission, since the current intercepted by the gun electrodes is neglected.
3. Beam Transmission through the R-f Region of the Drift Space — This refers to the ratio of the collector current to the current passing beyond the launch electrodes. It is the least severe description of beam transmission not only because it neglects the current received by the electron gun and launch electrodes, but also because the electrons are required to travel the shortest spatial distance in order to arrive at the collector.

Although the three curves exhibit definite maxima and minima, it must be explained that the results reflect the critical adjustments

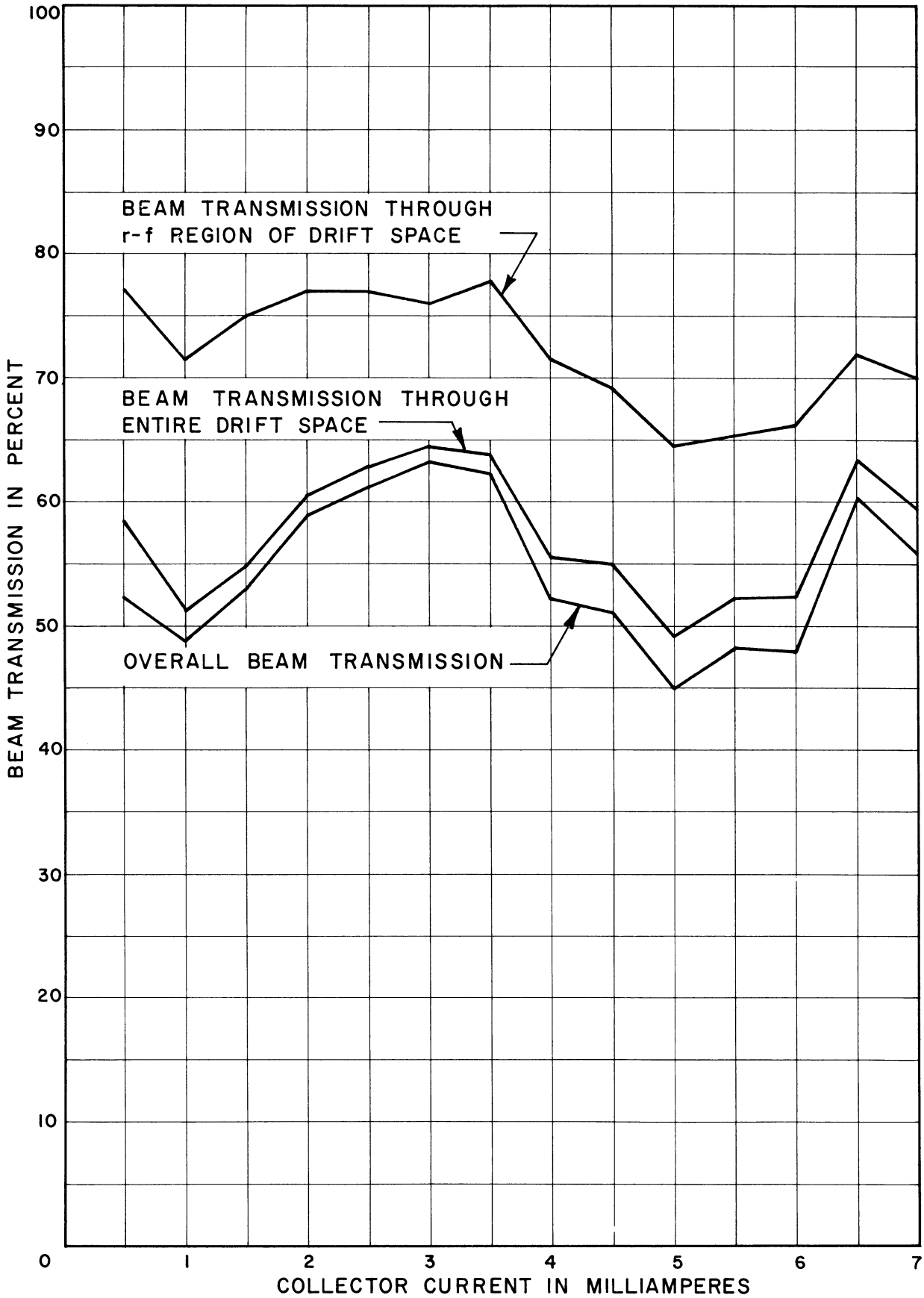

FIG. 4.4 BEAM TRANSMISSION CHARACTERISTICS OF THE EXPERIMENTAL DEVICE.

necessary to maintain the beam on its proper trajectory. Since the sole-to-circuit voltage exerts the greatest influence over beam transmission, the most probable cause of these peaks and troughs is an inability to achieve the optimum sole voltage adjustment for each value of collector current. A study of the curves shows that the average values of beam transmission, over the range of 0.5 to 7.0 ma of collector current, are approximately as given in the table below.

Table 4.8 Average Beam Transmission Characteristics of the Experimental E-Type Device

Type of Transmission	Average Value in Percent
R-f Region of Drift Space	71
Entire Drift Space	58
Overall Beam Transmission	54

The writer expected the beam transmission characteristics to exhibit an overall downward trend as the collector current is increased, because of the space-charge forces in the beam. The fact that such a trend is not evident from the experimental results presented in Fig. 4.4 suggests that currents in excess of those recorded can be successfully focused by centrifugal-electrostatic means, using the large center-of-the-beam-electron radius employed here. This is a rather significant finding since the theoretical results have pointed to the desirability of large beam radii in order to achieve a large value of gain per unit spatial angle. Moreover, there is reason to believe that even greater beam transmission figures can be realized by improving the design of the

electron gun and injection system. The radial electric field should be started as close to the final gun electrode as possible to minimize radial spreading of the beam. The distance of almost one-quarter of an inch, used in the experimental device, could probably be decreased to less than one-fifth of this spacing.

In addition to these findings, several qualitative observations have tended to confirm the assertion that stable beams can be obtained for the present electron radius. The first of these pertains to the fact that, when the equilibrium potentials were properly adjusted, the sole current was always zero, even for the largest collector current recorded. Thus, the center-of-the-beam electron was apparently following the desired trajectory after leaving the electron gun. The radial space-charge spreading forces, as well as beam rippling, are probably responsible for the helix interception current which increases with collector current. The second observation involves the fact that, although the proper sole voltage adjustment becomes increasingly more difficult with larger collector currents, equilibrium conditions can always be achieved over the range of beam currents recorded. Moreover, the value of the sole-to-circuit voltage remained unchanged within the limits of collector current employed. Once the proper adjustment of equilibrium potentials had been made, the currents received by the various electrodes remained unchanged, unless external disturbances present on the electrical supply lines upset the critical balance of forces.

A third set of observations were made when the tube was opened for inspection and repair. An optical examination revealed that the darkened area of the collector created by the electron beam was sharply

defined and situated on the portion of the collector face nearest to the slow-wave circuit. It therefore appears that the electron beam is following a circular path close to the r-f structure (this is consistent with the absence of sole current under equilibrium conditions). In addition, the fact that the darkened area was not observed to "spill over" the upper and lower extremities of the collector suggests that the "end hats" attached to the sole are serving their intended purpose of preventing vertical spreading of the beam.

The actual operating conditions observed with a collector current of 7 ma are recorded in Table 4.9. A comparison of these results with the corresponding "design values" given in Table 4.6 shows that the beam current and power are only slightly less than had been sought. However, the design values neglect the current intercepted by the launch electrodes, so that the beam current arriving at the collector is somewhat less than anticipated. Likewise, the observed perveance value of 0.347 micropervs is less than the critical value of 0.43 micropervs, thereby implying the presence of beam rippling. It was decided not to attempt further increases in beam current by raising the heater voltage, since earlier tests showed that the filament failed within one hour when more than 9.5 volts are applied to the tungsten ribbon. An increase of beam current achieved by raising the voltage on the mask electrode leads to excessive amounts of power dissipation at that element.

Table 4.9 Operating Conditions for the Experimental Device

Electrode	Voltage	Current, ma
Helix	0	3.00
Collector	0	7.00
Sole	-450	0
Launch Electrode No. 3	-80	0.30
Launch Electrode No. 2	-78	0.30
Launch Electrode No. 1	-100	1.20
Gun Electrode No. 4	-88	0.50
Gun Electrode No. 3	-460	0
Gun Electrode No. 2	-39	0.25
Mask Electrode	-867	115.00
Filament	-1046	127.55

Heater Operation: 8.4 volts 6 amps. 50.4 watts

Beam Current Leaving Electron Gun = 11.8 ma.

Beam Power = 11.3 watts.

Beam Perveance = 0.347 micropervs.

Power Dissipated at Mask Electrode = 20.5 watts.

Overall Beam Transmission = 55.8 percent.

Beam Transmission through Entire Drift Region = 59.3 percent.

Beam Transmission through R-f Region of Drift Space = 70 percent.

Vacuum Pressure = $5 \cdot 10^{-7}$ mm of Mercury.

If the same effective interaction impedance is assumed to exist at a frequency of 5 kmc as that given in Table 4.5, it follows that the gain parameter corresponding to a collector current of 7 ma becomes

$$C = \sqrt[3]{\frac{30.8(7\cdot10^{-3})}{2(1046)}} = 0.047$$

This magnitude, which is only slightly less than the "midband" value of 0.06 appearing in Table 4.7, leads to an angle of

$$\Phi = \beta_e C\theta = 131 \text{ electrical degrees,}$$

and the growing-wave gain is estimated to be 2 db from the d = 0 curve in Fig. I.9 (this value can only be regarded as approximate, since the curves in Appendix I explicitly apply to the case that C = 0.06).

It should be noted that the relatively small values of gain dealt with here could be substantially increased by sufficiently decreasing the synchronous beam potential. While a reduction in V_o would require an appropriate decrease in the wave phase velocity along the helix (if operation in the vicinity of synchronism between the spatial angular velocities of the electron beam and r-f wave is to be maintained), both β_e and C would be raised by this change, so that the real part of the growing-wave incremental propagation constant now acquires a larger value. In addition, the electrical angle Φ, which is directly proportional to β_e and C, would become greater, thereby contributing to further increases in growing-wave gain.

However, this reduction in beam voltage must be made at the expense of the beam power and, therefore, the r-f power output. In addition, the required perveance of the electron gun would have to be

increased if the beam current were to be held constant. Nevertheless, the results presented in Appendix I reveal that more than 10 db of gain could be achieved for the same spatial angle as used here, with a two-to-one reduction of V_o and with a collector current of 7 ma.

Several attempts to observe growing-wave gain were unsuccessful, because of the dielectric loss of the ceramic mandrel. In addition, the dielectric constant of this support is thought to be of sufficient size* to produce further detrimental effects. Thus, a high value of dielectric constant not only decreases the intensity of the r-f fields in the interaction space, which decreases the structure impedance and gain, but it also reduces the azimuthal component of wave phase velocity along the slow-wave circuit. Since the theoretical analysis has revealed that the largest gain values are realized when the spatial angular velocities of the electron stream and r-f wave are in synchronism, it becomes necessary to reduce the velocity of the beam entering the interaction region. However, the accompanying reduction of electron gun anode voltage also decreases the beam current and gain parameter. An effort to raise the beam current through an increase in beam voltage, results in a loss of synchronism between the beam and the wave. These effects, which degrade gain, act in addition to the decrease of r-f field intensity produced by the insertion loss of the slow-wave circuit.

---

* The dielectric constant is thought to lie in the range of 4 to 8, which is typical of such materials (notably the vacuum sealing glasses) used in the fabrication of electron beam devices.

CHAPTER V. CONCLUSIONS

5.1 Basic Characteristics of E-Type Devices

The theoretical analysis presented in Chapters II and III has provided a general approach to the small-signal study of E-type traveling-wave devices. Among the important consequences of this investigation, the following are particularly significant:

1. The treatment advanced here was primarily concerned with the properties of the complementary mode, azimuthally nonre-entrant E-type traveling-wave tube, for which the small-argument approximations to the radial functions are valid. The characteristics of the slow-wave structure are such that only one axial and one azimuthal space-harmonic component are presumed to interact with the ribbon beam.
2. The ribbon electron stream is assumed to be so constituted that the "critical perveance" condition is always satisfied, thereby eliminating the radial variations associated with beam rippling. In addition, the ribbon-shaped beam satisfies the Brillouin flow, Eulerian fluid hypothesis which requires that electrons at all radial positions follow parallel trajectories with the same spatial angular velocity. The beam is also presumed to be sufficiently thin that essentially the same r-f fields act on all stream particles. Finally, it is assumed that electron bunching, produced by the velocity-modulating r-f fields on the circuit, generates an a-c space-charge field whose direction is wholly azimuthal.

3. The small-signal incremental propagation constants possess properties that resemble those found in O-type traveling-wave tubes. The waves associated with δ_1, δ_2 and δ_3, for example, are characterized by x-versus-b and y-versus-b curves that are similar to corresponding solutions of O-type devices.

4. The solutions of the determinantal equation have revealed, however, that the propagation constants of the E-type traveling-wave device exhibit properties similar to those of M-type. Among these are the fact that a "low velocity limit" for the electron beam exists below which growing-wave gain ceases, even when space charge is not present. In addition, there exists a region of the y-b plane for which y_1 and y_2 are greater than zero, thereby indicating that the growing- and declining-waves travel faster than the electron beam which creates them. Thin, nonslipping-stream beams in M-type devices give rise to the same phenomenon.

5. Apart from these resemblances to M- and O-type devices, it is found that the incremental propagation constants of E-type tubes have certain distinctive characteristics. The "pattern splitting" behavior of the x-versus-b curve, which accompanies small values of β_e and C as well as large negative values of Q, does not occur in other types of traveling-wave tubes. Furthermore, E-type devices are associated with a "synchronous" space-charge wave in addition to the "fast" and "slow" space-charge waves of O-type tubes. At large positive values of b in the forward-wave device, and large negative values of b in

the backward-wave device, this "synchronous" space-charge wave is identified by the incremental propagation constant δ_4, which describes a wave that never travels faster than the electron beam. The investigation has also shown that E-type devices exhibit a "radial" wave characterized by the complete absence of azimuthal propagation.

6. The growing-wave gain of E-type devices is enhanced by an increase in the gain parameter C, and is degraded by loss, much as with other types of traveling-wave tubes. However, the gain of E-type tubes is found to be strongly influenced by the radius of curvature of the ribbon beam. The analysis shows that, in order to obtain a large value of gain in a single transit of the electrons through the interaction region, the radius of curvature of the beam should be large. This, unfortunately, is in direct conflict with the requirements imposed by "beam stiffness" considerations. Moreover, a reduction of the beam radius exerts an influence over the start-oscillation characteristics of the E-type backward-wave oscillator that is equivalent to a comparable reduction of the gain parameter.
7. The study has shown that the a-c component of the space-charge fields (corresponding to solutions involving nonzero Q) reduces the growing-wave gain of the forward-wave amplifier, similar to a comparable behavior of O-type devices[7]. In addition, the introduction of loss gives rise to a growing-wave component produced by the positive real part of δ_4. Under typical circumstances x_4, which vanishes in the absence of loss, reaches its maximum value for slightly positive values of b, where the

electron beam travels faster than the wave on the r-f structure. This is in contrast with the real part x_1 which attains its maximum value near synchronism between the spatial angular velocities of the electron beam and the r-f wave.

8. The azimuthal component of a-c convection current is found to be much larger than the radial component, so that interaction between the electron beam and the r-f wave is principally an azimuthally-oriented phenomena. Since radial motion is negligible, it follows that the r-f structure could be situated outside, rather than inside, the electron beam. This conclusion, which agrees with the findings of Pantell[24], is significant for E-type devices intended to operate at very high frequencies where the components of the slow-wave circuit become exceedingly small.
9. The analysis shows that the efficiency, based on the small-signal study presented here, of E-type traveling-wave tubes is comparable to that of O-type devices.

5.2 Refinements of the Small-Signal Theory

The small-signal analysis of all types of traveling-wave tubes customarily involves the assumption that electron trajectories do not cross. The "Eulerian fluid hypothesis" is therefore a reasonable premise on which to develop the theory of E-type devices. Furthermore, the separate, but important, simplification concerning the small amplitude of the perturbations as compared to the unvarying quantities is widely accepted.

In the E-type device, however, slipping-stream motion is of sufficient importance as to warrant greater attention in a further

treatment of the theory. Likewise, the finite thickness of the beam must be considered if a more accurate determination of electron-wave energy transformations are to be made. The steady space-charge fields of the beam should also be examined in order to determine their effects upon the operation of this class of traveling-wave tubes. All of these factors may be expected to modify the results obtained here.

5.3 Refinements of the Experimental Device

In the course of constructing the experimental small-signal forward-wave amplifier it has become apparent that certain improvements could be incorporated into future E-type devices. These modifications are recommended with a view toward improving the electrical or mechanical characteristics of the tube.

Considerable experience with problems posed by the electron gun has pointed to the desirability of reducing its physical size. The relatively large dimensions of the structure used result from a conservative design approach, since (approximate) analytical techniques were employed instead of the more customary experimental method[6]. The overall size of the gun electrodes was therefore made large in proportion to the aperture dimensions so as to assure the proper static electric field contour in the region of the beam. The exact limits to which these electrodes may be reduced can be determined with the aid of an electrolytic tank.

Another basic component which should receive further design attention is the slow-wave circuit. While the flattened helix appears to have good electrical characteristics, it is evident that the structure impedance is seriously degraded by the use of a high-dielectric mandrel. In the present tube, some attempt was made to "undercut" the mandrel

surface along the flat portion near the outside edge of the helix. However, in order for the dielectric loading of the mandrel to be reduced significantly the undercut should be accomplished on both the inside and outside edges of the helix support. In view of the danger of breakage during the machining of such a complex configuration, it was decided to undercut the ceramic along the outside surface only. Nevertheless, a subsequent design should take this problem into consideration, with the possibility of changing the mandrel radically. It has occurred to the author that two round sapphire rods might be bent into a circle of prescribed radius and fixed in height by means of three (vertical) stainless steel supports. One of these supports would be situated at the mid-point of the circular arc of the helix mandrel, while the remaining two would be located at its extremities. A mandrel of this type would appear to offer the smallest amount of dielectric loading since the region between the upper and lower circular supports is almost entirely free space.

Aside from these important details pertaining to an improvement in the structure impedance through a reduction of dielectric loading, there is also the question of obtaining a proper match at the r-f input and output terminals. Inasmuch as the numerical results have clearly shown that the application of loss severely degrades the gain of E-type devices, it is desirable to achieve as nearly reflectionless an impedance match as possible. The line-above-ground matching technique employed in the present experimental device is only one of a large class of r-f feed systems. Since round coupled-helix couplers are very effective in O-type traveling-wave devices, an investigation of their flattened helix counterpart seems warranted. Other feed systems should also be examined

with regard to their low VSWR and insertion loss characteristics over wide frequency ranges.

APPENDIX A. DERIVATION OF THE SCALAR WAVE EQUATION IN CYLINDRICAL COORDINATES

Several procedures exist for deriving the scalar wave equation in cylindrical coordinates from the vector electric and magnetic field intensities. The method presented by Stratton[9] makes use of the fact that an electromagnetic field can be resolved into two partial fields associated with the Hertz electric and magnetic polarization potentials. These partial fields can then be derived from a scalar function which satisfies the scalar wave equation.

The derivation given here involves the substitution of prescribed forms of electric and magnetic field intensity expressions into Maxwell's equations, and subsequently simplifying the relations by a sequence of vector algebraic operations. A development which in some respects is similar to the present treatment is outlined by Waldron[16], and although the field components can be specified to have certain intended variations, the reduction process is somewhat more tedious.

It will be convenient to define the complex vector functions

$$\bar{\psi} = (\bar{\psi}_T + \bar{1}_z \psi_z)\, e^{j(\omega t - \gamma z)} \quad , \tag{A.1}$$

$$\bar{\xi} = (\bar{\xi}_T + \bar{1}_z \xi_z)\, e^{j(\omega t - \gamma z)} \quad , \tag{A.2}$$

where $\bar{\psi}_T$, $\bar{\xi}_T$ = transverse vector functions of r and θ,

ψ_z, ξ_z = axial scalar functions of r and θ only,

$\bar{1}_z$ = unit vector in the axial direction,

ω = $2\pi f$ = electrical angular velocity of the r-f wave in electrical radians/second,

f = frequency of the r-f wave in electrical cycles/second,

γ = axial propagation constant in electrical radians/meter,

z = axial coordinate variable in meters,

t = time in seconds.

The vector functions have been chosen so that

$$\overline{E} = \text{Re}\ \overline{\psi} \quad , \quad \text{and} \quad \overline{H} = \text{Re}\ \overline{\xi} \quad , \tag{A.3}$$

where $\overline{E}$ = vector electric field intensity in volts/meter,

$\overline{H}$ = vector magnetic field intensity in ampere-turns/meter.

In homogeneous, lossless, isotropic media containing no charge, Maxwell's equations take the form

$$\nabla \times \overline{E} = -\mu_m \frac{\partial \overline{H}}{\partial t} \quad , \tag{A.4}$$

$$\nabla \times \overline{H} = \epsilon_m \frac{\partial \overline{E}}{\partial t} \quad , \tag{A.5}$$

$$\nabla \cdot \overline{E} = 0 \quad , \tag{A.6}$$

$$\nabla \cdot \overline{H} = 0 \quad , \tag{A.7}$$

where μ_m = permeability of the medium in henry/meter,

ϵ_m = permittivity of the medium in farad/meter.

The conditions under which relations A.1 and A.2 satisfy Maxwell's equations may be investigated by substituting A.3 into Eqs. A.4 and A.5. The equations become

$$\text{Re}\ (\nabla \times \overline{\psi}) = \text{Re}\left(-\mu_m \frac{\partial \overline{\xi}}{\partial t}\right) \quad , \tag{A.8}$$

$$\mathrm{Re}\,(\nabla \times \xi) = \mathrm{Re}\left(\epsilon_m \frac{\partial \psi}{\partial t}\right) , \qquad (A.9)$$

where the operations of taking the real part and partial differentiation have been interchanged owing to the linear character of these transformations. The above relations can be satisfied separately by functions whose real parts are equal, irrespective of their imaginary parts. However, the two relations can be satisfied <u>simultaneously</u> only when the real and imaginary parts of the left and right members of each equation are equal. This results from the fact that, for harmonic time variation, partial differentiation with respect to time can be replaced by the $j\omega$ operator. Since multiplication by j is equivalent to interchanging the real and imaginary parts of a given complex function, it follows at once that Eqs. A.8 and A.9 can <u>both</u> be satisfied provided

$$\nabla \times \bar{\psi} = -\mu_m \frac{\partial \bar{\xi}}{\partial t} , \qquad (A.10)$$

$$\nabla \times \bar{\xi} = \epsilon_m \frac{\partial \bar{\psi}}{\partial t} , \qquad (A.11)$$

so that the relations A.1 and A.2 are seen to satisfy Maxwell's equations.

Equations A.1 and A.2 can now be substituted into Eqs. A.4 and A.5 to obtain after expansion and simplification

$$\nabla \times \bar{\psi}_T + \nabla \psi_z \times \bar{1}_z - j\gamma\, \bar{1}_z \times \bar{\psi}_T = -jZ_m k_m (\bar{\xi}_T + \bar{1}_z \xi_z) , \qquad (A.12)$$

$$\nabla \times \bar{\xi}_T + \nabla \xi_z \times \bar{1}_z - j\gamma\, \bar{1}_z \times \bar{\xi}_T = j\left(\frac{k_m}{Z_m}\right)(\bar{\psi}_T + \bar{1}_z \psi_z) , \qquad (A.13)$$

where $k_m = \omega\sqrt{\mu_m \epsilon_m}$ = wave propagation constant of the medium in electrical radians/meter,

$Z_m = \sqrt{\mu_m/\epsilon_m}$ = wave impedance of the medium in ohms.

Forming the vector product of $\bar{l}_z$ with each member of the above equations, and making use of the relations

$$\bar{l}_z \times (\nabla \times \bar{\psi}_T) = 0, \quad \bar{l}_z \times (\nabla\psi_z \times \bar{l}_z) = \nabla\psi_z, \quad \bar{l}_z \times (\bar{l}_z \times \bar{\psi}_T) = -\bar{\psi}_T,$$

Eqs. A.12 and A.13 lead to

$$\nabla \psi_z + j\gamma\bar{\psi}_T = jZ_m k_m (\bar{\xi}_T \times \bar{l}_z) \quad , \tag{A.14}$$

$$\nabla \xi_z + j\gamma\bar{\xi}_T = -j\left(\frac{k_m}{Z_m}\right) (\bar{\psi}_T \times \bar{l}_z) \quad . \tag{A.15}$$

The divergence of Eqs. A.14 and A.15 is found to be

$$\nabla^2 \psi_z + j\gamma \nabla\cdot\bar{\psi}_T = j Z_m k_m \nabla\cdot(\bar{\xi}_T \times \bar{l}_z) \quad , \tag{A.16}$$

$$\nabla^2 \xi_z + j\gamma \nabla\cdot\bar{\xi}_T = -j\left(\frac{k_m}{Z_m}\right) \nabla\cdot(\bar{\psi}_T \times \bar{l}_z) \quad . \tag{A.17}$$

The scalar product of both members of Eqs. A.12 and A.13 with $\bar{l}_z$ yields

$$\bar{l}_z\cdot\nabla \times \bar{\psi}_T = -jZ_m k_m \xi_z \quad , \tag{A.18}$$

$$\bar{l}_z\cdot\nabla \times \bar{\xi}_T = j\left(\frac{k_m}{Z_m}\right) \psi_z \quad , \tag{A.19}$$

since $(\nabla\psi_z \times \bar{l}_z)$, $(\bar{l}_z \times \bar{\psi}_T)$, $(\nabla\xi_z \times \bar{l}_z)$ and $(\bar{l}_z \times \bar{\xi}_T)$, all lie normal to the axial unit vector. These expressions can be substituted into Eqs. A.16 and A.17 to obtain

$$\nabla^2 \psi_z + j\gamma \nabla\cdot\bar{\psi}_T = k_m^2 \psi_z \quad , \tag{A.20}$$

$$\nabla^2 \xi_z + j\gamma \nabla\cdot\bar{\xi}_T = -k_m^2 \xi_z \quad , \tag{A.21}$$

because of the cyclical permutation associated with the scalar triple product. If Eq. A.1 is used in conjunction with Eq. A.6, and Eq. A.2 with Eq. A.7, there results

$$\nabla\cdot\bar{\psi}_T = j\gamma\,\psi_z \quad , \tag{A.22}$$

$$\nabla\cdot\bar{\xi}_T = j\gamma\,\xi_T \quad , \tag{A.23}$$

since, evidently the conditions that

$$\mathrm{Re}(\nabla\cdot\bar{\psi}) = 0 \quad , \quad \text{and} \quad \mathrm{Re}(\nabla\cdot\bar{\xi}) = 0 \quad ,$$

can be satisfied if the entire arguments are equal to zero. The desired relations are obtained by substituting Eq. A.22 into Eq. A.20, and Eq. A.23 into Eq. A.21, thus yielding

$$(\nabla^2_{r,\theta} + k^2)\,\psi_z = 0 \quad , \tag{A.24}$$

$$(\nabla^2_{r,\theta} + k^2)\,\xi_z = 0 \quad , \tag{A.25}$$

where $k^2 = (k_m^2 - \gamma^2)$,

$$\nabla^2_{r,\theta} = \frac{1}{r}\frac{\partial}{\partial r}\left(r\,\frac{\partial}{\partial r}\right) + \frac{1}{r^2}\,\frac{\partial^2}{\partial\theta^2} \quad .$$

The transformation from ∇^2 to $\nabla^2_{r,\theta}$ follows from the fact that the axial scalar potentials ψ_z and ξ_z are functions of r and θ only.

APPENDIX B. THE SMALL-ARGUMENT APPROXIMATIONS TO THE REAL AND HYPERBOLIC BESSEL FUNCTIONS

A number of situations arise in the solution of electromagnetic boundary value problems that require fairly extensive tables of the real and hyperbolic Bessel functions when precise results are required. It is an unfortunate fact that the accumulated data is rather sparse for certain of these functions and entirely nonexistent for others. One of the more complete tabulations was prepared by Jahnke and Emde[4], which also contains many important recursion relations, although additional information has been published by Morse and Feshback[5], Watson[10], Dwight[12], Marcuvitz[15] and Waldron[16]. A review of these sources reveals, however, that only functions of integral order, or rational fractional order, are presented. While it is apparent that the computational labor may become quite considerable in many cases, a rather severe limitation is imposed upon the study of azimuthally nonre-entrant systems where general, nonintegral order, functions arise. It is of course possible to enlist the aid of a digital computer, assuming these facilities are available, but this has the effect of particularizing a broad theoretical treatment to special cases in numerical analysis.

An effort has been made to partially circumvent these problems by replacing the general Bessel relations with suitable small-argument approximations. The particular choice of simplifications employed, however, suggest the importance of properly interpreting the physical conditions surrounding this assumption.

B.I. The Real and Hyperbolic Bessel Functions of the First Kind

The power series expansion for the Bessel function of the first kind and real argument x is known to be[4,5]

$$J_p(x) = \frac{(x/2)^p}{p!}\left[1 - \frac{(x/2)^2}{(p+1)} + \frac{(x/2)^4}{2!(p+1)(p+2)} - \frac{(x/2)^6}{3!(p+1)(p+2)(p+3)} + \cdots\right] , \tag{B.1}$$

where the index p may be any positive or negative integer (including zero), or it must be greater than zero if it is nonintegral. The Bessel function of the first kind and imaginary argument is related to a function known alternatively as the modified or hyperbolic Bessel function $I_p(x)$. The latter terminology is used here, following the designation of Morse and Feshback[5], since this function is related to the corresponding Bessel function of real argument in a manner similar to that of the more elementary trigonometric and hyperbolic functions. The hyperbolic Bessel function of the first kind is thus written

$$I_p(x) = \frac{(jx/2)^p}{p!}\left[1 - \frac{(jx/2)^2}{(p+1)} + \frac{(jx/2)^4}{2!(p+1)(p+2)} - \frac{(jx/2)^6}{3!(p+1)(p+2)(p+3)} + \cdots\right](j)^{-p} , \tag{B.2}$$

from which it follows, by a comparison with Eq. B.1, that

$$I_p(x) = (j)^{-p} J_p(jx) . \tag{B.3}$$

The small-argument approximations to the real and hyperbolic Bessel functions of the first kind become, in view of Eqs. B.1 and B.2,

$$J_p(x) \approx \frac{(x/2)^p}{p!} \qquad |x| \ll 1 , \tag{B.4}$$

$$I_p(x) \approx \frac{(x/2)^p}{p!} \qquad |x| \ll 1 \quad . \tag{B.5}$$

It is interesting to observe that these functions reduce to a common form when their arguments have a small magnitude.

B.II. The Real and Hyperbolic Bessel Functions of the Second Kind

Although an explicit, but somewhat unwieldy, series expansion may be written for the Bessel function of the second kind and real argument x, a more compact mathematical expression is

$$N_p(x) = \frac{J_p(x) \cos p\pi - J_{-p}(x)}{\sin p\pi} \quad , \tag{B.6}$$

where the same limitations are imposed on the index p as in the case of $J_p(x)$. Upon carrying out a detailed limit process, it may be shown[4] that as x approaches zero

$$N_p(x) \approx -\frac{(p-1)!}{\pi}\left(\frac{2}{x}\right)^p \qquad |x| \ll 1, \quad p > 0 \quad . \tag{B.7}$$

The hyperbolic Bessel function of the second kind is related to the foregoing functions by means of the equation[5]

$$K_p(x) = \frac{\pi}{2}(j)^{p+1}\left[J_p(jx) + jN_p(jx)\right] \quad . \tag{B.8}$$

In order to determine the form which $K_p(x)$ assumes as x approaches zero, Eqs. B.3, B.5 and B.7 may be used in conjunction with Eq. B.8 to obtain

$$K_p(x) \approx \frac{\pi}{2}(j)^{p+1}\left[(j)^p \frac{(x/2)^p}{p!} - (j)^{-p+1}\frac{(p-1)!}{\pi}\left(\frac{2}{x}\right)^p\right] \quad ,$$

$$\approx \frac{(p-1)!}{2}\left(\frac{2}{x}\right)^p \qquad |x| \ll 1, \quad p > 0 \quad . \tag{B.9}$$

B.III. The First Derivatives of the Small-Argument Approximations

The application of the boundary conditions to the general solutions of the scalar wave equation leads to the requirement that the first derivatives of the real and hyperbolic Bessel functions be known under certain conditions. In the process of developing the expressions appropriate to the small-argument approximations, caution must be exercised with the two types of Bessel functions of the second kind since each possesses a singular point at the origin. It will be assumed, therefore, that over the range of x for which these approximations are valid the small-argument functions are finite, continuous and differentiable, and that they approach a finite value for any limit point within this range.

Subject to these restrictions, the first derivatives of the real and hyperbolic Bessel functions of the first kind may be written with the aid of Eqs. B.4 and B.5

$$J_p'(x) = I_p'(x) = \frac{x^{p-1}}{2^p(p-1)!} \qquad |x| \ll 1 , \qquad (B.10)$$

where the prime indicates differentiation with respect to x. The corresponding relations for the real and hyperbolic functions of the second kind become, in view of Eqs. B.7 and B.9,

$$N_p'(x) = \frac{2^p p!}{\pi x^{p+1}} \qquad |x| \ll 1, \quad p > 0 , \qquad (B.11)$$

$$K_p'(x) = \frac{-2^{p-1} p!}{x^{p+1}} \qquad |x| \ll 1, \quad p > 0 . \qquad (B.12)$$

B.IV. Derivation of the Special Relations

The act of imposing the boundary conditions in the coaxial-cylindrical system inevitably leads to general expressions of the following forms, involving the real or hyperbolic Bessel functions and their first derivatives.

$$X_{\beta_o}(k_n r) = J_{\beta_o}(k_n r)\, N_{\beta_o}(k_n r_s) - N_{\beta_o}(k_n r)\, J_{\beta_o}(k_n r_s) \quad , \qquad (B.13)$$

$$X'_{\beta_o}(k_n r) = J'_{\beta_o}(k_n r)\, N_{\beta_o}(k_n r_s) - N'_{\beta_o}(k_n r)\, J_{\beta_o}(k_n r_s) \quad , \qquad (B.14)$$

$$Z_{\beta_o}(k_n r) = J_{\beta_o}(k_n r)\, N'_{\beta_o}(k_n r_s) - N_{\beta_o}(k_n r)\, J'_{\beta_o}(k_n r_s) \quad , \qquad (B.15)$$

$$Z'_{\beta_o}(k_n r) = J'_{\beta_o}(k_n r)\, N'_{\beta_o}(k_n r_s) - N'_{\beta_o}(k_n r)\, J'_{\beta_o}(k_n r_s) \quad , \qquad (B.16)$$

$$V_{\beta_o}(k_n r) = I_{\beta_o}(k_n r)\, K_{\beta_o}(k_n r_s) - K_{\beta_o}(k_n r)\, I_{\beta_o}(k_n r_s) \quad , \qquad (B.17)$$

$$V'_{\beta_o}(k_n r) = I'_{\beta_o}(k_n r)\, K_{\beta_o}(k_n r_s) - K'_{\beta_o}(k_n r)\, I_{\beta_o}(k_n r_s) \quad , \qquad (B.18)$$

$$Y_{\beta_o}(k_n r) = I_{\beta_o}(k_n r)\, K'_{\beta_o}(k_n r_s) - K_{\beta_o}(k_n r)\, I'_{\beta_o}(k_n r_s) \quad , \qquad (B.19)$$

$$Y'_{\beta_o}(k_n r) = I'_{\beta_o}(k_n r)\, K'_{\beta_o}(k_n r_s) - K'_{\beta_o}(k_n r)\, I'_{\beta_o}(k_n r_s) \quad . \qquad (B.20)$$

Under the assumption that the arguments of these functions are small compared with unity, the approximations developed in the preceding sections of this appendix may be used to show that

$$X_{\beta_o}(k_n r) = \frac{-1}{\pi \beta_o r_s^{\beta_o}} \left[r^{\beta_o} - \frac{r_s^{2\beta_o}}{r^{\beta_o}} \right] \quad , \qquad (B.21)$$

$$X'_{\beta_o}(k_n r) = \frac{-1}{\pi k_n r_s^{\beta_o}} \left[r^{\beta_o - 1} + \frac{r_s^{2\beta_o}}{r^{\beta_o+1}} \right] , \qquad (B.22)$$

$$Z_{\beta_o}(k_n r) = \frac{1}{\pi k_n r_s^{\beta_o+1}} \left[r^{\beta_o} + \frac{r_s^{2\beta_o}}{r^{\beta_o}} \right] , \qquad (B.23)$$

$$Z'_{\beta_o}(k_n r) = \frac{\beta_o}{\pi k_n^2 r_s^{\beta_o+1}} \left[r^{\beta_o - 1} - \frac{r_s^{2\beta_o}}{r^{\beta_o+1}} \right] , \qquad (B.24)$$

$$V_{\beta_o}(k_n r) = \frac{1}{2\beta_o r_s^{\beta_o}} \left[r^{\beta_o} - \frac{r_s^{2\beta_o}}{r^{\beta_o}} \right] , \qquad (B.25)$$

$$V'_{\beta_o}(k_n r) = \frac{1}{2k_n r_s^{\beta_o}} \left[r^{\beta_o - 1} + \frac{r_s^{2\beta_o}}{r^{\beta_o+1}} \right] , \qquad (B.26)$$

$$Y_{\beta_o}(k_n r) = \frac{-1}{2k_n r_s^{\beta_o+1}} \left[r^{\beta_o} + \frac{r_s^{2\beta_o}}{r^{\beta_o}} \right] , \qquad (B.27)$$

$$Y'_{\beta_o}(k_n r) = \frac{-\beta_o}{2k_n^2 r_s^{\beta_o+1}} \left[r^{\beta_o - 1} - \frac{r_s^{2\beta_o}}{r^{\beta_o+1}} \right] . \qquad (B.28)$$

It is important to observe that the arguments $k_n r$ and $k_n r_s$ replace the general variable x used in the previous sections. Therefore, the appropriate substitutions must first be carried out using the entire argument before cancelling common factors in k_n.

APPENDIX C. DERIVATION OF THE FIELD-RATIO EXPRESSION

In the course of deriving the ballistic equations in the equivalent circuit analysis of Chapter III, a point in the development is reached at which a knowledge of the radial-to-azimuthal r-f electric field intensity ratio becomes essential. The expressions for the radial and azimuthal intensities in the interaction space were derived in the electromagnetic analysis given in Chapter II. It will be recalled that these relations are valid in the region surrounding the slow-wave circuit provided the beam is not present. However, this is not a serious limitation in the equivalent circuit analysis since the fields produced by the charges in the beam are accounted for separately. Therefore, Eqs. 2.64 and 2.65 of Chapter II can be used to compute the desired ratio*

$$\frac{E_r}{E_\theta} = \frac{\mathrm{Re} \sum_{n,\beta_o} \epsilon^{j\omega t} \sin\left(\frac{n\pi}{L} z\right) \xi_r(r)\, e^{-j\beta_o\theta}}{\mathrm{Re} \sum_{n,\beta_o} \epsilon^{j\omega t} \sin\left(\frac{n\pi}{L} z\right) \xi_\theta(r)\, e^{-j\beta_o\theta}} \quad , \tag{C.1}$$

where

$$\xi_r(r) = F_{n\beta_o}\left(\frac{-n\pi}{k_n L}\right) V'_{\beta_o}(k_n r) + G_{n\beta_o}\left(\frac{-j\omega\mu_o\beta_o}{k_n^2 r}\right) Y_{\beta_o}(k_n r) \quad ,$$

$$\xi_\theta(r) = F_{n\beta_o}\left(\frac{jn\pi\beta_o}{k_n^2 r L}\right) V_{\beta_o}(k_n r) + G_{n\beta_o}\left(\frac{-\omega\mu_o}{k_n}\right) Y'_{\beta_o}(k_n r) \quad .$$

---

* The subscript "1" is dropped here because only the fields in the interaction space will be considered.

The above expression can be simplified by assuming that only one axial eigenvalue and one azimuthal space harmonic are significant. The summation over n and β_o can thus be simplified to a single term, leading to the form

$$\frac{E_r}{E_\theta} = \left[\frac{F_{n\beta_o}\left(\frac{-n\pi}{L}\right) V'_{\beta_o}(k_n r) + G_{n\beta_o}\left(\frac{-j\omega\mu_o\beta_o}{k_n r}\right) Y_{\beta_o}(k_n r)}{F_{n\beta_o}\left(\frac{jn\pi\beta_o}{k_n rL}\right) V_{\beta_o}(k_n r) + G_{n\beta_o}(-\omega\mu_o)\, Y'_{\beta_o}(k_n r)} \right]_{\substack{n,\beta_o \\ \text{fixed}}} \quad . \quad (C.2)$$

It is interesting to observe that in the presence of both E- and H-modes the field ratio is complex since $F_{n\beta_o}$ and $G_{n\beta_o}$ are real constants. However, the existence of only E-mode waves, corresponding to the condition $F_{n\beta_o} = 0$, yields a purely imaginary value for the ratio.

Since several important r-f structures contain many linear radiating elements aligned parallel to the axis of the coaxial-cylindrical system, it does not appear unduly restrictive to suppose that only E-mode waves are excited in the interaction space. If the radial behavior of these fields is assumed to possess the hyperbolic Bessel behavior, it follows that they must be the cutoff modes described in Chapter II. Furthermore, only the first axial eigenvalue n=1, corresponding to a single half-cycle of variation along the z-axis, is considered to exist in the analysis presented in Chapter III. Under these conditions the field ratio reduces to

$$\frac{E_r}{E_\theta} = j\left(\frac{k_1 r}{\beta_o}\right)\left[\frac{V'_{\beta_o}(k_1 r)}{V_{\beta_o}(k_1 r)}\right], \quad (C.3)$$

where $k_1 = \sqrt{(\pi/L)^2 - \omega^2 \mu_o \epsilon_o}$ electrical radians/meter.

While this expression is much simpler than the general relation given by Eq. C.1, it still requires a knowledge of the hyperbolic Bessel function. A further reduction can be made by assuming that the arguments $k_1 r$ and $k_1 r_s$ are much smaller than unity, so that the simplification developed in Appendix B may be employed. Although this approach seems attractive, it is important to investigate the physical significance of the assumption. Since the largest radius to be encountered is r_s, the discussion will be limited to a study of $k_1 r_s$. The radius r_s is not generally greater than about 2.0 cm for E-type devices*, because it is difficult to achieve adequate electron beam stiffness in large-radius structures[34,35]. The magnitude of k_1 will therefore determine the degree to which the above inequality is satisfied.

Although the expression below Eq. C.3 can be made as small as desired at a given frequency by sufficiently increasing the guide height L, it is of interest to examine the consequences of making k_1 very small. The treatment presented in the second chapter emphasized that k_1^2 is less than zero for axially-propagating waves in the interaction space, while it is greater than zero for axially-cutoff modes in the same region. The point at which this quantity changes sign is precisely

$$\omega_{co_1}^2 \mu_o \epsilon_o \equiv \left(\frac{\pi}{L}\right)^2 ,$$

---

* For the experimental device described in Chapter IV the radius r_s is approximately 1.75 cm.

or alternatively

$$f_{co_1} \equiv \frac{1}{2L\sqrt{\mu_o \epsilon_o}} \quad . \tag{C.4}$$

The corresponding expression for the axial cutoff frequency of waves propagating along the slow-wave circuit is given by

$$f_{co_2} \equiv \frac{1}{2L\sqrt{\mu_o \epsilon_2}} \quad ,$$

$$\equiv \frac{f_{co_1}}{\sqrt{\epsilon'}} \quad , \tag{C.5}$$

where $\epsilon_2 = \epsilon' \epsilon_o$. It is assumed here that the waveguide height is the same for both the interaction and slow-wave-circuit regions.

In view of the fact that the electron beam primarily encounters the azimuthal component of the r-f wave in the interaction space, the crucial issue involving the size of k_1 is that pertaining to the azimuthal-space-harmonic variation in the frequency range near cutoff for axial propagation in the interaction space. The question is rather complex, however, because it requires a knowledge of the conditions of wave propagation along the slow-wave circuit. For this reason it is desirable to consider the slow-wave and interaction regions separately.

The exact nature of the azimuthal-space-harmonic frequency dependence in the vicinity of axial cutoff on the r-f structure is uniquely determined by characteristics peculiar to a particular slow-wave circuit. Nevertheless, certain generalizations seem plausible. Within the frequency interval surrounding f_{co_2} the azimuthal as well as the axial wave phase velocity is likely to be highly dispersive. In this range of the r-f spectrum a large number of azimuthal space harmonics associated with

the wave on the circuit might be expected to have nearly equal spatial characteristics*. Under these circumstances the premise, that the dielectric slow-wave structure can replace the actual r-f circuit for investigating a single axial and azimuthal space harmonic, is invalid owing to the "spatial degeneracy" which the harmonic components exhibit near cutoff. However, at frequencies greatly removed from the value given by Eq. C.5 the assumption that the harmonics possess distinctive spatial characteristics is justified.

A further examination of Eq. C.5 reveals that the axial cutoff frequency for waves on the slow-wave circuit is substantially removed from the corresponding cutoff frequency in the interaction space, provided the structure exhibits a large value of axial slowing (which is equivalent to a large value of ϵ'). In this event the r-f circuit produces a negligible effect upon the fields in the interaction space. However, for circuits in which this axial slowing is small, such as the vane structure where ϵ' equals unity, the axial cutoff frequencies in the two regions approach each other. The slow-wave circuit then exerts a strong influence over the spatial characteristics of the field in the interaction space, in the vicinity of the common cutoff frequency.

Under the assumption that f_{co_1} significantly differs from f_{co_2}, it becomes possible to limit attention to the control exercised over the characteristics of the space harmonics produced by the axial cutoff frequency in the interaction space. While it is difficult to assert the exact nature of this control, it is well-known that for propagating waves

---

* It must be admitted that this assertion is an extrapolation of the well-known behavior of the helix and "filter-type" structures employed in O-type traveling-wave devices. On this basis the conjecture seems warranted.

the conditions become highly dispersive as the cutoff frequency f_{co_1} is approached. It would be conservative, therefore, to assume a comparable behavior exists for the cutoff modes, with the associated degeneracy of a large number of azimuthal space harmonics, in the vicinity of f_{co_1}. The use of the small-argument approximation will accordingly carry the following assumptions in the present treatment:

1. The cutoff frequency for axial propagation along the slow-wave structure is sufficiently displaced from the corresponding frequency of the interaction space that the r-f circuit exerts negligible effect over the characteristics of the space harmonics in the interaction region. This, in turn, implies the use of a biperiodic structure exhibiting a large axial slowing factor.

2. The waveguide height L will be properly chosen so that, within a specified frequency range, the value of k_1 is small enough to achieve the condition

$$k_1 r_s < 1 \ .$$

However, it will be assumed that k_1 is sufficiently large as to exclude operation in the immediate vicinity of the cutoff frequency for the interaction space. This permits an analysis which is limited to a study of one axial and one azimuthal space-harmonic component.

Within the limitations imposed by these restrictions Eq. C.3 can be simplified with the aid of Eqs. B.25 and B.26 to obtain

$$\frac{E_r}{E_\theta} = j\left[\frac{1 + (r_s/r)^{2\beta_o}}{1 - (r_s/r)^{2\beta_o}}\right] ,$$

$$= j\, F(r) \quad . \qquad \text{(C.6)}$$

The equations derived in the last section of Appendix B can likewise be used to develop the corresponding expression for E_r/E_θ when only H-wave cutoff modes are assumed to exist in the interaction region. Those relations also permit a derivation of the field ratio relations applicable when E- or H-mode <u>propagating</u> waves are present in the space surrounding the r-f circuit. In each case, however, the consequences of the small-argument approximation should be carefully examined to determine its compatability with the assumption of only one axial and one azimuthal space-harmonic component.

APPENDIX D. DERIVATION OF THE RADIAL- AND AZIMUTHAL-COUPLING FACTOR EXPRESSIONS

The ballistic and circuit equations, derived in Chapter III, involve expressions requiring a knowledge of the radial and azimuthal r-f electric field intensities at the circuit and at the center of the ribbon beam. The relations for these field intensity ratios will be developed here under the same assumptions used in Appendix C.

1. Only E-wave cutoff modes are considered to be present in the interaction space.
2. Only one axial and one azimuthal space harmonic predominates in the electron-wave interaction process.
3. The small-argument approximation is valid within the frequency range under investigation. The limitations on the size of k_1 are compatible with the single-space-harmonic assumption, as explained in Appendix C.

The general expressions for the radial- and azimuthal-coupling factors may be written, with the aid of Eqs. 2.64 and 2.65 of Chapter II,

$$k_r = \frac{\operatorname{Re} \sum_{n,\beta_o} \epsilon^{j\omega t} \sin\left(\frac{n\pi}{L} z\right) \xi_r(r_o)\, e^{-j\beta_o\theta}}{\operatorname{Re} \sum_{n,\beta_o} \epsilon^{j\omega t} \sin\left(\frac{n\pi}{L} z\right) \xi_r(r_c)\, e^{-j\beta_o\theta}} , \qquad (D.1)$$

$$k_\theta = \frac{\mathrm{Re}\sum_{n,\beta_o} \epsilon^{j\omega t} \sin\left(\frac{n\pi}{L} z\right) \xi_\theta(r_o)\, e^{-j\beta_o\theta}}{\mathrm{Re}\sum_{n,\beta_o} \epsilon^{j\omega t} \sin\left(\frac{n\pi}{L} z\right) \xi_\theta(r_c)\, e^{-j\beta_o\theta}} , \qquad (D.2)$$

where

$$\xi_r(r_o) = F_{n\beta_o}\left(\frac{-n\pi}{k_n L}\right) V'_{\beta_o}(k_n r_o) + G_{n\beta_o}\left(\frac{-j\omega\mu_o\beta_o}{k_n^2 r_o}\right) Y_{\beta_o}(k_n r_o) ,$$

$$\xi_r(r_c) = F_{n\beta_o}\left(\frac{-n\pi}{k_n L}\right) V'_{\beta_o}(k_n r_c) + G_{n\beta_o}\left(\frac{-j\omega\mu_o\beta_o}{k_n^2 r_c}\right) Y_{\beta_o}(k_n r_c) ,$$

$$\xi_\theta(r_o) = F_{n\beta_o}\left(\frac{jn\pi\beta_o}{k_n^2 r_o L}\right) V_{\beta_o}(k_n r_o) + G_{n\beta_o}\left(\frac{-\omega\mu_o}{k_n}\right) Y'_{\beta_o}(k_n r_o) ,$$

$$\xi_\theta(r_c) = F_{n\beta_o}\left(\frac{jn\pi\beta_o}{k_n^2 r_c L}\right) V_{\beta_o}(k_n r_c) + G_{n\beta_o}\left(\frac{-\omega\mu_o}{k_n}\right) Y'_{\beta_o}(k_n r_c) .$$

Within the range of limitations stated above, the radial- and azimuthal-coupling factors simplify to

$$k_r = \frac{V'_{\beta_o}(k_1 r_o)}{V'_{\beta_o}(k_1 r_c)} , \qquad (D.3)$$

$$k_\theta = \frac{r_c}{r_o}\left[\frac{V_{\beta_o}(k_1 r_o)}{V_{\beta_o}(k_1 r_c)}\right] , \qquad (D.4)$$

where k_n is replaced by k_1 in the arguments of the foregoing functions, since only the axial eigenvalue n = 1 is assumed to exist.

The final forms of k_r and k_θ are obtained by substituting Eqs. B.26 and B.25 into Eqs. D.3 and D.4 after evaluating the expressions at the radii r_o and r_c. The desired results are

$$k_r = \left(\frac{r_o}{r_c}\right)^{\beta_o - 1} \left[\frac{1 + \left(\frac{r_s}{r_o}\right)^{2\beta_o}}{1 + \left(\frac{r_s}{r_c}\right)^{2\beta_o}} \right], \tag{D.5}$$

$$k_\theta = \left(\frac{r_o}{r_c}\right)^{\beta_o - 1} \left[\frac{1 - \left(\frac{r_s}{r_o}\right)^{2\beta_o}}{1 - \left(\frac{r_s}{r_c}\right)^{2\beta_o}} \right]. \tag{D.6}$$

The special relations developed in Appendix B may also be used to compute k_r and k_θ when H-wave cutoff modes, or E- or H-mode propagating waves, are present in the region surrounding the slow-wave structure.

APPENDIX E

THE FORWARD-WAVE INCREMENTAL PROPAGATION CONSTANTS OF THE E-TYPE DEVICE

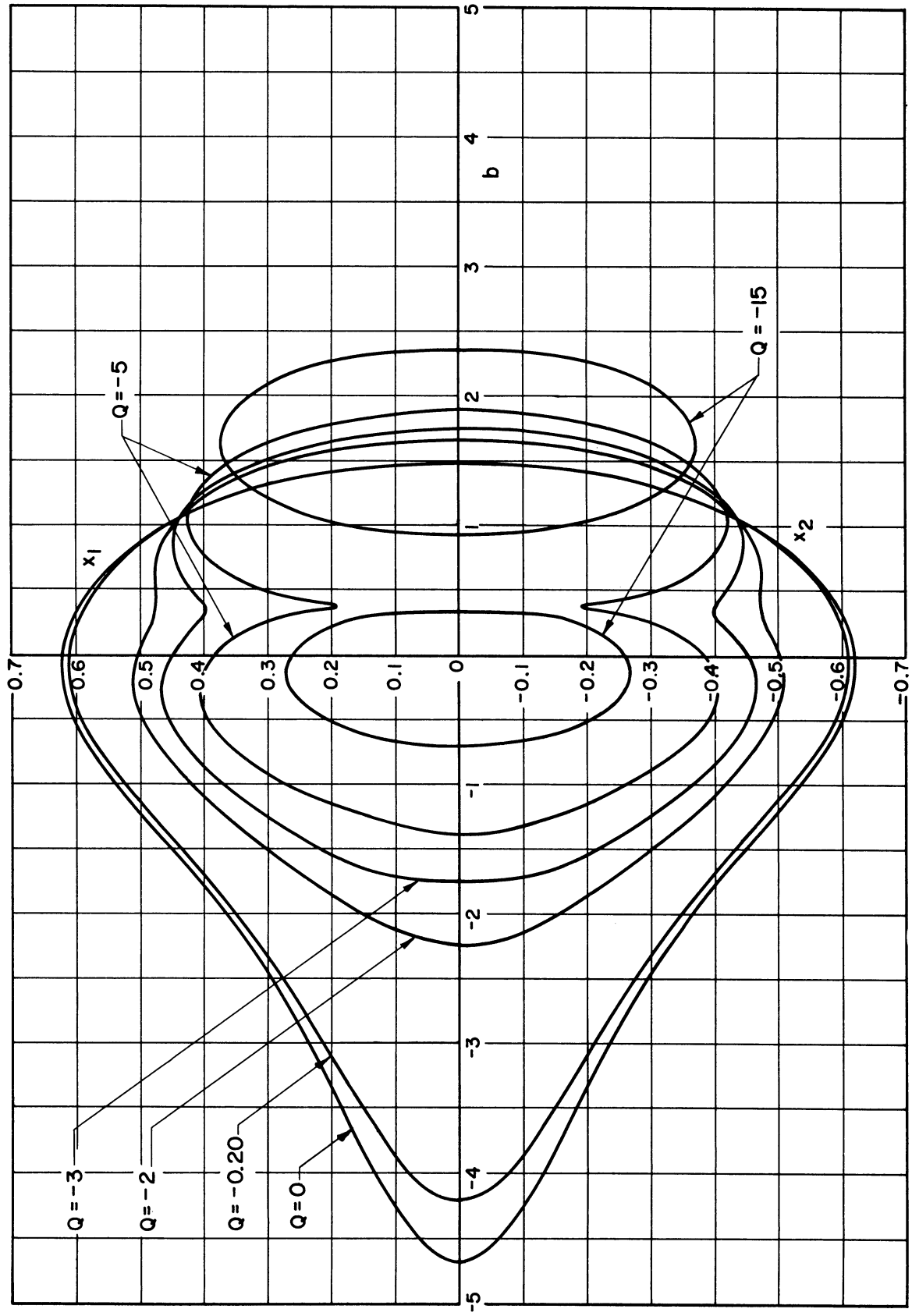

Fig. E. 1 $\beta_e = 50$, C = 0.05, d = 0

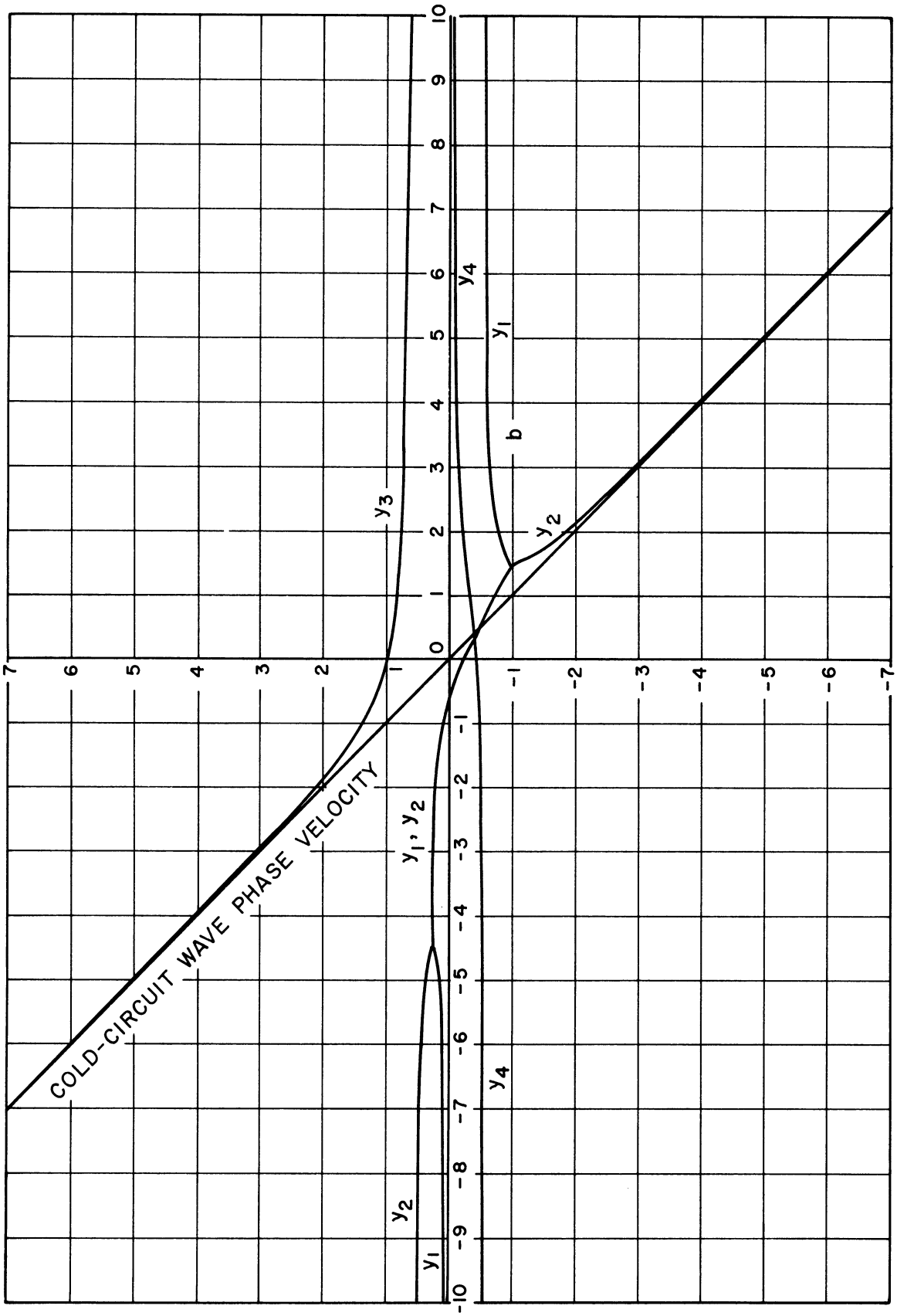

Fig. E.2 β_e=50, C=0.05, d=0, Q=0

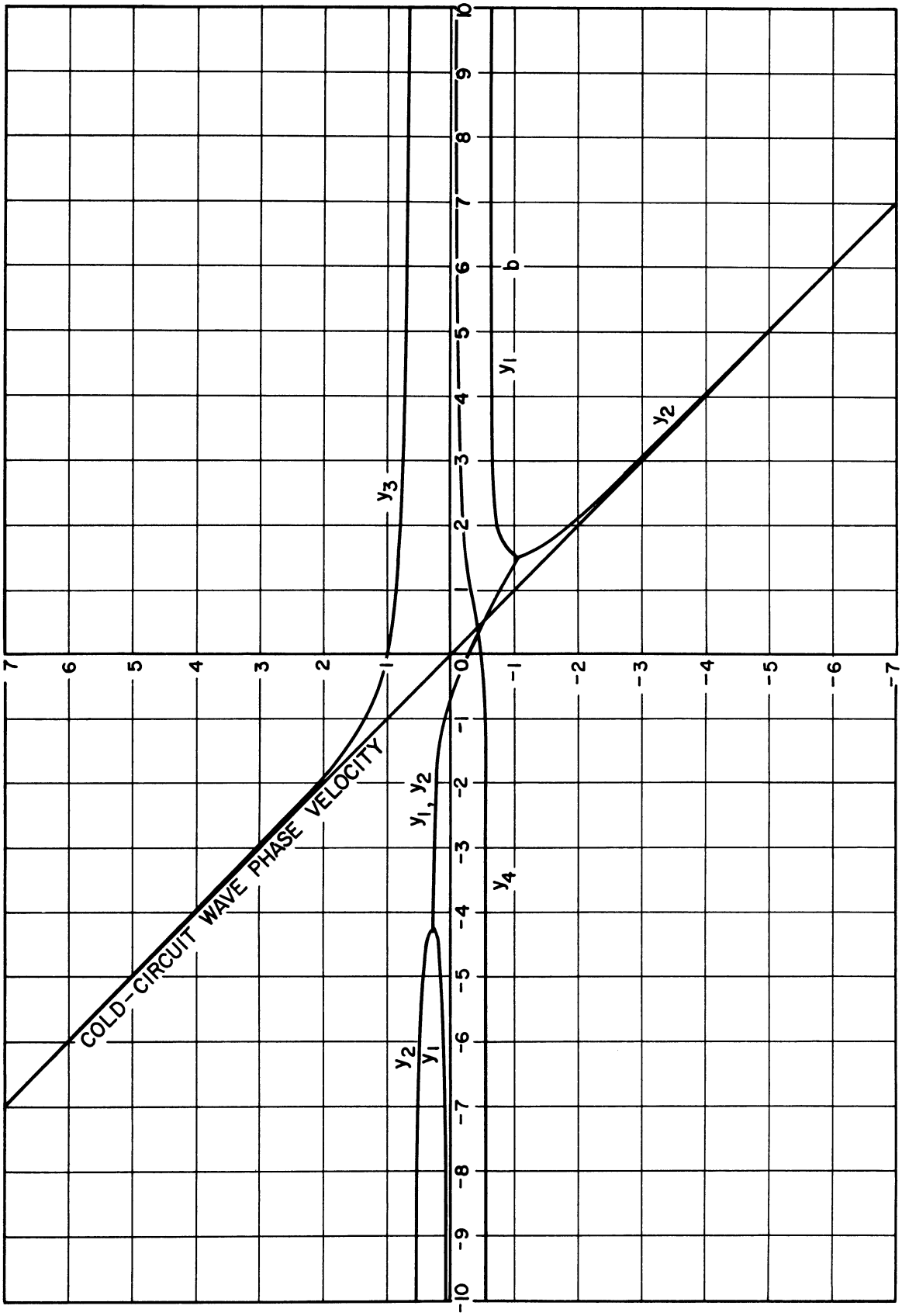

Fig. E. 3 $\beta_e = 50$, $C = 0.05$, $d = 0$, $Q = -0.20$

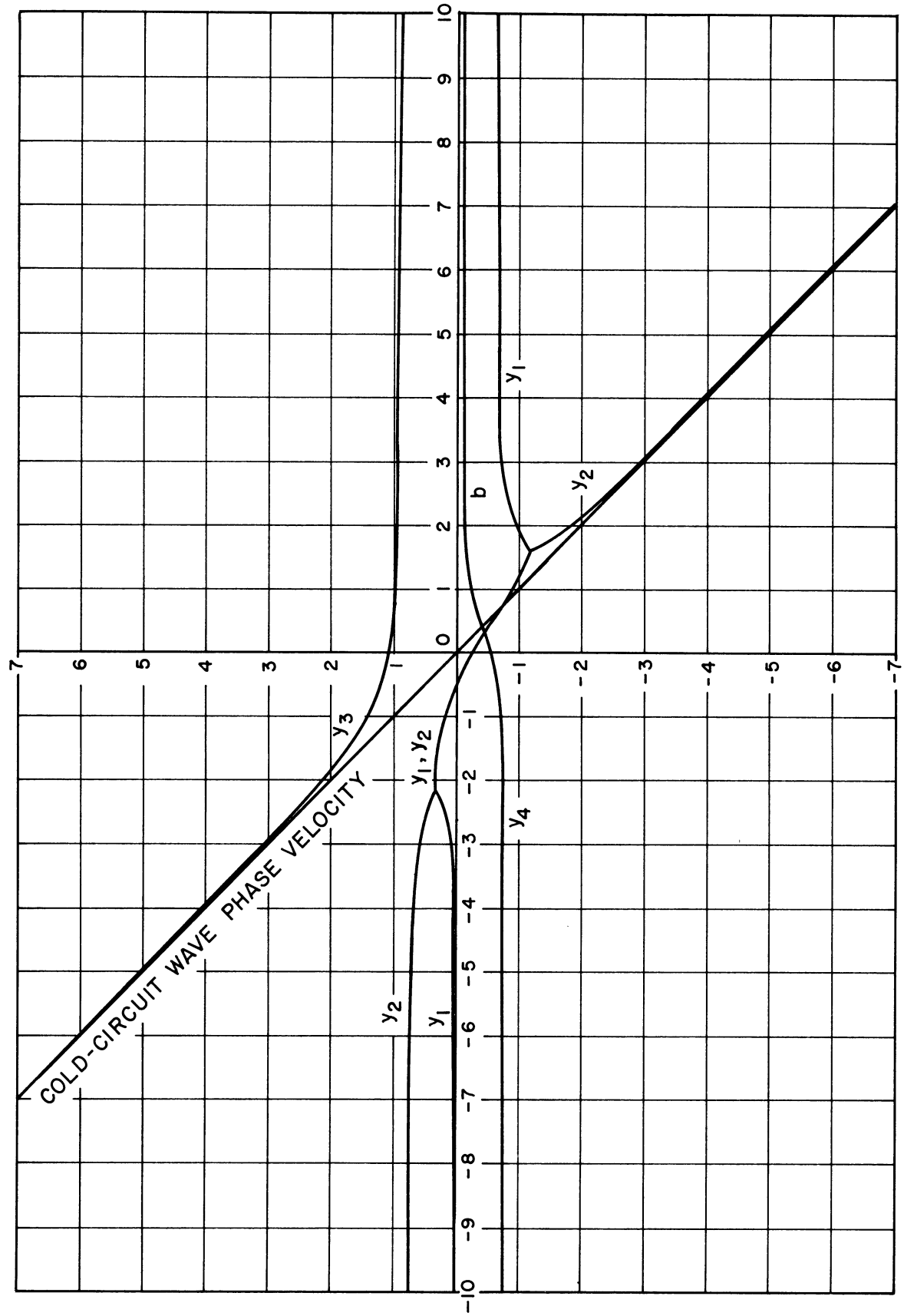

Fig. E. 4 β_e=50, C=0.05, d=0, Q=-2.0

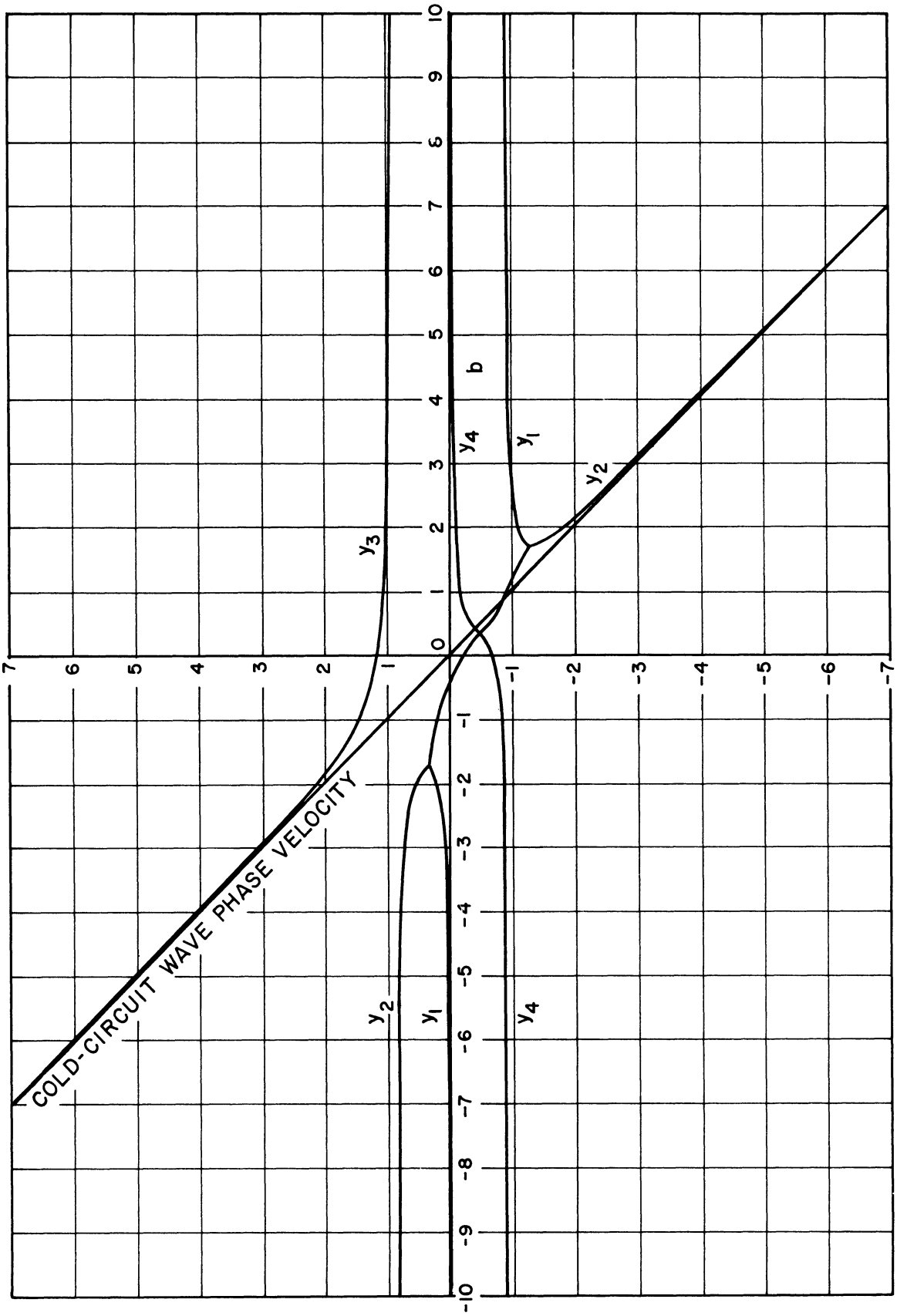

Fig. E.5 β_e=50, C=0.05, d=0, Q = - 3.0

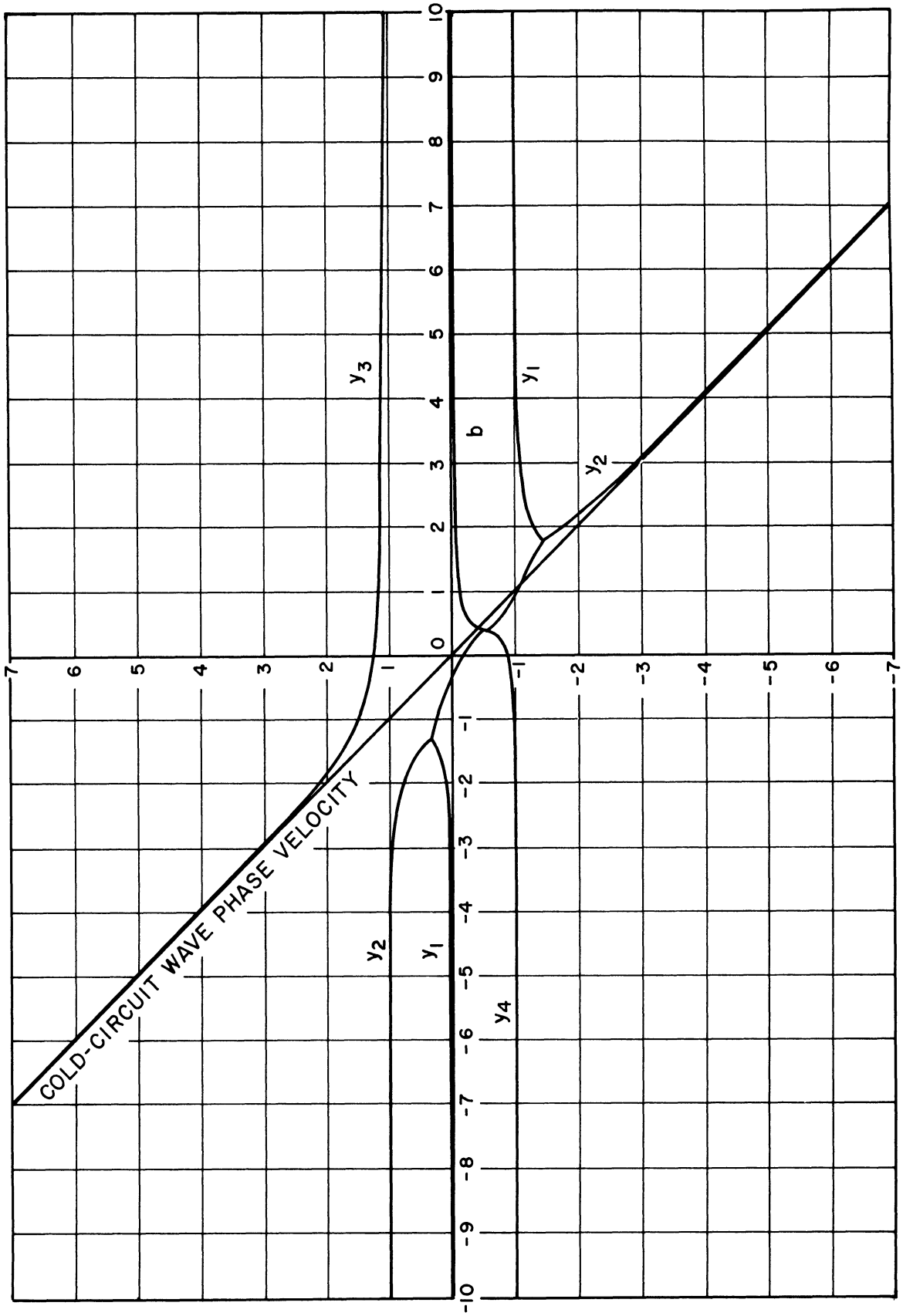

Fig. E.6 β_e=50, C=0.05, d=0, Q=-5.0

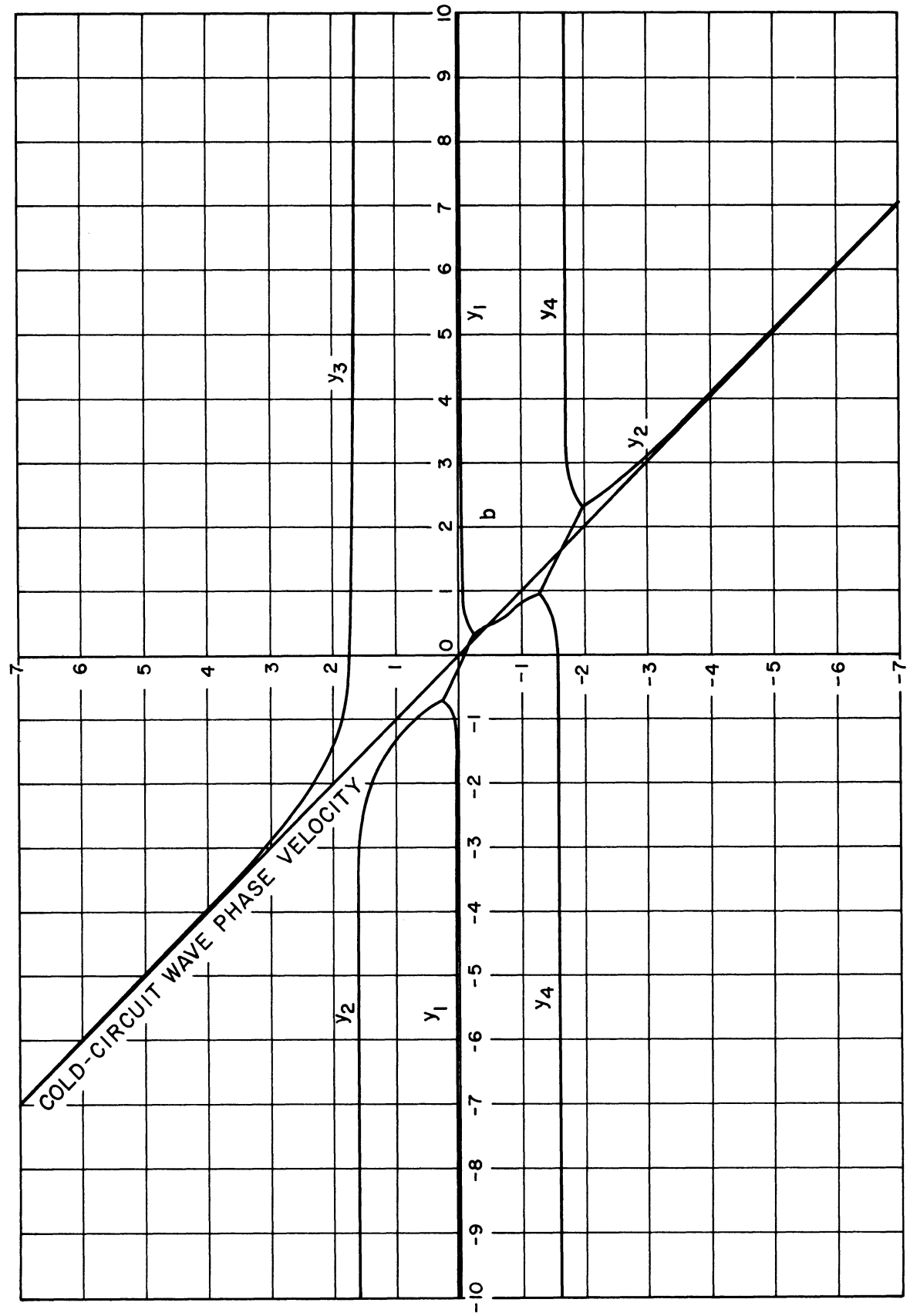

Fig. E. 7 β_e=50, C=0.05, d=0, Q=-15

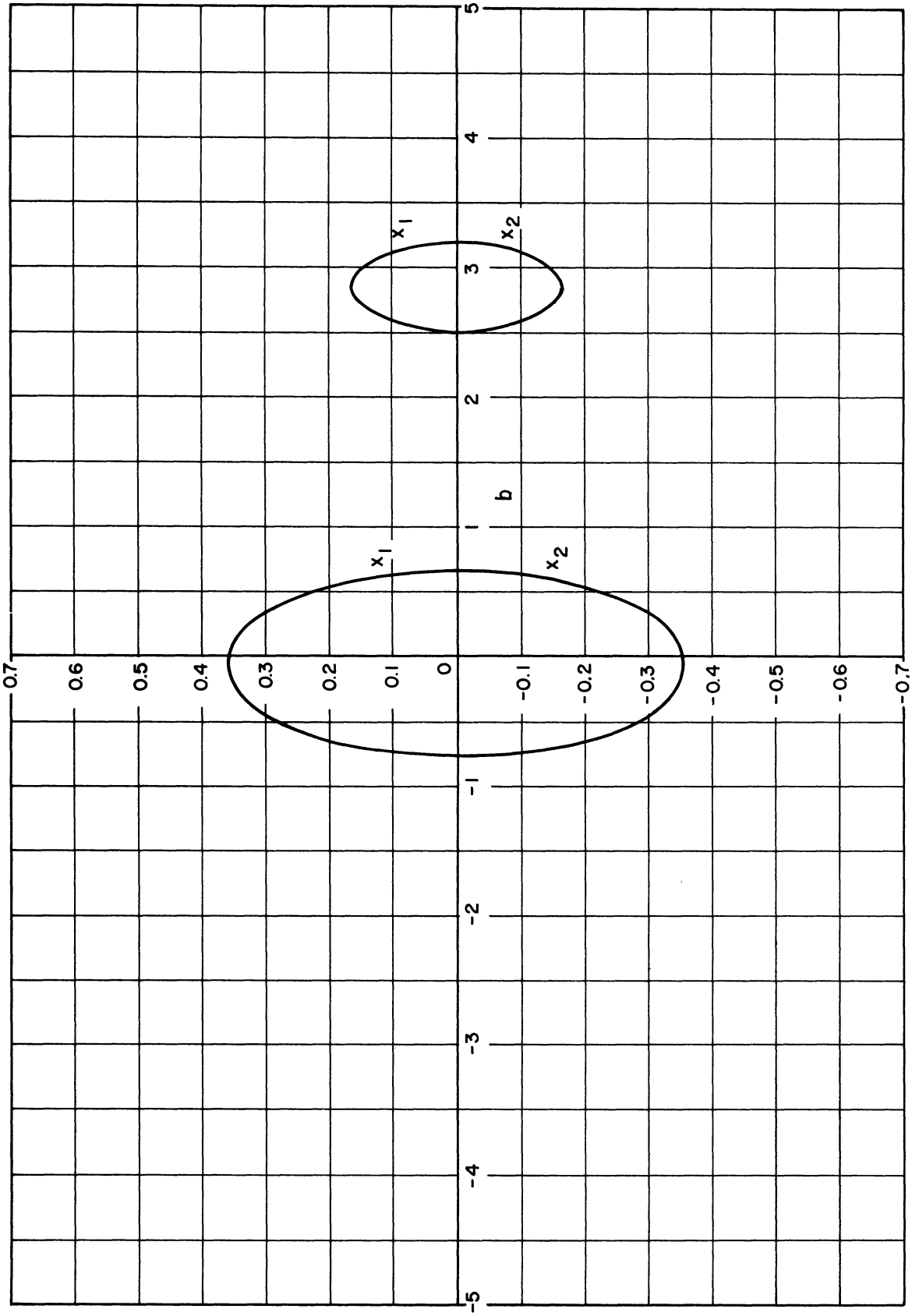

Fig. E.8 β_e=50, C=0.01, d=0, Q=0

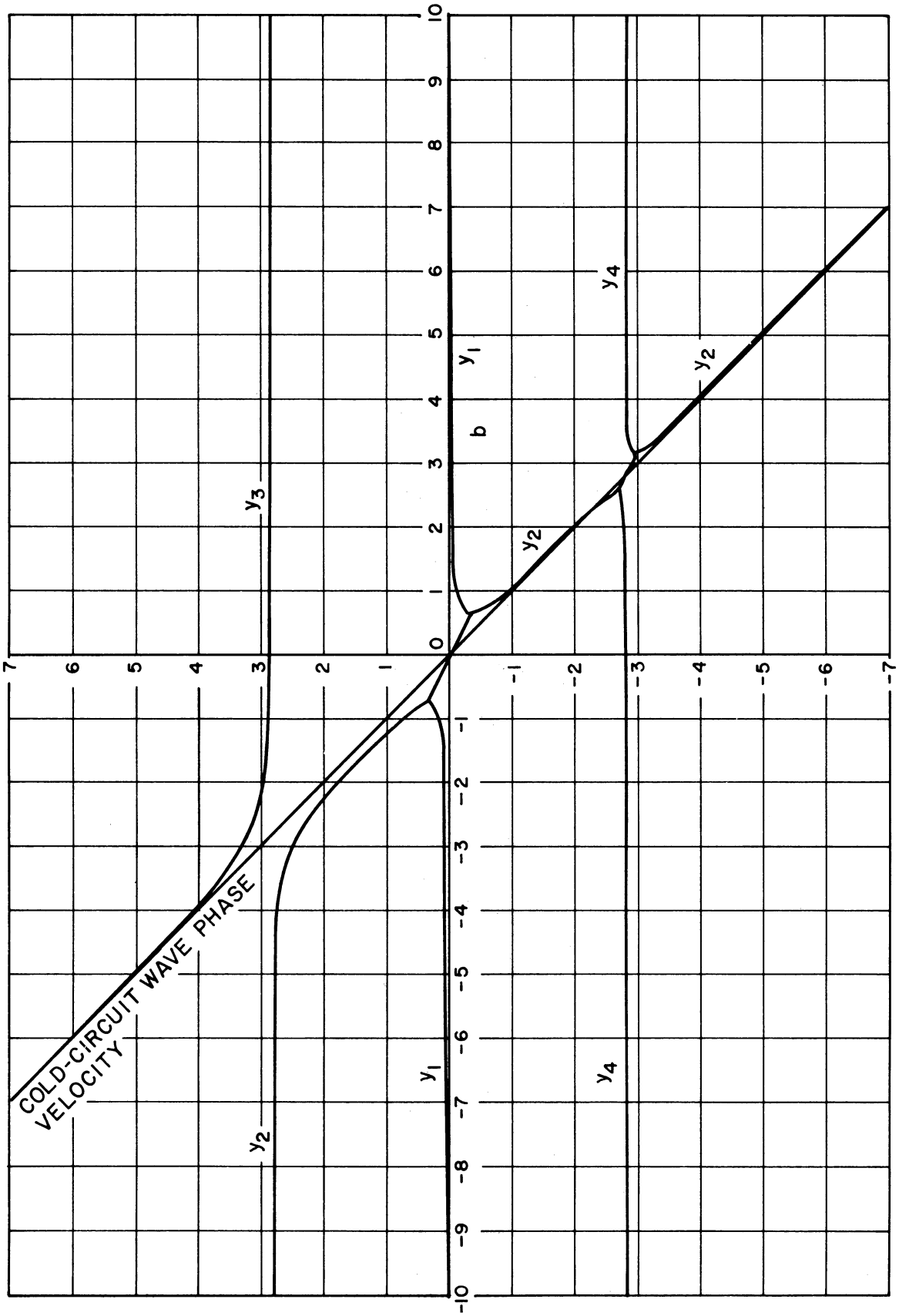

Fig. E.9 $\beta_e = 50$, C=0.01, d=0, Q=0

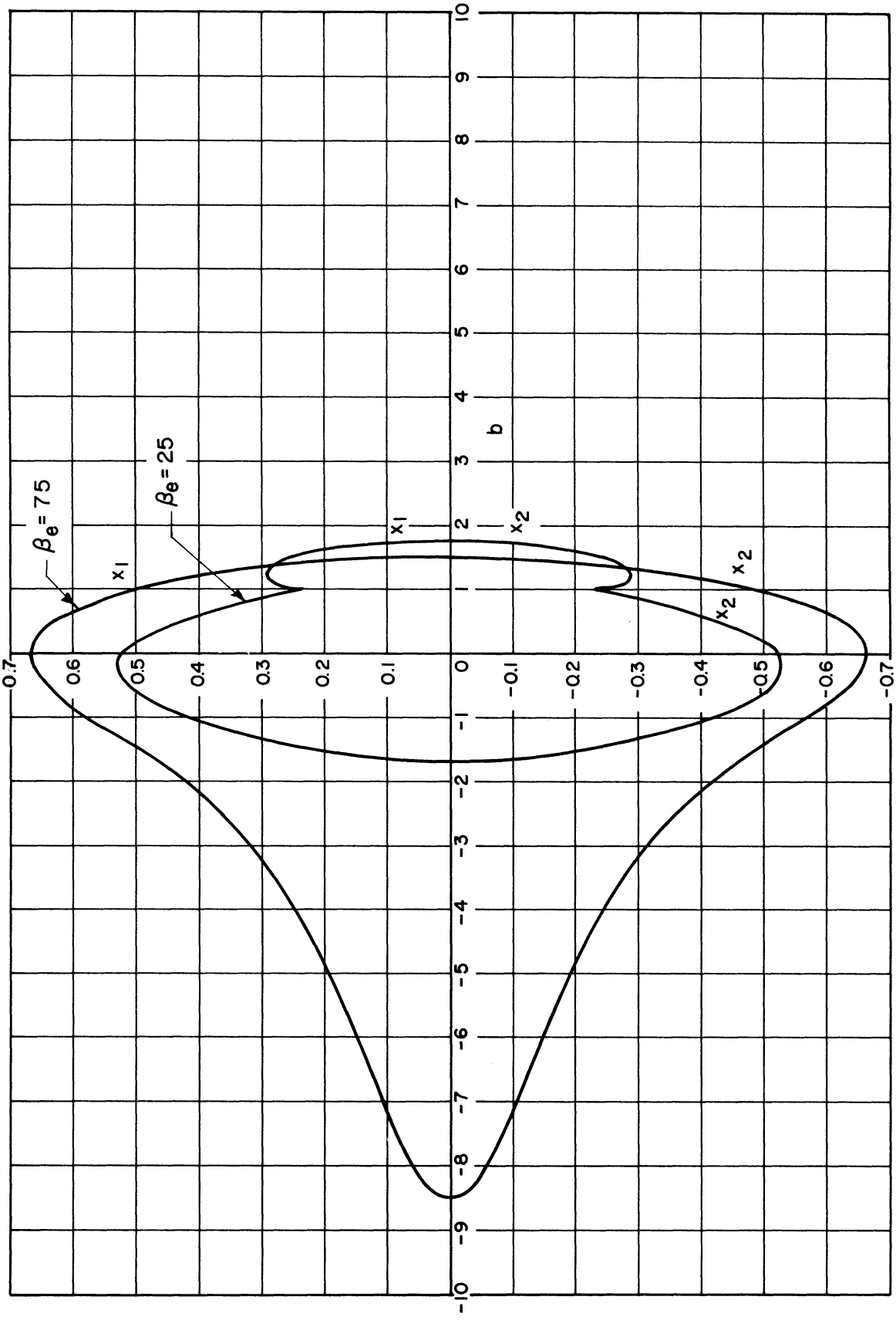

Fig. E. 10 C = 0.05, d = 0, Q = 0

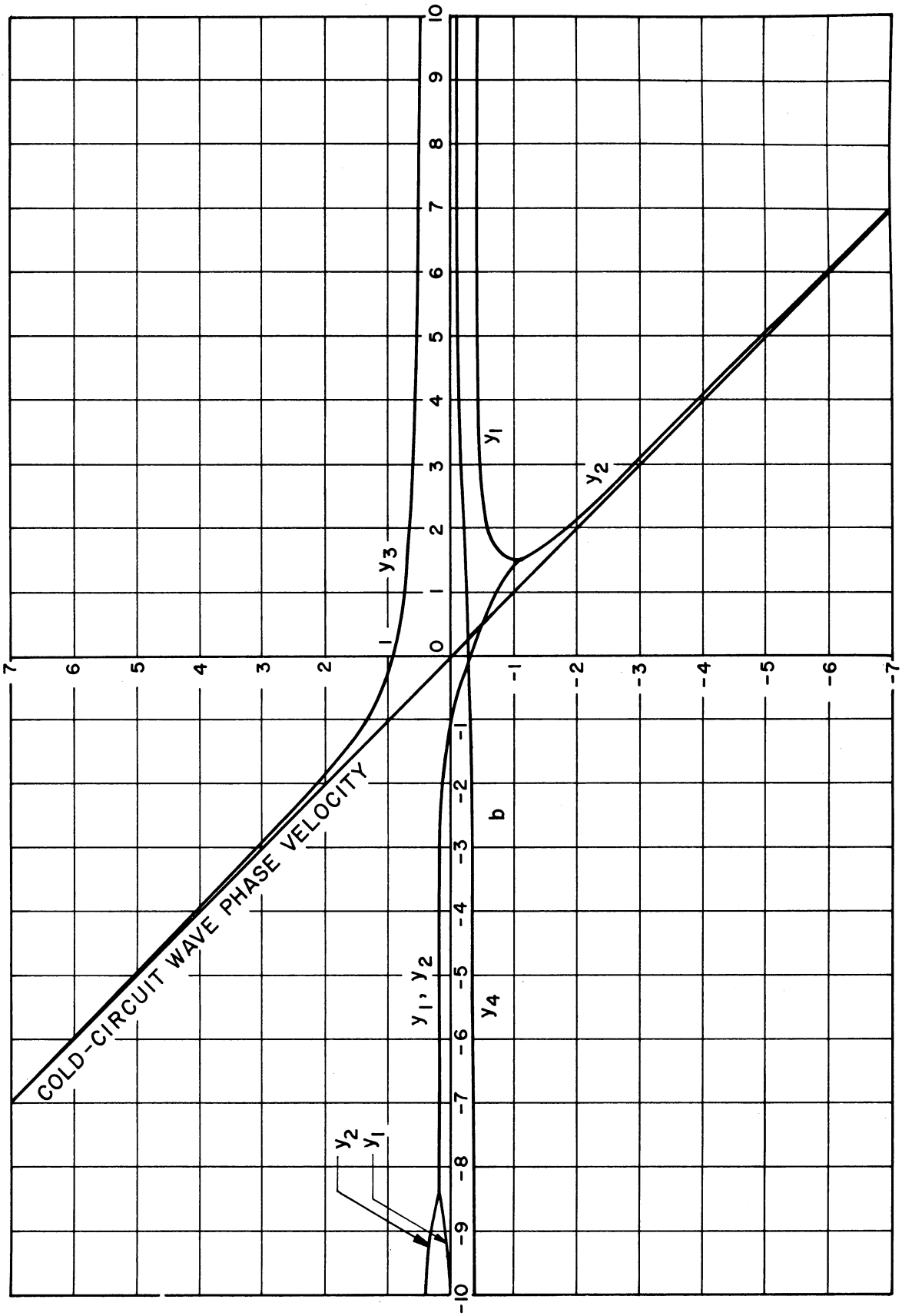

Fig. E.11 $\beta_e = 75$, C=0.05, d=0, Q=0

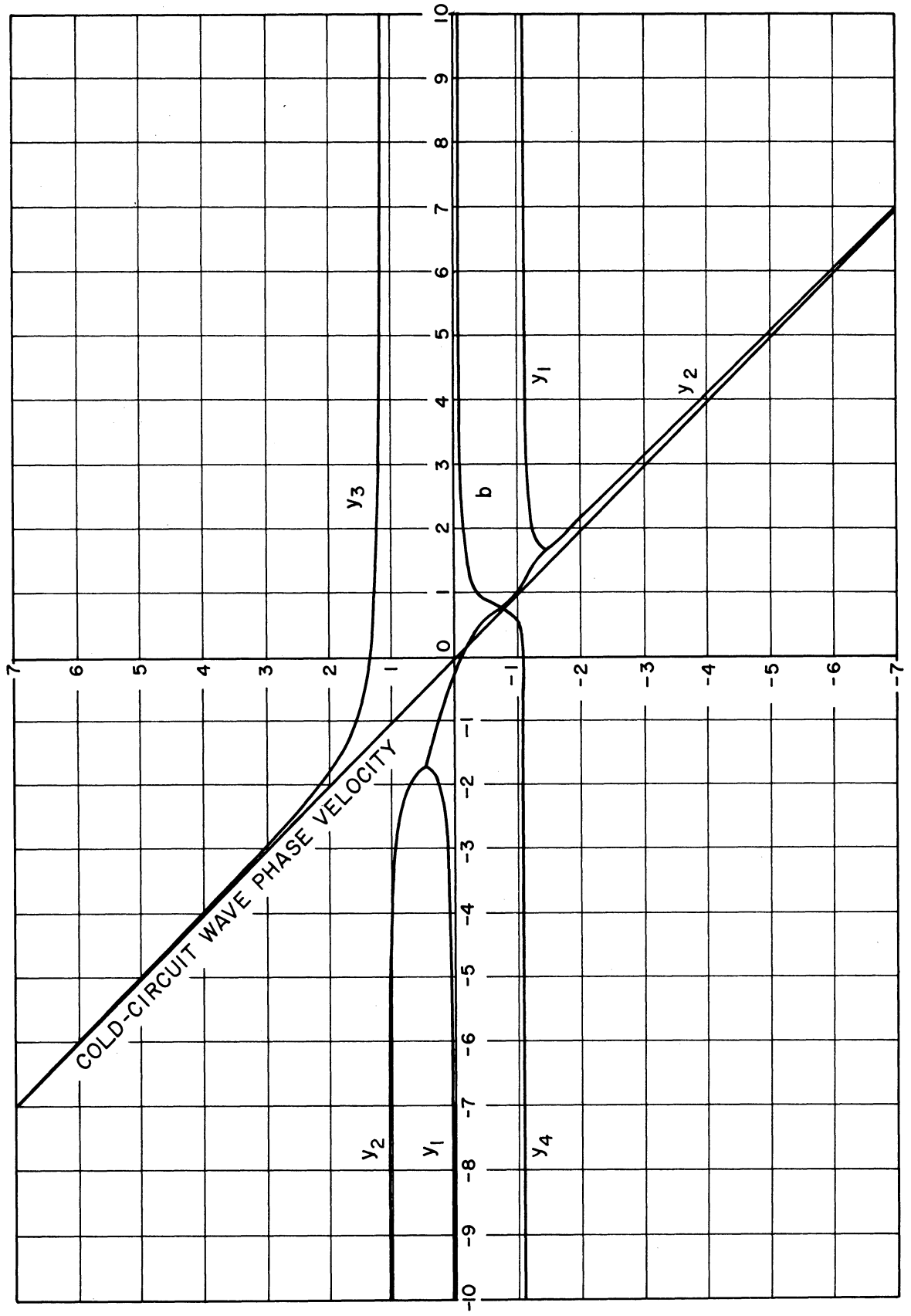

Fig. E. 12 $\beta_e = 25$, C=0.05, d = 0, Q = 0

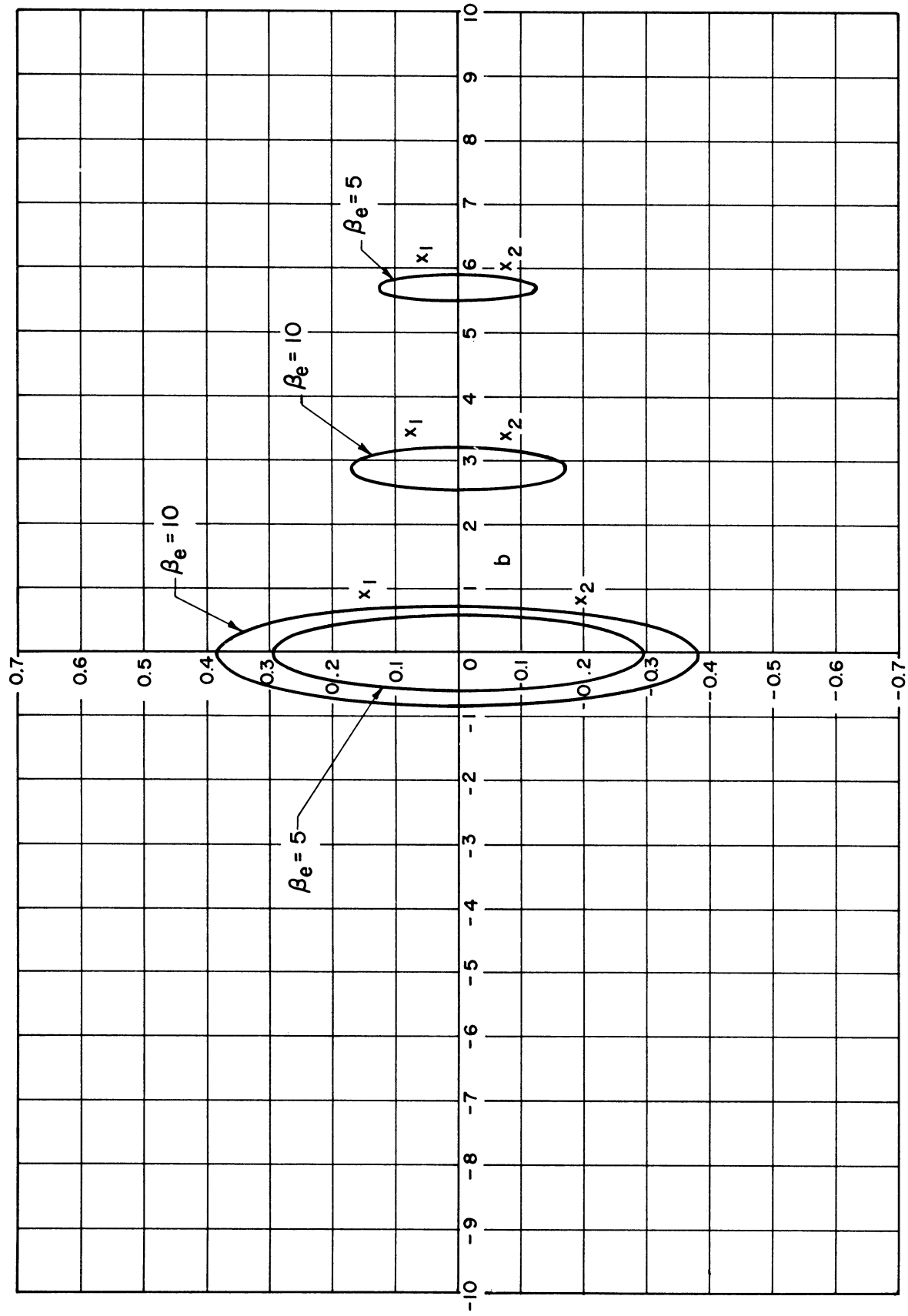

Fig. E. 13 C=0.05, d=0, Q=0

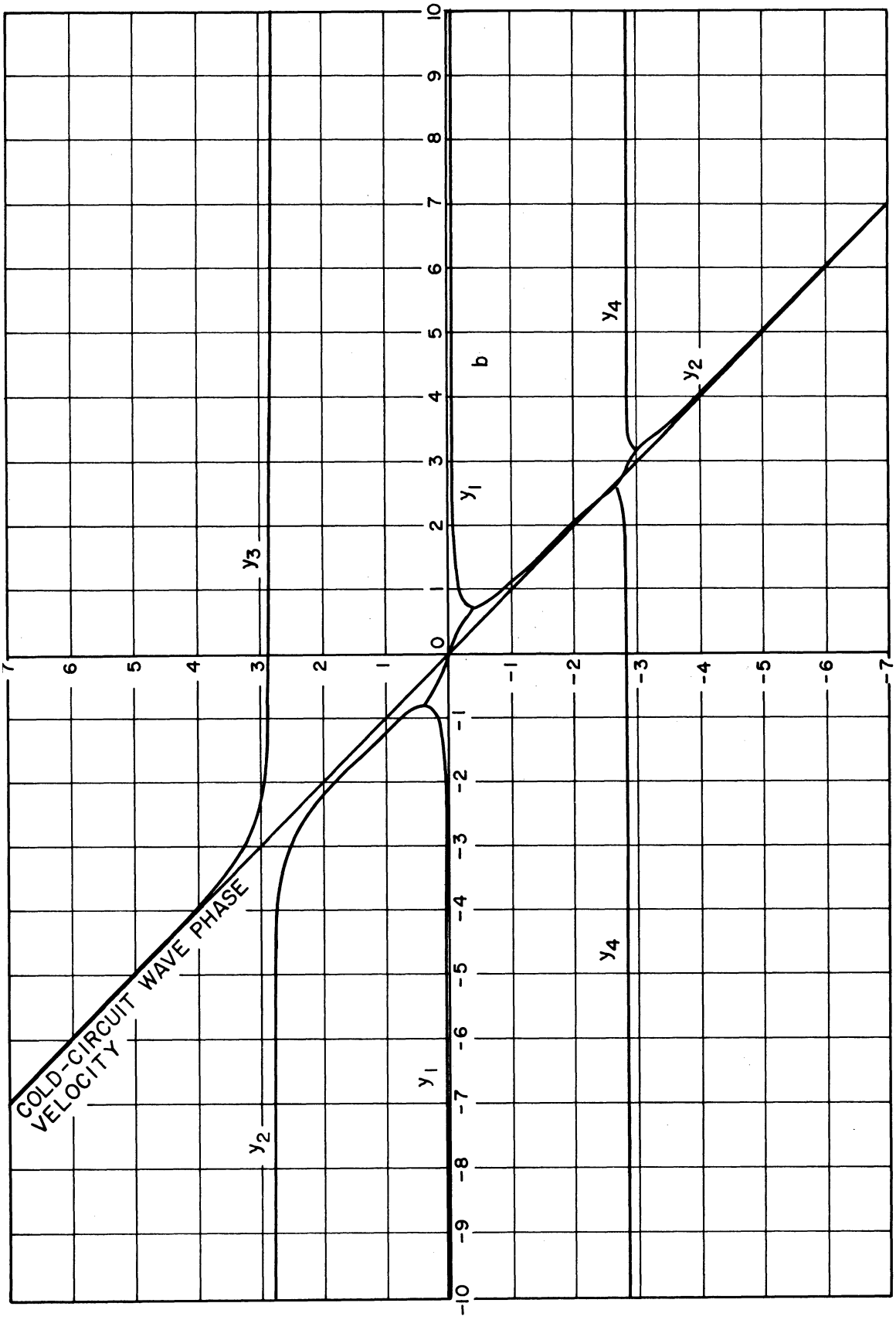

Fig. E. 14 β_e=10, C=0.05, d=0, Q=0

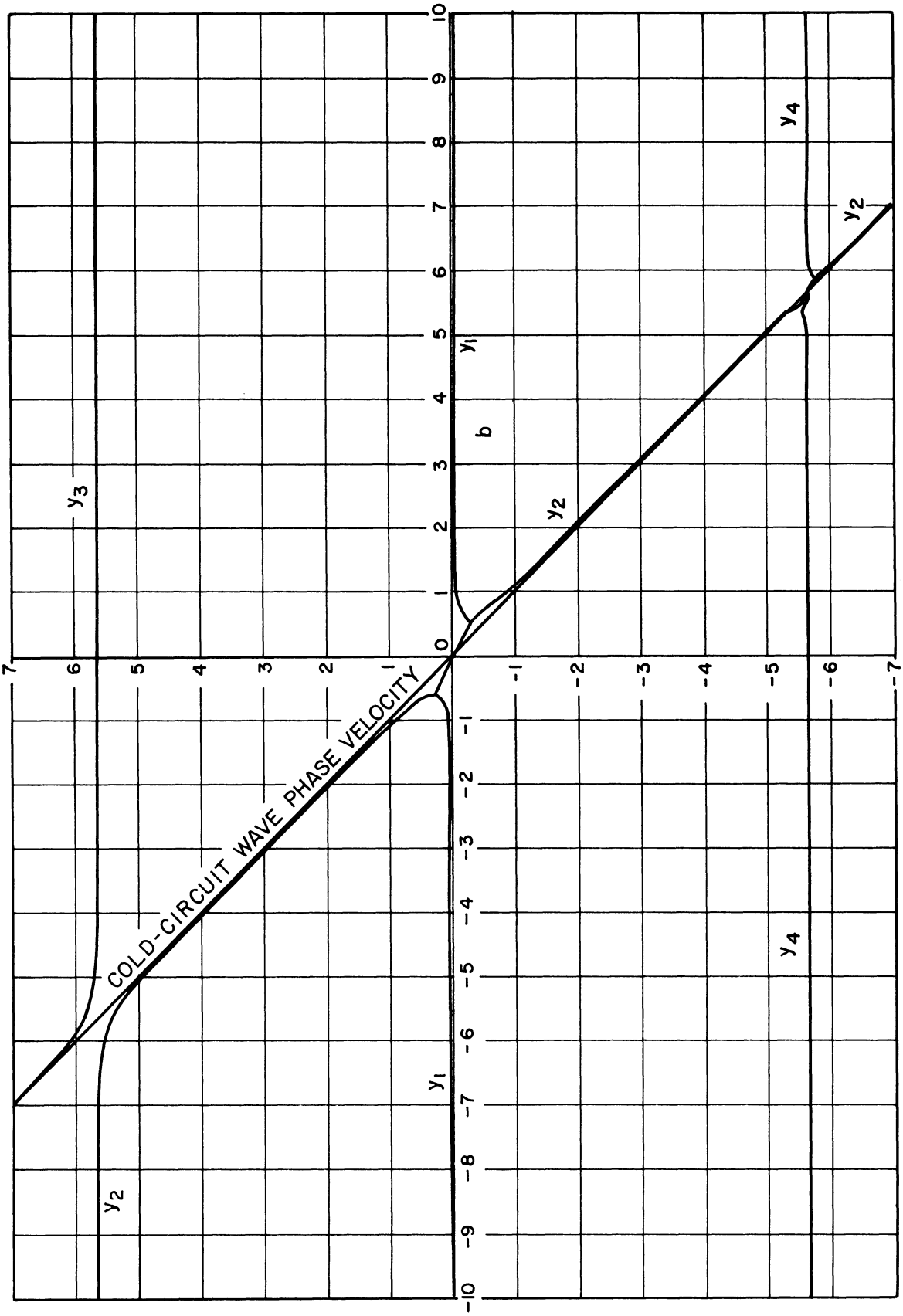

Fig. E. 15 $\beta_e = 5$, C = 0.05, d = 0, Q = 0

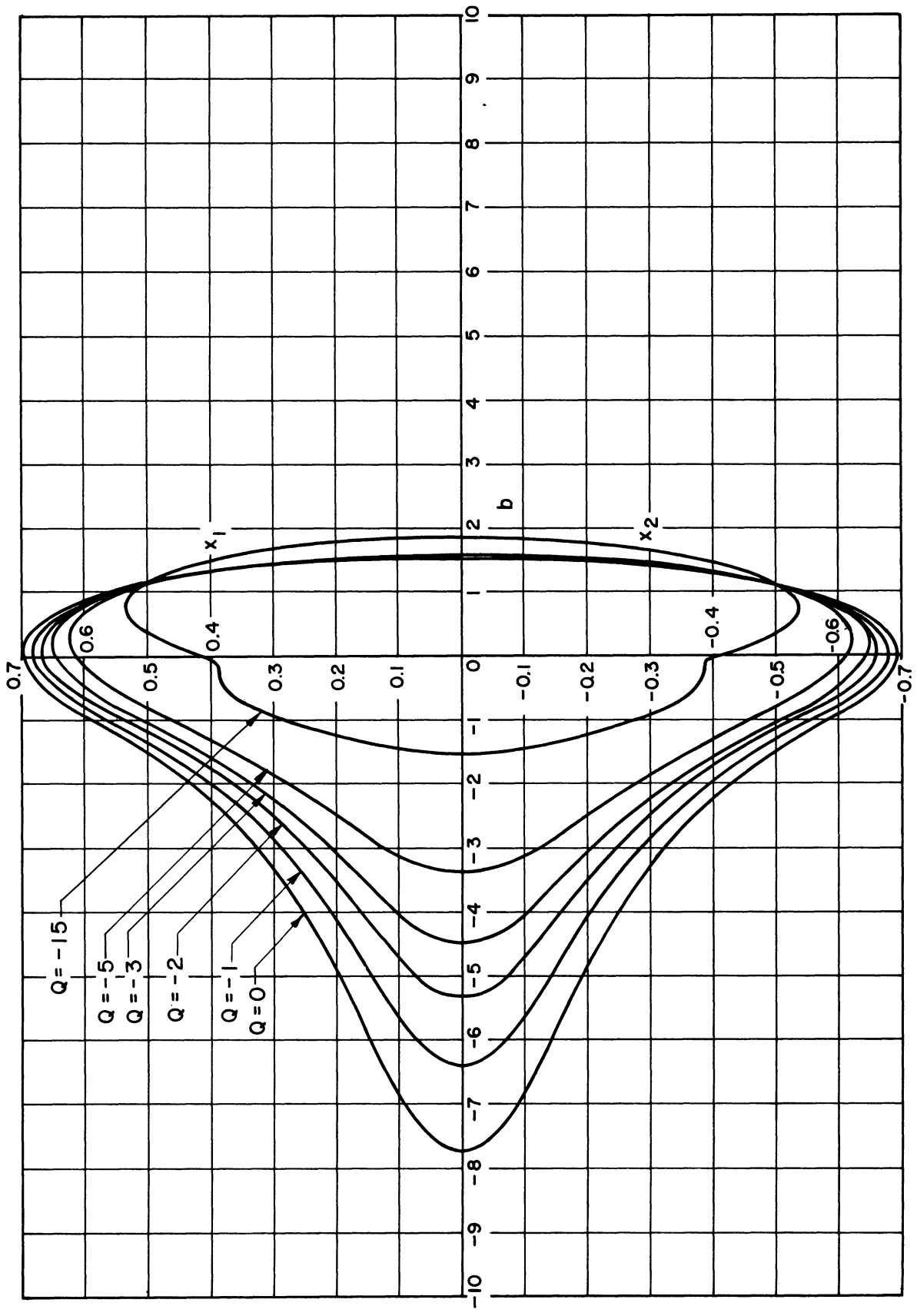

Fig. E. 16 $\beta_e = 50$, C = 0.10, d = 0

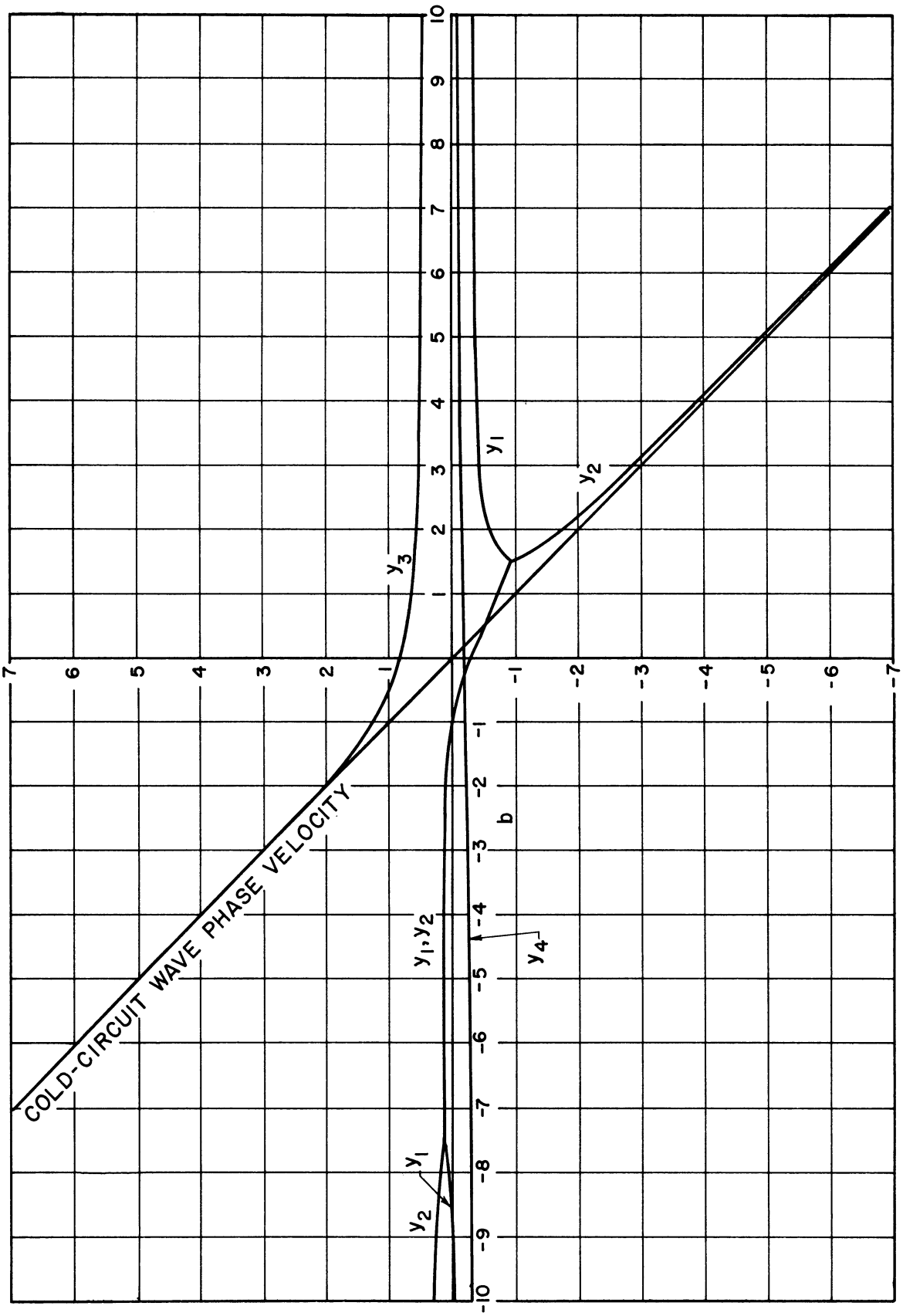

Fig. E. 17 β_e=50, C=0.10, d=0, Q=0

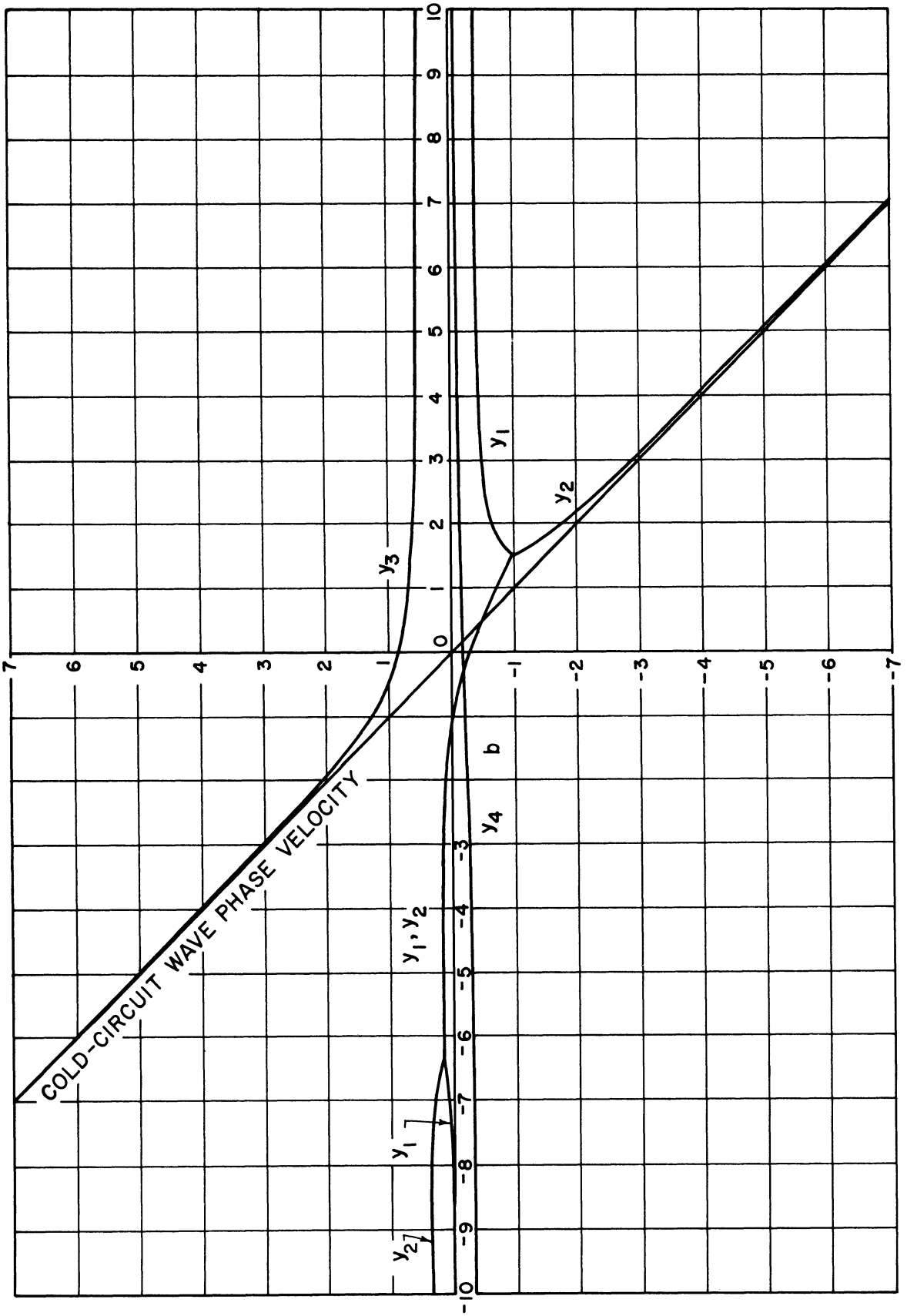

Fig. E. 18 β_e=50, C=0.10, d=0, Q = -1.0

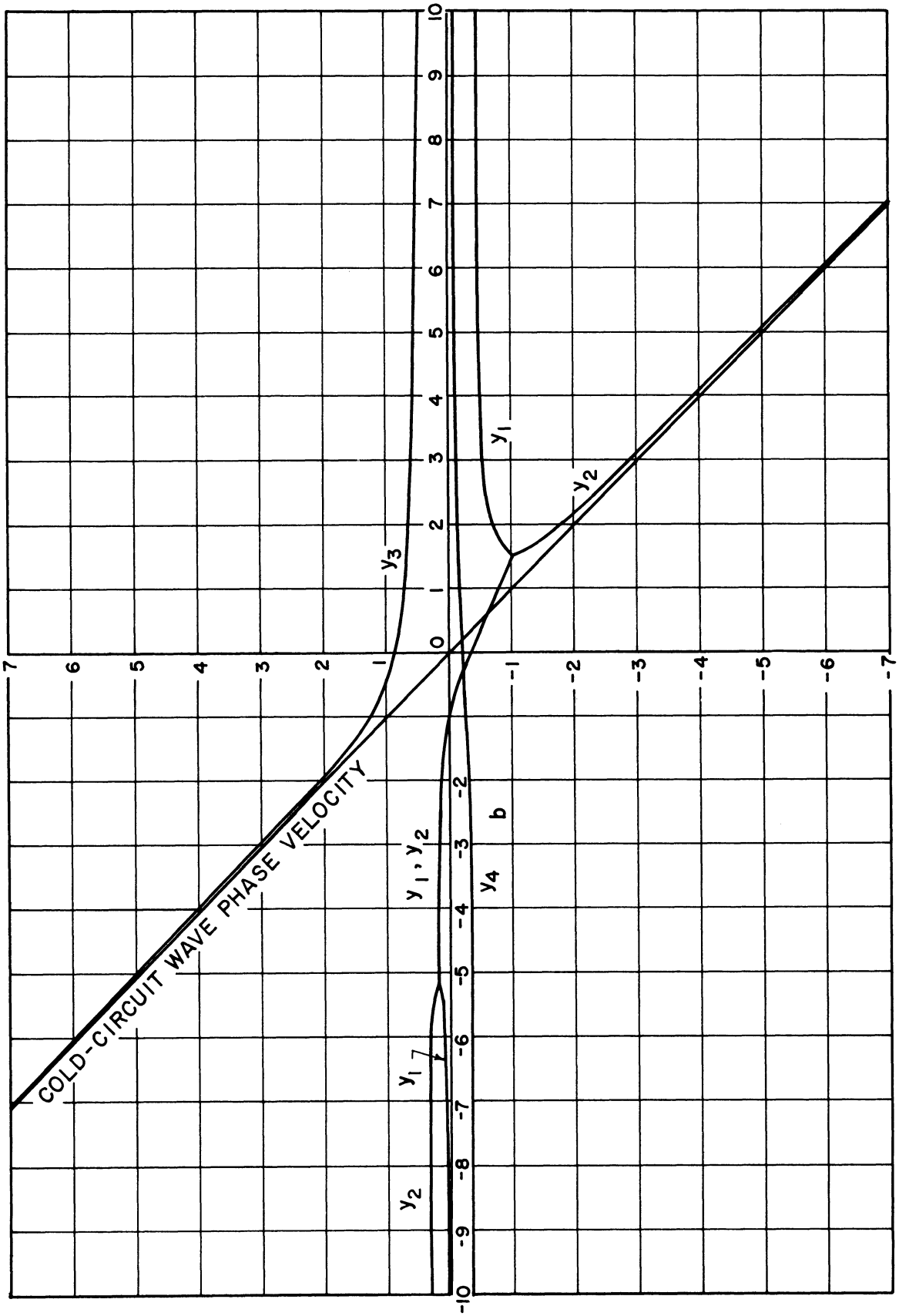

Fig. E.19 β_e=50, C=0.10, d=0, Q=-2.0

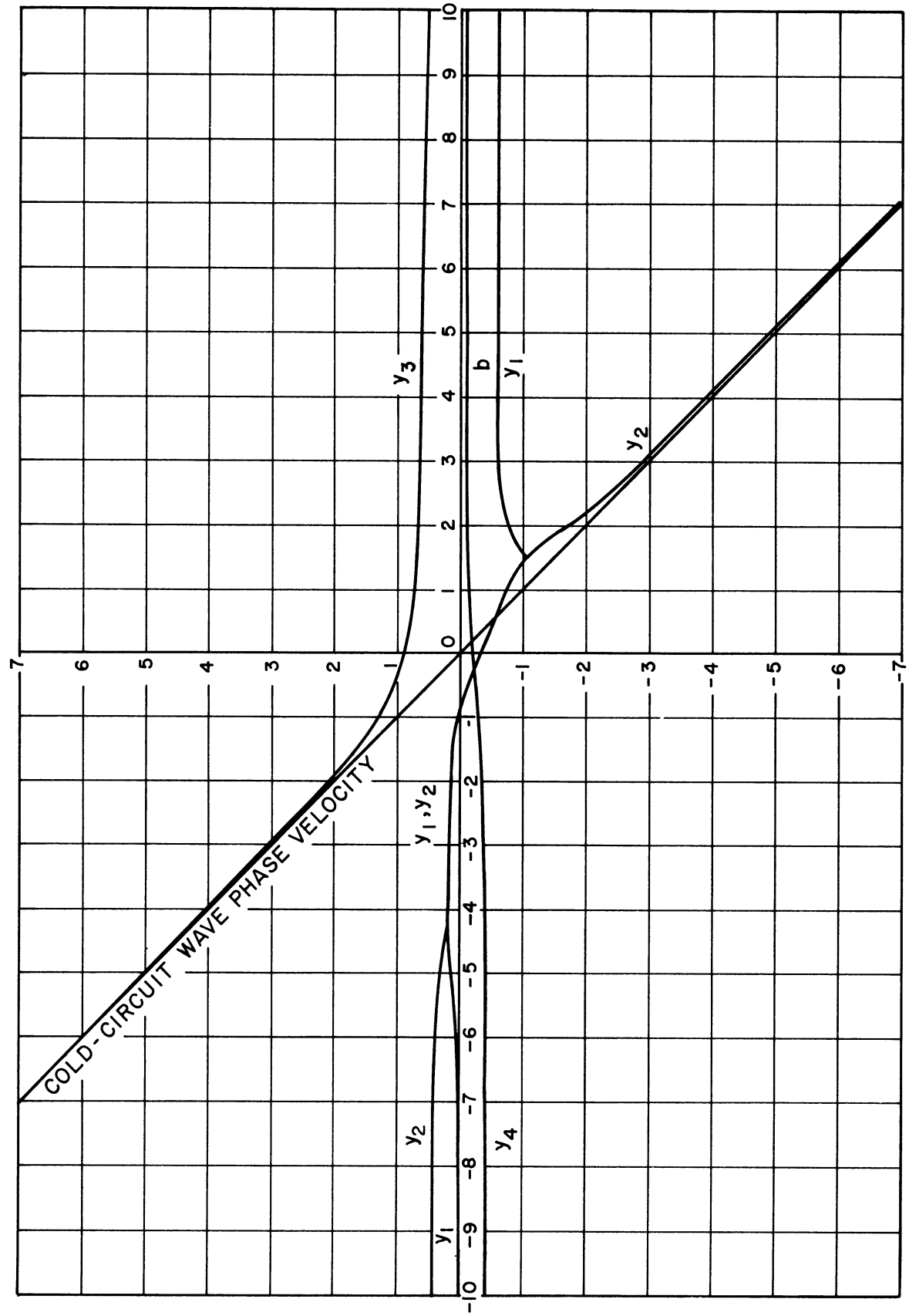

Fig. E.20 β_e=50, C=0.10, d=0, Q=-3.0

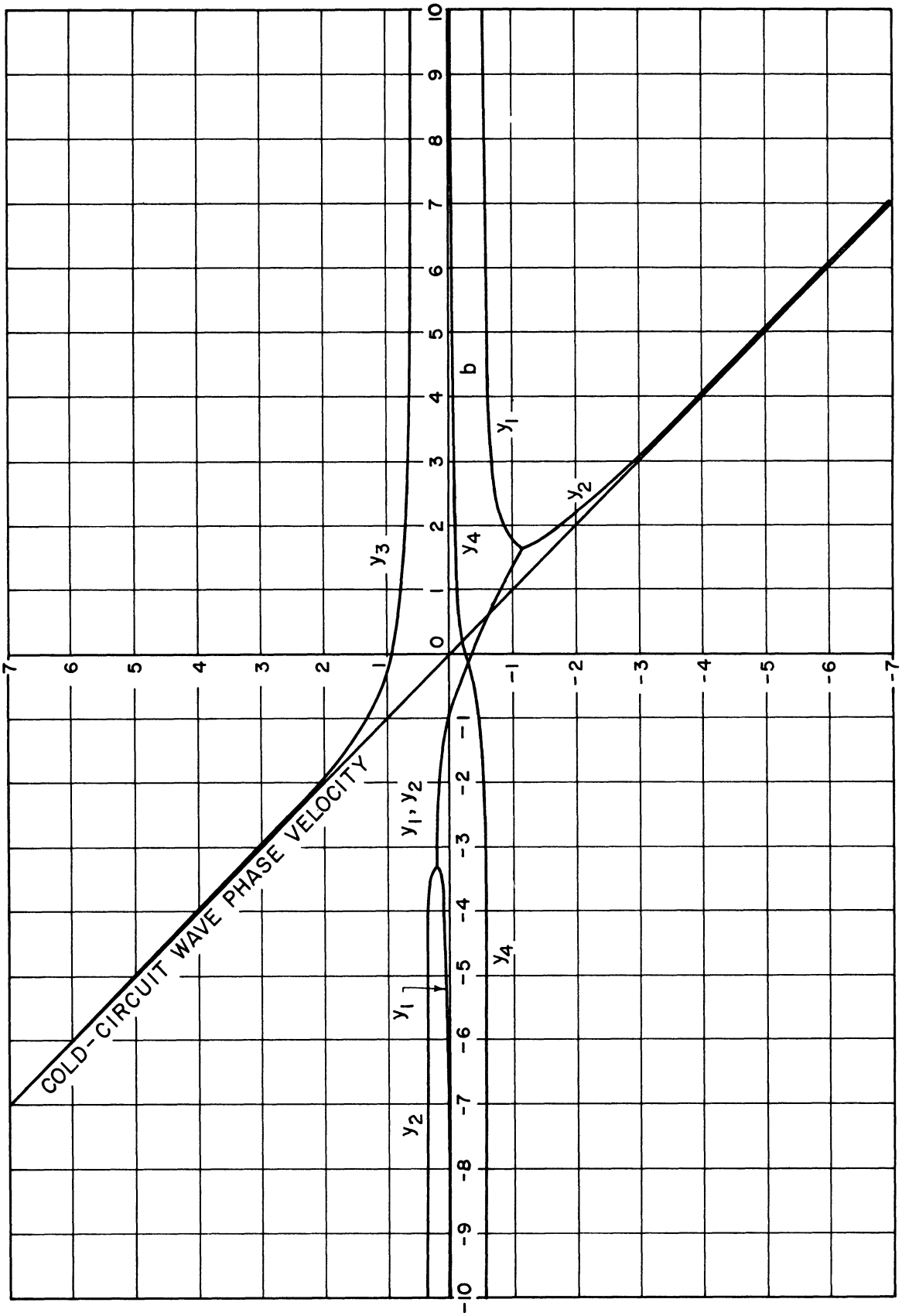

Fig. E.21 β_e=50, C=0.10, d=0, Q=-5.0

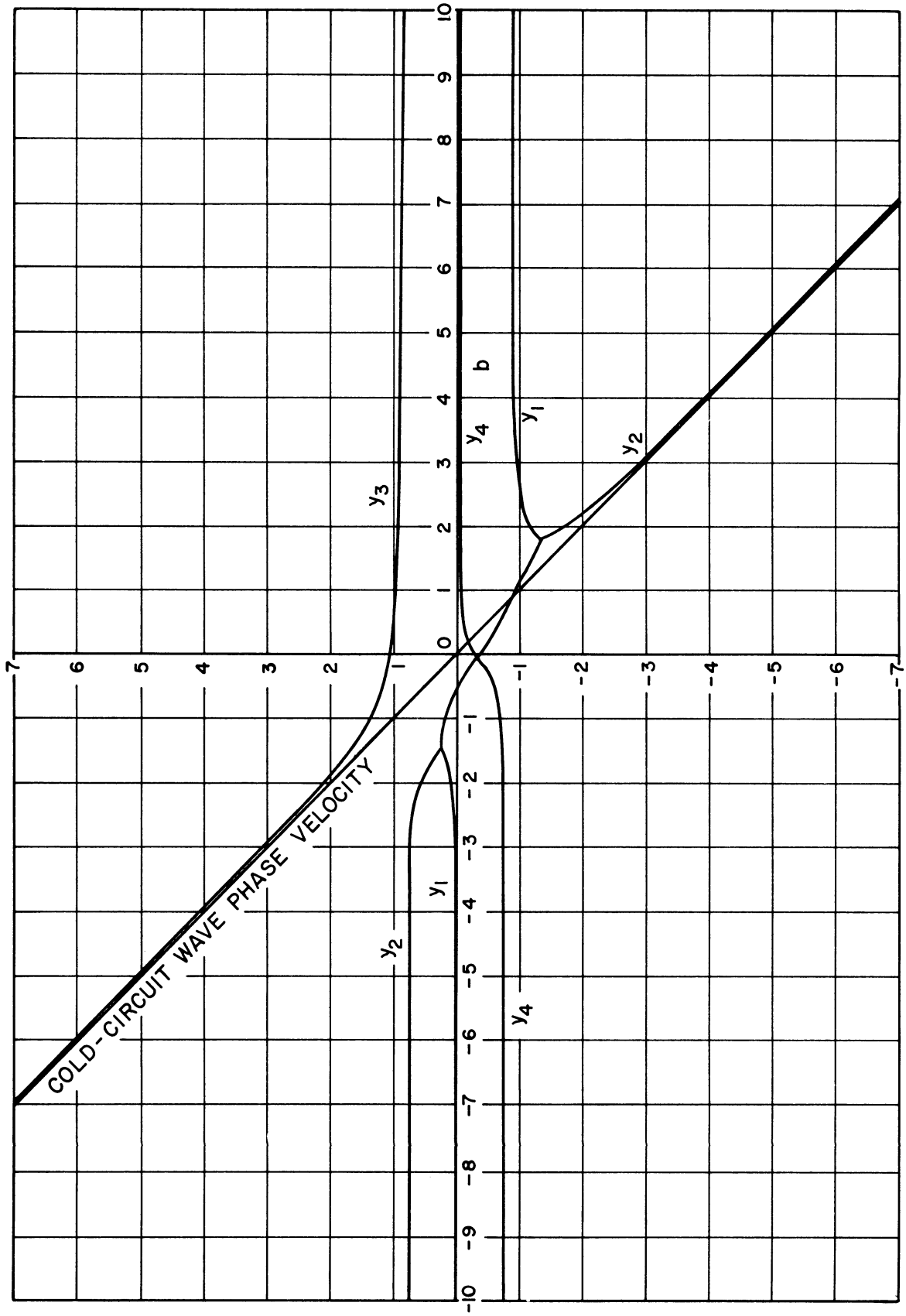

Fig. E. 22 β_e=50, C=0.10, d=0, Q=-15

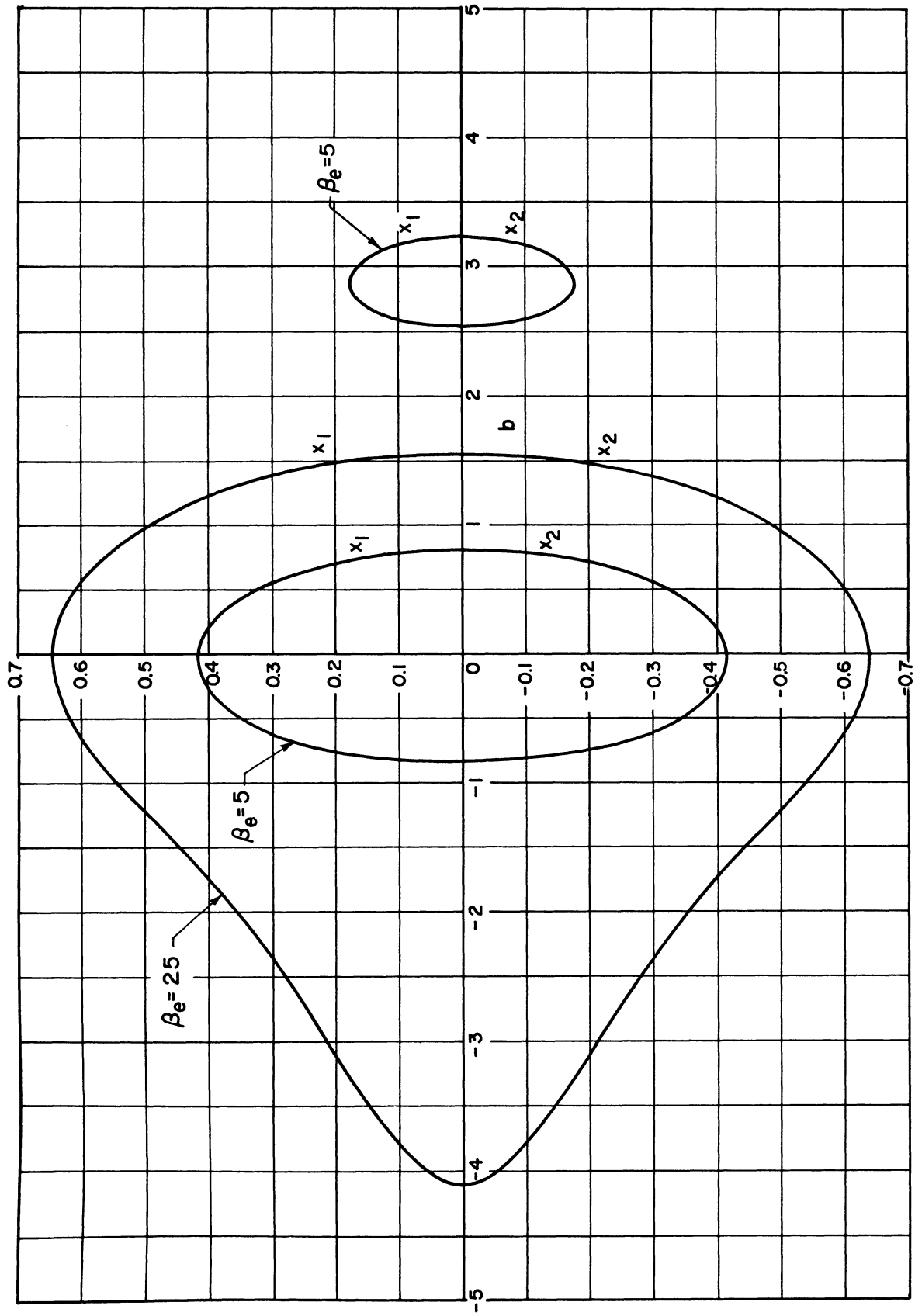

Fig. E.23 C=0.10, d=0, Q=0

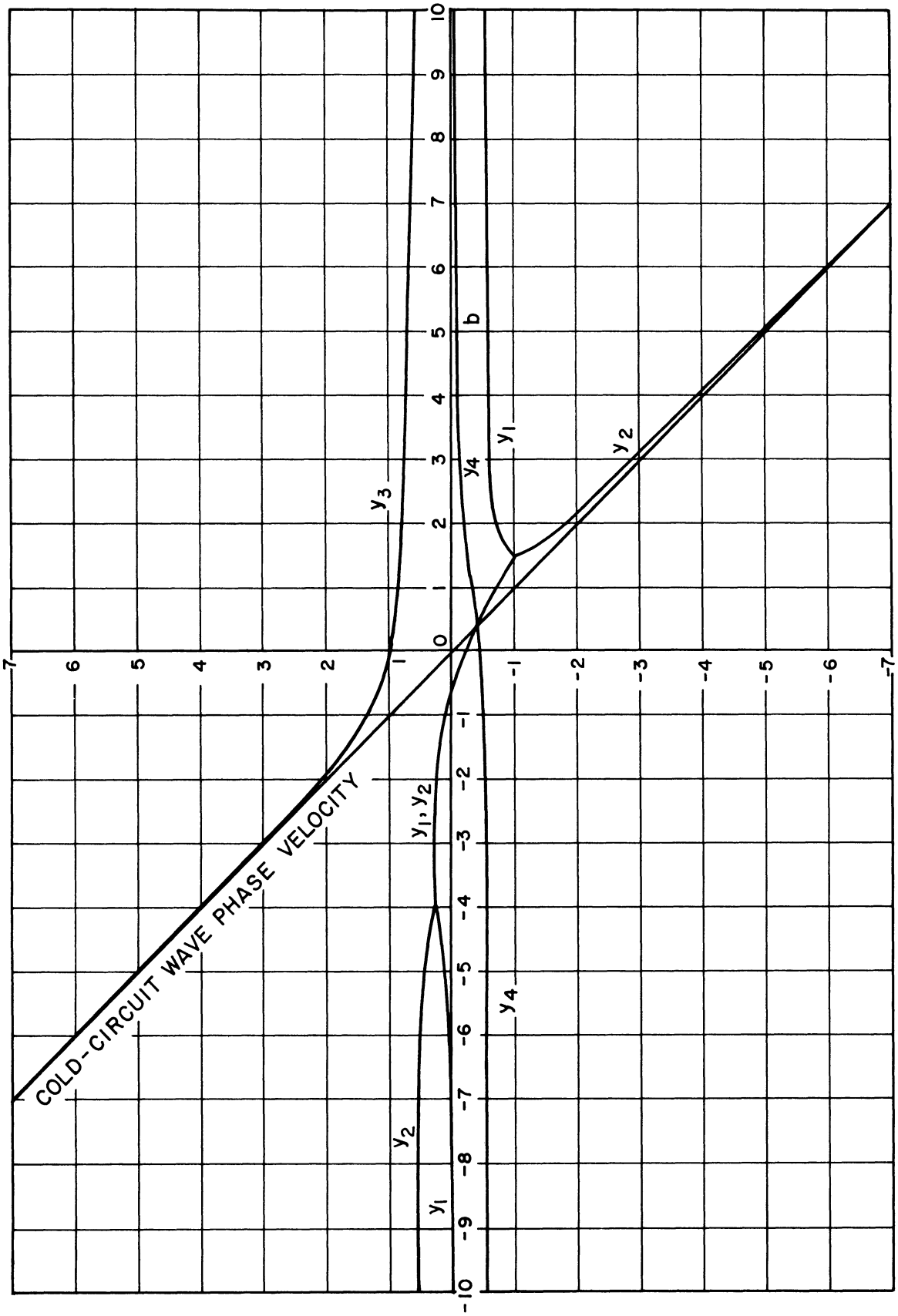

Fig. E. 24 β_e=25, C=0.10, d=0, Q=0

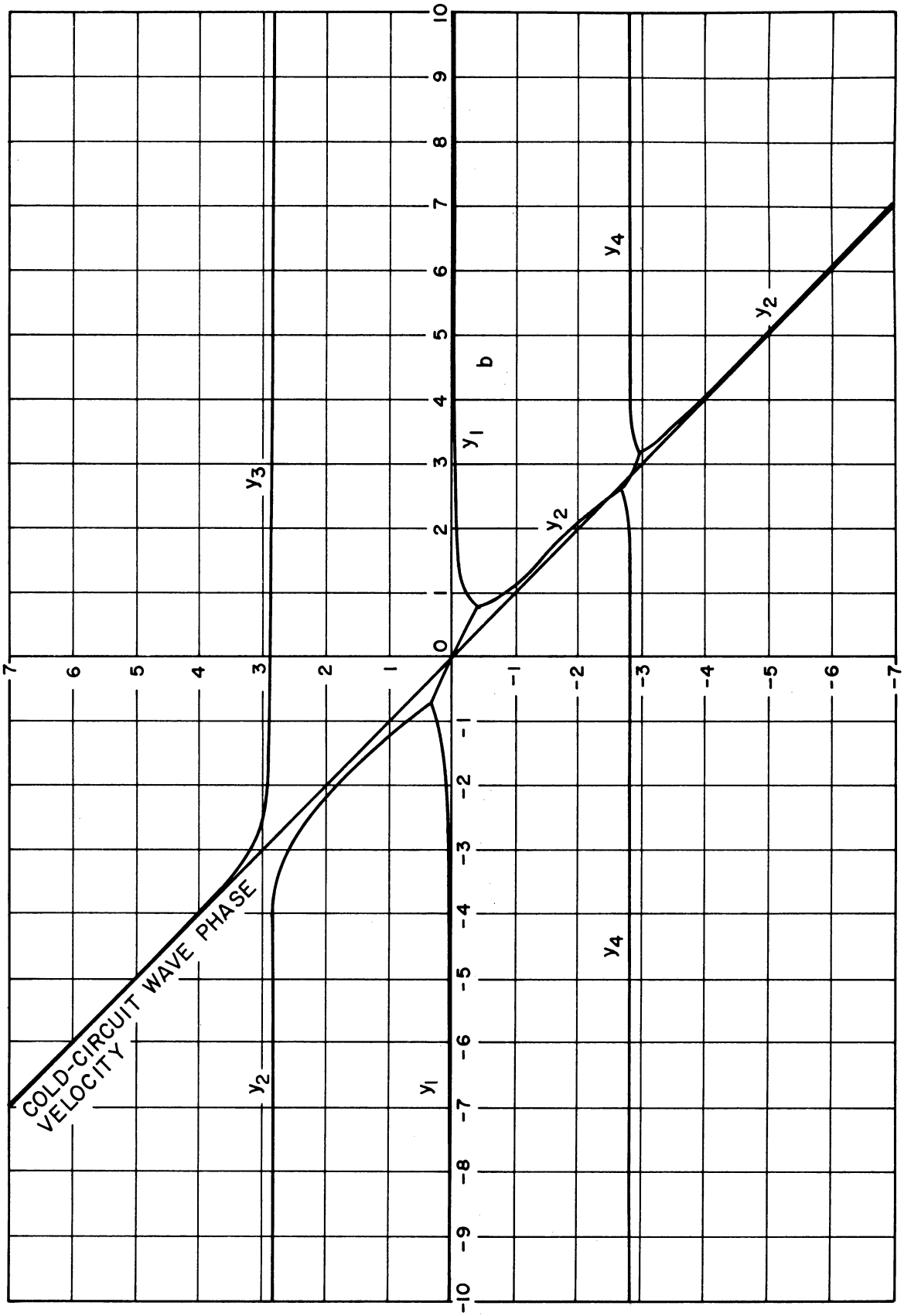

Fig. E. 25 $\beta_e = 5.0$, C=0.10, d=0, Q=0

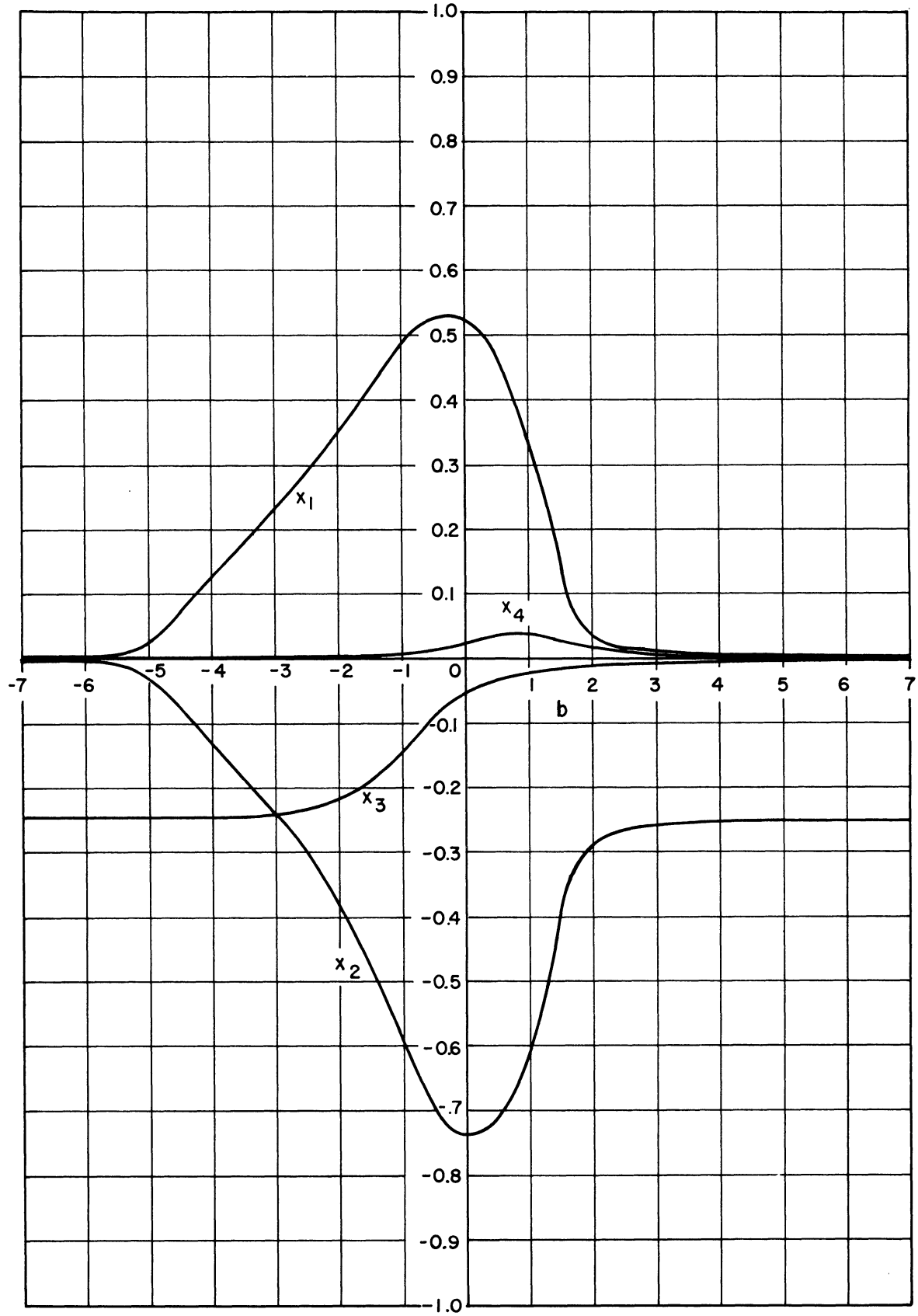

Fig. E. 26 $\beta_e = 50$, C=0.05, d=0.25, Q=0

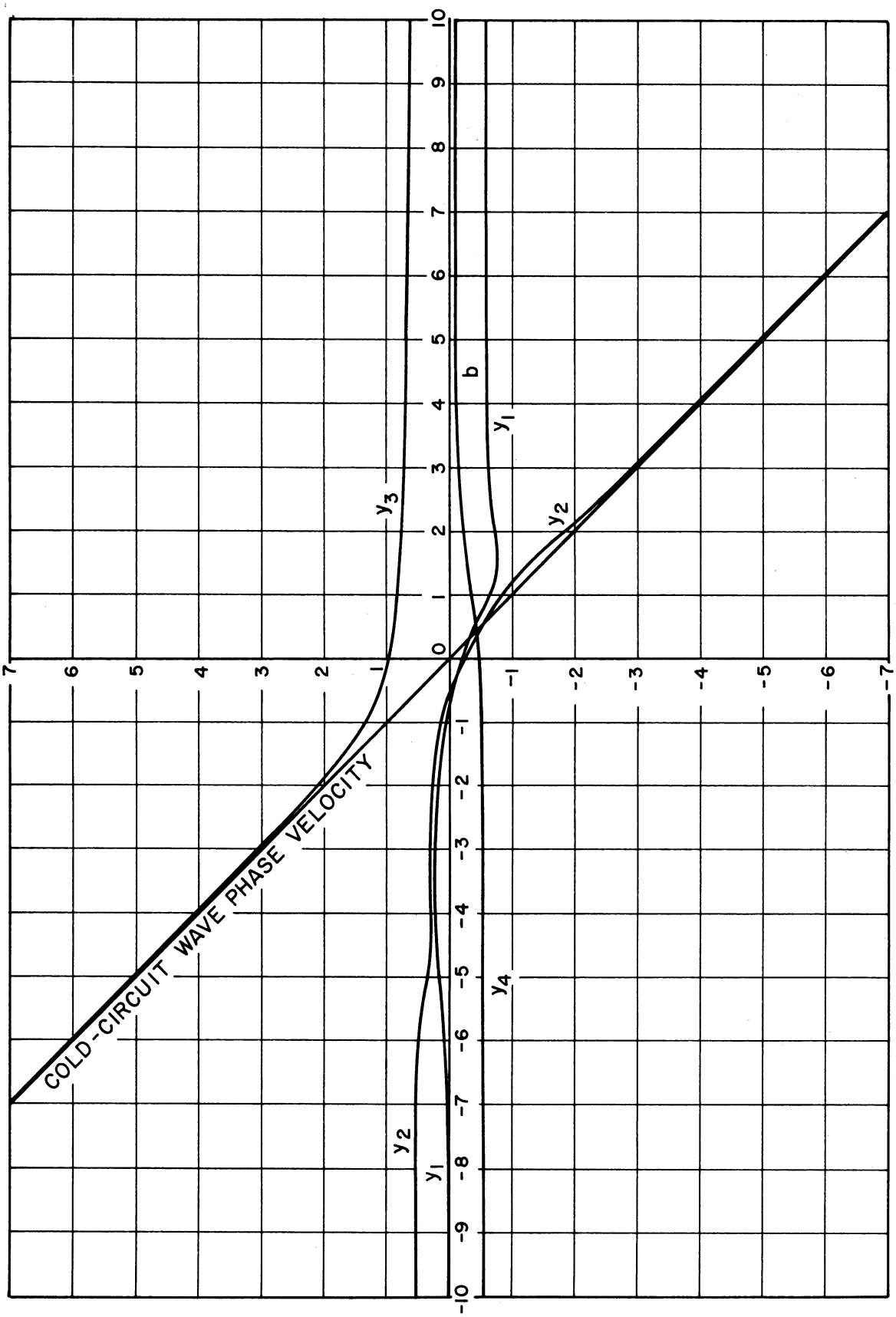

Fig. E.27 β_e=50, C=0.05, d=0.25, Q=0

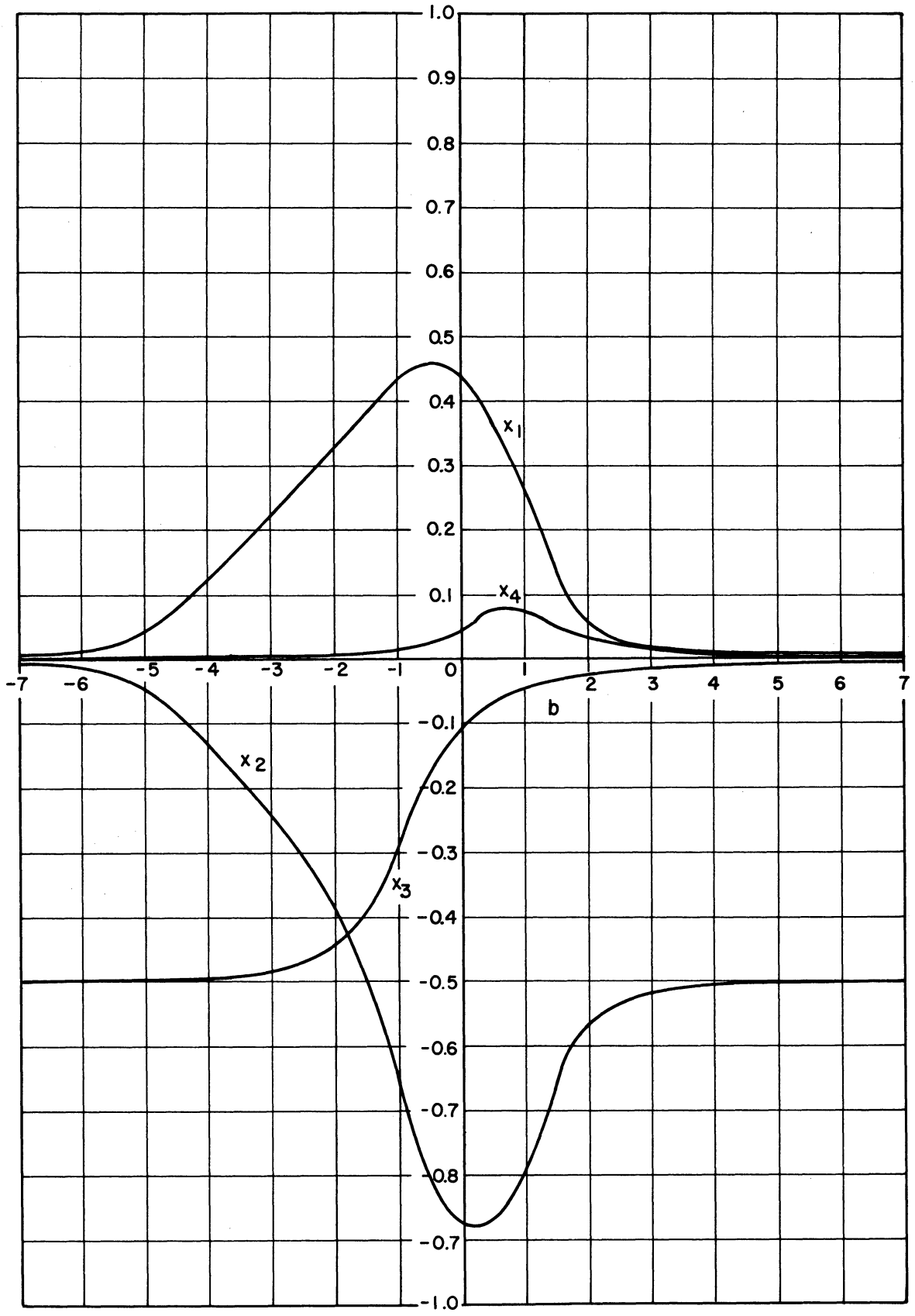

Fig. E. 28 $\beta_e = 50$, $C = 0.05$, $d = 0.50$, $Q = 0$

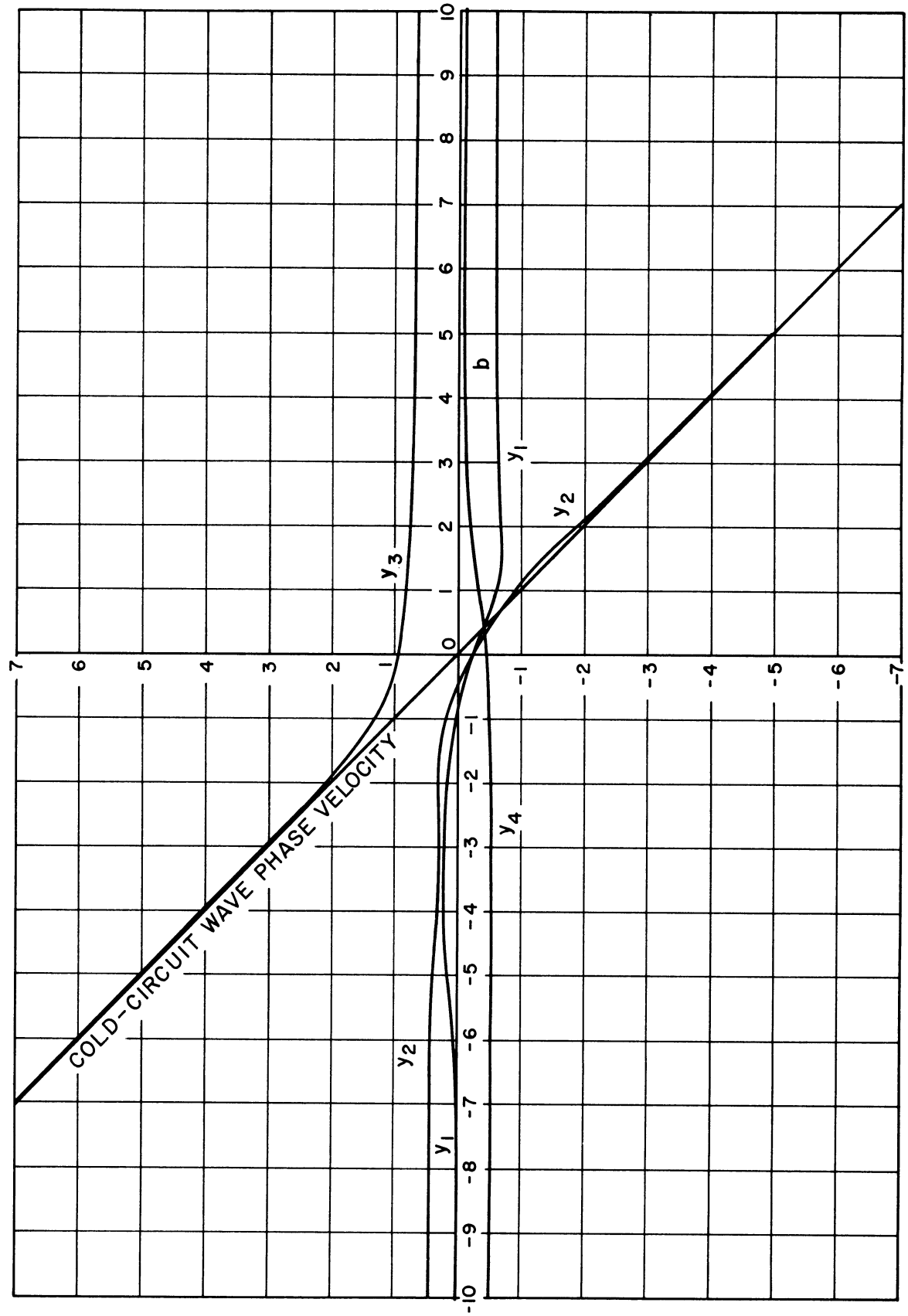

Fig. E. 29 $\beta_e = 50$, C=0.05, d=0.50, Q=0

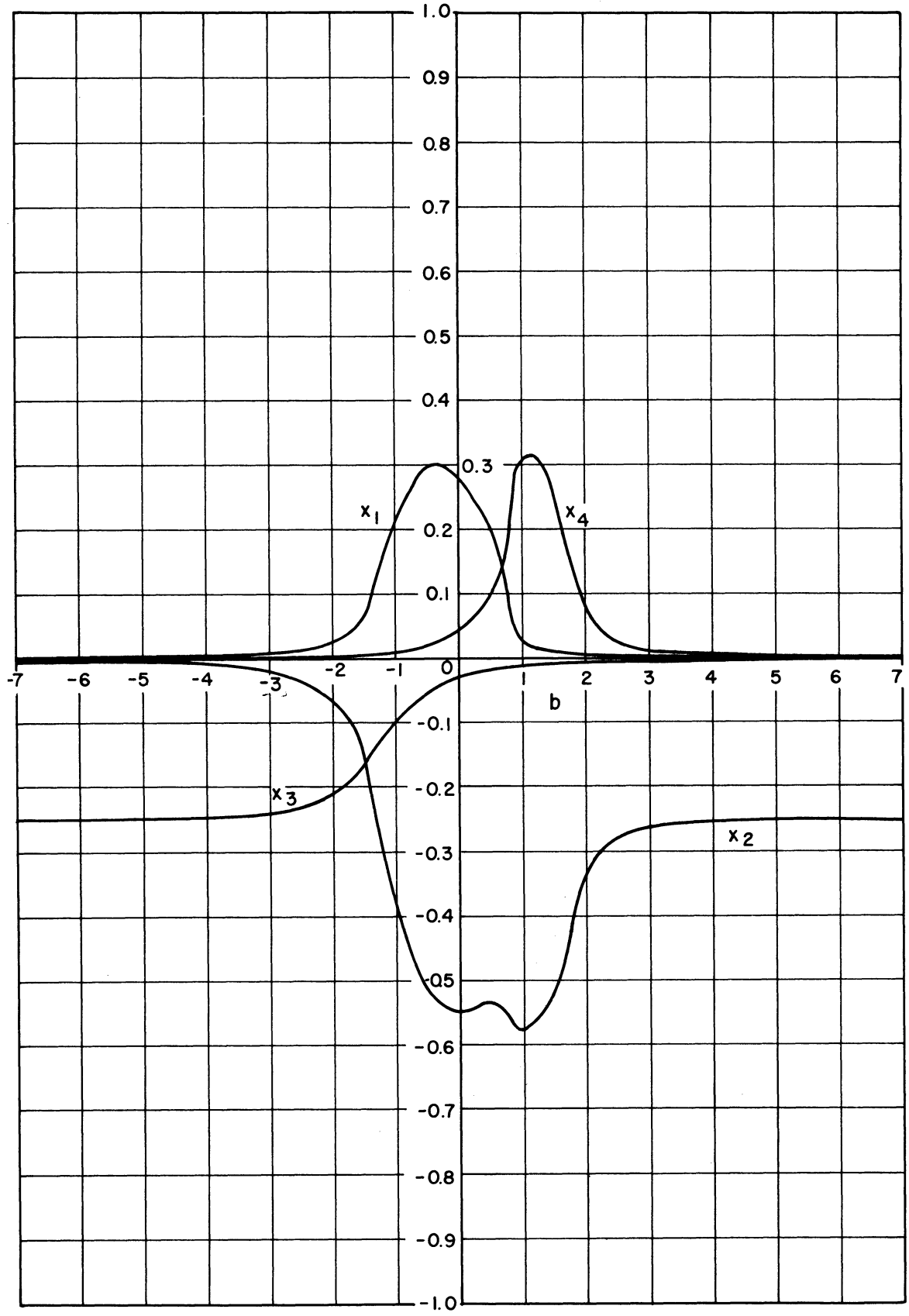

Fig. E. 30 β_e=50, C=0.05, d=0.25, Q=-5.0

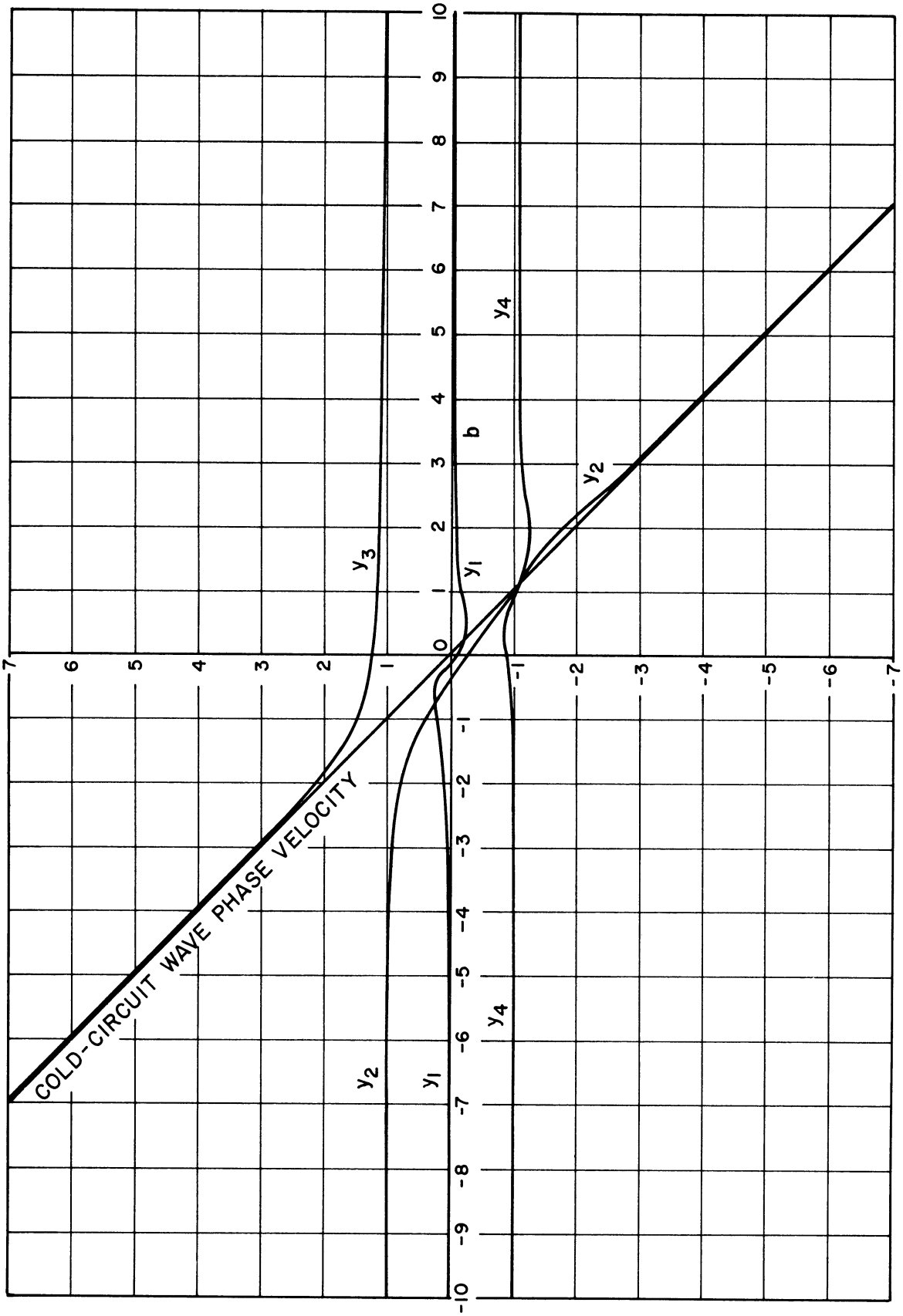

Fig. E.31 β_e=50, C=0.05, d=0.25, Q=-5.0

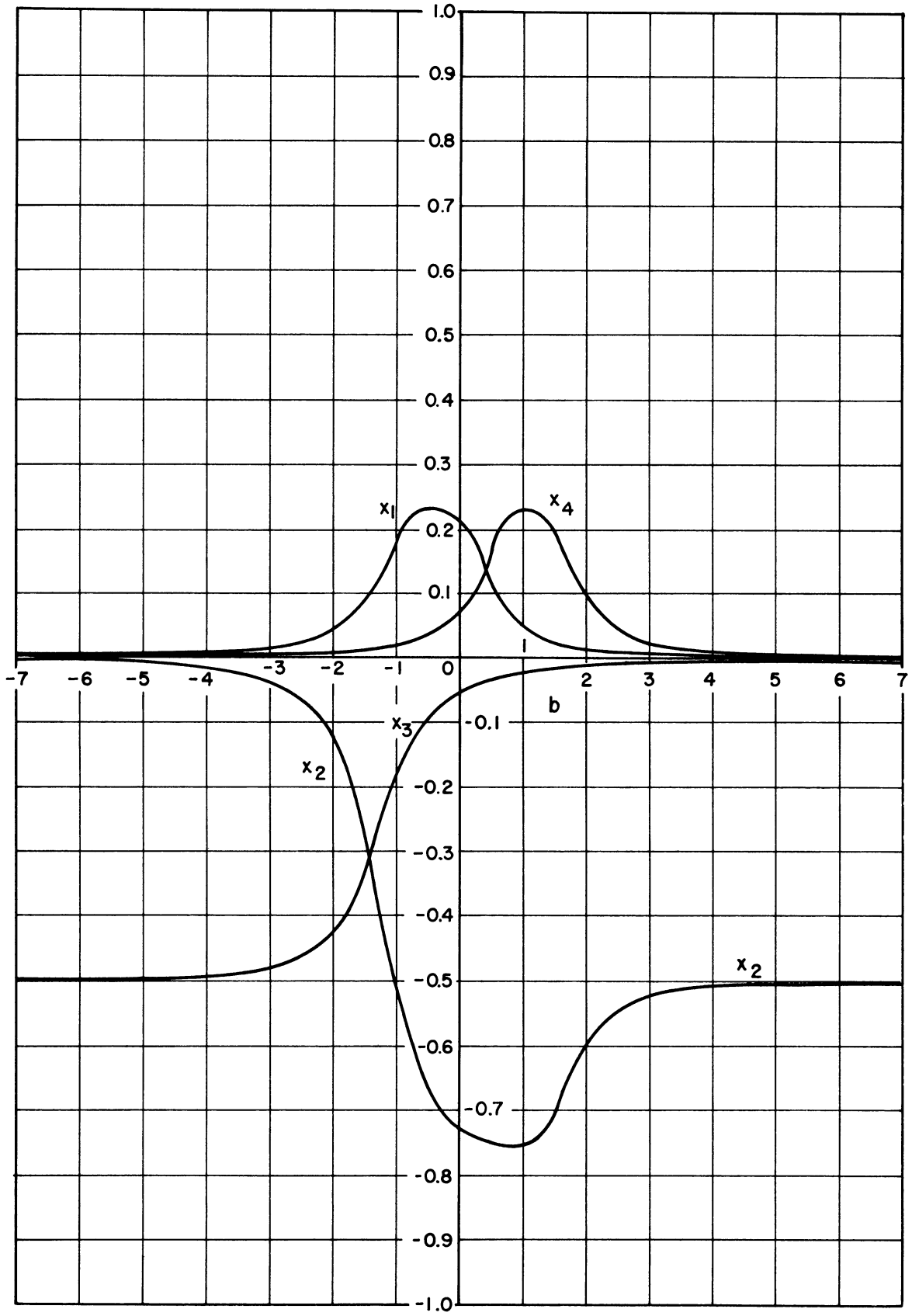

Fig. E. 32 $\beta_e = 50$, C=0.05, d=0.50, Q=-5.0

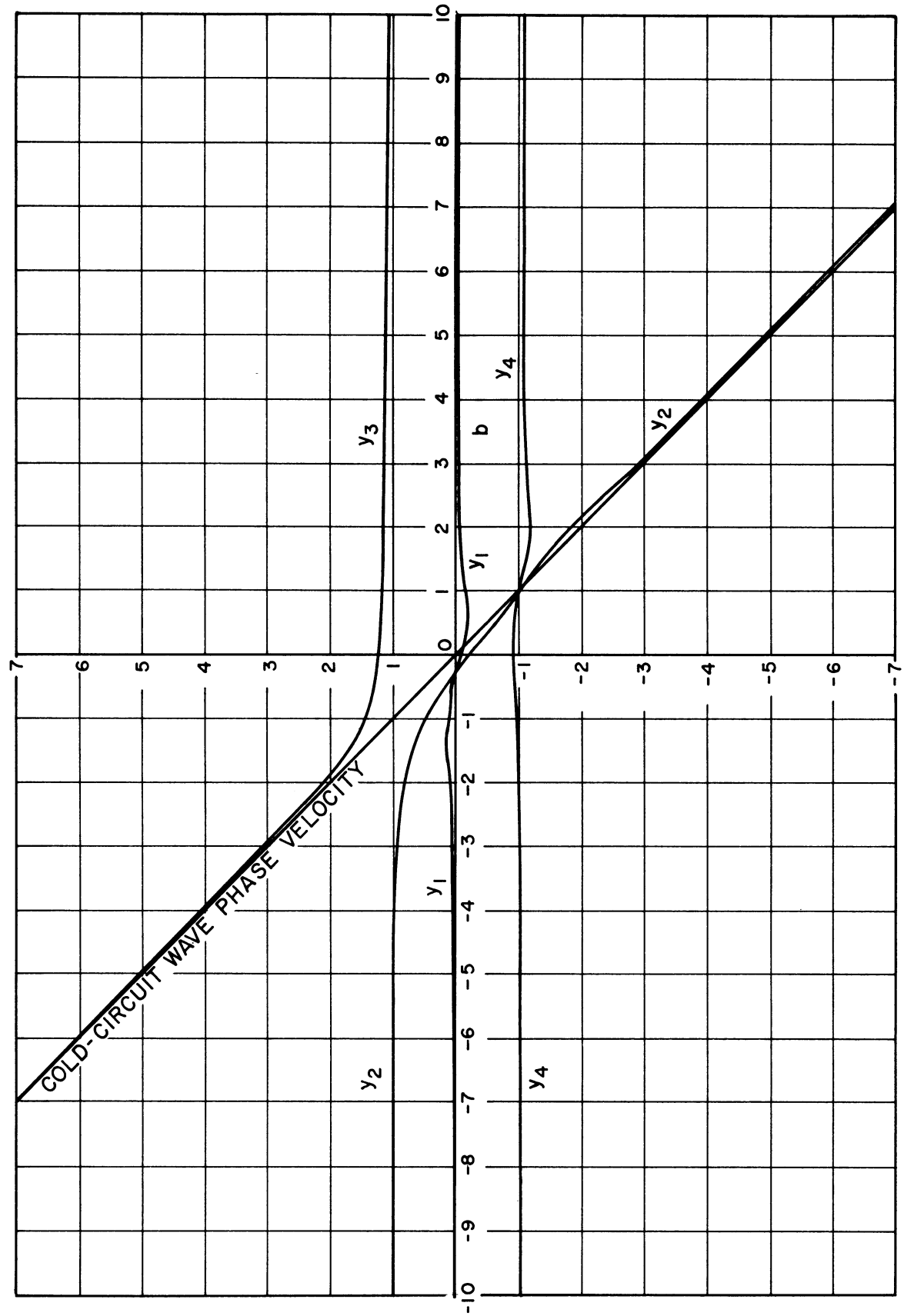

Fig. E.33 β_e=50, C=0.05, d=0.50, Q=-5.0

APPENDIX F

THE GROWING- AND BEATING-WAVE GAIN CHARACTERISTICS OF THE E-TYPE DEVICE

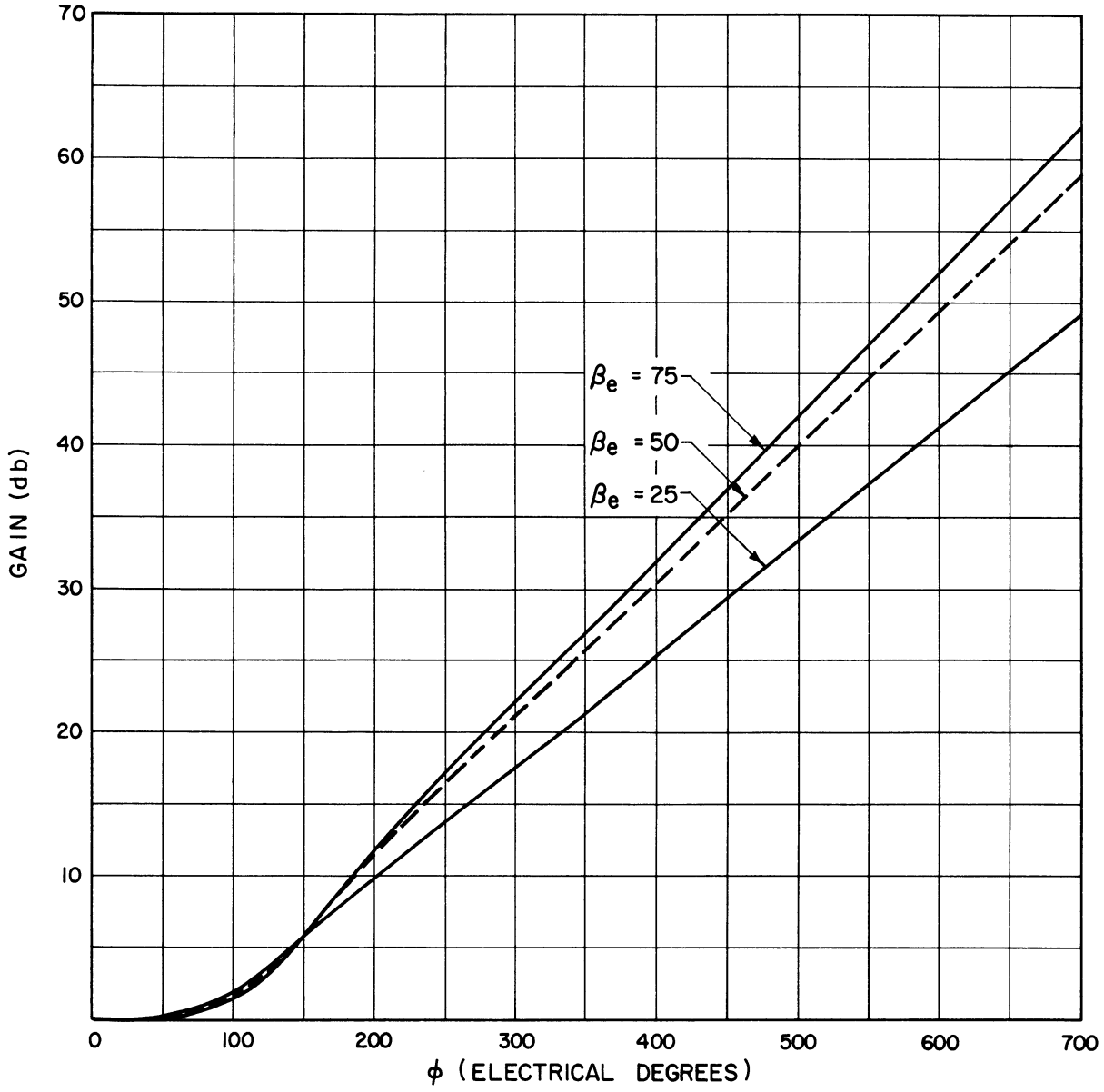

Fig. F. 1 b = 0, C = 0.05, d = 0, Q = 0

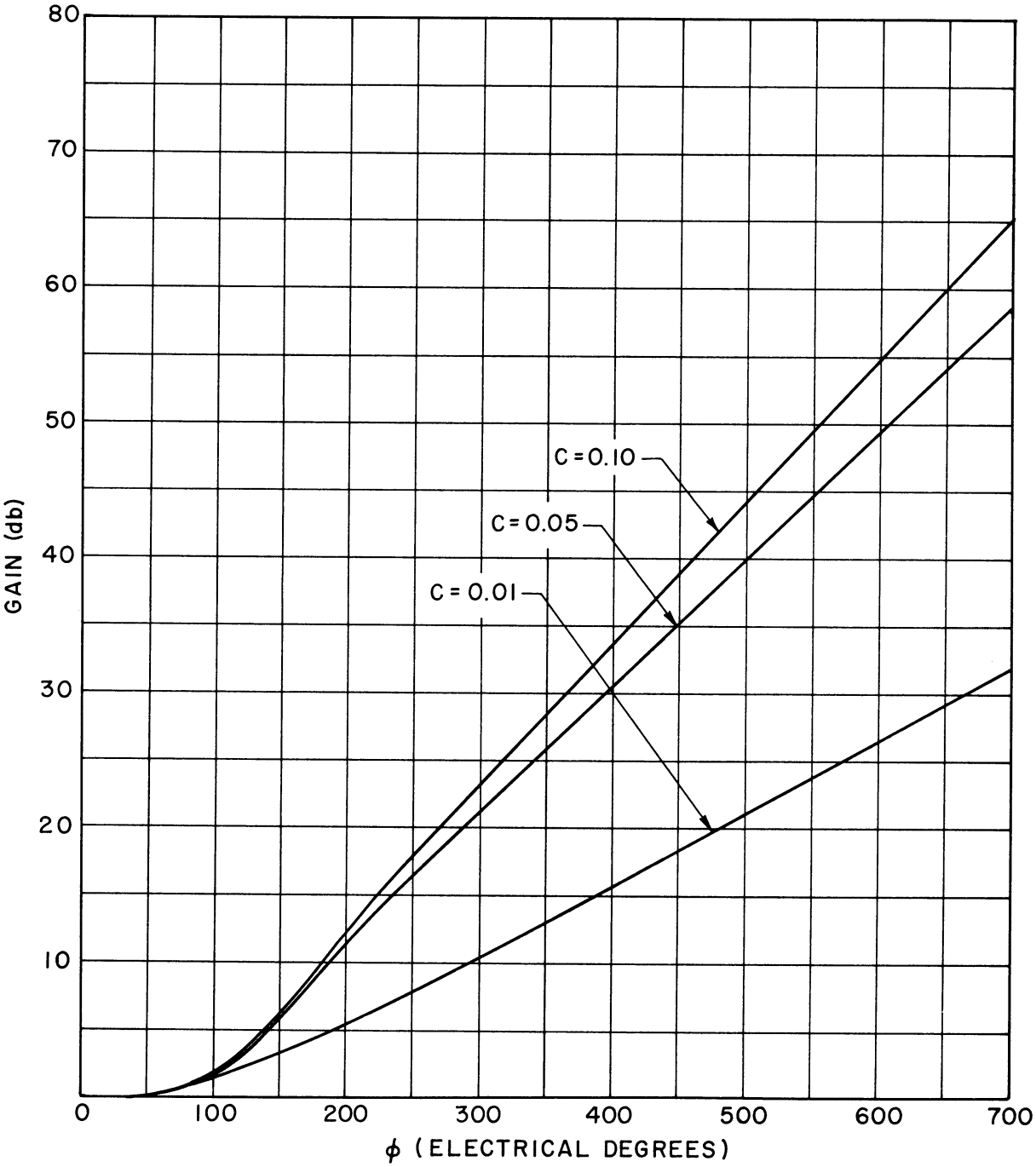

Fig. F. 2 $\beta_e = 50$, d = 0, b = 0, Q = 0

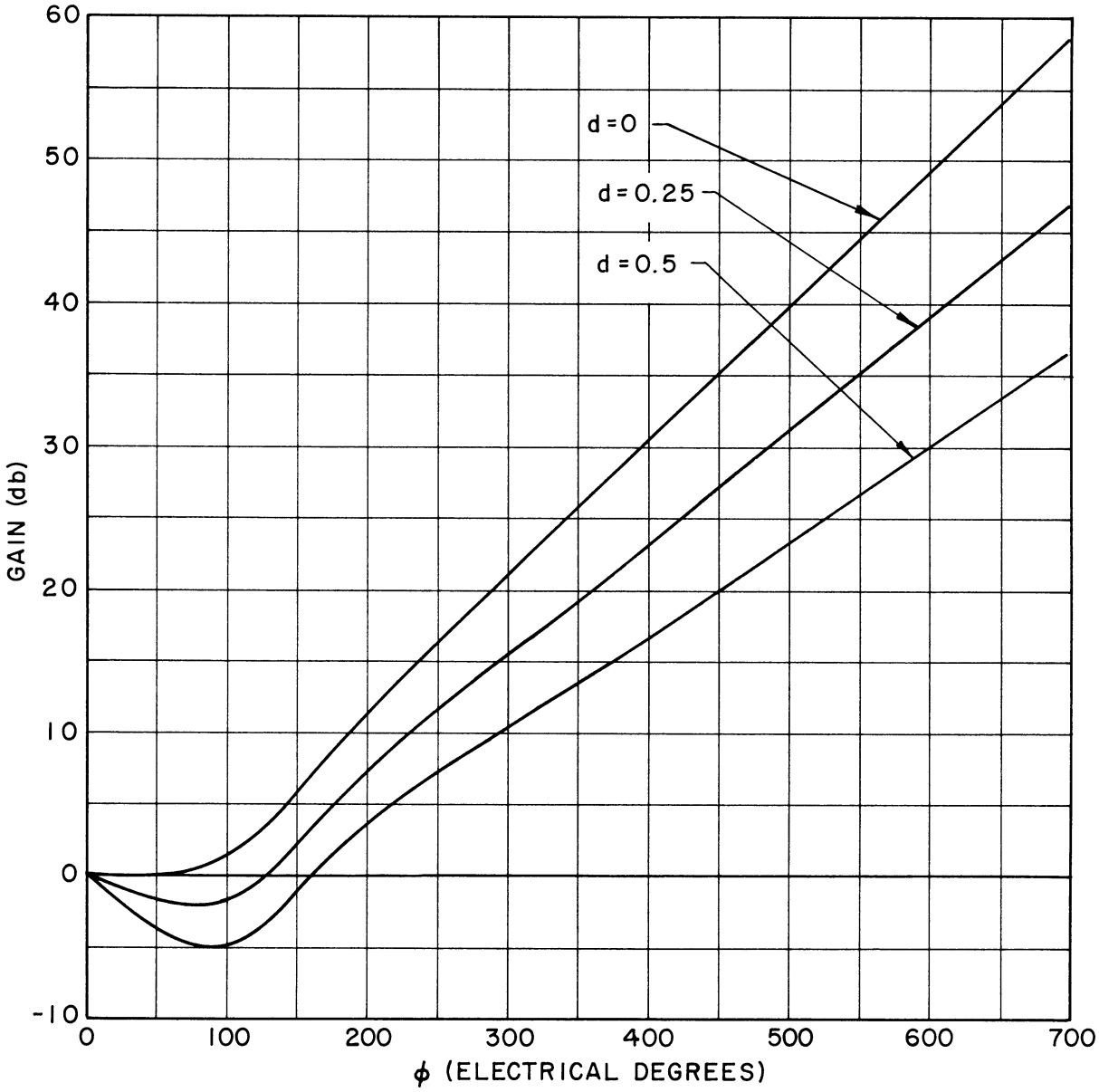

Fig. F.3 $\beta_e = 50$, b = 0, C = 0.05, Q = 0

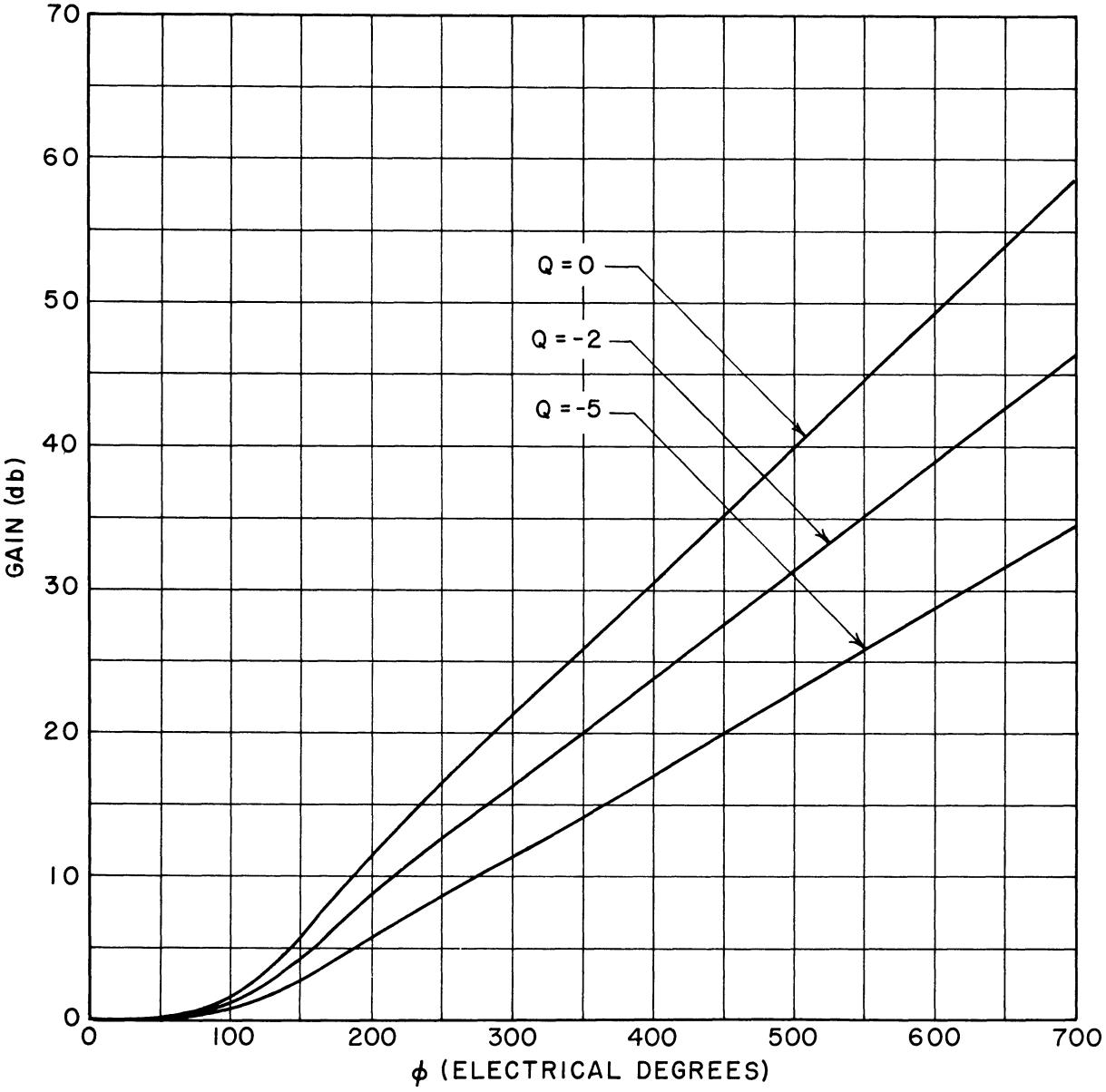

Fig. F. 4 β_e=50, b=0, C=0.05, d=0

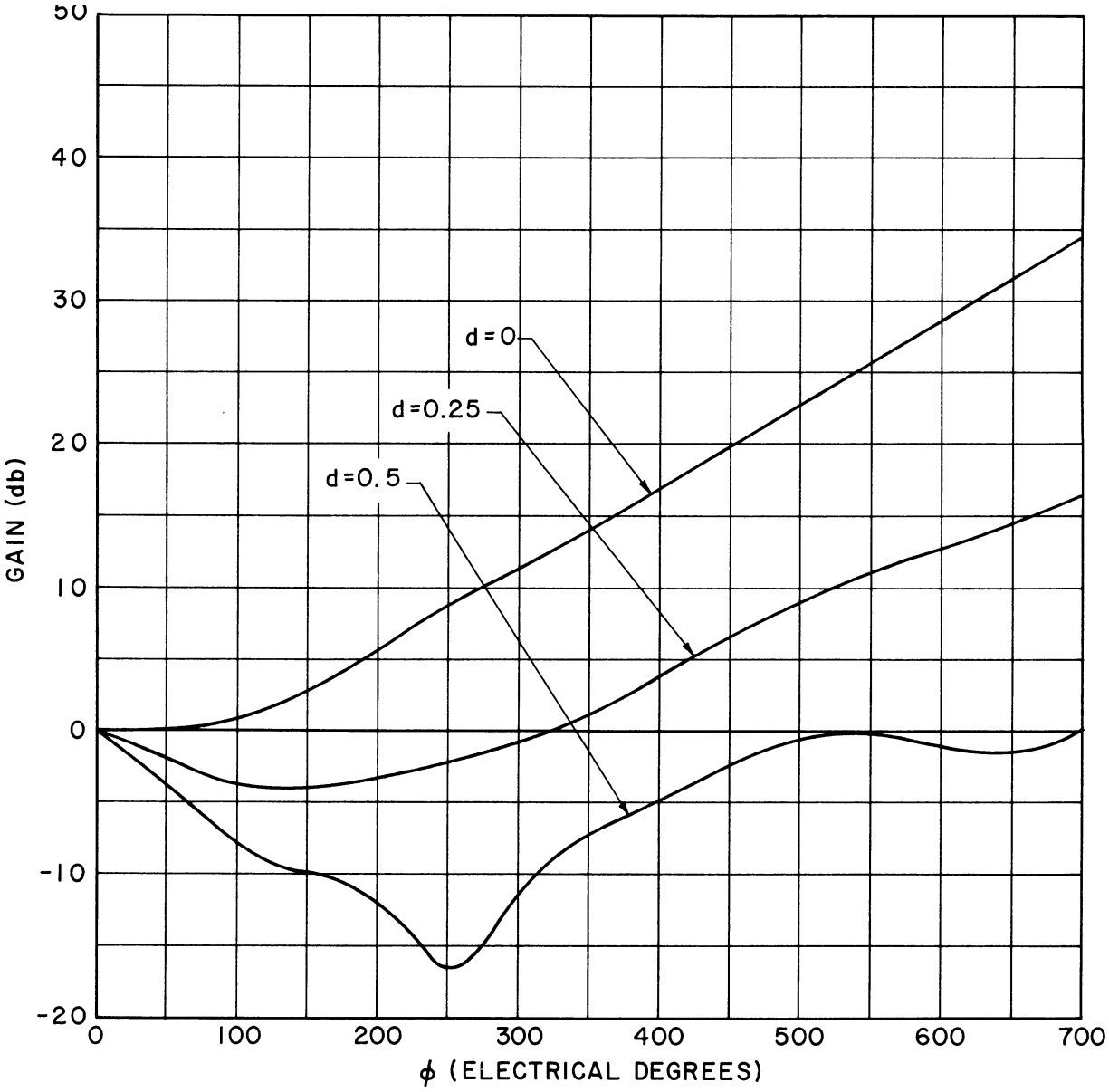

Fig. F. 5 β_a=50, b=0, C=0.05, Q=-5.0

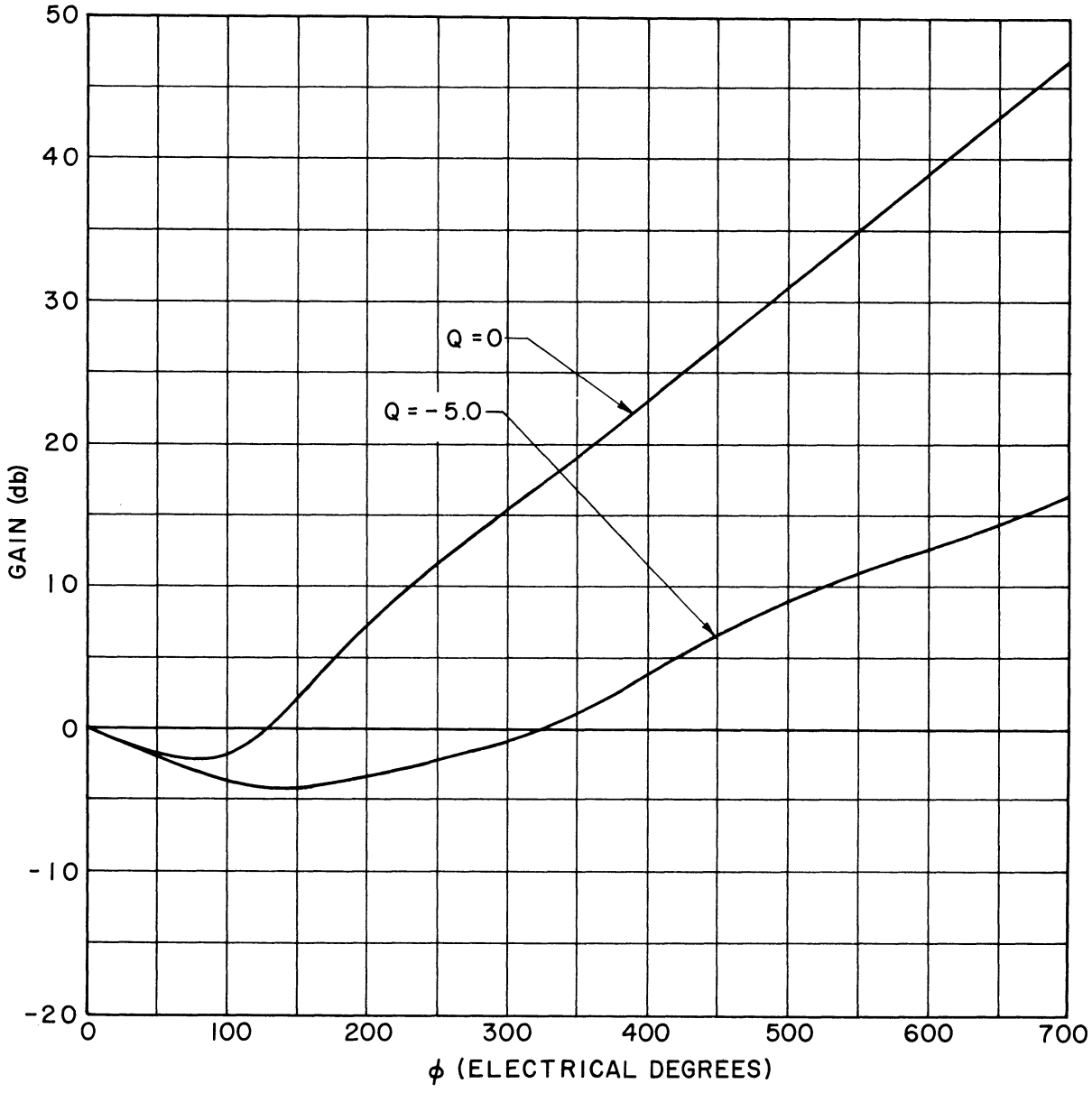

Fig. F.6 $\beta_e = 50$, b = 0, C = 0.05, d = 0.25

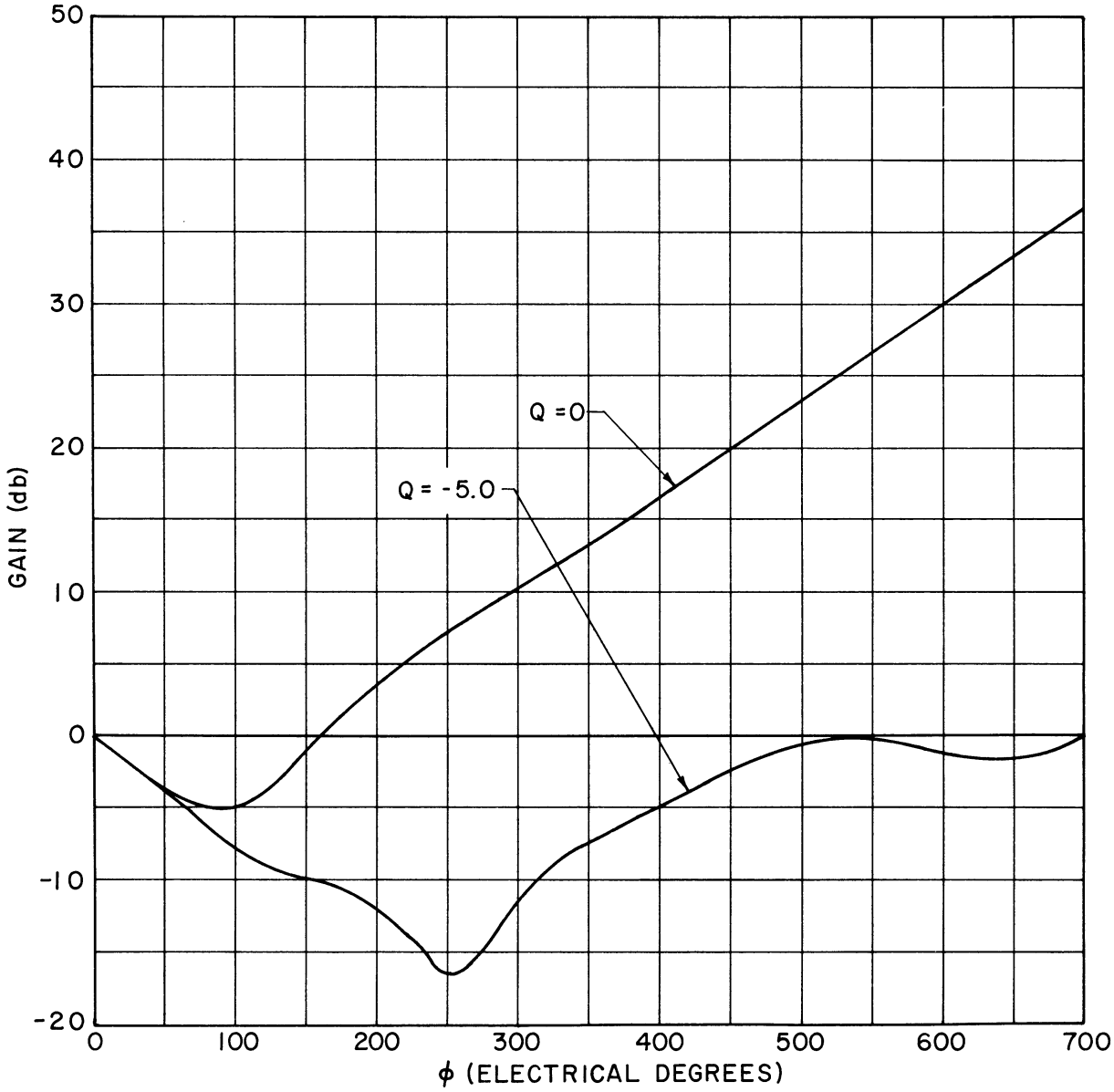

Fig. F. 7 $\beta_e = 50$, b = 0, C = 0.05, d = 0.5

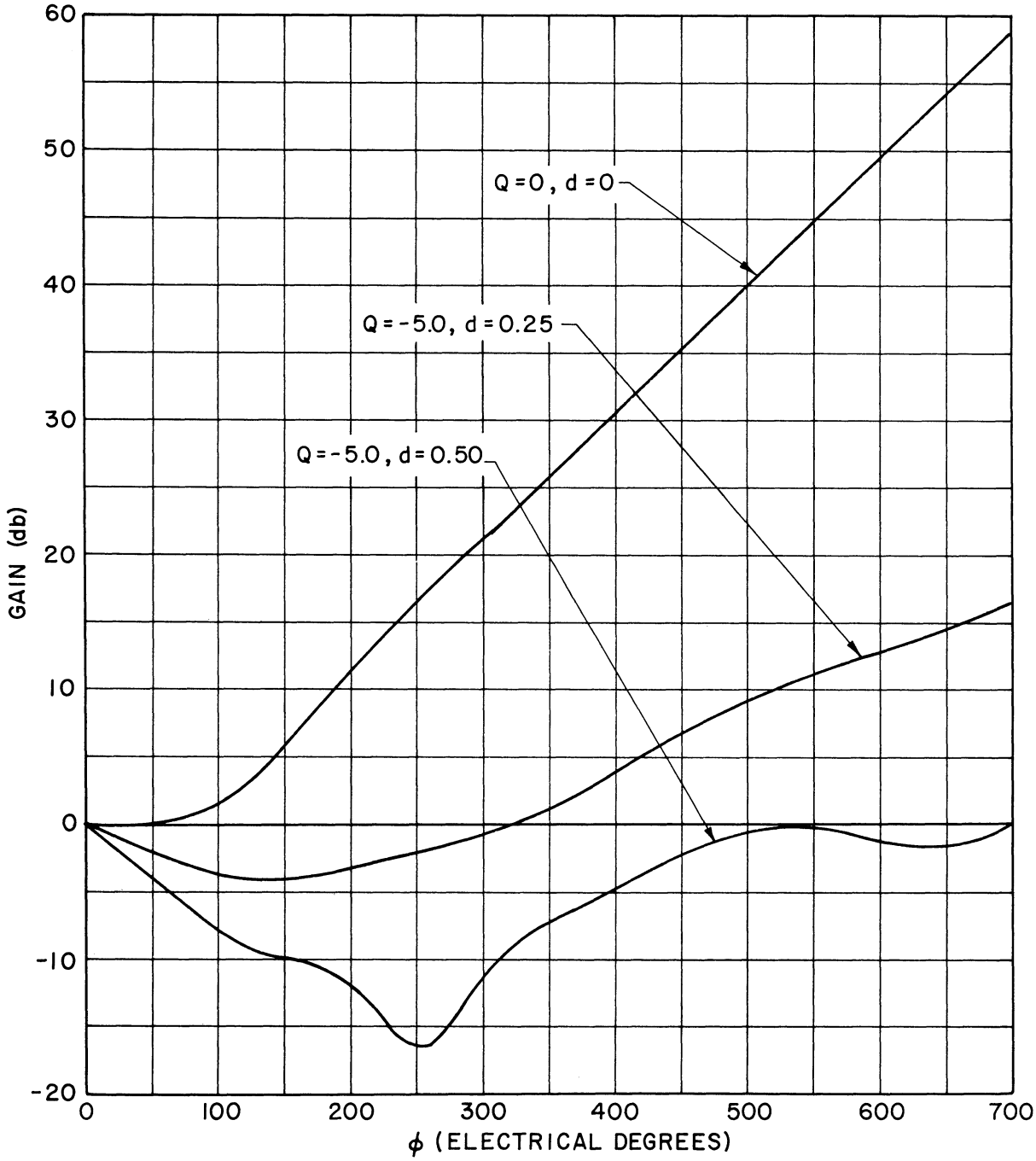

Fig. F. 8 $\beta_e = 50$, b = 0, C = 0.05

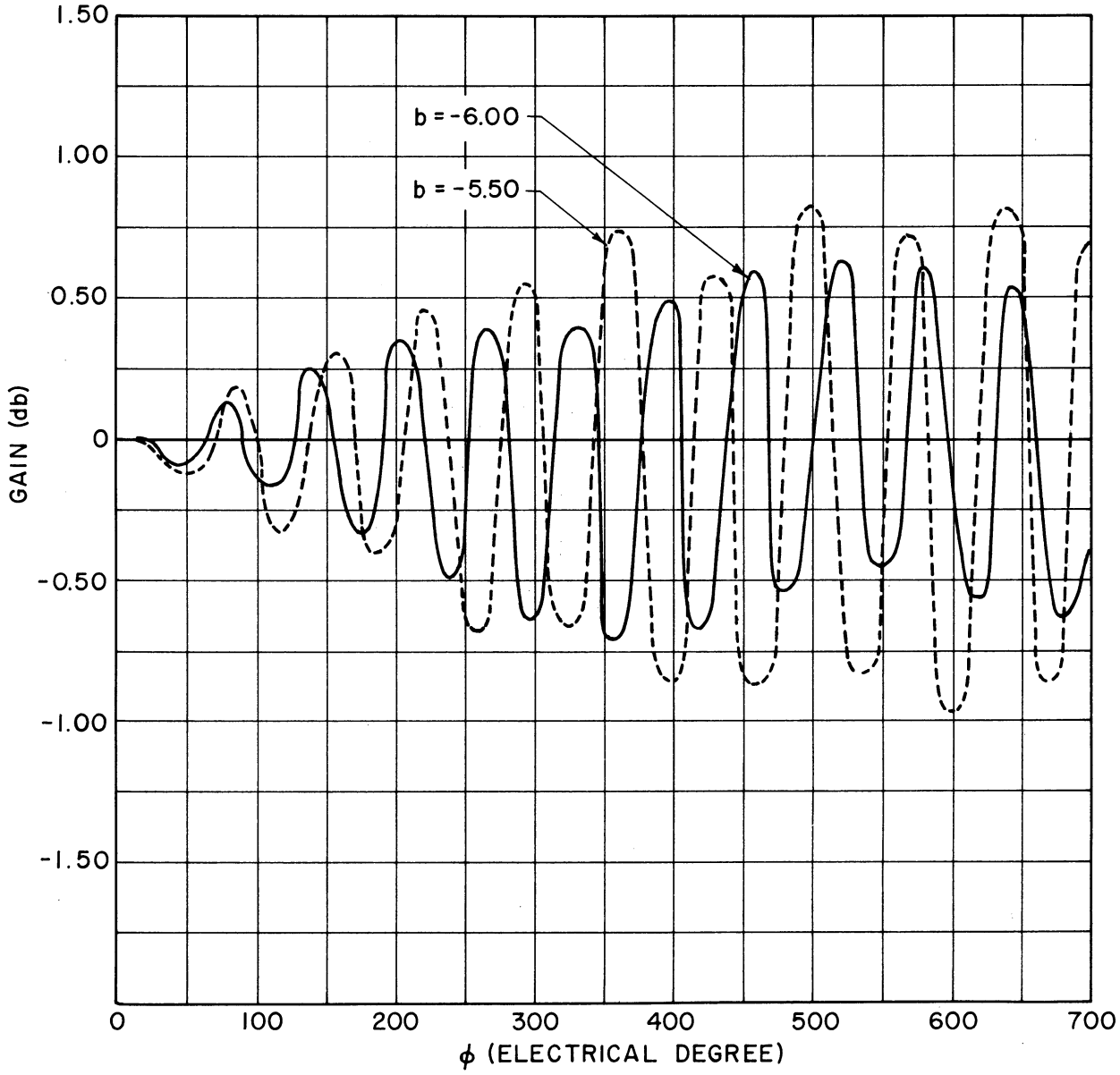

Fig. F.9 $\beta_e = 50$, C=0.05, d=0, Q=-0.2

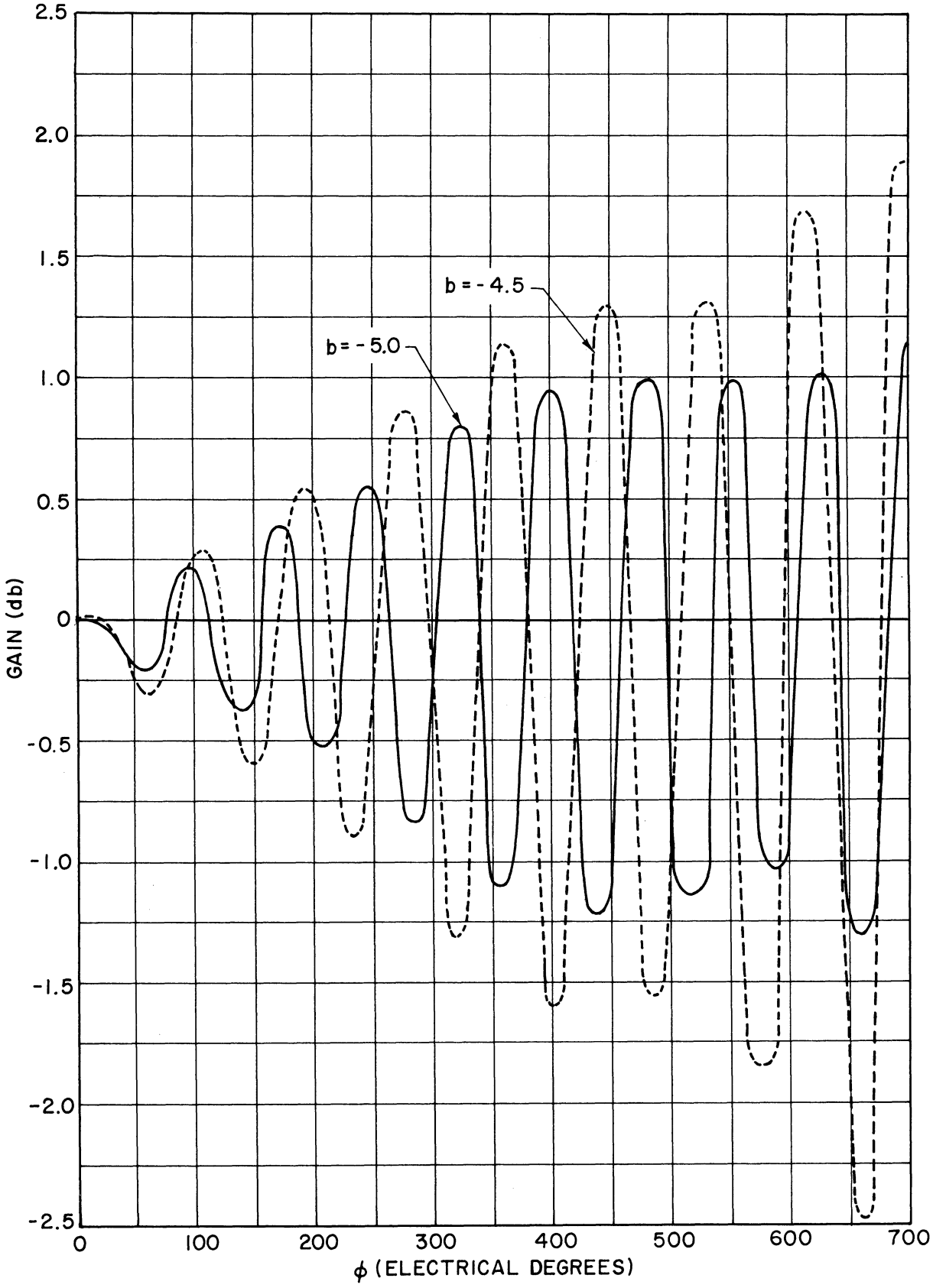

Fig. F. 10 $\beta_e = 50$, C=0.05, d=0, Q=-0.2

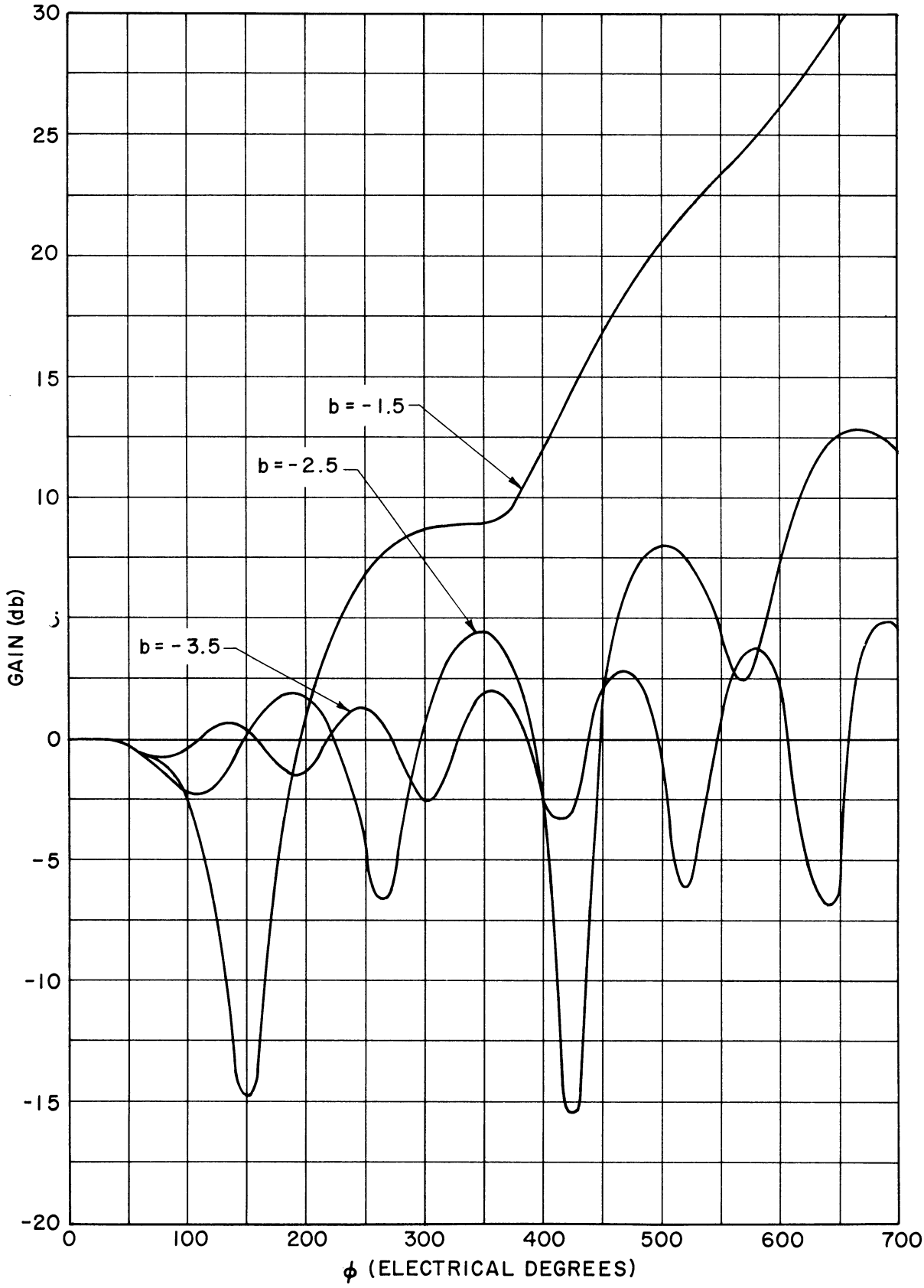

Fig. F. 11 $\beta_e = 50$, C = 0.05, d = 0, Q = -0.20

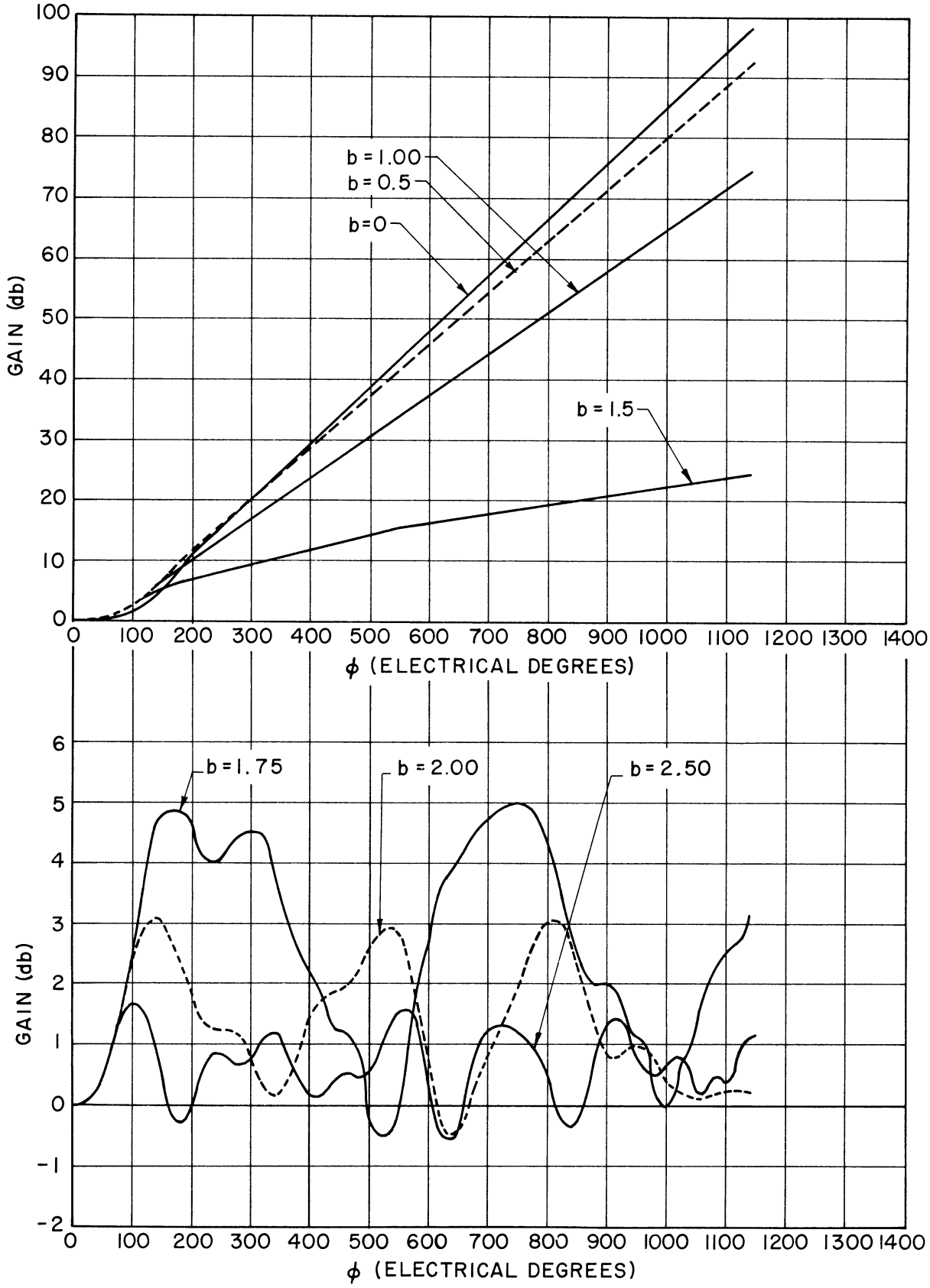

Fig. F. 12 β_e= 50, C = 0.05, d = 0, Q = -0.20

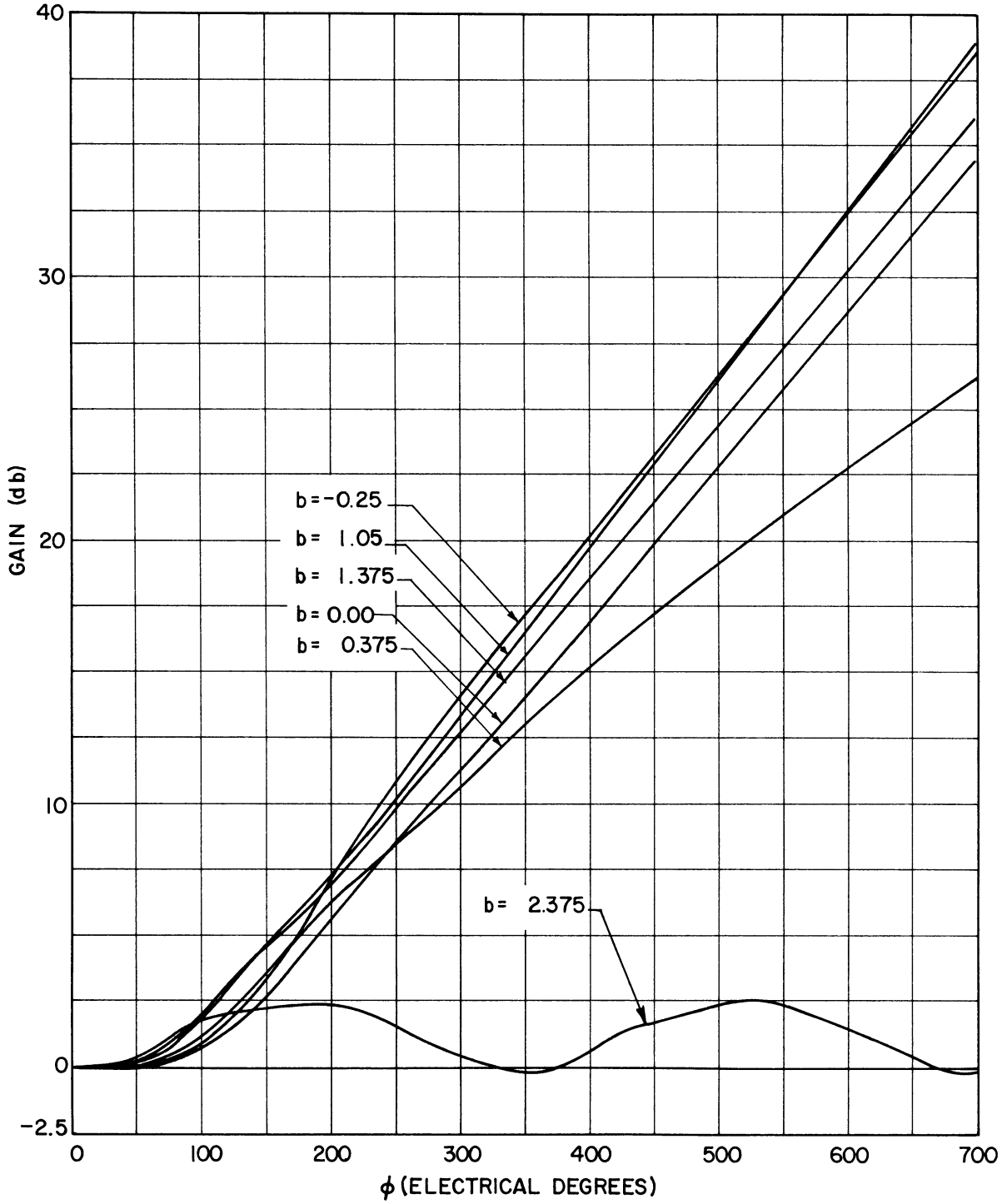

Fig. F. 13 $\beta_e = 50$, C = 0.05, d = 0, Q = -5.0

APPENDIX G

THE BACKWARD-WAVE INCREMENTAL PROPAGATION CONSTANTS OF THE E-TYPE DEVICE

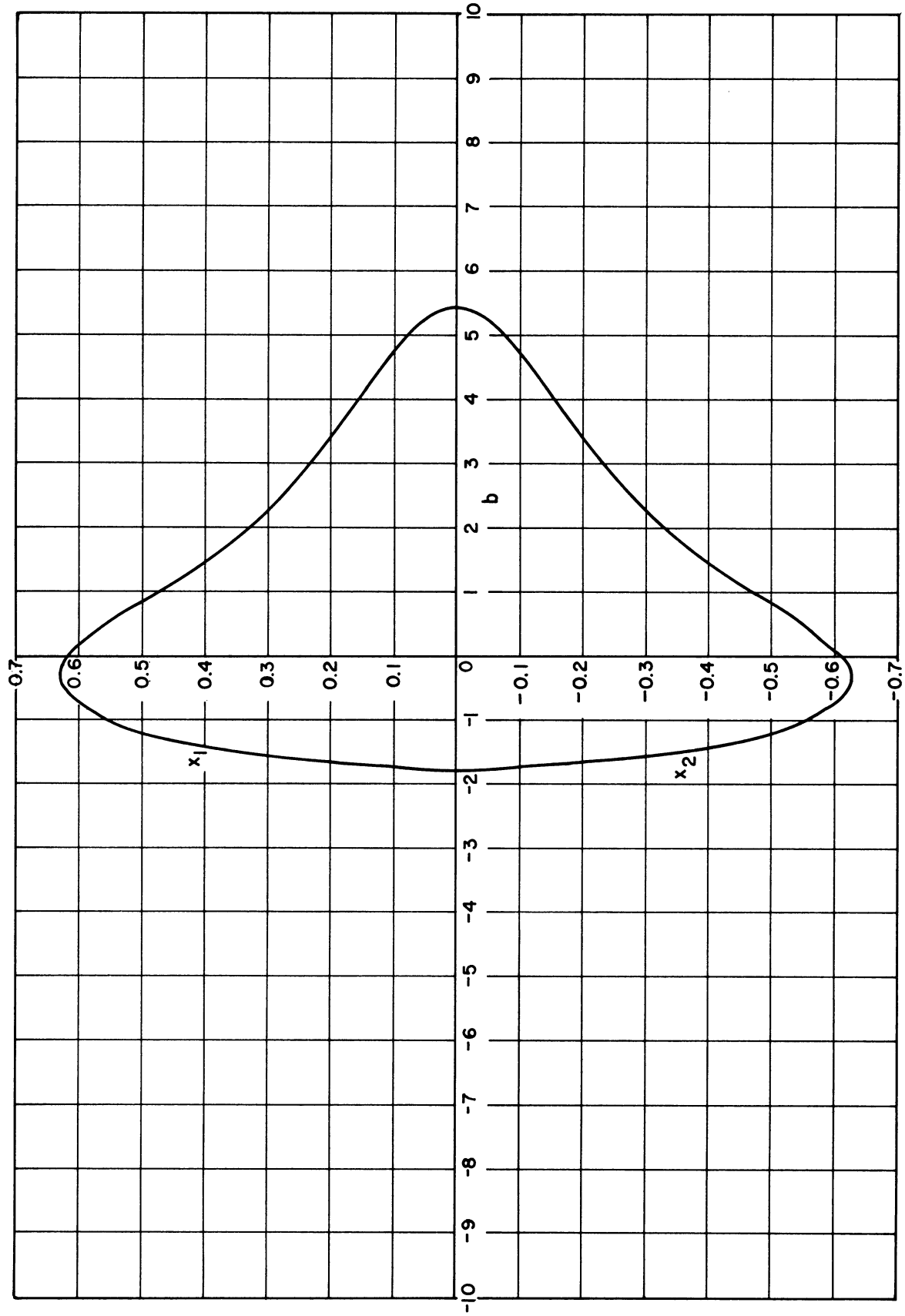

Fig. G.1 $\beta_e = 50$, $C = 0.05$, $d = 0$, $Q = 0$

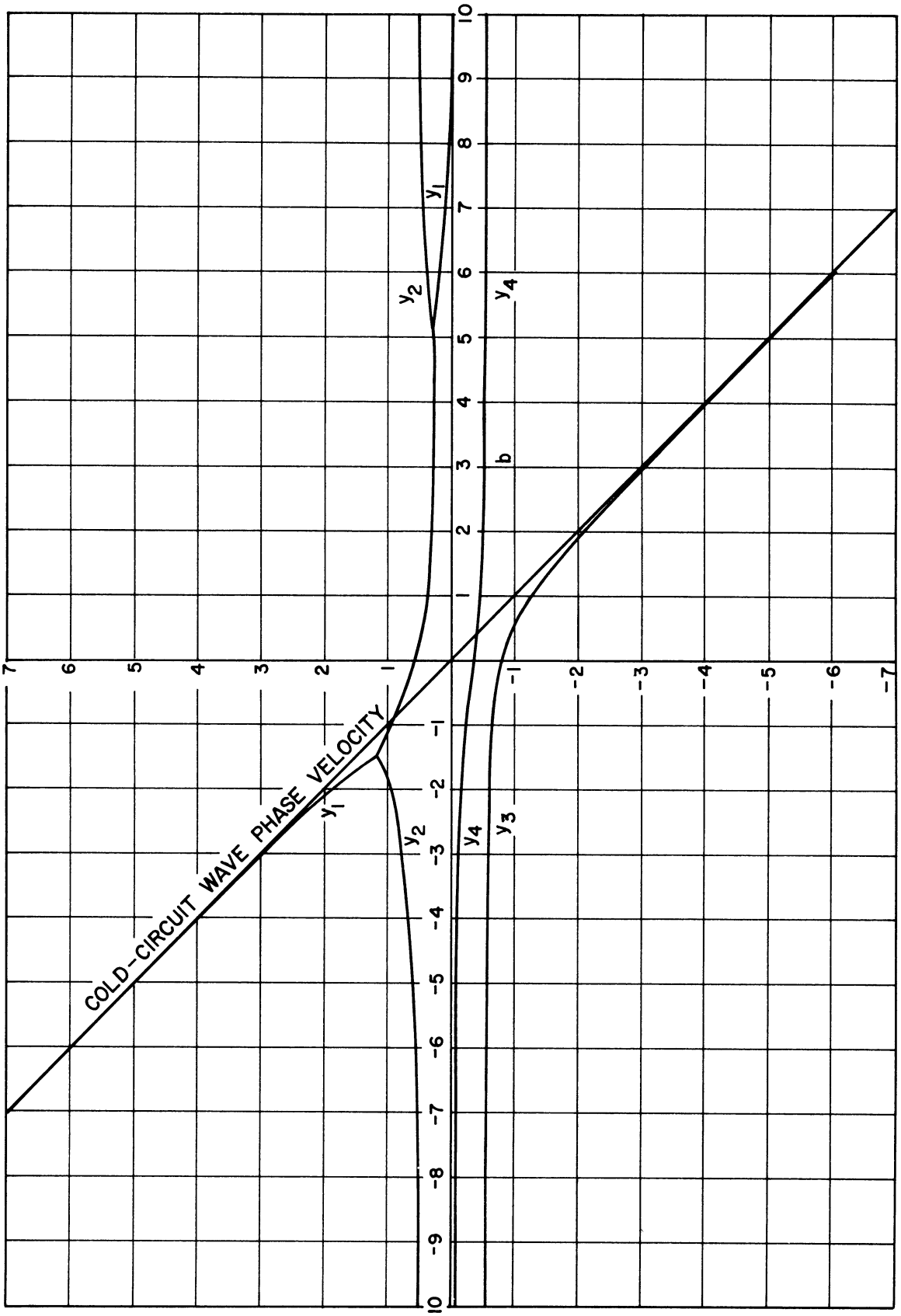

Fig. G. 2 $\beta_e = 50$, C = 0.05, d = 0, Q = 0

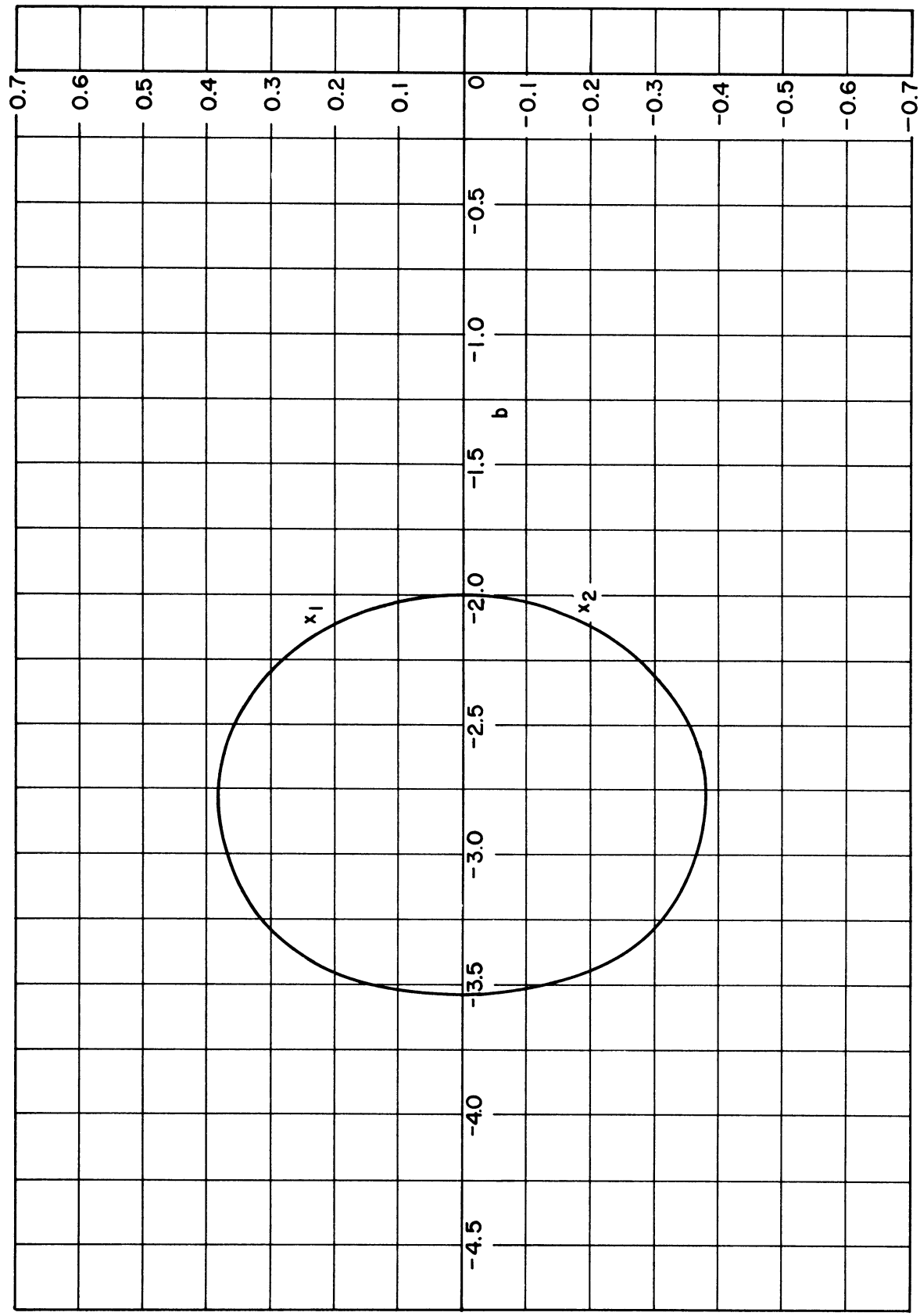

Fig. G.3 $\beta e = 50$, $C = 0.01$, $d = 0$, $Q = 0$

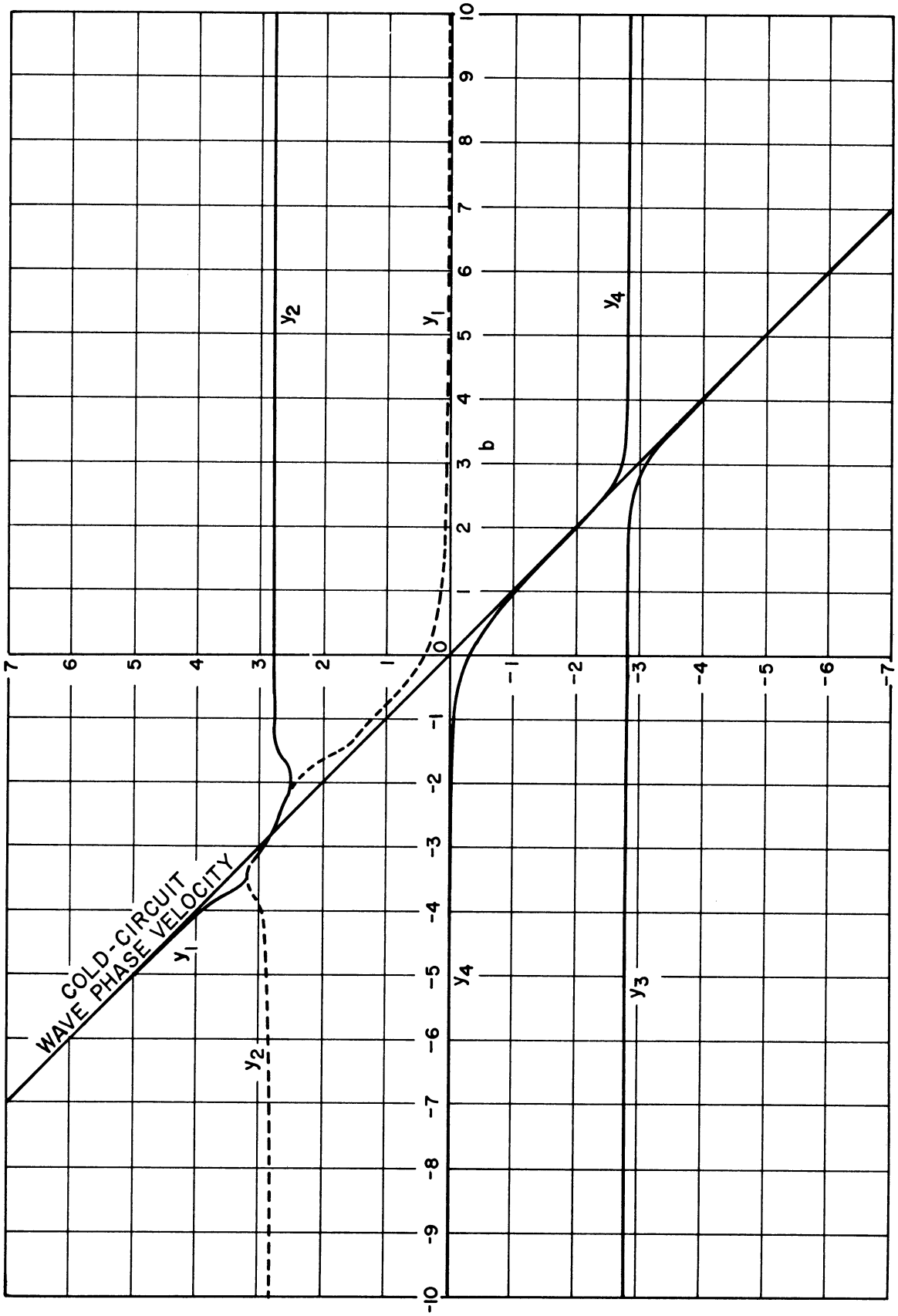

Fig. G.4 $\beta_e = 50$, C = 0.01, d = 0, Q = 0

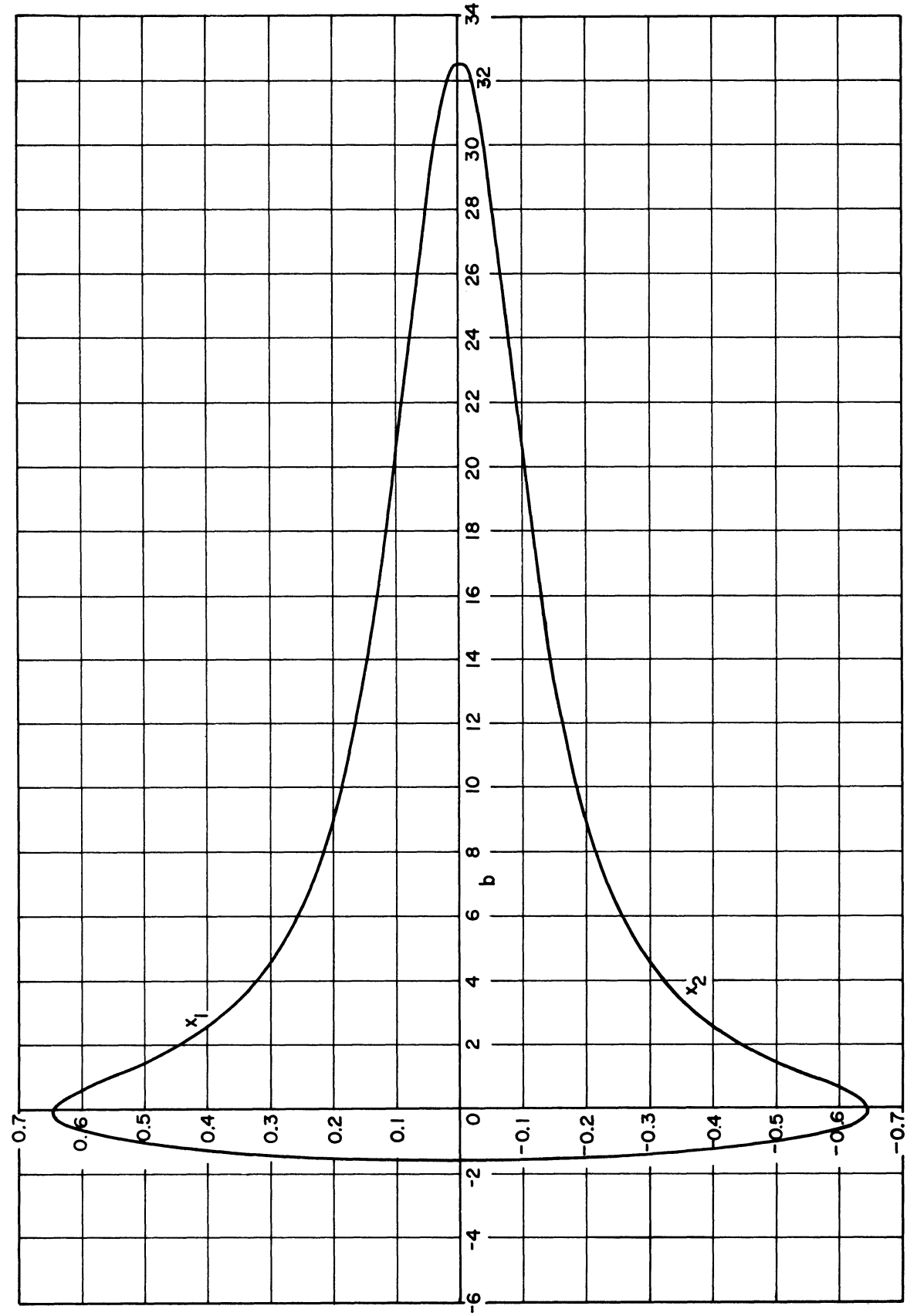

Fig. G.5 $\beta e = 50$, $C = 0.10$, $d = 0$, $Q = 0$

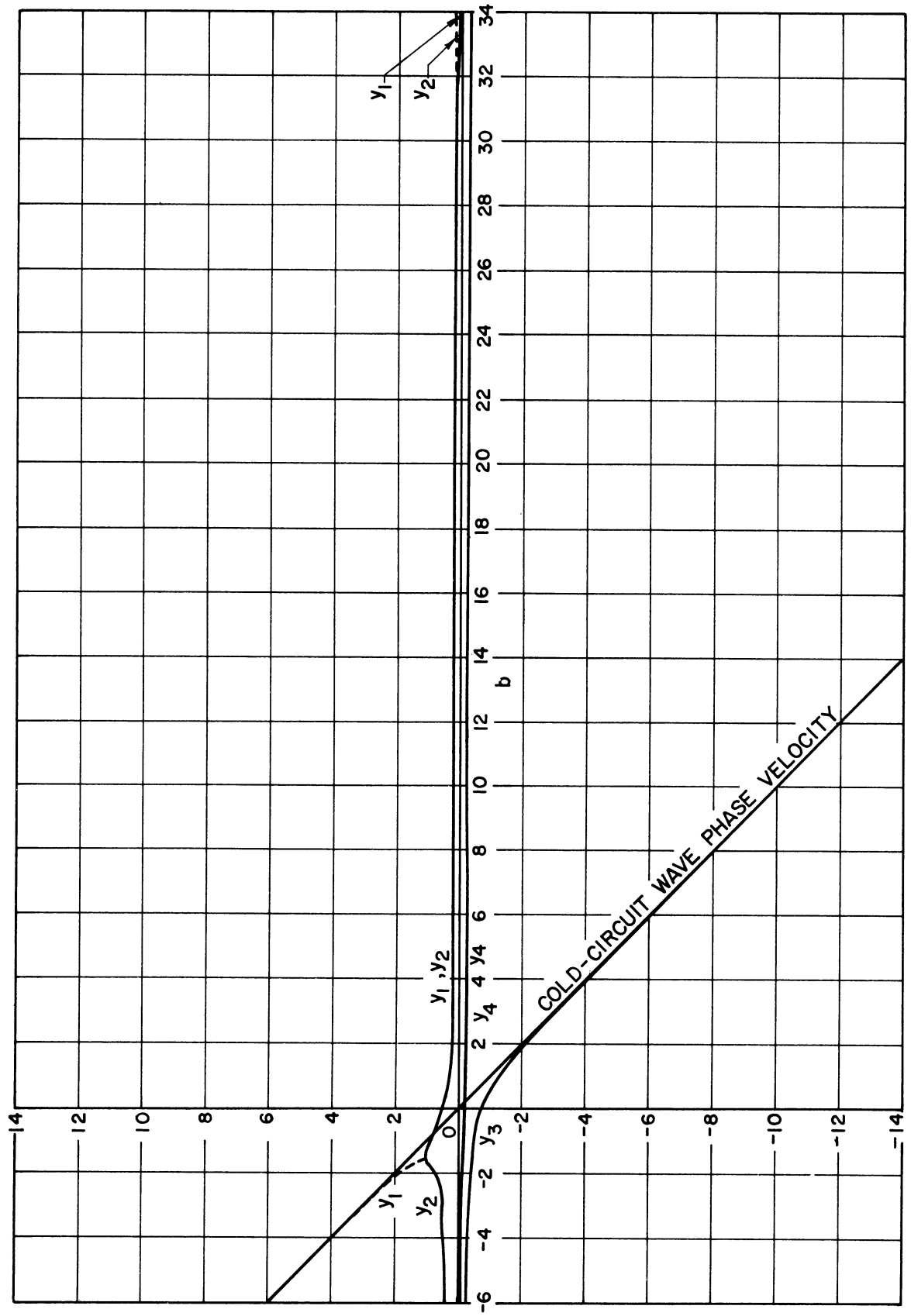

Fig. G.6 $\beta_e = 50$, C = 0.10, d = 0, Q = 0

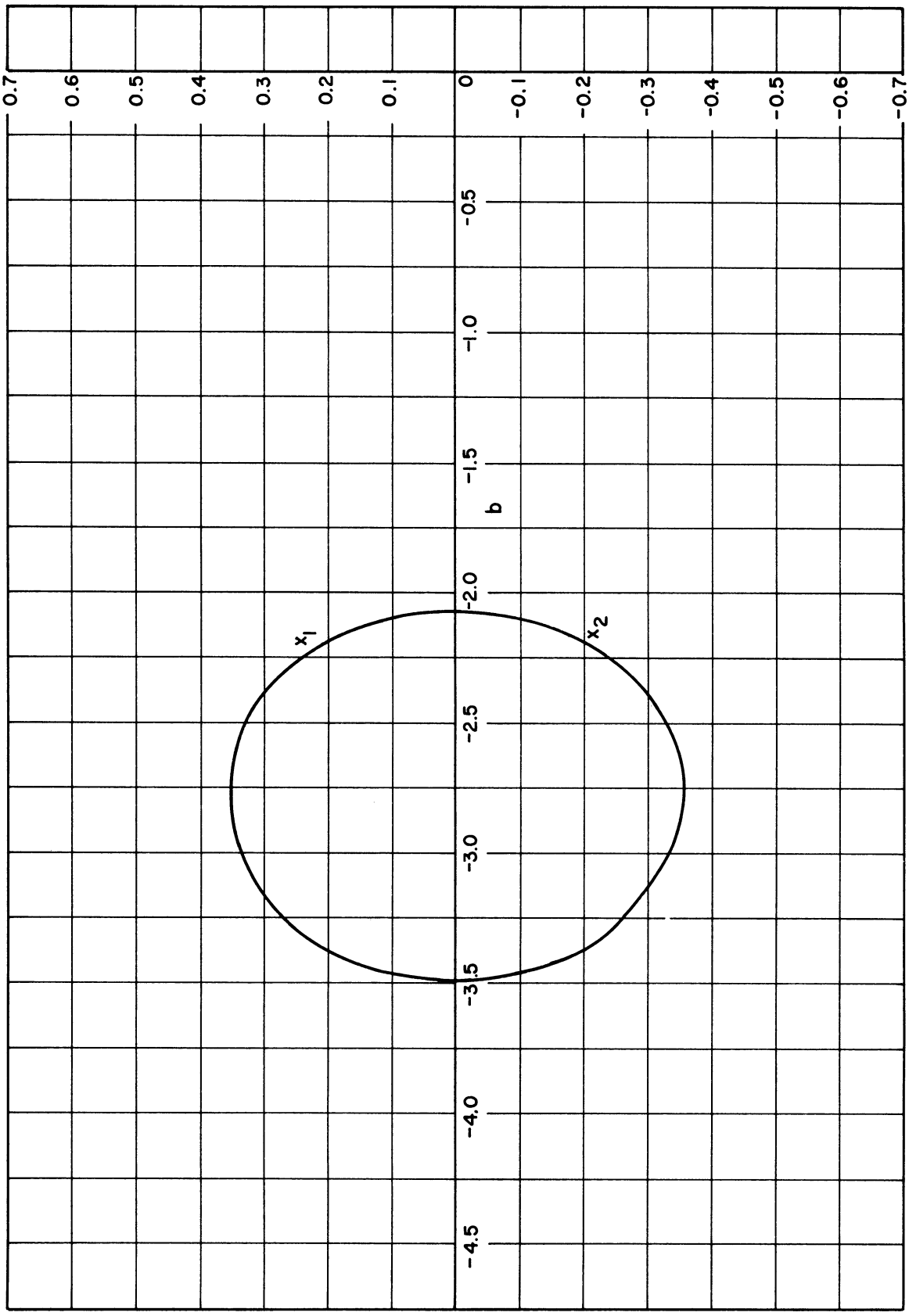

Fig. G.7 $\beta_e = 10$, $C = 0.05$, $d = 0$, $Q = 0$

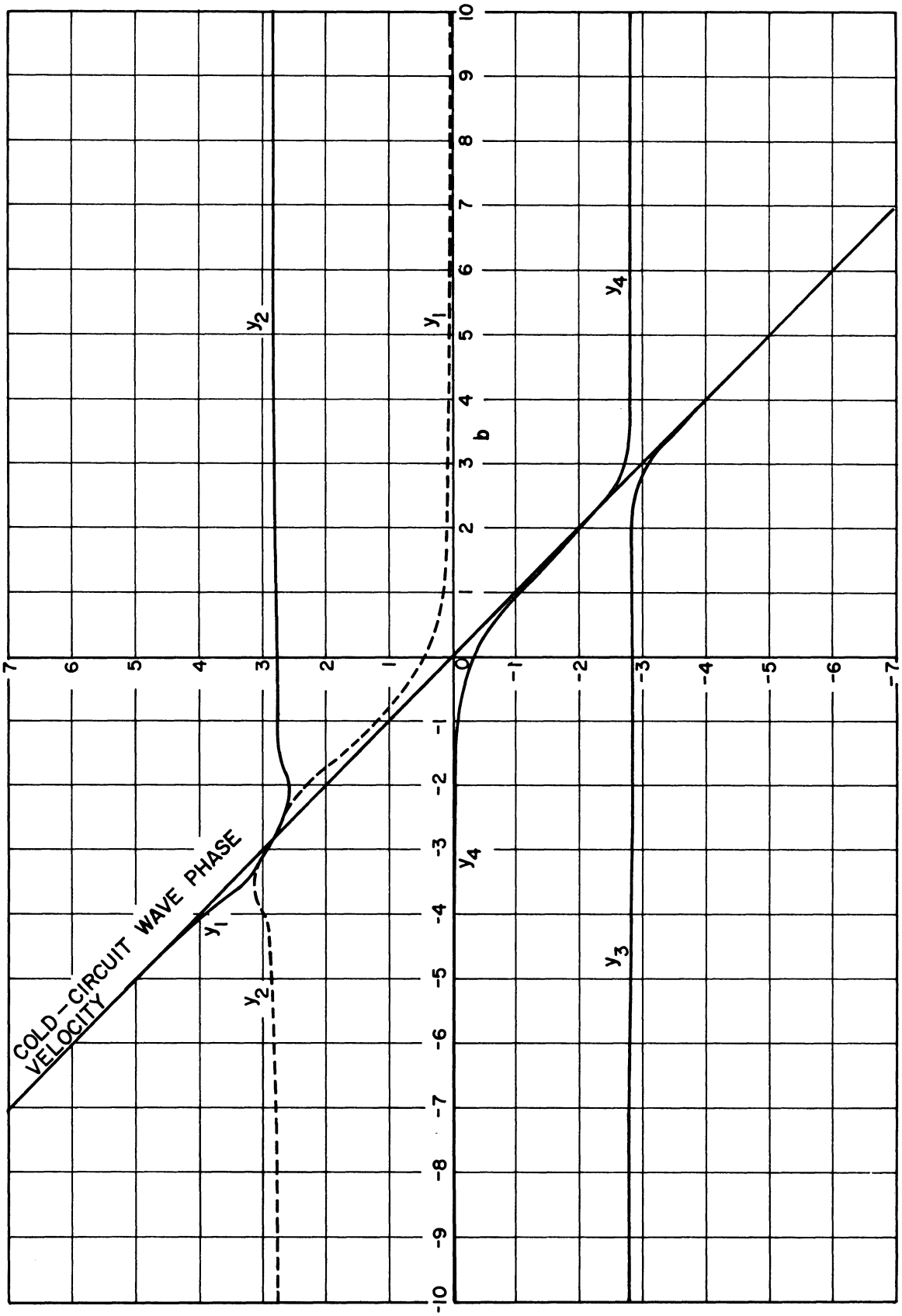

Fig. G.8 $\beta_e = 10$, C=0.05, d=0, Q=0

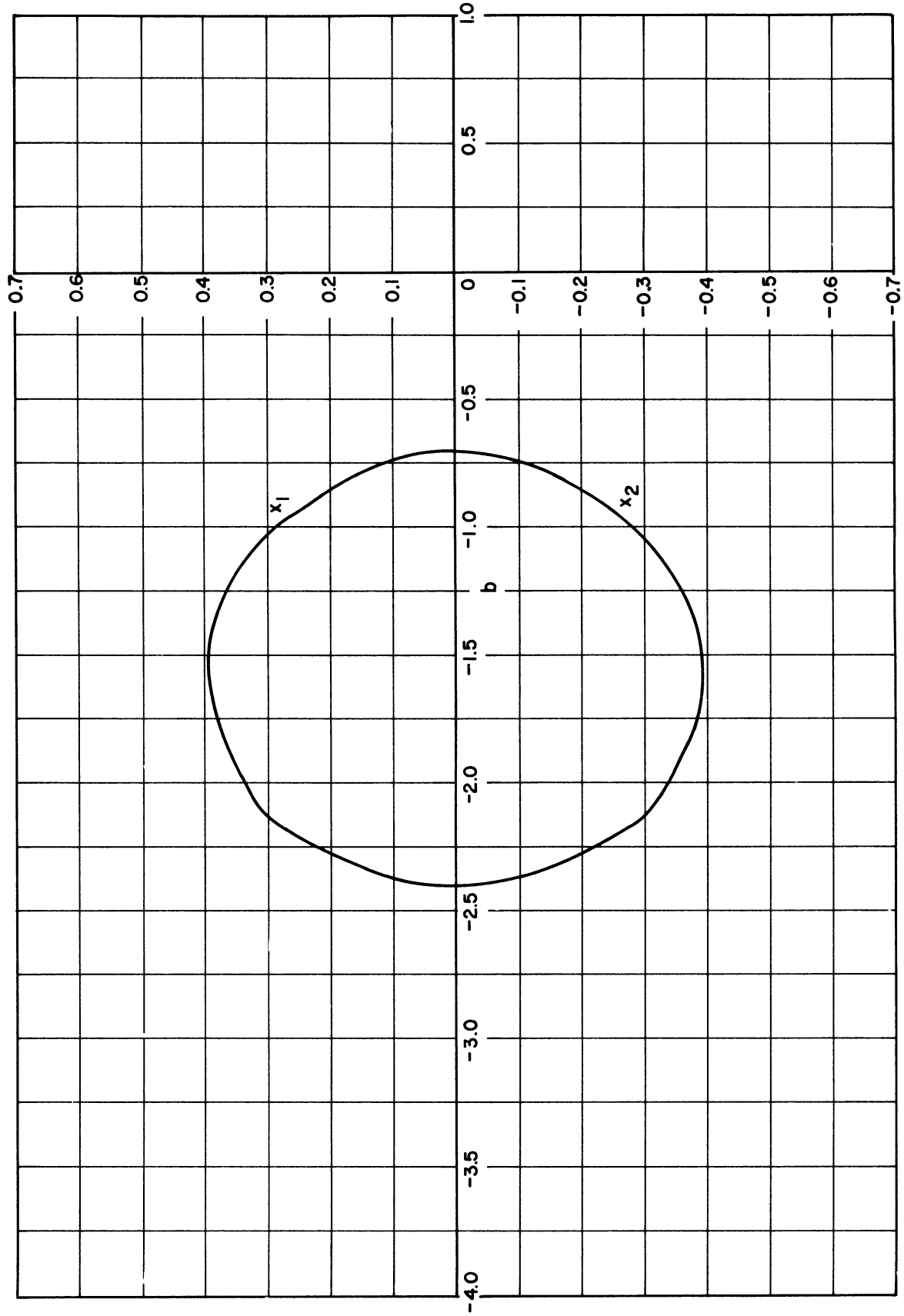

Fig. G.9 $\beta_e = 50$, C=0.05, d=0, Q=-15

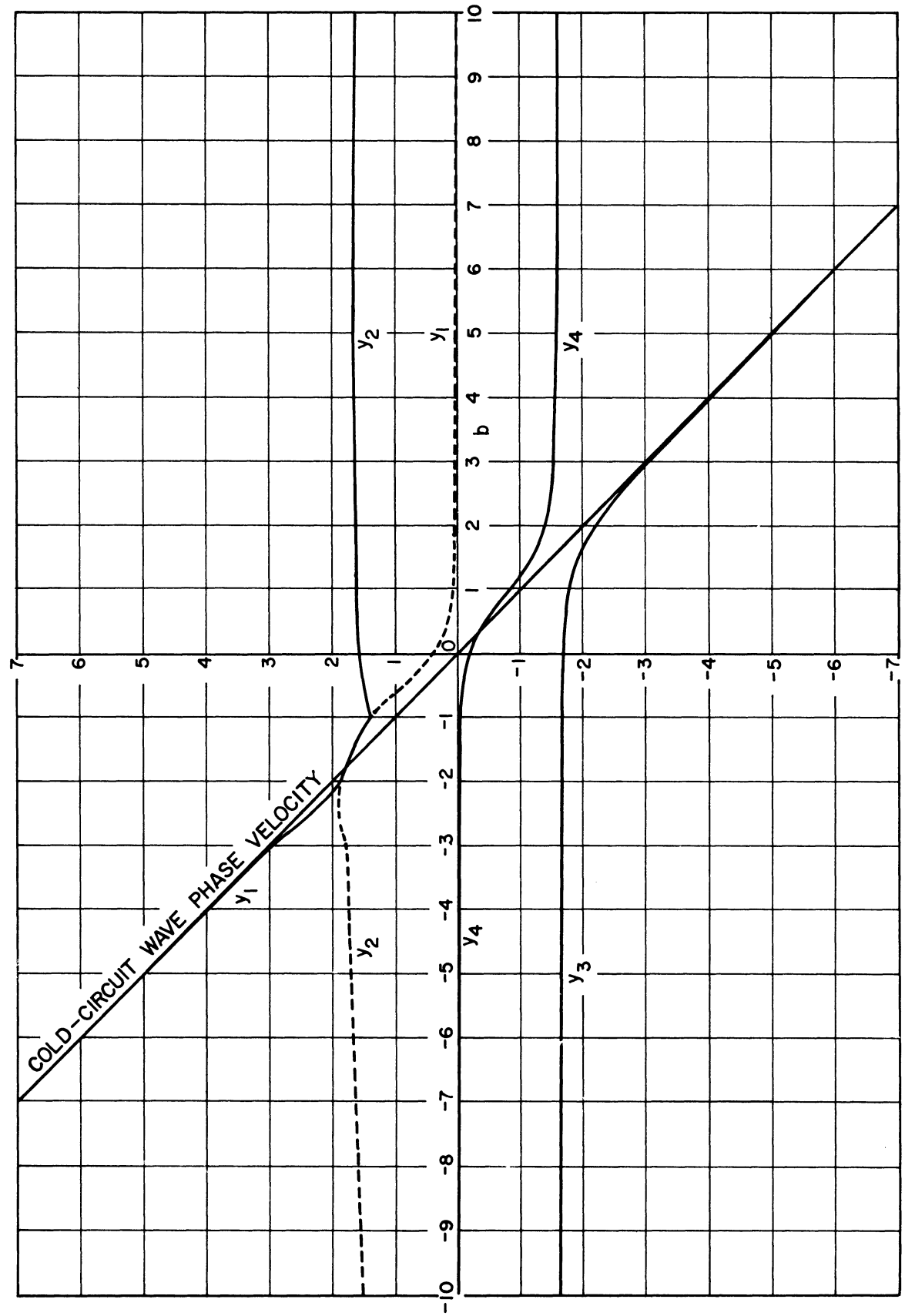

Fig. G.10 $\beta_e = 50$, C=0.05, d=0, Q=-15

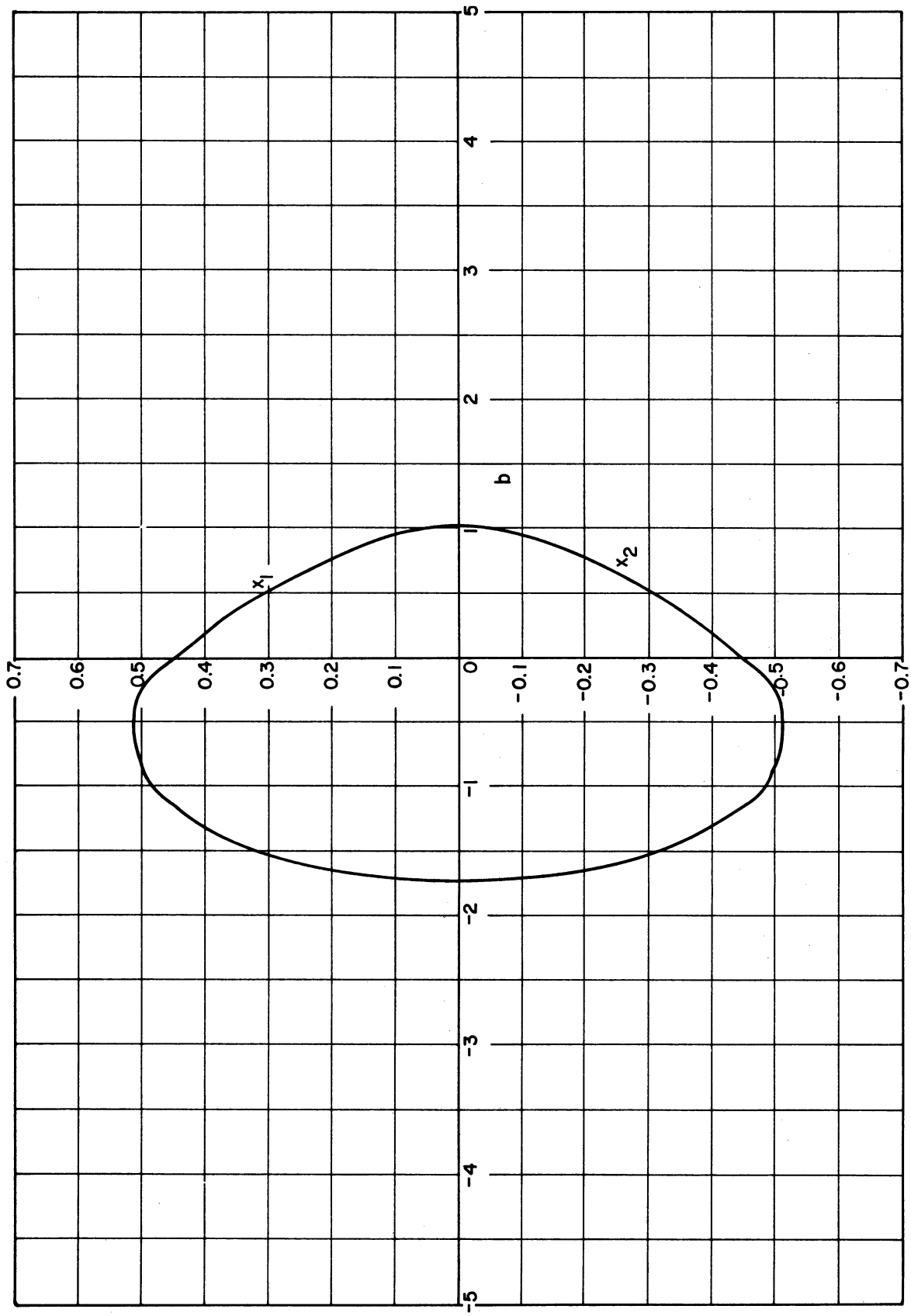

Fig. G.11 $\beta e = 50$, $C = 0.10$, $d = 0$, $Q = -15$

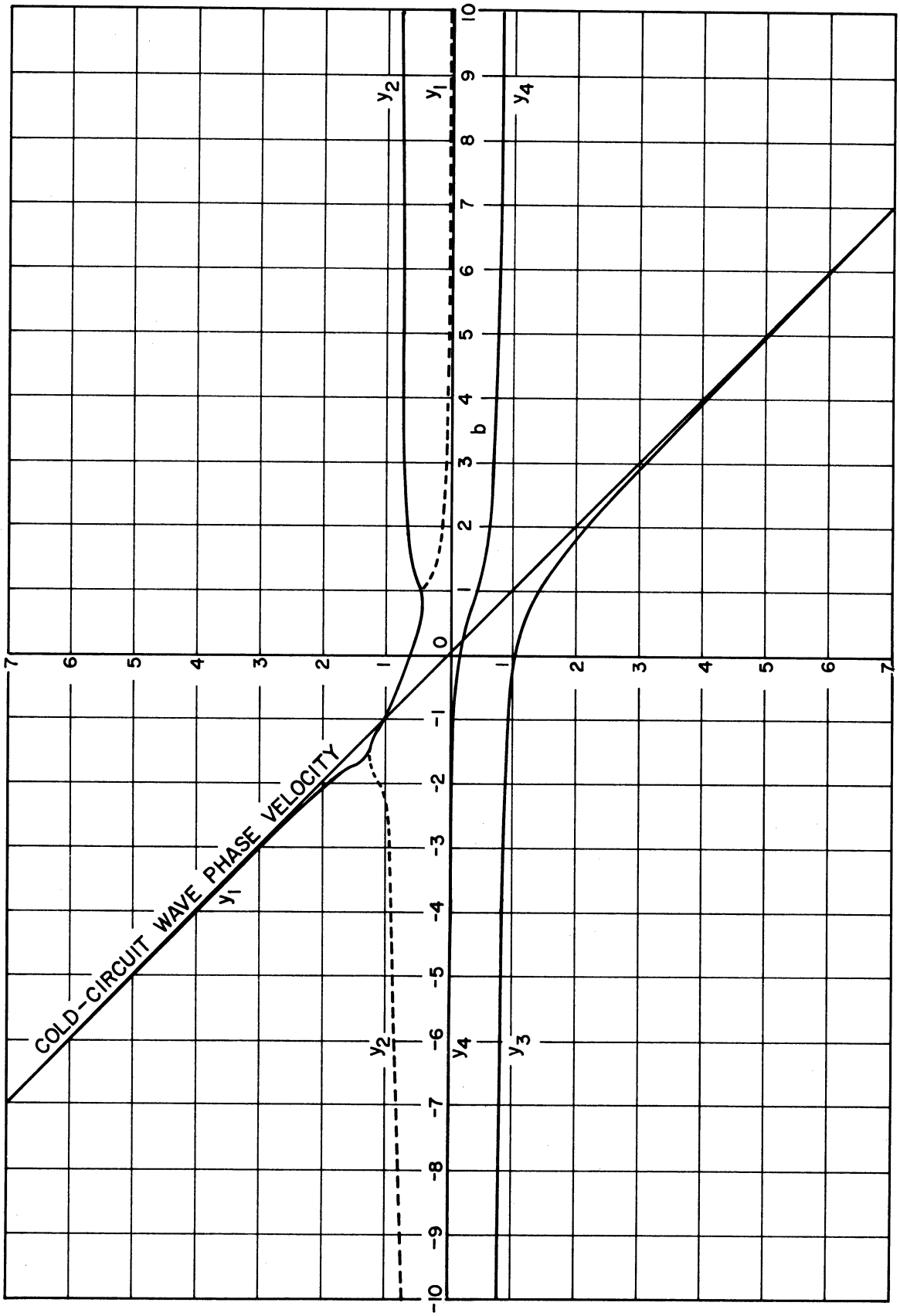

Fig. 6.12 $\beta_e = 50$, C = 0.10, d = 0, Q = -15

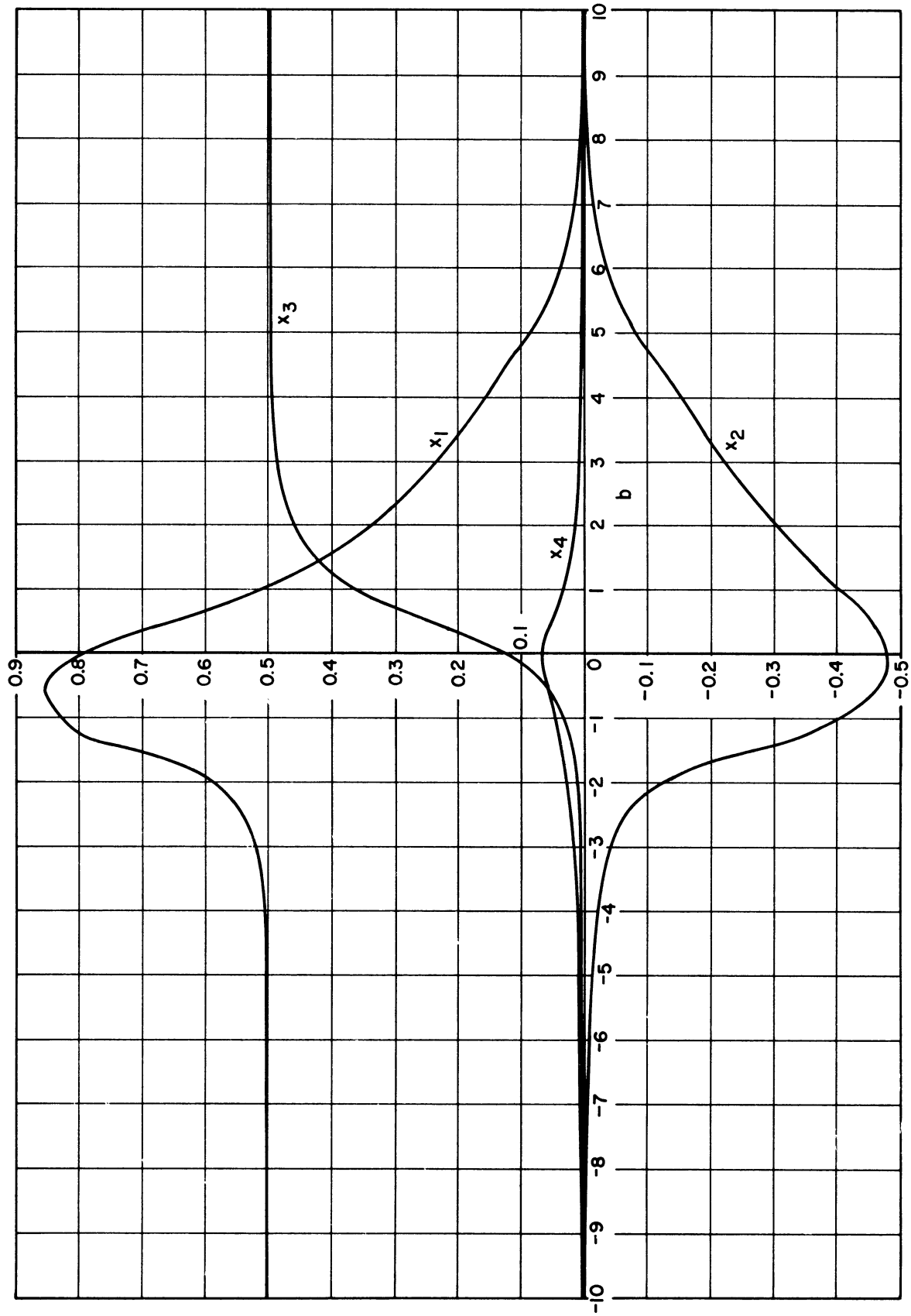

Fig. G. 13 $\beta_e = 50$, C = 0.05, d = 0.5, Q = 0

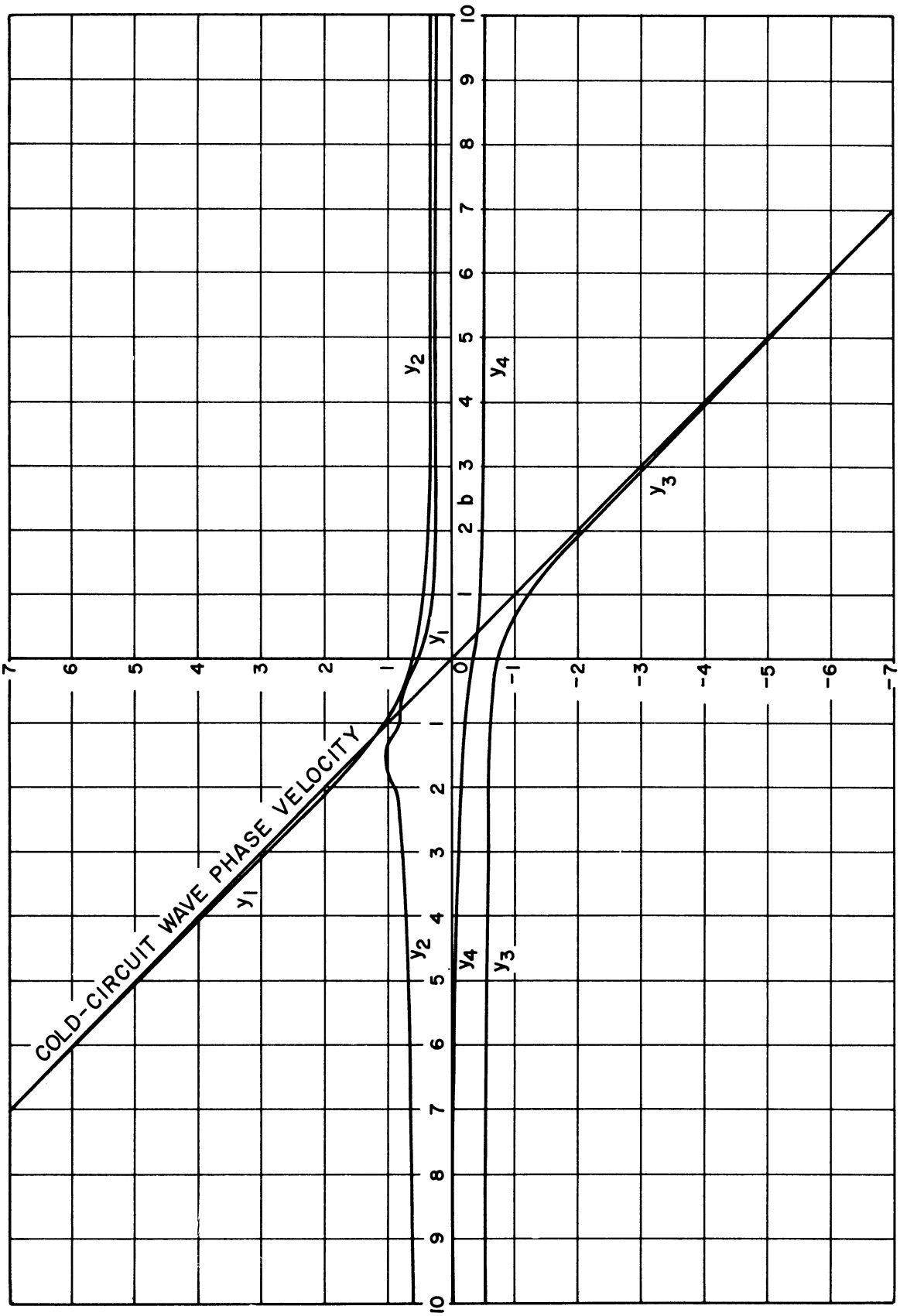

Fig. G. 14 $\beta e = 50$, C=0.05, d=0.5, Q=0

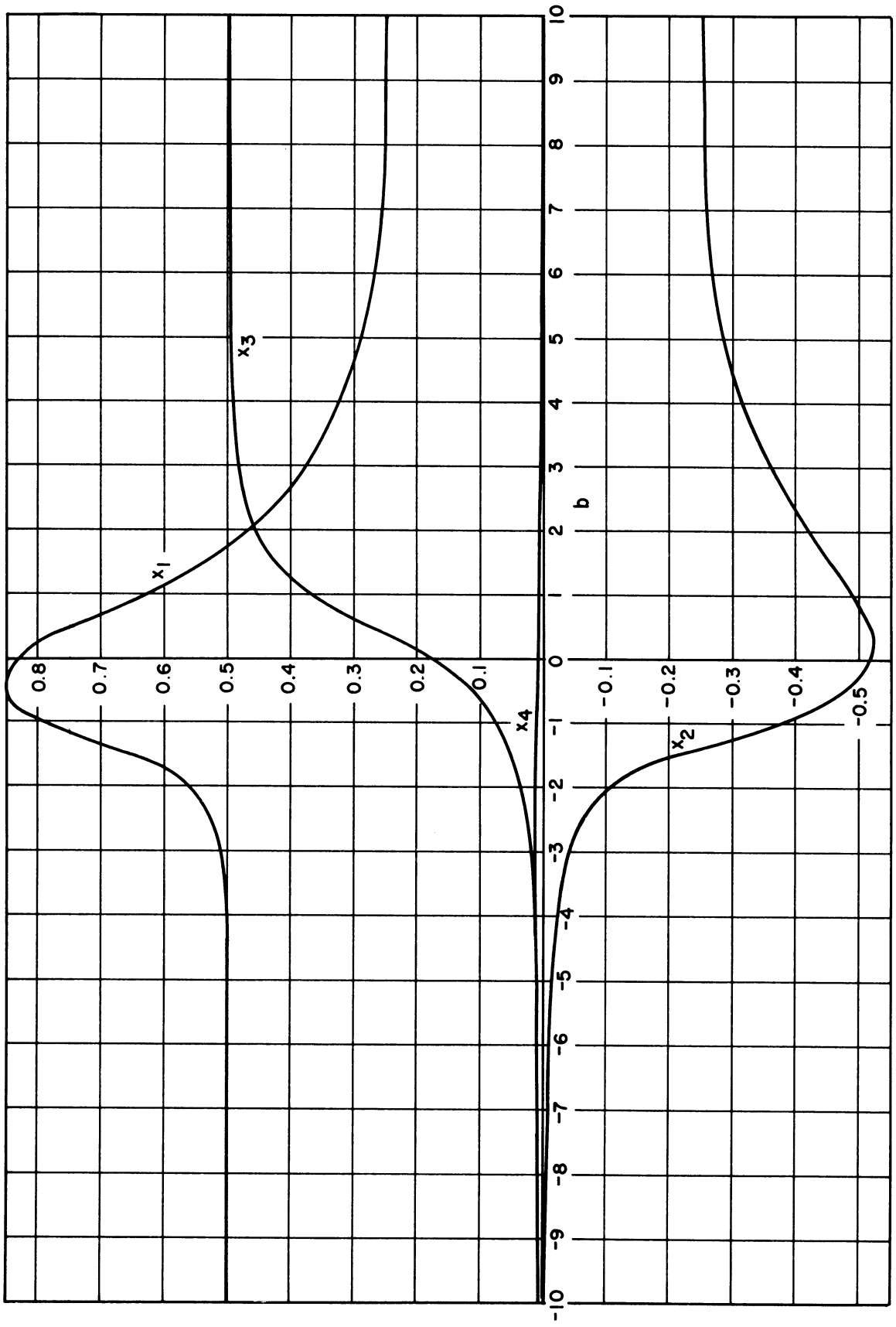

Fig. G.15 β_e=50, C=0.1, d=0.5, Q=0

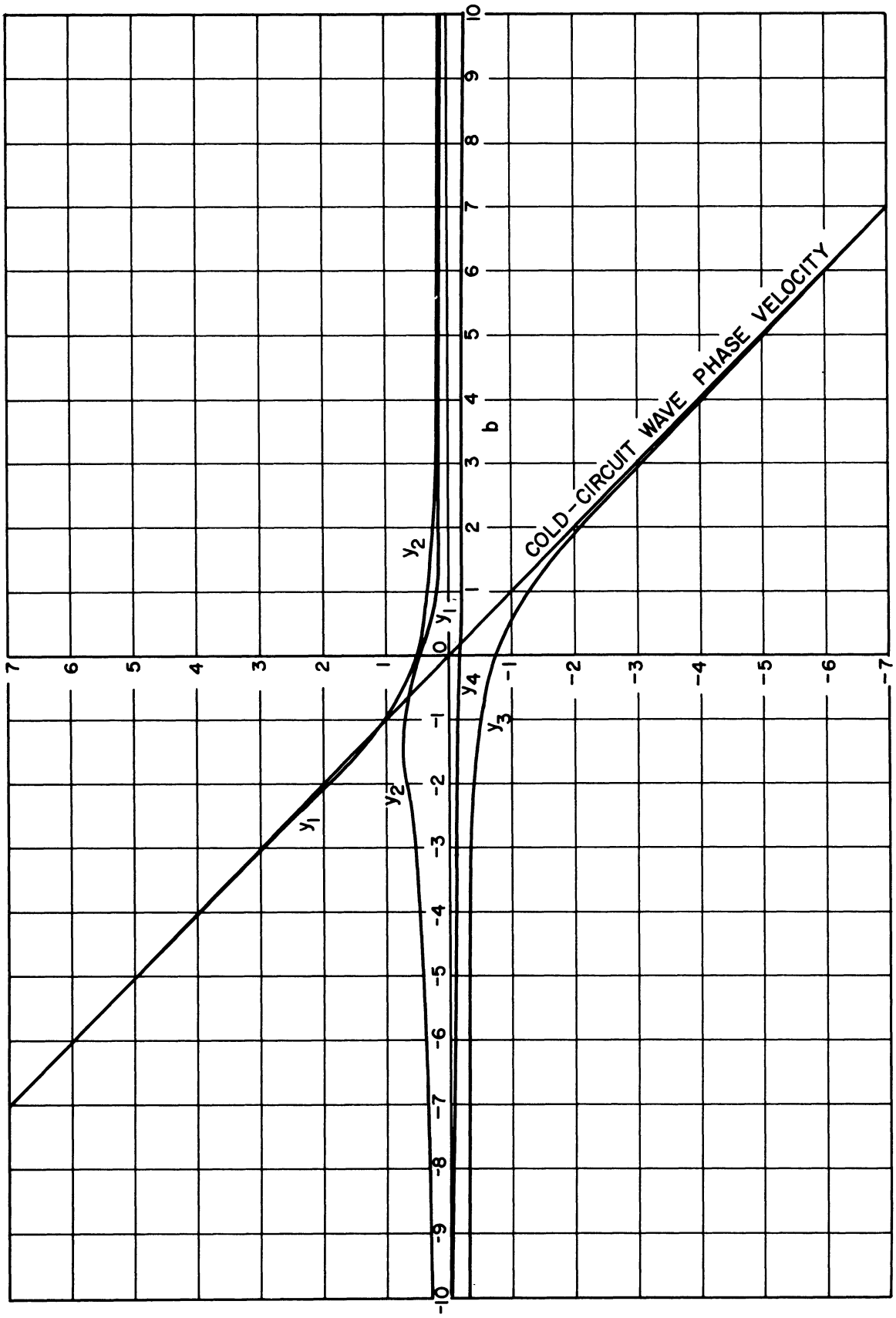

Fig. G.16 $\beta e = 50$, $C = 0.1$, $d = 0.5$, $Q = 0$

APPENDIX H

THE START-OSCILLATION CHARACTERISTICS OF THE E-TYPE DEVICE

Table H.1 The Start-Oscillation Characteristics of the E-Type Device

$\beta_e = 50$ Q = 0 d = 0

C	b at osc	Φ(radians) at osc	$\delta_1 = x_1 + jy_1$	$\delta_2 = x_2 + jy_2$	$\delta_3 = x_3 + jy_3$	$\delta_4 = x_4 + jy_4$
0.01	0.074121458	4.288002	0+j0.3577685	0+j2.7752945	0-j2.8379883	0-j0.3692091
0.05	0.968852	2.4778982	0.47365946 +j0.378388	-0.47365946 +j0.378388	0-j1.2697031	0-j0.45626242
0.10	1.0486882	2.3693846	0.5518693 +j0.26254803	-0.5518693 +j0.26254804	0-j1.3603228	0-j0.2148807

C = 0.05 Q = 0 d = 0

β_e						
10	0.076794875	4.0167567	0+j0.38132517	0+j2.7795098	0-j2.8383456	0-j0.39964991
25	0.69438533	2.6857529	0+j0.62672117	0+j0.71884874	0-j1.2759887	0-j0.76430979
50	0.968852	2.4778982	0.47365946 +j0.378388	-0.47365946 +j0.378388	0-j1.2697031	0-j0.45626242

$\beta_e = 50$ C = 0.05 d = 0

Q						
0	0.968852	2.4778982	0.47365946 +j0.378388	-0.47365946 +j0.378388	0-j1.2697031	0-j0.45626242
-5	1.3167581	11.156832	0+j0.17453361	0+j0.90197626	0-j1.6131906	0-j0.78039175

$\beta_e = 50$ $\quad$ C = 0.05 $\quad$ Q = 0

d	b at osc	Φ(radians) at osc	$\delta_1 = x_1 + jy_1$	$\delta_2 = x_2 + jy_2$	$\delta_3 = x_3 + jy_3$	$\delta_4 = x_4 + jy_4$
0	0.968852	2.4778982	0.47365946 +j0.378388	-0.47365946 +j0.378388	0-j1.2697031	0-j0.45626242
0.5	0.81227385	3.3303739	0.56909303 +j0.29021367	-0.42800931 +j0.46269843	0.32097365 -j1.1116805	0.037950462 -j0.4538404

$\beta_e = 23$ $\quad$ C = 0.06 $\quad$ Q = -2.0 $\quad$ d = 0.0

1.5432049	4.9073023	0+j0.10313917	0+j1.3782161	0-j1.8328602	0-j1.1919929

APPENDIX I

THEORETICAL PREDICTIONS OF THE EXPERIMENTAL SMALL-SIGNAL E-TYPE FORWARD-WAVE AMPLIFIER PROPAGATION CONSTANTS AND GAIN

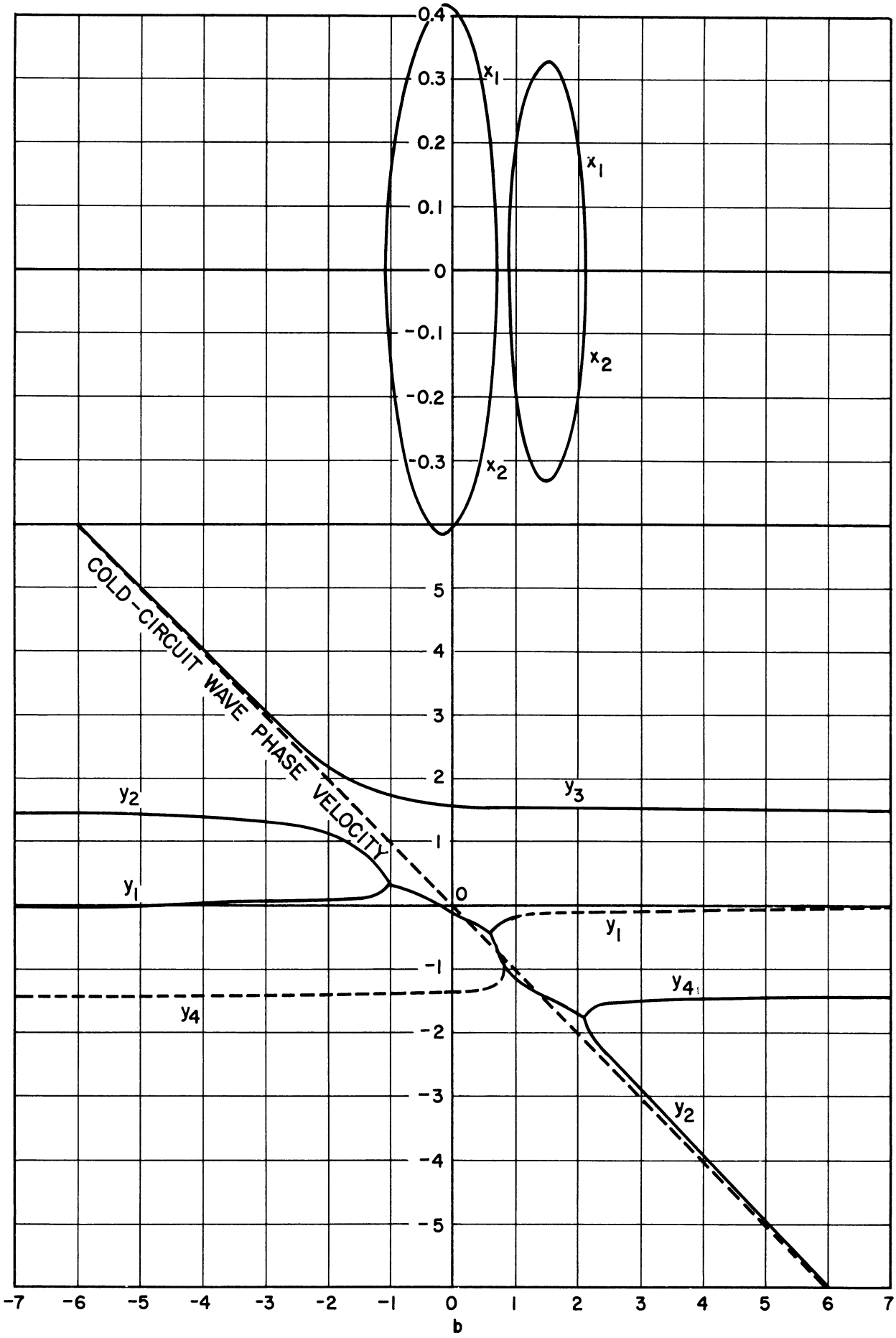

Fig. I. 1 $\beta_e = 23$, C = 0.06, d = 0, Q = -2.0

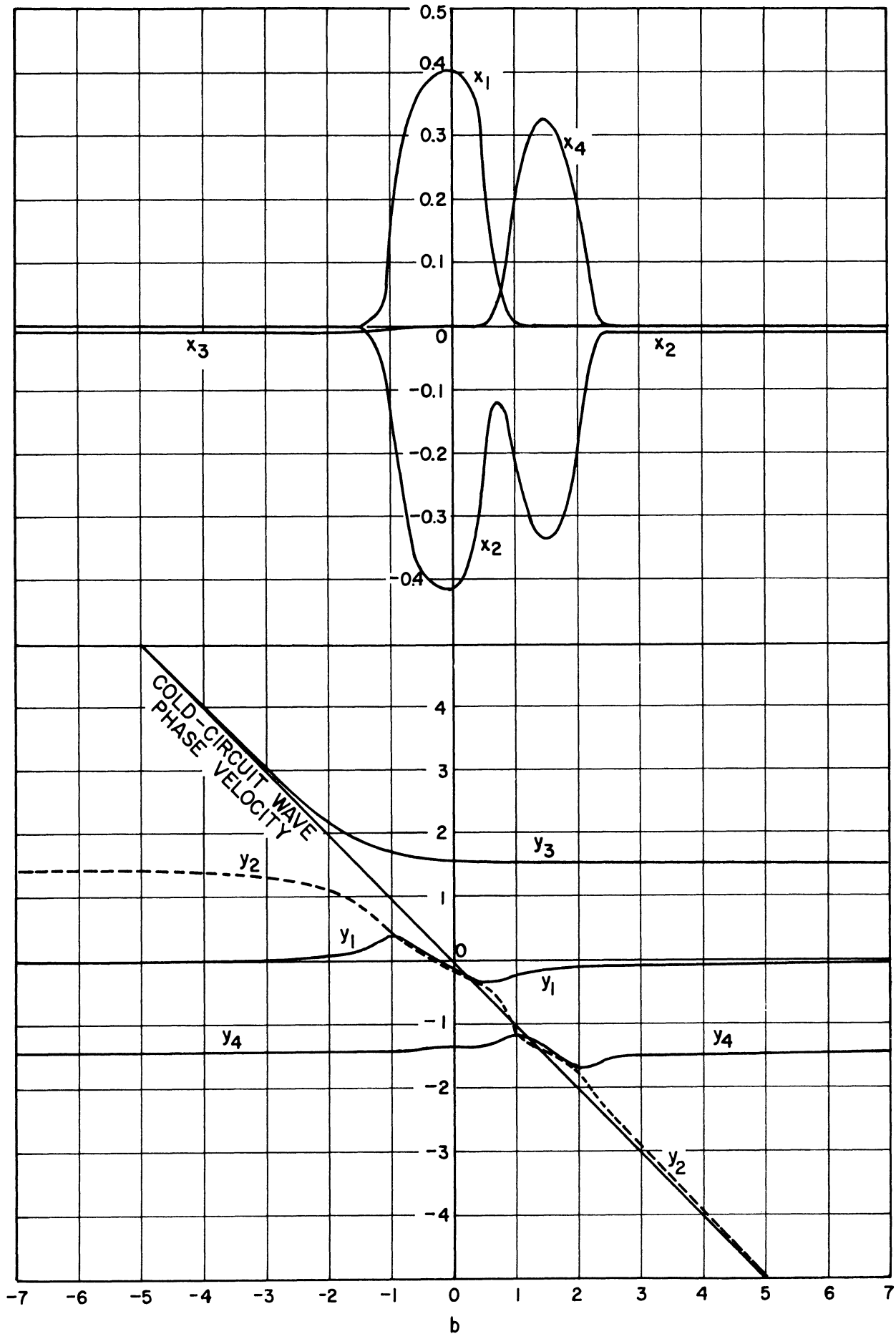

Fig. I.2 $\beta_e = 23$, C = 0.06, d = 0.010, Q = -2.0

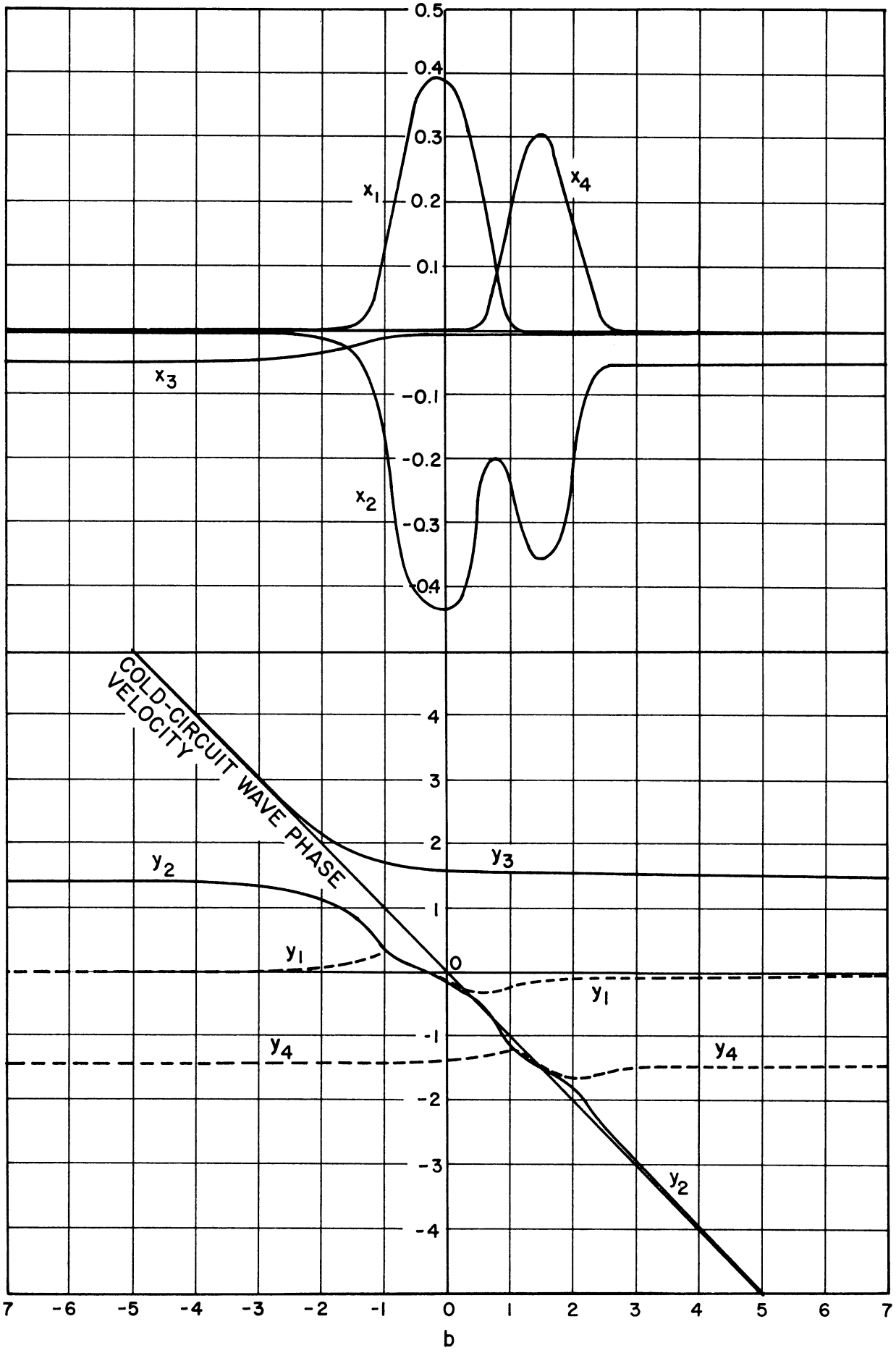

Fig. I.3 $\beta_e = 23$, C = 0.06, d = 0.05, Q = -2.0

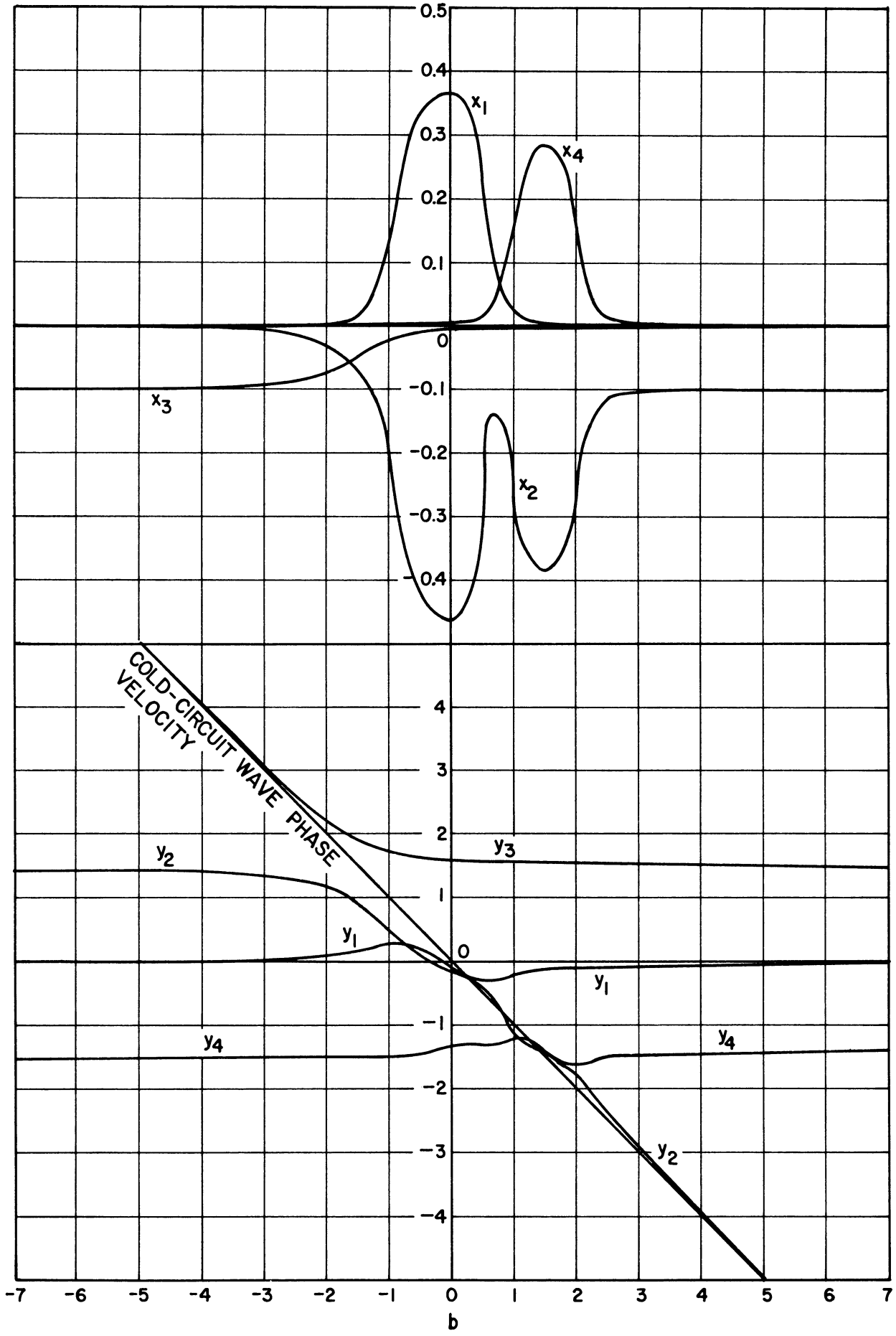

Fig. I.4 $\beta_e = 23$, C = 0.06, d = 0.100, Q = −2.0

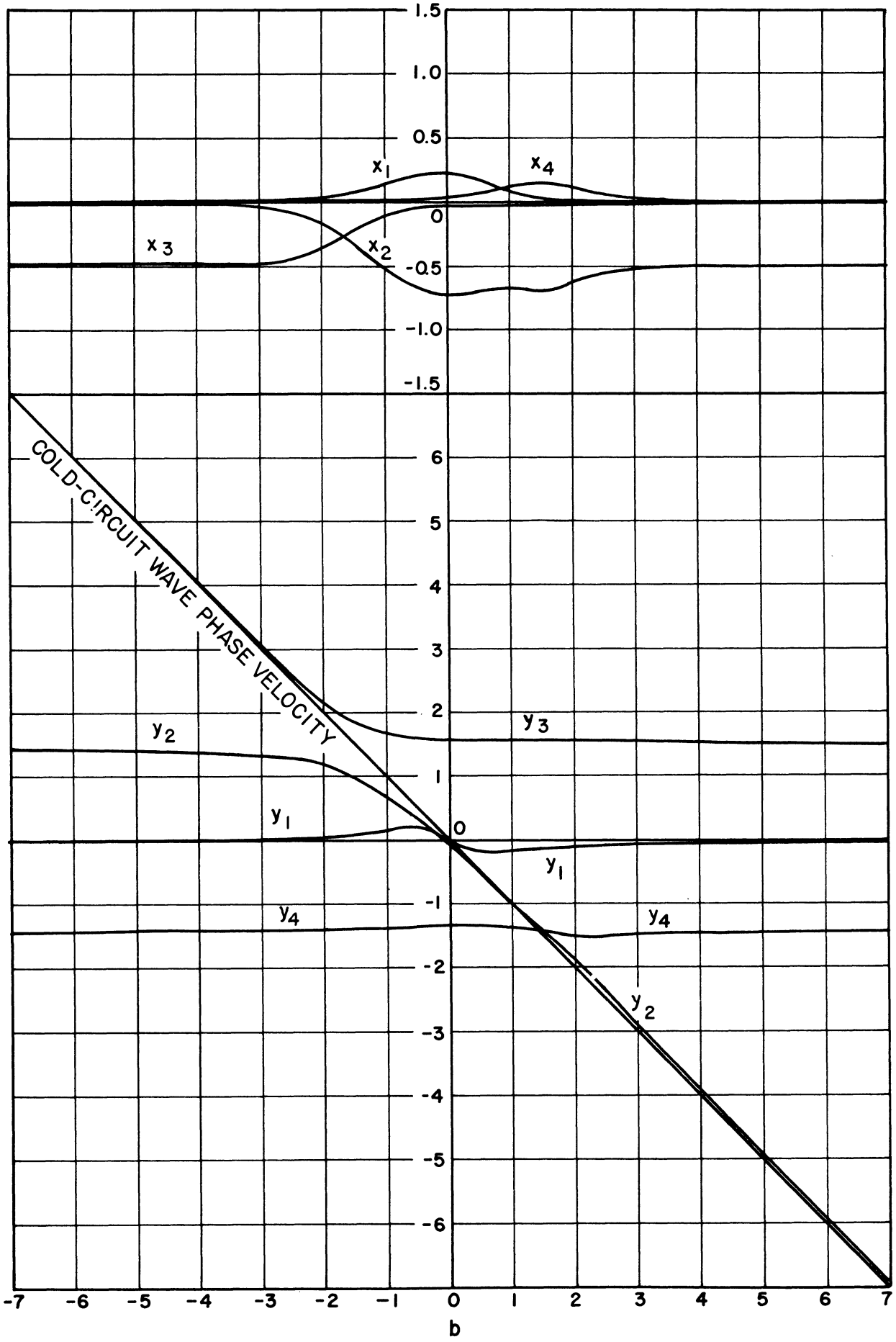

Fig. I. 5 β_e=23, C=0.06, d=0.50, Q=-2.0

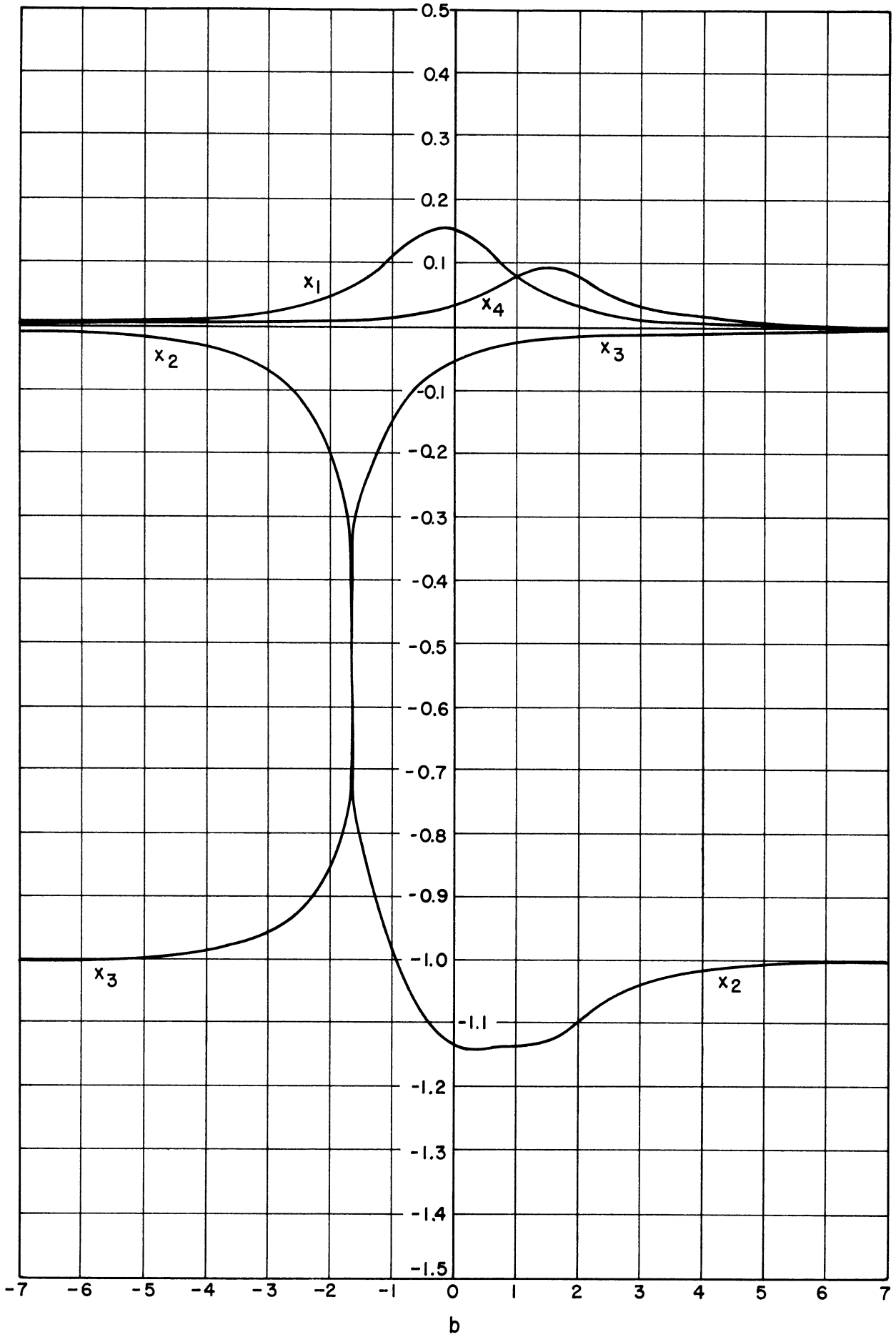

Fig. I. 6 β_e=23, C=0.06, d=1.00, Q=-2.0

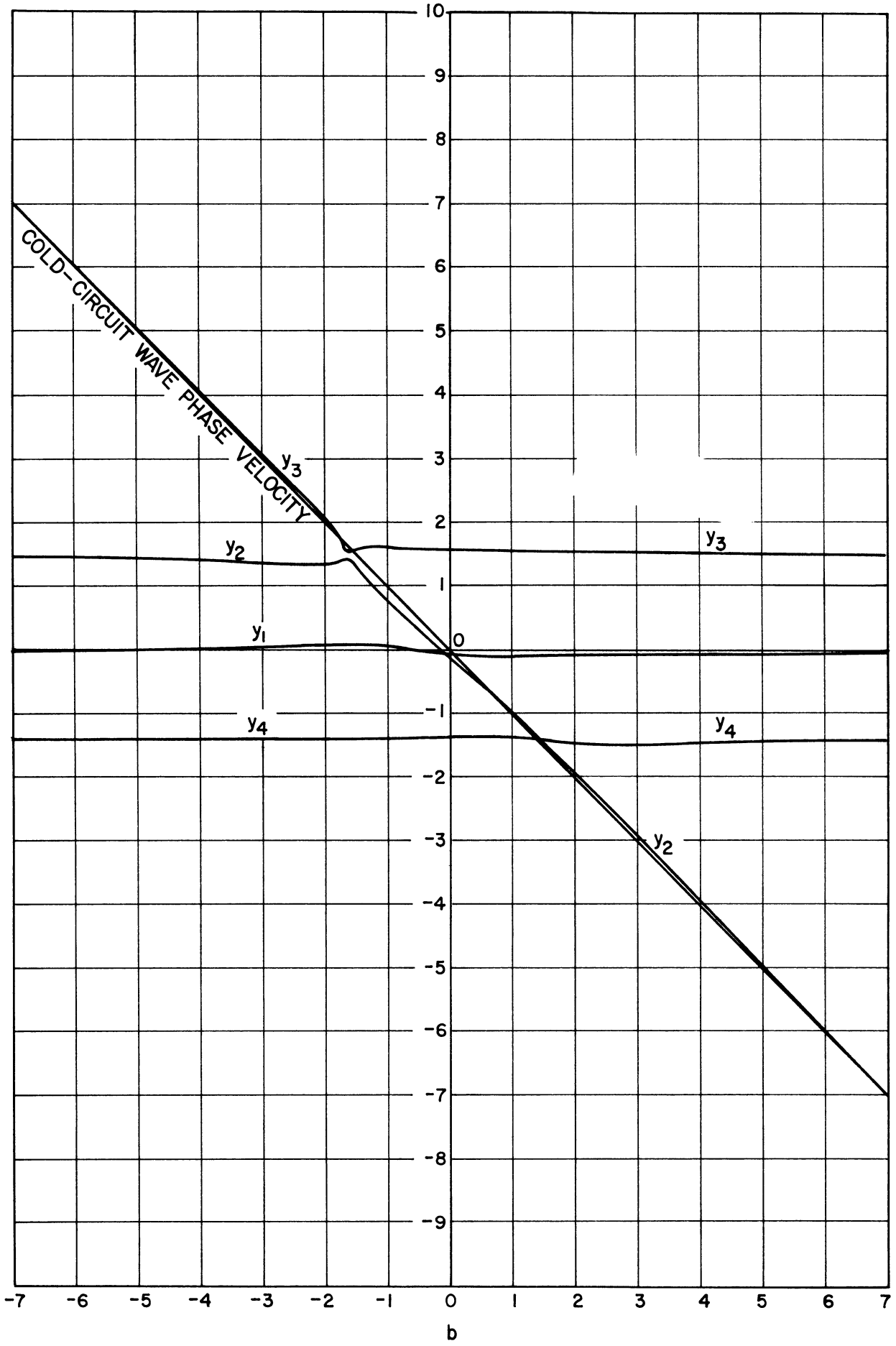

Fig. I.7 $\beta_e = 23$, C = 0.06, d = 1.00, Q = −2.0

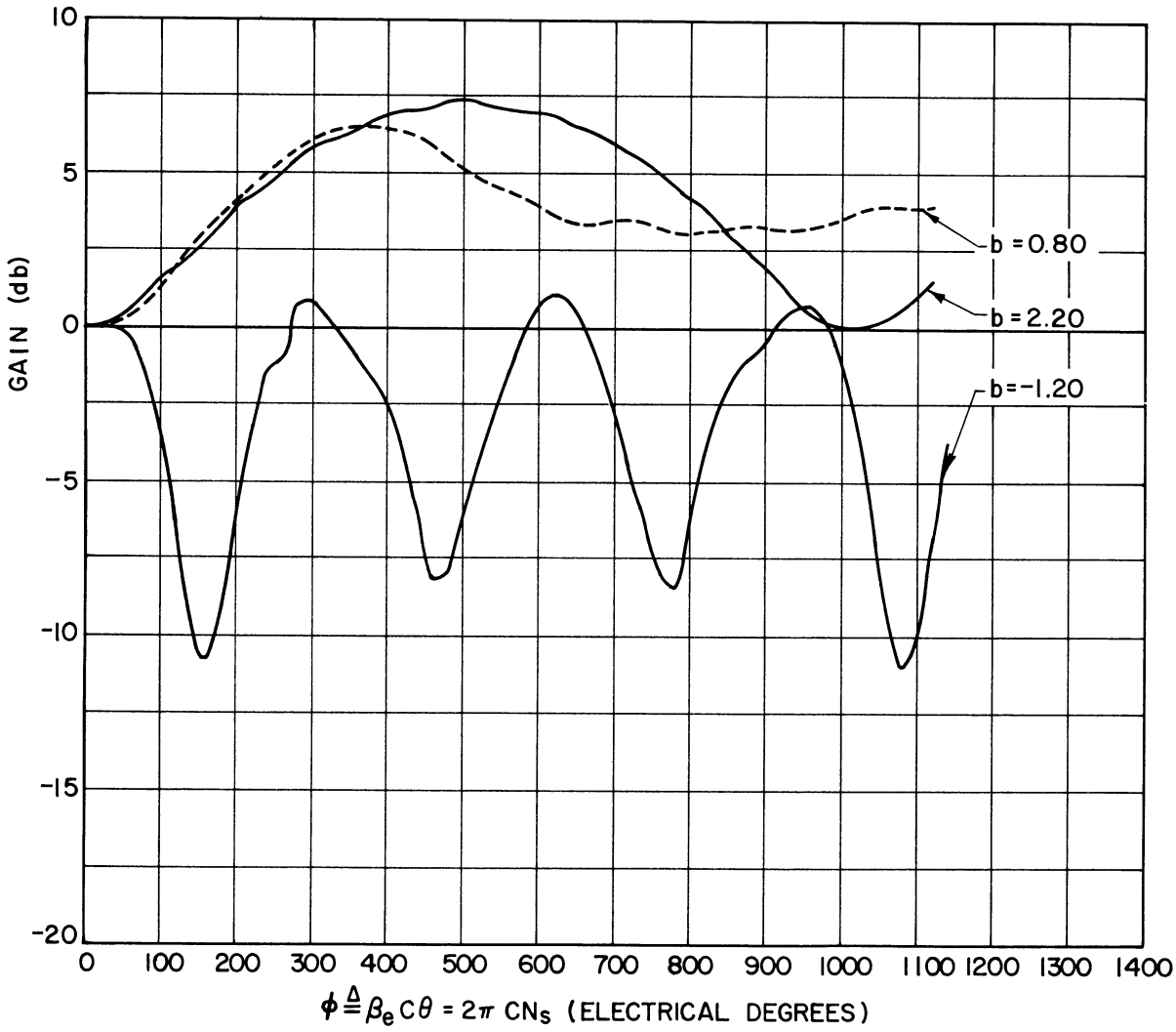

Fig. I.8 $\beta_e = 23$, C = 0.06, d = 0, Q = -2.0

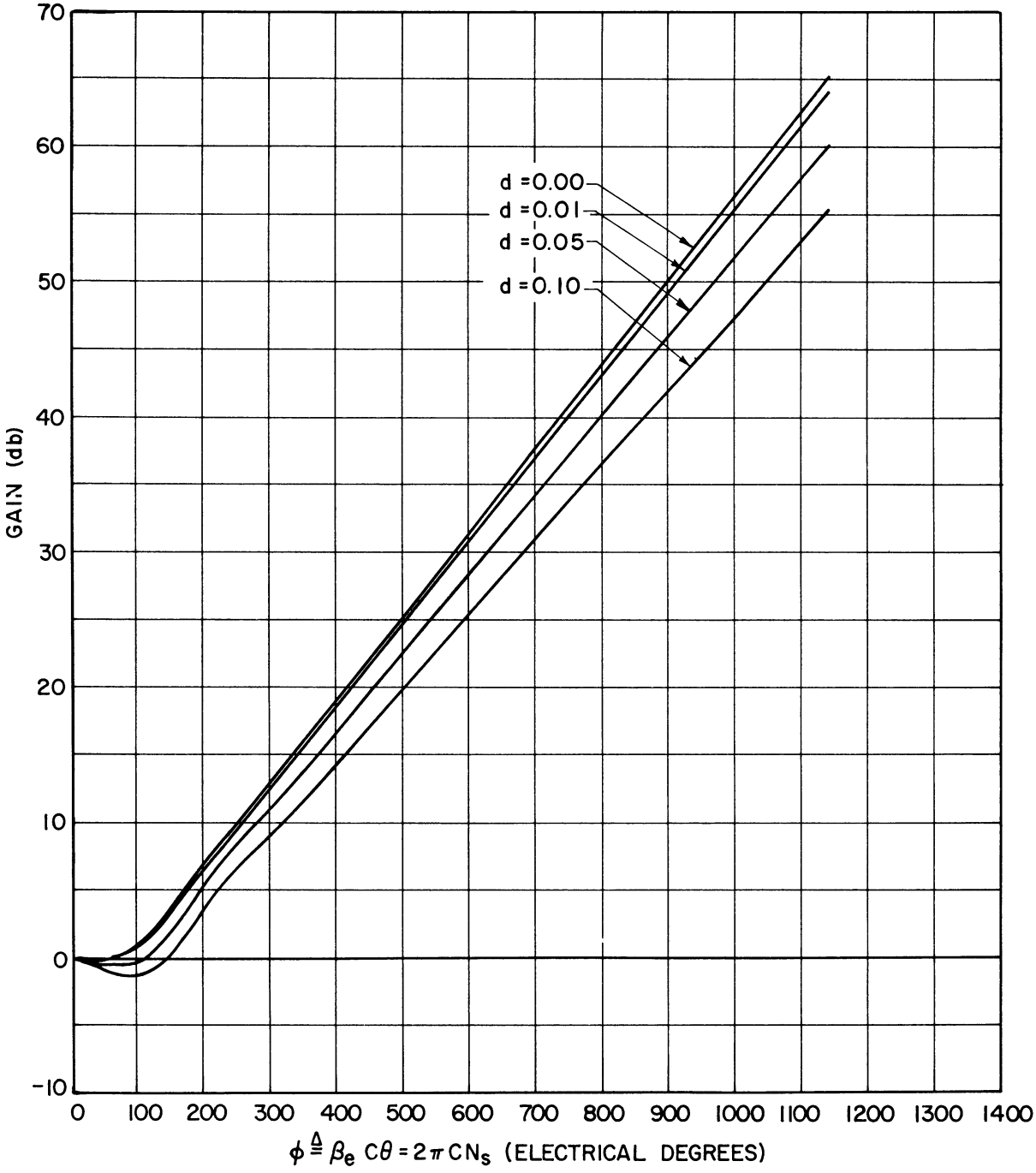

Fig. I.9 $\beta_e = 23$, b=0, C=0.06, Q=-2.0

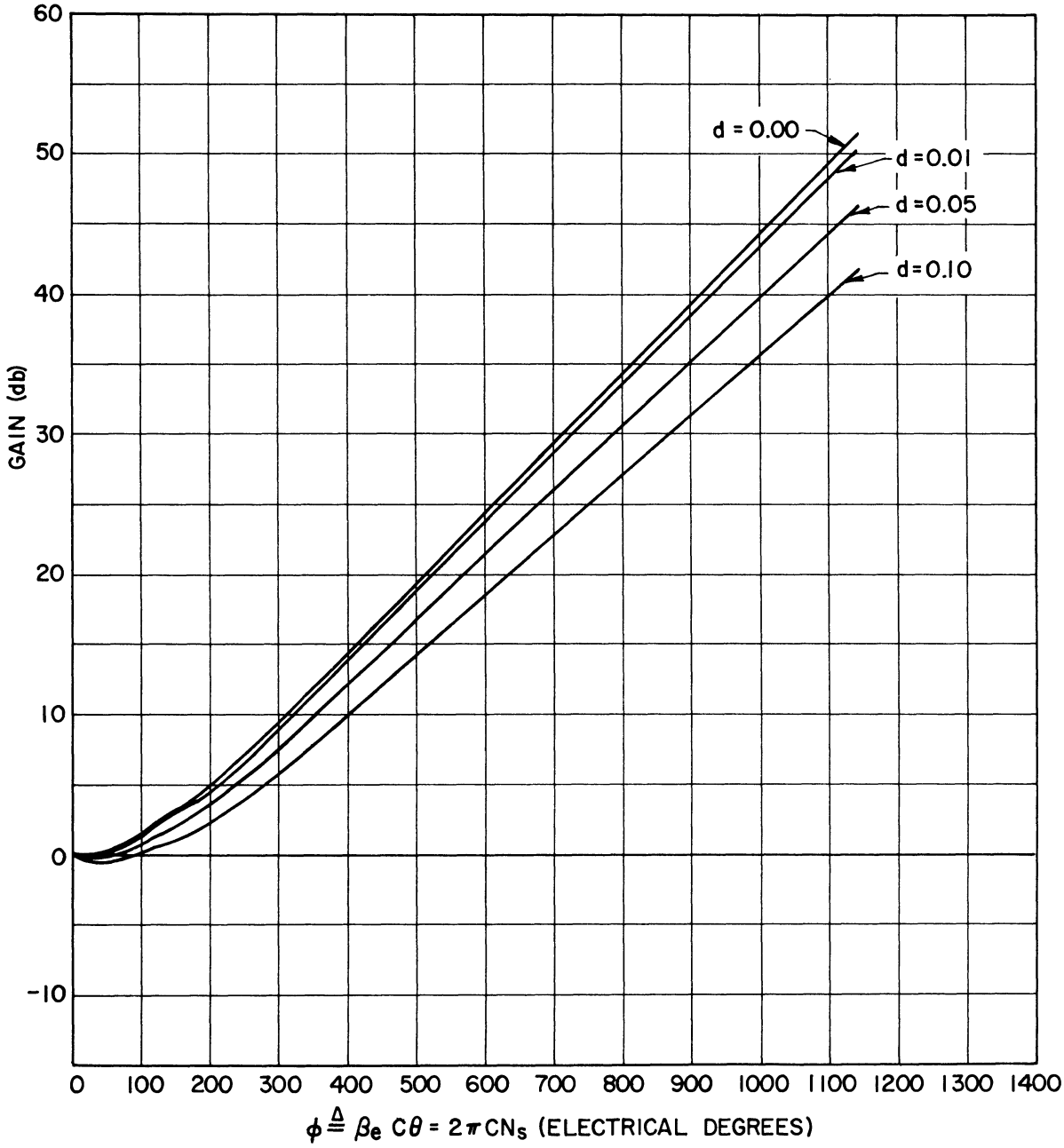

Fig. I.10 $\beta_e = 23$, b = 1.50, C = 0.06, Q = -2.0

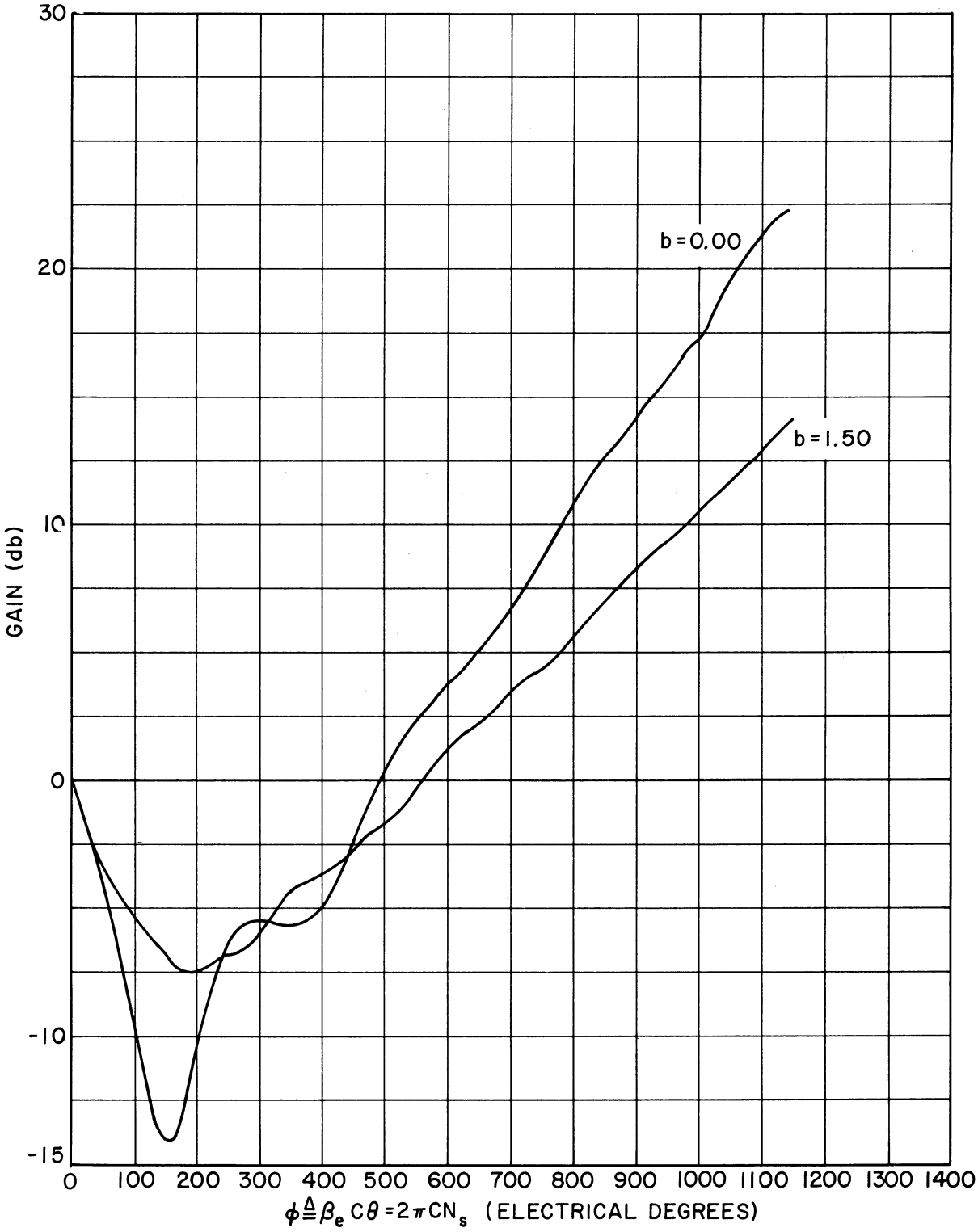

Fig. I. 11 $\beta_e = 23$, C=0.06, d=0.50, Q=-2.0

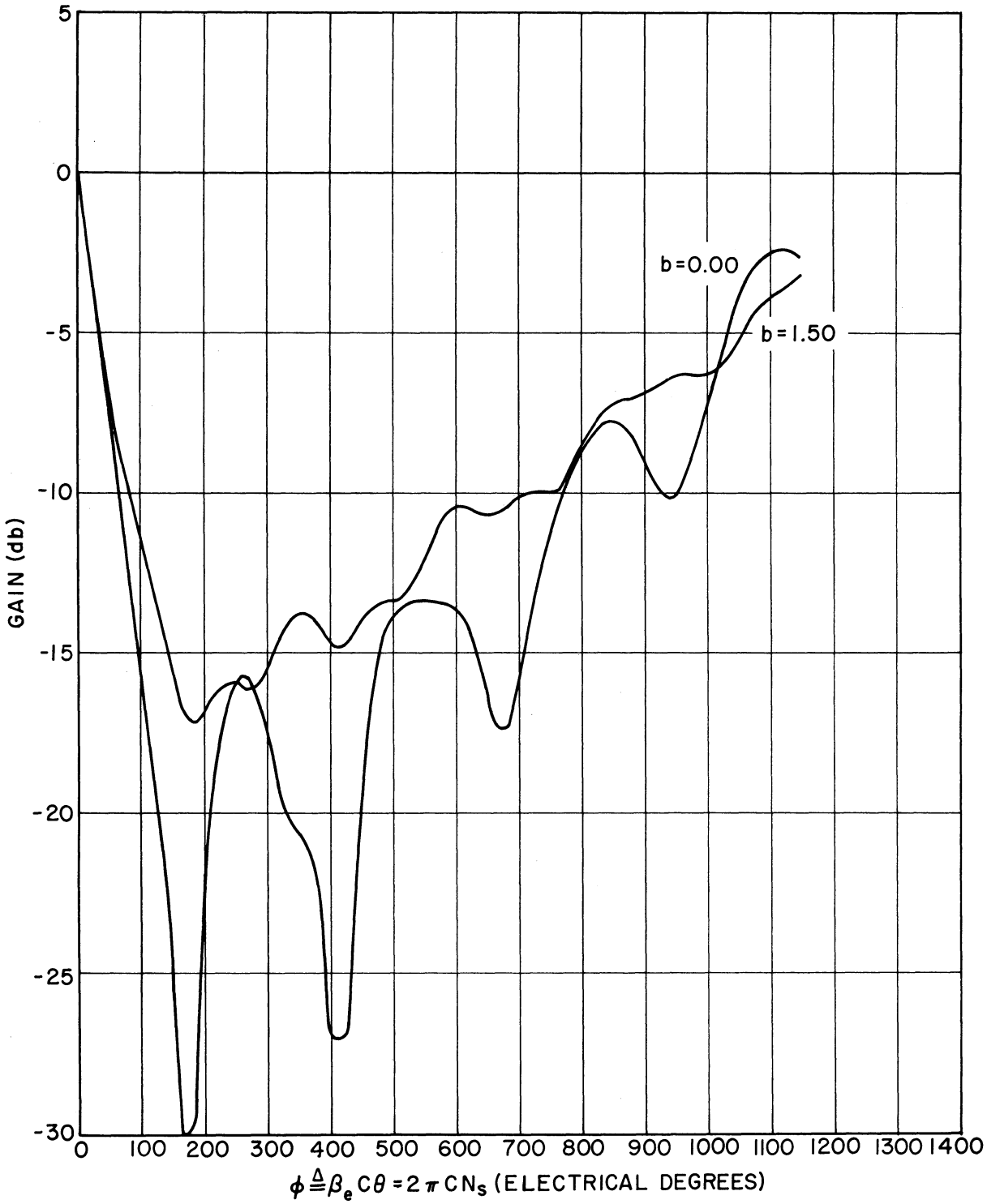

Fig. I.12 β_e=23, C=0.06, d=1.00, Q=-2.0

BIBLIOGRAPHY

General References

1. Brillouin, L., Wave Propagation in Periodic Structures, Dover Publications, New York; 1953.

2. Goldstein, H., Classical Mechanics, Addison-Wesley Publishing Co., Inc., Reading, Massachusetts; 1959.

3. Guillemin, E. A., The Mathematics of Circuit Analysis, John Wiley and Sons, Inc., New York; 1949.

4. Jahnke, E., and Emde, F., Tables of Functions, Dover Publications, New York; 1945.

5. Morse, P. M., and Feshback, H., Methods of Theoretical Physics, Parts I and II, McGraw-Hill Book Co., Inc., New York; 1953.

6. Pierce, J. R., Theory and Design of Electron Beams, 2nd Edition, D. Van Nostrand Co., Inc., New York; 1954.

7. Pierce, J. R., Traveling-Wave Tubes, D. Van Nostrand Co., Inc., New York; 1950.

8. Schelkunoff, S. A., Electromagnetic Waves, D. Van Nostrand Co., Inc., New York; 1943.

9. Stratton, J. A., Electromagnetic Theory, McGraw-Hill Book Co., Inc., New York; 1941.

10. Watson, G. N., Treatise on the Theory of Bessel Functions, Macmillan and Co., New York; 1944.

References Pertaining to the Electromagnetic Analysis

11. Buchholz, H., "Effect of Curvature of Rectangular Hollow Conductors on the Phase Constant of Ultra-Short Waves", Elektrische Nachrichten-Technik, 16, No. 3, 73-85; March, 1939.

12. Dwight, H. B., "Tables of Roots for Natural Frequencies in Coaxial Type Cavities", Journal of Mathematics and Physics, vol. 27, pp. 84-89; April, 1948.

13. Kalähne, A., "Electrical Oscillations in Ring-Shaped Metal Tubes", Annalen der Physik, vol. 18, pp. 92-127; 1905; Annalen der Physik, vol. 19, pp. 80-115; 1906.

14. Kline, M., "Some Bessel Equations and Their Application to Guide and Cavity Theory", Journal of Mathematics and Physics, vol. 27, pp. 37-48; April, 1948.

15. Marcuvitz, N., Waveguide Handbook, vol. 10, M. I. T. Radiation Laboratory Series, McGraw-Hill Book Co., Inc., New York; 1951 (pp. 72-80).

16. Waldron, R. A., "Theory of the Helical Waveguide of Rectangular Cross-Section", Journal of the British IRE, vol. 17, No. 10, pp. 577-592; October, 1957.

17. Waldron, R. A., "A Helical Coordinate System and Its Applications in Electromagnetic Theory", Quarterly Journal of Mechanics and Applied Mathematics, vol. XI, Pt. 4, pp. 438-461; 1958.

References Pertaining to E-Type and Related Devices

18. Guenard, P., and Doehler, O., "E and C Type Traveling-Wave Devices", Letter to the Editor, Proc. IRE, vol. 44, No. 2, pp. 261; February, 1956.

19. Harman, W. W., Fundamentals of Electronic Motion, McGraw-Hill Book Co., Inc., New York; 1953 (pp. 41-47).

20. Heffner, H., and Watkins, D. A., "The Practicability of E-Type Traveling-Wave Devices", Letter to the Editor, Proc. IRE, vol. 43, No. 7, pp. 1007-1008; August, 1955.

21. Huber, H., "A Traveling-Wave Tube with Purely Electrostatic Focusing", Patent No. 993.492, Patent Office of the Republic of France, Paris; June 21, 1949.

22. Johnson, C. C., "Impedance and Dispersion Characteristics of the Flattened Helix", Trans. PGED-IRE, ED-6, No. 2, pp. 189-194; April, 1959.

23. Pantell, R. H., "Backward-Wave Oscillations in an Unloaded Waveguide", Letter to the Editor, Proc. IRE, vol. 47, No. 6, pp. 1164; June, 1959.

24. Pantell, R. H., "Small-Signal Analysis of the Helitron Oscillator", Trans. PGED-IRE, ED-7, No. 1, pp. 22-29; January, 1960.

25. Rowe, J. E., "Transmission-Line Equations for Wave Propagation in a Two-Dimensional Anisotropic Lattice", Electron Physics Laboratory Memorandum No. 59-2-2854, Electrical Engineering Department, The University of Michigan; March 9, 1959.

26. Rowe, J. E., "Theory of the Crestatron: A Forward-Wave Amplifier", Proc. IRE, vol. 47, pp. 536-545; April, 1959.

27. Tchernov, Z. S., "'The Spiratron' — A Traveling-Wave Tube with Centrifuged Electrostatic Beam Focusing", Proceedings of the International Conference of Microwave Tubes, vol. II, Sect. 5.03, pp. 27-35, Paris; May 29-June 2, 1956.

28. Tchernov, Z. S., "Interaction of Electromagnetic Waves and Electron Beams with Centrifugal-Electrostatic Focusing", Electronic Waveguides, Polytechnic Institute of Brooklyn Microwave Research Institute Symposia Series, vol. VIII; April, 1958 (pp. 339-344).

29. Versnel, A., and Jonker, J. L. H., "A Magnetless Magnetron", Philips Research Reports, vol. 9, pp. 458-459; December, 1954.

30. Versnel, A., "Magnetless Magnetron", Proceedings of the International Conference of Microwave Tubes, vol. II, Sect. 5.02, pp. 22-26, Paris; May 29-June 2, 1956.

31. Wada, G., and Pantell, R. H., "Design, Theory, and Characteristics of the Helitron — A New Type of Microwave Oscillator", IRE WESCON Convenction Record, Pt. 3, Electron Devices, pp. 92-102, San Francisco; August 18-21, 1959.

32. Waters, W. E., "Beam Rippling in an E-Type Oscillator", Diamond Ordnance Fuze Laboratories, Internal Technical Memorandum; August 28, 1957.

33. Waters, W. E., "Motion of Electrons between Concentric Cylinders", Diamond Ordnance Fuze Laboratories, Tech. Rpt. No. TR-525; November 1, 1957.

34. Waters, W. E., "Rippling of Thin Electron Ribbons", Journal of Applied Physics, vol. 29, No. 1, pp. 100-104; January, 1958.

35. Waters, W. E., "Some Properties of Electron Sheet Beams in E-Type Oscillators", Diamond Ordnance Fuze Laboratories Memorandum No. M340-58-6; August 18, 1958.

36. Waters, W. E., "Paraxial Properties of Crossed-Field Electron Sheet Beams", Stanford Electronics Laboratories Technical Report No. 901-2, Microwave Laboratory Report No. 603; May, 1959.

37. Waters, W. E., "A Simple Formula for Calculation of the Minimum Useable Circuit Interaction Impedance for an E-Type Oscillator", Diamond Ordnance Fuze Laboratories, Internal Technical Memorandum; August 18, 1959.

38. Watkins, D. A., and Wada, G., "The Helitron Oscillator", Proc. IRE, vol. 46, No. 10, pp. 1700-1705; October, 1958.

39. Rowe, J. E., and Sobol. H., "Start-Oscillation Conditions in Modulated and Unmodulated O-Type Oscillators", Electron Physics Laboratory Technical Report No. 35, Electrical Engineering Department, The University of Michigan; February, 1960.

LIST OF SYMBOLS*

A	An arbitrary real constant defined in connection with Eqs. 2.33-2.38.
$A_1,\ldots,A_4$	Constants of integration associated with Eqs. 2.10 and 2.11.
$A_{n\beta_o}$	A quantity defined in connection with Eqs. 2.53-2.58.
B	An arbitrary real constant defined in connection with Eqs. 2.45-2.50.
$B_{n\beta_o}$	A quantity defined in connection with Eqs. 2.53-2.58.
b	The relative injection velocity parameter.
C	The small-signal gain parameter.
$C_1,\ldots,C_4$	Arbitrary constants defined in connection with Eq. 2.15.
C_1, C_2	Constants of integration used in the slipping-stream analysis.
C_1	Slipping-stream gain parameter associated with the outside segment of the beam.
C_2	Slipping-stream gain parameter associated with the inside segment of the beam.
$C_{\theta n}$	A coefficient defined by Eq. 3.95.
$C_{\nu n}$	A coefficient defined by Eq. 3.96.
$C_{\mu n}$	A coefficient defined by Eq. 3.97.
$(CN_s)_{so}$	The start-oscillation length.
c	The velocity of light in free space in meters/second.
$D_1,\ldots D_4$	Arbitrary constants defined in connection with Eq. 2.16.
D_{n1}	Elements of the D-matrix defined by Eq. 3.101.
d	The small-signal loss parameter.

---

* Special symbols used in connection with the experimental device are defined in Table 4.6 of Chapter IV.

$\bar{E}$ Vector electric field intensity, defined according to Eq. A.3, in volt/meter.

E_r Scalar component of radial r-f electric field intensity in volt/meter.

$E(r)$ The d-c radial electric field intensity at radius r in volt/meter.

$E(r_o)$ The d-c radial electric field intensity at radius r_o in volt/meter.

E_r^o The steady component of radial electric field intensity, defined according to Eq. 3.16, in volt/meter.

$E_{r\ max}$ The maximum value of radial r-f electric field intensity in volt/meter.

E_θ Scalar component of azimuthal r-f electric field intensity in volt/meter.

$E_{\theta s}$ The azimuthal r-f electric field intensity produced by electron beam bunching in volt/meter.

$E_{\theta\ max}$ The maximum value of azimuthal r-f electric field intensity in volt/meter.

E_z Scalar component of axial r-f electric field intensity in volt/meter.

e The negative charge of the electron in coulomb.

e The base of natural logarithms.

F_o The field ratio expression defined by Eq. 3.51.

F_1, F_2 Arbitrary constants defined by Eq. 2.61.

$F_{n\beta_o}$ A quantity defined in connection with Eqs. 2.62-2.67.

$F(r)$ The field ratio expression defined by Eq. C.6.

f The frequency of the r-f wave in cycles/second.

f_{co_1} The cutoff frequency for the interaction space, defined by Eq. C.4, in cycles/second.

f_{co_2} The cutoff frequency for the slow-wave structure, defined by Eq. C.5, in cycles/second.

$G_{n\beta_o}$ A quantity defined in connection with Eqs. 2.62-2.67.

$\bar{H}$ Vector r-f magnetic field intensity, defined according to Eq. A.3, in ampere-turn/meter.

H_r Scalar component of radial r-f magnetic field intensity in ampere-turn/meter.

H_θ Scalar component of azimuthal r-f magnetic field intensity in ampere-turn/meter.

H_z Scalar component of axial r-f magnetic field intensity in ampere-turn/meter.

$H^{(1)}_{\beta_o}(kr)$ The Hankel function of the first kind with argument kr and order β_o.

$H^{(2)}_{\beta_o}(kr)$ The Hankel function of the second kind with argument kr and order β_o.

h The height of the ribbon-shaped electron beam parallel to the z-axis in meters.

I_θ The total azimuthal current in amperes.

I_o The steady component of azimuthal current in amperes.

I_{so} The start-oscillation current in amperes.

$I_{\beta_o}(kr)$ The hyperbolic Bessel function of the first kind with argument kr and order β_o.

i_r The radial r-f current in amperes.

$i_{r\ max}$ The maximum value of the radial r-f current in amperes.

i_θ The azimuthal r-f current in amperes.

$i_{\theta n}$ The azimuthal r-f current of the nth wave in amperes.

$i_{\theta\ max}$ The maximum value of the azimuthal r-f current in amperes.

$J_{\beta_o}(kr)$ The real Bessel function of the first kind with argument kr and order β_o.

K The magnitude of the effective interaction impedance in ohms.

$K_{\beta_o}(kr)$ The hyperbolic Bessel function of the second kind with argument kr and order β_o.

k The wave propagation constant, defined in connection with Eqs. A.24 and A.25, in electrical radian/meter.

k_m The wave propagation constant of a medium whose permittivity is ϵ_m, defined in connection with Eqs. A.12 and A.13, in electrical radian/meter.

k_n A wave propagation constant, defined in connection with Eq. C.1, in electrical radian/meter.

k_{1n} A wave propagation constant, defined in connection with Eq. 2.59, in electrical radian/meter.

k_{2n} A wave propagation constant, defined in connection with Eq. 2.52, in electrical radian/meter.

k_r The radial coupling factor.

k_θ The azimuthal coupling factor.

L The height of the waveguide parallel to the z-axis in meters.

m The mass of the electron in kilograms.

N The number of "wave angles" along the r-f structure in the presence of the beam.

N_s A quantity related to the number of "wave angles" along the r-f structure in the presence of the beam.

$N_{\beta_o}(kr)$ The real Bessel function of the second kind with argument kr and order β_o.

P_c The critical perveance for an unrippled beam.

P_r The average radial r-f power transferred to the wave in watts.

P_θ The average azimuthal r-f power transferred to the wave in watts.

Q The small-signal space-charge parameter.

Q_b The total charge contained in the beam in coulombs.

Q_1 The slipping-stream space-charge parameter associated with the outside segment of the beam.

Q_2 The slipping-stream space-charge parameter associated with the inside segment of the beam.

R A scalar function of the radial coordinate.

r The radial coordinate variable in meters.

r_a The radius of the inside wall of the curved rectangular waveguide, as shown in Fig. 2.2, in meters.

r_c The radius of the slow-wave circuit, as shown in Figs. 1.1 and 2.2, in meters.

r_o The radius of the center-of-the-beam electron, as shown in Fig. 1.1, in meters.

r_s The radius of the sole, as shown in Fig. 1.1, in meters.

r_s The radius of the outside wall of the curved rectangular waveguide, as shown in Fig. 2.2, in meters.

r_1 The radius of the outside edge of the beam in meters.

r_2 The radius of the inside edge of the beam in meters.

s The scalar magnitude of arc length in meters.

t Time in seconds.

U A scalar function of r and θ.

u_{n1} The real part of the nth initial wave amplitude.

V A static potential function of r alone in volts.

V_c The d-c potential of the circuit measured relative to the cathode in volts.

V_n The amplitude of the r-f voltage of the nth wave in volts.

V_o The d-c potential of an electron at radius r_o in volts.

V_{RO} The total r-f voltage applied to the circuit at $\theta = 0$ in volts.

V_s The d-c potential of the sole measured relative to the cathode in volts.

V_{so} The beam potential at start-oscillation in volts.

$V(z,\theta,t)$ The r-f voltage on the biperiodic structure, defined in connection with Eq. 3.53, in volts.

$V_{\beta_o}(kr)$ A quantity defined in connection with Eqs. 2.62-2.67.

V_1 The d-c potential at the outside edge of the beam in volts.

V_2 The d-c potential at the inside edge of the beam in volts.

v The linear tangential velocity of an electron at radius r in meter/second.

$(v)_r$ The linear tangential velocity of the r-f wave at radius r in the absence of electrons in meter/second.

$(v_1)_{r_o}$ The linear tangential velocity of the r-f wave at radius r_o in the presence of electrons in meter/second.

v_o The linear tangential velocity of an electron at radius r_o in meter/second.

v_2 The phase velocity of electromagnetic waves in a medium of permittivity ϵ_m, defined by Eq. 2.51, in meter/second.

$v_{o,o}$ The linear tangential phase velocity (at the r-f circuit radius) of an azimuthally-directed wave, defined in connection with Eq. 3.53, in meter/second.

$v_{o,1}$ The axial component of wave phase velocity, defined in connection with Eq. 3.53, in meter/second.

v_{n1} The imaginary part of the nth initial wave amplitude.

$X_{\beta_o}(kr)$ The function defined in connection with Eqs. 2.33-2.38.

x_n The real part of the incremental propagation constant of the nth wave.

$Y_{\beta_o}(kr)$ A quantity defined in connection with Eqs. 2.62-2.67.

y_n The imaginary part of the incremental propagation constant of the nth wave.

Z_m The wave impedance of a medium of permittivity ϵ_m and permeability μ_m in ohms.

$Z_{o,o}$ The azimuthal component of circuit impedance at the surface of the r-f structure, defined in connection with Eq. 3.53, in ohms.

$Z_{o,1}$ The axial component of the circuit impedance at the surface of the r-f structure, defined in connection with Eq. 3.53, in ohms.

$Z_{\beta_o}(kr)$ A function defined in connection with Eqs. 2.45-2.50.

z The axial coordinate variable in meters.

α A quantity defined by Eq. 3.138.

β The circular propagation constant in the presence of the beam in electrical radian/spatial radian.

β_e The circular propagation constant of the electron beam in electrical radian/spatial radian.

β_{e1} The circular propagation constant of the outside segment of the electron beam in electrical radian/spatial radian.

β_{e2} The circular propagation constant of the inside segment of the electron beam in electrical radian/spatial radian.

β_n The circular propagation constant of the nth wave in the presence of the beam in electrical radian/spatial radian.

β_o The circular propagation constant of the r-f wave in the absence of electrons in electrical radian/spatial radian.

γ The axial propagation constant of the r-f wave in the presence and absence of electrons in electrical radian/meter.

Δ_s The system determinant defined by Eq. 3.40.

δ The incremental propagation constant.

δ_n The incremental propagation constant of the nth wave.

ϵ_m The permittivity of medium m in farad/meter.

ϵ_o The permittivity of free space in farad/meter.

ϵ' The relative dielectric constant of medium m.

ζ The complex gain vector.

ζ_{ss} The slipping-stream gain vector.

$|\zeta|$ The magnitude of the gain vector.

$|\zeta_1|$ The magnitude of the complex gain vector associated with the outside segment of the beam.

$|\zeta_2|$ The magnitude of the complex gain vector associated with the inside segment of the beam.

η The magnitude of the electron's charge-to-mass ratio in coulomb/kilogram.

η_θ The small-signal efficiency of E-type devices.

Θ A scalar function of θ alone.

θ The azimuthal coordinate variable in radians.

θ_g The spatial "wave angle" of the r-f wave along the slow-wave structure in the presence of the beam in radians.

μ The radial perturbation function in meters.

μ_m The permeability of medium m in henry/meter.

μ_n The radial perturbation function of the nth wave in meters.

μ_o The permeability of free space in henry/meter.

ν The azimuthal velocity perturbation function in spatial radian/second.

ν_n The azimuthal velocity perturbation function of the nth wave in spatial radian/second.

$\overline{\xi}_T$ Vector field intensity function lying in a plane normal to the cylindrical axis defined in connection with Eq. A.2.

$\xi_r(r)$ A quantity defined in connection with Eq. C.1.

$\xi_r(r_c)$ A quantity defined in connection with Eq. D.1.

$\xi_r(r_o)$ A quantity defined in connection with Eq. D.1.

$\xi_\theta(r)$ A quantity defined in connection with Eq. C.1.

$\xi_\theta(r_c)$ A quantity defined in connection with Eq. D.2.

$\xi_\theta(r_o)$ A quantity defined in connection with Eq. D.2.

ξ_z Scalar axial field intensity function defined in connection with Eq. A.2.

ρ The total volume charge density of the beam in coulomb/cubic meter.

ρ_o The d-c component of volume charge density of the beam in coulomb/cubic meter.

σ The radial width of the beam in meters.

τ The total ring charge density of the beam in coulomb/meter.

τ_o The d-c component of ring charge density of the beam in coulomb/meter.

τ_1 The r-f component of ring charge density of the beam in coulomb/meter.

τ_1^* The effective r-f component of ring charge density of the beam, defined in connection with Eq. 3.53, in coulomb/meter.

Φ Electrical angle in radians.

Φ_{so} Electrical angle at start-oscillation in radians.

Φ_1, Φ_2 Electrical angles associated with the outside and inside beam segments in radians.

Ψ The angle associated with the complex gain vector.

Ψ_1, Ψ_2 The angles associated with the complex gain vectors of the outside and inside segments of the beam.

$\bar{\psi}_T$ Vector field intensity function lying in a plane normal to the cylindrical axis defined in connection with Eq. A.1.

ψ_z Scalar axial field intensity function defined in connection with Eq. A.1.

Ω_o The unperturbed spatial angular velocity of an electron at radius r_o in spatial radian/second.

Ω_r The spatial angular velocity of an electron at radius r in spatial radian/second.

Ω_w Spatial angular velocity of r-f wave in the absence of electrons in spatial radian/second.

Ω_{w1} Spatial angular velocity of r-f wave in the presence of electrons in spatial radian/second.

Ω_1 Spatial angular velocity of an electron at outside edge of beam in spatial radian/second.

Ω_2 Spatial angular velocity of an electron at inside edge of beam in spatial radian/second.

ω The electrical angular velocity of r-f wave in electrical radian/second.

$\bar{1}_r$ The unit radial vector as shown in Fig. 2.1.

$\bar{1}_\theta$ The unit azimuthal vector as shown in Fig. 2.1.

$\bar{1}_z$ The unit axial vector as shown in Fig. 2.1.

DISTRIBUTION LIST

No. Copies	Agency
10	Dr. Robert T. Young, Chief, Electron Tube Branch, Diamond Ordnance Fuze Laboratories, Washington 25, D. C.
1	Commanding General, U. S. Army Signal Research & Development Laboratory, Fort Monmouth, New Jersey, ATTN: Chief, Technical Documents Center
1	Director, Evans Signal Laboratory, Belmar, New Jersey, ATTN: Dr. Gerald E. Pokorney, Microwave Tubes Branch, Electron Devices Division
10	Commander, Armed Services Technical Information Agency, Arlington Hall Station, Arlington 12, Virginia
1	Electronics Engineer, Signal Corps Engineering Laboratory, Evans Signal Laboratories, Belmar, New Jersey, ATTN: Mr. Harold J. Hersh
1	Commander, Rome Air Development Center, Griffiss Air Force Base, Rome, New York, ATTN: Mr. H. Chiosa, RCLRR-3
1	Commander, Rome Air Development Center, Griffiss Air Force Base, Rome, New York, ATTN: Lt. B. O. Werle, RCLRR-3
1	Bureau of Ships, Code 691A4, Department of Navy, Washington 25, D. C., ATTN: Mr. W. J. Riegger
1	Electronics Research Laboratory, Stanford University, Stanford, California, ATTN: Mr. David C. Bacon, Assistant Director
1	Spencer Laboratory Library, Raytheon Company, Wayside Road, Burlington, Massachusetts, ATTN: Mr. W. W. Teich
1	Spencer Laboratory, Raytheon Company, Wayside Road, Burlington, Massachusetts, ATTN: Mr. William C. Brown
1	Mr. Rudolf C. Hergenrother, Lab. Manager, Raytheon Manufacturing Company, Waltham, Massachusetts
1	Varian Associates, 611 Hansen Way, Palo Alto, California, ATTN: Mrs. Helen Dean, Technical Library
1	Sylvania Electric Products, Inc., Mountain View, California, ATTN: Dr. Jules Needle
1	University of California, Berkeley 4, California, ATTN: The Electronics Research Laboratory, 427 Cory Hall

No. Copies	Agency
1	Polytechnic Institute of Brooklyn, Microwave Research Institute, 55 Johnson Street, Brooklyn 1, New York, ATTN: Dr. M. Ettenberg
1	Harvard University, Technical Reports Collection, Room 303A, Pierce Hall, Cambridge 38, Massachusetts, ATTN: M. L. Cox, Librarian
1	Ohio State University, Department of Electrical Engineering, Columbus 10, Ohio, ATTN: Professor E. M. Boone
1	General Electric Company, Electron Tube Division of the Research Laboratory, The Knolls, Schenectady, New York, ATTN: Mr. E. D. McArthur
1	Hughes Aircraft Company, Electron Tube Laboratory, Culver City, California, ATTN: Mr. John Mendel
1	Litton Industries, 1025 Brittan Avenue, San Carlos, California, ATTN: Dr. Joseph F. Hull
1	Radio Corporation of America, RCA Laboratories, Princeton, New Jersey, ATTN: Technical Library
1	Sylvania Electric Products, Inc., Physics Laboratory, 208-20 Willetts Point Blvd., Bayside, L. I., New York, ATTN: Dr. Louis R. Bloom
1	Microwave Laboratory, W. W. Hansen Laboratories of Physics, Stanford University, Stanford, California, ATTN: Librarian
1	Sperry Corporation, Electronic Tube Division, Gainesville, Florida, ATTN: Mr. P. Bergman
1	Microwave Electronic Corporation, 4061 Transport Street, Palo Alto, California, ATTN: Dr. S. F. Kaisel
1	Dr. J. H. Bryant, Bendix Aviation Corporation, Research Laboratories, Northwestern Highway and 10-1/2 Mile Road, Detroit 35, Michigan
1	Mr. A. G. Peifer, Bendix Aviation Corporation, Research Laboratories, Northwestern Highway and 10-1/2 Mile Road, Detroit 35, Michigan
1	Commander, Wright Air Development Division, Wright-Patterson Air Force Base, Ohio, ATTN: Mr. K. Hutchinson
1	Hughes Research Laboratories, Electron Tube Laboratory, Malibu, California, ATTN: Mr. George R. Brewer

No. Copies	Agency
1	California Institute of Technology, Department of Electrical Engineering, Pasadena, California, ATTN: Dr. R. W. Gould
1	University of Minnesota, Department of Electrical Engineering, Minneapolis, Minnesota, ATTN: Dr. W. G. Shepherd
1	Head, Vacuum Tube Laboratory, Massachusetts Institute of Technology, Research Laboratory of Electronics, Cambridge 39, Massachusetts, ATTN: Professor L. D. Smullin
1	Sperry Gyroscope Company, Electron Tubes Division, Great Neck, Long Island, New York, ATTN: Dr. V. Learned
1	ITT Laboratories, 500 Washington Avenue, Nutley 10, New Jersey, ATTN: Mr. Robert W. Wilmarth
1	Zenith Radio Corporation, Chicago, Illinois, ATTN: Dr. Robert Adler, Vice President and Associate Director of Research
1	Mr. Gerald Klein, Manager, Microwave Tubes Section, Applied Research Department, Westinghouse Electric Corporation, Box 746, Baltimore 3, Maryland
1	Microwave Electronic Corporation, 4061 Transport Street, Palo Alto, California, ATTN: Dr. William E. Waters

AD_____

The University of Michigan, Electron Physics Laboratory, Ann Arbor, Michigan. A SMALL-SIGNAL ANALYSIS OF E-TYPE TRAVELING-WAVE DEVICES, by W. M. Nunn, Jr., August, 1960, 325 pp. incl. illus. (Proj. No. 31030) (DA-49-186-502-ORD-720) Unclassified Report

This report is concerned with a small-signal analysis, both theoretical and experimental, of E-type traveling-wave tubes. The electromagnetic analysis yields the important characteristics of the fields present in the interaction space, while the equivalent circuit analysis leads to a prediction of the propagation constants and the initial wave amplitudes excited when a ribbon beam encounters the impressed r-f wave. The circuit and ballistic relations are derived and used in formulating the determinantal equations of both forward- and backward-wave devices. The growing- and beating-wave gain, and the backward-wave start-oscillation characteristics, are then obtained from solutions of the input boundary problem. The study reveals that the efficiency of E-type devices, based on a small-signal estimate, is comparable to that of O-type tubes. Although some similarities to other tubes exist, the E-type device possesses the property that its gain and start-oscillation characteristics are influenced by the radius of curvature of the beam.

UNCLASSIFIED

1. Introduction
2. The Electromagnetic Analysis
3. The Equivalent Circuit Analysis
4. The Experimental Small-Signal E-Type Traveling-Wave Amplifier
5. Conclusions

I. Nunn, Walter M., Jr.

II. Diamond Ordnance Fuze Laboratories

UNCLASSIFIED

AD_____

The University of Michigan, Electron Physics Laboratory, Ann Arbor, Michigan. A SMALL-SIGNAL ANALYSIS OF E-TYPE TRAVELING-WAVE DEVICES, by W. M. Nunn, Jr., August, 1960, 325 pp. incl. illus. (Proj. No. 31030) (DA-49-186-502-ORD-720) Unclassified Report

This report is concerned with a small-signal analysis, both theoretical and experimental, of E-type traveling-wave tubes. The electromagnetic analysis yields the important characteristics of the fields present in the interaction space, while the equivalent circuit analysis leads to a prediction of the propagation constants and the initial wave amplitudes excited when a ribbon beam encounters the impressed r-f wave. The circuit and ballistic relations are derived and used in formulating the determinantal equations of both forward- and backward-wave devices. The growing- and beating-wave gain, and the backward-wave start-oscillation characteristics, are then obtained from solutions of the input boundary problem. The study reveals that the efficiency of E-type devices, based on a small-signal estimate, is comparable to that of O-type tubes. Although some similarities to other tubes exist, the E-type device possesses the property that its gain and start-oscillation characteristics are influenced by the radius of curvature of the beam.

UNCLASSIFIED

1. Introduction
2. The Electromagnetic Analysis
3. The Equivalent Circuit Analysis
4. The Experimental Small-Signal E-Type Traveling-Wave Amplifier
5. Conclusions

I. Nunn, Walter, M., Jr.

II. Diamond Ordnance Fuze Laboratories

UNCLASSIFIED

AD_____

The University of Michigan, Electron Physics Laboratory, Ann Arbor, Michigan. A SMALL-SIGNAL ANALYSIS OF E-TYPE TRAVELING-WAVE DEVICES, by W. M. Nunn, Jr., August, 1960, 325 pp. incl. illus. (Proj. No. 31030) (DA-49-186-502-ORD-720) Unclassified Report

This report is concerned with a small-signal analysis, both theoretical and experimental, of E-type traveling-wave tubes. The electromagnetic analysis yields the important characteristics of the fields present in the interaction space, while the equivalent circuit analysis leads to a prediction of the propagation constants and the initial wave amplitudes excited when a ribbon beam encounters the impressed r-f wave. The circuit and ballistic relations are derived and used in formulating the determinantal equations of both forward- and backward-wave devices. The growing- and beating-wave gain, and the backward-wave start-oscillation characteristics, are then obtained from solutions of the input boundary problem. The study reveals that the efficiency of E-type devices, based on a small-signal estimate, is comparable to that of O-type tubes. Although some similarities to other tubes exist, the E-type device possesses the property that its gain and start-oscillation characteristics are influenced by the radius of curvature of the beam.

UNCLASSIFIED

1. Introduction
2. The Electromagnetic Analysis
3. The Equivalent Circuit Analysis
4. The Experimental Small-Signal E-Type Traveling-Wave Amplifier
5. Conclusions

I. Nunn, Walter, M., Jr.

II. Diamond Ordnance Fuze Laboratories

UNCLASSIFIED

AD_____

The University of Michigan, Electron Physics Laboratory, Ann Arbor, Michigan. A SMALL-SIGNAL ANALYSIS OF E-TYPE TRAVELING-WAVE DEVICES, by W. M. Nunn, Jr., August, 1960, 325 pp. incl. illus. (Proj. No. 31030) (DA-49-186-502-ORD-720) Unclassified Report

This report is concerned with a small-signal analysis, both theoretical and experimental, of E-type traveling-wave tubes. The electromagnetic analysis yields the important characteristics of the fields present in the interaction space, while the equivalent circuit analysis leads to a prediction of the propagation constants and the initial wave amplitudes excited when a ribbon beam encounters the impressed r-f wave. The circuit and ballistic relations are derived and used in formulating the determinantal equations of both forward- and backward-wave devices. The growing- and beating-wave gain, and the backward-wave start-oscillation characteristics, are then obtained from solutions of the input boundary problem. The study reveals that the efficiency of E-type devices, based on a small-signal estimate, is comparable to that of O-type tubes. Although some similarities to other tubes exist, the E-type device possesses the property that its gain and start-oscillation characteristics are influenced by the radius of curvature of the beam.

UNCLASSIFIED

1. Introduction
2. The Electromagnetic Analysis
3. The Equivalent Circuit Analysis
4. The Experimental Small-Signal E-Type Traveling-Wave Amplifier
5. Conclusions

I. Nunn, Walter M., Jr.

II. Diamond Ordnance Fuze Laboratories

UNCLASSIFIED

AD_____

The University of Michigan, Electron Physics Laboratory, Ann Arbor, Michigan. A SMALL-SIGNAL ANALYSIS OF E-TYPE TRAVELING-WAVE DEVICES, by W. M. Nunn, Jr., August, 1960, 325 pp. incl. illus. (Proj. No. 31030) (DA-49-186-502-ORD-720) Unclassified Report

This report is concerned with a small-signal analysis, both theoretical and experimental, of E-type traveling-wave tubes. The electromagnetic analysis yields the important characteristics of the fields present in the interaction space, while the equivalent circuit analysis leads to a prediction of the propagation constants and the initial wave amplitudes excited when a ribbon beam encounters the impressed r-f wave. The circuit and ballistic relations are derived and used in formulating the determinantal equations of both forward- and backward-wave devices. The growing- and beating-wave gain, and the backward-wave start-oscillation characteristics, are then obtained from solutions of the input boundary problem. The study reveals that the efficiency of E-type devices, based on a small-signal estimate, is comparable to that of O-type tubes. Although some similarities to other tubes exist, the E-type device possesses the property that its gain and start-oscillation characteristics are influenced by the radius of curvature of the beam.

UNCLASSIFIED

1. Introduction
2. The Electromagnetic Analysis
3. The Equivalent Circuit Analysis
4. The Experimental Small-Signal E-Type Traveling-Wave Amplifier
5. Conclusions

I. Nunn, Walter M., Jr.

II. Diamond Ordnance Fuze Laboratories

UNCLASSIFIED

AD_____

The University of Michigan, Electron Physics Laboratory, Ann Arbor, Michigan. A SMALL-SIGNAL ANALYSIS OF E-TYPE TRAVELING-WAVE DEVICES, by W. M. Nunn, Jr., August, 1960, 325 pp. incl. illus. (Proj. No. 31030) (DA-49-186-502-ORD-720) Unclassified Report

This report is concerned with a small-signal analysis, both theoretical and experimental, of E-type traveling-wave tubes. The electromagnetic analysis yields the important characteristics of the fields present in the interaction space, while the equivalent circuit analysis leads to a prediction of the propagation constants and the initial wave amplitudes excited when a ribbon beam encounters the impressed r-f wave. The circuit and ballistic relations are derived and used in formulating the determinantal equations of both forward- and backward-wave devices. The growing- and beating-wave gain, and the backward-wave start-oscillation characteristics, are then obtained from solutions of the input boundary problem. The study reveals that the efficiency of E-type devices, based on a small-signal estimate, is comparable to that of O-type tubes. Although some similarities to other tubes exist, the E-type device possesses the property that its gain and start-oscillation characteristics are influenced by the radius of curvature of the beam.

UNCLASSIFIED

1. Introduction
2. The Electromagnetic Analysis
3. The Equivalent Circuit Analysis
4. The Experimental Small-Signal E-Type Traveling-Wave Amplifier
5. Conclusions

I. Nunn, Walter, M., Jr.

II. Diamond Ordnance Fuze Laboratories

UNCLASSIFIED

AD_____

The University of Michigan, Electron Physics Laboratory, Ann Arbor, Michigan. A SMALL-SIGNAL ANALYSIS OF E-TYPE TRAVELING-WAVE DEVICES, by W. M. Nunn, Jr., August, 1960, 325 pp. incl. illus. (Proj. No. 31030) (DA-49-186-502-ORD-720) Unclassified Report

This report is concerned with a small-signal analysis, both theoretical and experimental, of E-type traveling-wave tubes. The electromagnetic analysis yields the important characteristics of the fields present in the interaction space, while the equivalent circuit analysis leads to a prediction of the propagation constants and the initial wave amplitudes excited when a ribbon beam encounters the impressed r-f wave. The circuit and ballistic relations are derived and used in formulating the determinantal equations of both forward- and backward-wave devices. The growing- and beating-wave gain, and the backward-wave start-oscillation characteristics, are then obtained from solutions of the input boundary problem. The study reveals that the efficiency of E-type devices, based on a small-signal estimate, is comparable to that of O-type tubes. Although some similarities to other tubes exist, the E-type device possesses the property that its gain and start-oscillation characteristics are influenced by the radius of curvature of the beam.

UNCLASSIFIED

1. Introduction
2. The Electromagnetic Analysis
3. The Equivalent Circuit Analysis
4. The Experimental Small-Signal E-Type Traveling-Wave Amplifier
5. Conclusions

I. Nunn, Walter M., Jr.

II. Diamond Ordnance Fuze Laboratories

UNCLASSIFIED

AD_____

The University of Michigan, Electron Physics Laboratory, Ann Arbor, Michigan. A SMALL-SIGNAL ANALYSIS OF E-TYPE TRAVELING-WAVE DEVICES, by W. M. Nunn, Jr., August, 1960, 325 pp. incl. illus. (Proj. No. 31030) (DA-49-186-502-ORD-720) Unclassified Report

This report is concerned with a small-signal analysis, both theoretical and experimental, of E-type traveling-wave tubes. The electromagnetic analysis yields the important characteristics of the fields present in the interaction space, while the equivalent circuit analysis leads to a prediction of the propagation constants and the initial wave amplitudes excited when a ribbon beam encounters the impressed r-f wave. The circuit and ballistic relations are derived and used in formulating the determinantal equations of both forward- and backward-wave devices. The growing- and beating-wave gain, and the backward-wave start-oscillation characteristics, are then obtained from solutions of the input boundary problem. The study reveals that the efficiency of E-type devices, based on a small-signal estimate, is comparable to that of O-type tubes. Although some similarities to other tubes exist, the E-type device possesses the property that its gain and start-oscillation characteristics are influenced by the radius of curvature of the beam.

UNCLASSIFIED

1. Introduction
2. The Electromagnetic Analysis
3. The Equivalent Circuit Analysis
4. The Experimental Small-Signal E-Type Traveling-Wave Amplifier
5. Conclusions

I. Nunn, Walter M., Jr.

II. Diamond Ordnance Fuze Laboratories

UNCLASSIFIED

ERRATA*

for

A SMALL-SIGNAL ANALYSIS OF E-TYPE TRAVELING-WAVE DEVICES

by

Walter M. Munn, Jr.

Electron Physics Laboratory Technical Report No. 38,
DA-49-186-502-ORD-720

Page 9, second line from the top of the page: "However, it has also been asserted[24] that ..."

Page 27, last sentence on the page: "Hence, the phase velocity of plane electromagnetic waves ..."

Page 47, the exponential expressions should be: e^{jkr}, e^{-jkr}, e^{-kr}, e^{kr}.

Page 48, the exponential expressions should be: e^{-kr}, $e^{-j\beta_o\theta}$.

Page 49, ninth line from the top of the page: limited[31].

Page 72, the exponential expression should be: $e^{j(\omega t-\beta_o\theta)}$.

Page 100, the definition of V_n below Eq. 3.90: delete "and $r = r_o$".

Page 104, the exponential appearing in Eq. 3.105 should be: $e^{\Phi x_n}$.

Page 109, twelve lines from the top of the page: "...the independent variables b and Φ lead to".

Page 127, seventeen lines from the top of the page: "...which resembles an ..."

Page 138, twelve lines from the top of the page: "..., as contrasted to the forward-wave case, ...".

Page 151, seven lines from the top of the page: "...in Table 3.1 have been".

Page 154, the left member of Eq. 3.134 should be: P_θ.

Page 214, equation A.9 should read:

$$\mathrm{Re}(\nabla \times \bar{\xi}) = \mathrm{Re}\left(\epsilon_m \frac{\partial \bar{\Psi}}{\partial t}\right) , \qquad (A.9)$$

---

* The corrections are underlined, where appropriate, for emphasis.

Page 216, equation A.23 should read:

$$\nabla \cdot \bar{\xi}_T = j\gamma \xi_z \quad , \qquad (A.23)$$

Page 224, four lines below Eq. C.2:

$F_{n\beta_o} = 0$ should be replaced with $G_{n\beta_o} = 0$.

ADDENDA TO SECTION 4.5

The correctness of the diagnosis pertaining to the origin of the large values of insertion loss associated with the slow-wave circuit was borne out by several experiments conducted subsequent to the completion of this report. When a helix, having the same dimensions as that used in the tube, was wound on a teflon form, and when the line-above-ground feed system was replaced by a coaxial transmission system, an insertion loss of only 9 db was observed at a midband frequency of 5 kmc. In view of the relatively large VSWR of 2.1:1 recorded at the same frequency, the attenuation is primarily due to the "reflection component" rather than the "intrinsic component" of loss. While teflon is not suited to use in an actual E-type tube, because of its limited temperature range, the investigation has experimentally demonstrated that a low-loss flattened helix can be constructed by a careful selection of the mandrel material. The recommendation concerning the helix mandrel design, discussed in Chapter V, would therefore appear to alleviate the present difficulty.